PhD thesis presented by

Eduard Baeza Pérez

For the degree of doctor at

UNIVERSITAT POLITÈCNICA DE CATALUNYA

Development of the new AINA code and its application to the Safety Analysis of the European DEMO designs

April 2019

UNIVERSITAT POLITÈCNICA
DE CATALUNYA
BARCELONATECH

Directors:
Alfredo de Blas del Hoyo
Albert Riego Pérez

Table of Contents

Abbreviations

AINA	*Analyses of IN-vessel Accidents*
ASDEX	*Axially Symmetric Divertor Experiment*
BB	*Breeding Blanket*
BC	*Boundary Condition*
BLK	*Blanket*
BSS	*Back Supporting Structure*
BZ	*Breeding Zone*
CB	*Cassette Body*
CFD	*Computational Fluid Dynamics*
CH	*Cooling Channel*
CP	*Cooling Plate*
DCLL	*Dual Coolant Lithium Lead*
ELM	*Edge Localized Modes*
FCI	*Flow Channel Inserts*
FW	*First Wall*
FPSS	*Fast Plasma Shutdown*
HCLL	*Helium Cooled Lithium Lead*
HCPB	*Helium Cooled Pebble Bed*
HFS	*High Field Side*
HTS	*Heat Transfer System*
IB	*In Board*
IE	*Initiating Events*
IVT	*Inner Vertical Target*
ITER	*International Thermonuclear Experimental Reactor*
JET	*Joint European Torus*
LiOS	*Lithium-Orthosilicate*
LOCA	*Loss Of Coolant Accident*
LOPC	*Loss Of Plasma Control*
MAST	*Mega Ampere Spherical Tokamak*
MHD	*Magnetohydrodynamic*
MMS	*Multi-Module Segment*
NHD	*Nuclear Heating Density*
NWL	*Neutron Wall Loading*
OB	*Out Board*
OBC	*Outboard Central Segment*
OVT	*Outer Vertical Target*
PEG	*Plasma Enhancement Gases*
PFC	*Plasma Facing Component*
PFU	*Plasma Facing Unit*
PIE	*Postulated Initiating Events*
RDL	*Radiation Divertor Load*
RWL	*Radiation Wall Load*
SIC	*Safety Importance Classification*
SOL	*Scrape Off Layer*
SS	*Steady State*
TBD	*To Be Defined*
TBR	*Tritium Breeding Ratio*
UPC	*Polytechnic University of Catalonia-BarcelonaTech*
VV	*Vacuum Vessel*
WCDC	*Water Cooled Divertor Cassette*
WCLL	*Water Cooled Lithium Lead*
WCPB	Water Cooled Pebble-Bed

List of important variables

A_k	*Mass number of k*
a	*Minor radius*
A_i	*Average ion mass*
β_p	*Poloidal Beta*
β_T	*Toroidal Beta*
B_T	*Toroidal magnetic field*
c	*Heat capacity*
C_α	*Ratio of alpha particle confinement time to TAU-E*
C_H	*Ratio of fuel particle confinement time to TAU-E*
C_i	*Ratio of ion energy confinement time to TAU-E*
$C_{screen_{Z_i}}$	*Screening factor for the impurity i*
C_Z	*Ratio of impurity particle confinement time to TAU-E*
ε	*Reduced energy or emissivity in the thermal model*
E_0	*Projectile energy*
E_α	*Alpha's energy*
E_{fus}	*Fusion energy*
E_n	*Neutron energy*
E_s	*Surface binding energy*
E_{TF}	*Thomas Fermi energy*
E_{th}	*Threshold energy*
f_α	*Fraction of alpha power absorbed by ions*
f_{Ar}	*Ratio Argon density to electron density*
$f_{bootstrap}$	*Fraction of Bootstrap current*
f_{Br_Z}	*Fraction of the total radiation power of the impurity Z originated by Bremsstrahlung in PROCESS*
f_{COOL}	*Relative surface of the coolant tubes*
f_{core}	*Fraction of the radiation Line which enter into the core due to high and medium Z impurities*
f_{ext}	*Fraction of external power absorbed by ions*
F_{mult_BB}	*Neutron multiplication factor for the NWL estimation in the Breeder Blankets*
$f_{P_{li\_ScalingFactor}}$	*Factor to adapt the results to the desired operational state conditions in the power Line model*
f_{ripple}	*Alpha ripple-loss rate*
f_{Xe}	*Ratio Xenon density to electron density*
f_W	*Ratio Tungsten density to electron density*
$f_{WGT,R}$, $f_{WGT,P}$	*Coolant factor for the no in lines tubes*
f_Z	*Thermal ion fraction in PROCESS*
G_{Troyon}	*Troyon coefficient*
h	*Heat Transfer Coefficient*
$HEVA$	*Heat of evaporation*
$I_{bootstrap}$	*Bootstrap currents*
I_p	*Plasma current*
k	*Plasma elongation or thermal conductivity in thermal models*
k_T	*Thermal conductivity*
M_i	*Atomic mass*
μ	*Dynamic viscosity*
n_α	*Alpha density*
n_e	*Electron density*
n_H	*Fuel density*
n_i	*Ion density*
NWL	*Neutron wall load*
n_Z	*Impurity density*

n_{ZAr}	*Argon density*
n_{ZXe}	*Xenon density*
n_{ZW}	*Tungsten density*
P_{α}	*Alpha power*
P_{Br}	*Bremsstrahlung power*
P_{core_rad}	*Total radiative losses in plasma core*
P_{div_rad}	*Radiation from the divertor region*
P_{edge}	*Power in plasma edge*
P_{ext}	*External power*
P_{fus}	*Fusion power*
P_{ie}	*Ion-electron exchange power*
P_{li}	*Line power*
P_{Ohm}	*Ohmic heating power*
P_{rad}	*Total radiative heat flux against the wall*
P_{rad_total}	*Total radiative losses*
P_{sep}	*Separatrix power*
P_{SOL}	*Scrape off layer power*
P_{sy}	*Cyclotron power*
P_Z	*Radiation power in PROCESS*
Q	*Power gain or a fitting parameter for the physical sputtering model*
q_{95}	*Safety factor at 95% flux*
q_0	*Safety factor at plasma axis*
$\dot{q}_{erosion}$	*Flux emitted due to due to impurity flux leaving the wall*
$\dot{q}_{RadiationReflection}$	*Radiation reflected for every module of the blanket*
$\ddot{q}$	Volumetric nuclear heat deposition
R	*Major radius*
RDL	*Radiation divertor load*
RWL	*Radiation wall load*
ρ	*Density*
R_w	*Wall reflection coefficient of the Psy*
S_{α}	*Alpha generation*
$S_{Geeration\ Z_i}$	*Impurity generation source*
S_H	*Fuel Injection*
S_n	*Nuclear stopping cross section*
S_p	*Plasma surface*
Sup_{PFC}	*PFC surface*
S_{Wall}	*Wall surface*
S_{ZXe}	*Xenon source*
S_{ZW}	*Tungsten source*
S_{Z_i}	*Impurity source until the plasma core*
t	*Time*
T_e	*Electron temperature*
T_i	*Ion temperature*
$\tau_{E,e}$	*Energy confinement time for electrons*
$\tau_{E,i}$	*Energy confinement time for ions*
$\tau_{p,\alpha}$	*Particle confinement time for alphas*
$\tau_{p,H}$	*Particle confinement time for fuel*
$\tau_{p,Z}$	*Particle confinement time for impurities*
$\Gamma_{incident\ ions\ or\ neutral}$	*Ions or neutral particles flux against the PFC*
$\Gamma_{PhysSput}$	*Physical sputtering source flux*
Γ_{Subli_i}	*Thermal sublimation source flux*

Γ_{Total}	*Total impurity generation flux*
$\langle \sigma v \rangle_{DT}$	*Velocity averaged cross-section of the deuterium-tritium nuclear fusion reaction*
V	*Plasma volume*
v	*Velocity*
Z_j	*Atomic number*

1 Introduction

1.1 Framework

This PhD thesis research is framed under the activities carried out by EUROfusion (European Consortium for the Development of Fusion Energy, manages and funds European fusion research activities [1]) to develop concepts for DEMO. Specifically, the FEEL; working supervised by Centro de Investigaciones Energéticas, Medioambientales y Tecnológicas (CIEMAT), is within the research team which is responsible of the previous studies about radiological safety and environmental impact, specifically in the Work Package of Safety and Environment (WPSAE). These studies are necessary in the current design stage of DEMO. It should be noted that the performed tasks had to be approved by EUROfusion as well as reviewed by a group of experts.

1.2 State of the art

At the beginning of the project, a last version of a safety fusion code called AINA had been developed by the Fusion Energy Engineering Laboratory (FEEL) of the Technical University of Catalonia (UPC) Barcelona-Tech. This tool was able to evaluate plasma evolution and in vessel components strains for ITER (AINA 3.0) and the WCPB Japanese DEMO design without divertor (AINA 3.1). In addition, AINA was used to provide contributions to the safety analyses of those two reactors designs.

Moreover, other computer codes have been developed as important tools applied for the safety analyses of the fusion facilities during the design stages of ITER and DEMO; however, AINA is the only one capable of simulating transients of plasma physics and thermal wall behaviour at the same time. A more detailed explanation of this framework will be introduce in chapter 2.

1.3 Objectives

It is with this backdrop in mind that the objectives of this PhD thesis research were divided in two main parts; however, one of them makes up the basis and it is the necessary tool to achieve the other one successfully. These introduced targets are:

I. Developing contributions to safety analyses for the four different European designs of DEMO using the AINA code.
II. Developing a totally new AINA version for the four different European designs of DEMO.

As derived from the previous list, it is only possible to reach the first and main purpose if the second one is properly performed.

Likewise, it can be noted that, currently, DEMO design is focused on four different concepts. The major difference between them concerns the BB (Breeding Blanket). Moreover, it is also necessary to take into account that all these concepts are continuously updated; hence, the last available design in every particular case will be used at the relevant time. Nevertheless, it is expected and intended that AINA will be easily modifiable in order to add or adapt new updates without difficulty.

1.4 Schedule and milestones

For the purpose of reaching the previous objectives shown, a scheduling of the different tasks was planned:

I. During the **first year** of PhD thesis studies (be aware of activities were initiated at April 2016):
   a. Developing an in-depth critical analysis of the AINA code 3.0.
   b. Study of the state of the art of all the models of the code.
   c. Development a new AINA, using MATLAB framework, and validation from the perspective of ITER. Specifically, the plasma block and a first approach of the plasma-wall interaction block.
   d. First assembly of the code in order to adapt it to DEMO HCPB configuration using the thermal blanket block modeled by Marco Fabbri while performing as a member of the AINA development team [2] and identification of the future improvements.
   e. Estimation of some steady state (SS) scenarios for HCPB DEMO and benchmarking using or other validated code as PROCESS.
   f. Study of evolution of the SS scenarios for HCPB DEMO when a perturbation is inserted.
   g. Identification of some critical transients for the future safety analyses.

II. During the **second year** of PhD thesis studies:
   a. Implementation of the identified improvements from the task 1.d of the previous year and addition of a divertor model. Thus, this new code was called AINA 4.0 and is able to simulate the DEMO HCPB configuration.
   b. Development of the DEMO1 safety analysis of the DEMO HCPB configuration by means of AINA.
   c. Modification of the code to adapt it to DEMO DCLL configuration. This new code was called AINA 4.0 DCLL (great effort was necessary with regard to the new thermal blanket block).

III. During the **third year** of PhD thesis studies:
   a. Development of the DEMO1 safety analysis of the DEMO DCLL configuration by means of AINA.
   b. Modification of the code to adapt it to DEMO HCLL and WCLL configurations (AINA 4.0 HCLL and AINA 4.3 WCLL respectively; great effort was necessary with regard to the new thermal blanket blocks for each design).
   c. Development of the DEMO1 safety analyses of the DEMO DCLL and WCLL configurations by means of AINA.
   d. Development of the DEMO2 safety analyses.

1.5 Scope

The scope of the text includes from a brief explanation of fusion power, International Thermonuclear Experimental Reactor (ITER) and Demonstration Power Plant (DEMO) until a critical analysis of the previous AINA code versions, the numerical models implemented in the new AINA code and the architecture of it.

Nonetheless, as it already mentioned the main aim of the project has been the development of a tool (AINA 4.0) in order to outline contributions to safety analyses for the four different European designs of DEMO.

1.6 Fusion power

Nuclear fusion is the reaction by which two or more atomic nuclei collide and join together to form a new heavier atomic nucleus. The fusion of two nuclei with lower masses than iron or nickel (which have the largest binding energy per nucleon) generally releases energy, while the fusion of nuclei heavier than iron absorbs energy. The matter is not conserved during the process (mass defect) and this is exoenergetic. So, fusion generally occurs for lighter elements only and their mass loss is converted to energy released following the Einstein equation $E=m\cdot c^2$ [3].

In spite of this kind of energy release is generated by the stars by means of nuclear fusion of hydrogen nuclei into helium; their production artificially with the aim of generating electricity is a laborious task. This research and development work has been conducted for over the last 60 years and it has encountered with great scientific and technological challenges. The electrostatic repulsion force between the positively charged protons of the nuclei has to be overcome before fusion can occur. If two nuclei can be brought close enough together (very short distance between them), the nuclear force of attraction is stronger than the electrostatic and the last one can be surpassed. Therefore an important prerequisite for fusion is that the nuclei have enough kinetic energy that they can approach each other despite the electrostatic repulsion. This minimum energy is called the Coulomb barrier [3].

Three main variables must be kept in mind to achieve fusion in a laboratory: very high temperature (to provoke high-energy collisions); the plasma particle density (to increase the likelihood that collisions do occur); and the confinement time (to hold the plasma, which has a propensity to expand, within a defined volume) [4].

The modified Lawson criterion [5] defines the conditions needed for a fusion reaction to reach the ignition, that is, that the heating of the plasma by the products of the fusion reactions is sufficient to maintain the temperature of the plasma against all losses without external power input. The relationship to obtain the ignition is [3]:

$$n_3 \cdot T \cdot \tau_e \geq 10^{21} \frac{keV \cdot s}{m^3} \qquad (1)$$

Where n_e is the electron density, T is the plasma temperature and τ_e is the confinement time.

A previous milestone is called Breakeven and it occurs when the energy released by the fusion reaction equals the energy put in to heat the plasma. This state can be defined with a gain factor of one (Q = 1).

The reaction cross section σ is a measure of the probability of a reaction takes place. Moreover, the Coulomb barrier is smaller for isotopes of hydrogen since their nuclei contain only a single positive charge [3].

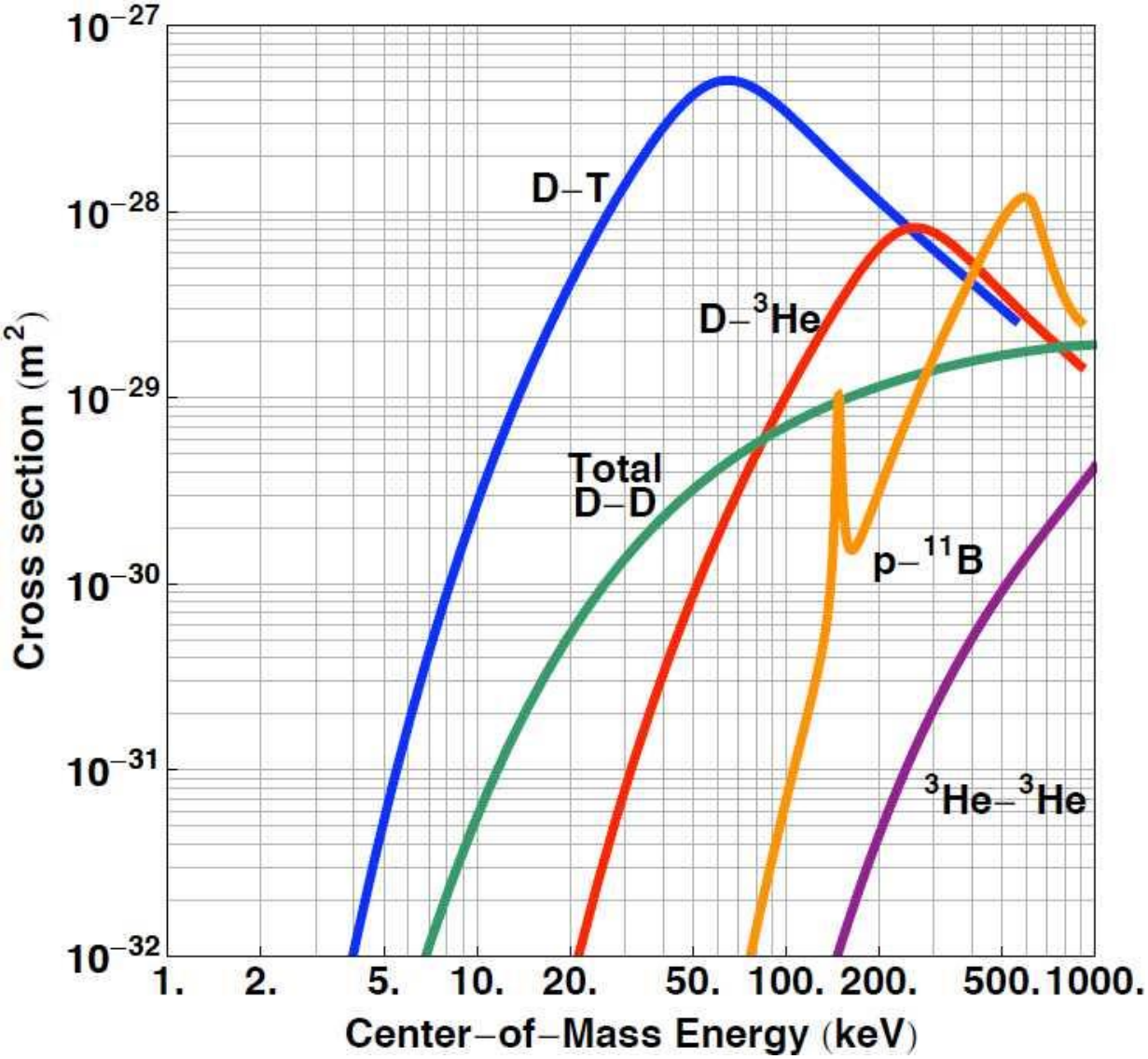

Figure 1: Cross section for different fusion reactions [3].

The previous graphic shows that the reaction D-T (Deuterium-Tritium) is the easiest to achieve. It needs a relatively low energy to reach the maximum probability to take place the fusion process [3].

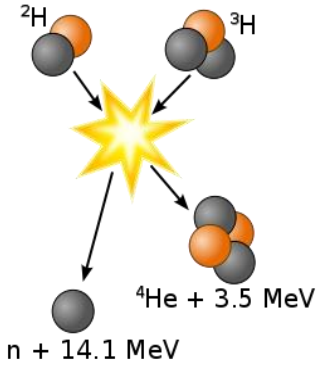

Figure 2: D-T fusion reaction [3].

As a result, the future fusion power reactors will use D-T because this reaction has been identified as the most efficient for fusion devices at low temperatures. Moreover, D can be found plentifully on Earth; on the other hand, T is extremely rare on nature because it is radioactive with 12.3 years half-life, but it can be created in another reaction using the neutrons produced in the fusion reaction after being moderated as noted the following expression [3]:

$$n + {}^{6}_{3}Li \rightarrow {}^{4}_{2}He + T$$

An important number of "fusion machines" have been gradually refined along the years. Multiple approaches have been proposed for producing fusion energy; however, inertial and magnetic confinement are the most important ways.

Inertial confinement fusion initiates nuclear fusion reactions by heating and compressing a fuel target which is usually as a pellet that contains the D-T mixture. Energy is distributed to the most external layer of the target by means of high-energy beams of laser light, electrons or ions. The heated outer layer evaporates producing a reaction force against the remainder of the target, accelerating it inwards and compressing the target. Thus, the density in the core increases and its temperature reaches the ignition point for fusion.

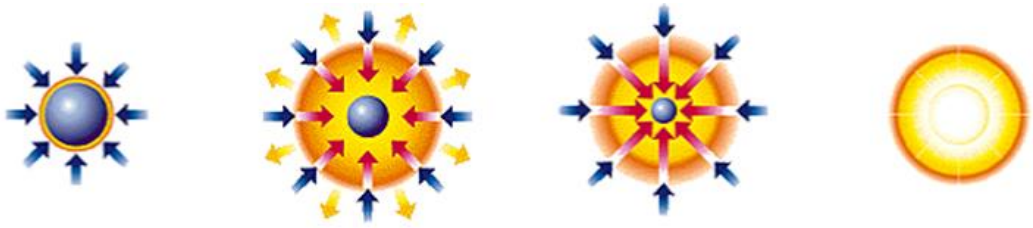

Figure 3: Inertial Confinement Process [6].

In magnetic confinement, since the plasma mainly consists of charged particles, ions and electrons, it is an excellent conductor. As a consequence, the plasma can be confined by means of high magnetic fields where the particles spiral along the corresponding magnetic field lines. The confinement times achieved using this method are higher than the obtained ones from inertial configuration facilities. Nowadays, the magnetic method is the most developed and two configurations can be used: the mirror confinement and the toroidal confinement. The second one is the most extended in which the magnetic field is formed by a toroidal component induced by external coils and a poloidal component that can be generated; on the one hand, by the plasma itself by inducing an external current with a central solenoid (transformer) and this approach is called Tokamak or; on the other hand, it can be generated by external coils receiving the name of Stellarator. In this thesis, the focus is on Tokamaks despite of the reactor works by pulses for the transformer operation as Faraday's law describes (It point out that an increasing of Bootstrap current could reduce this handicap).

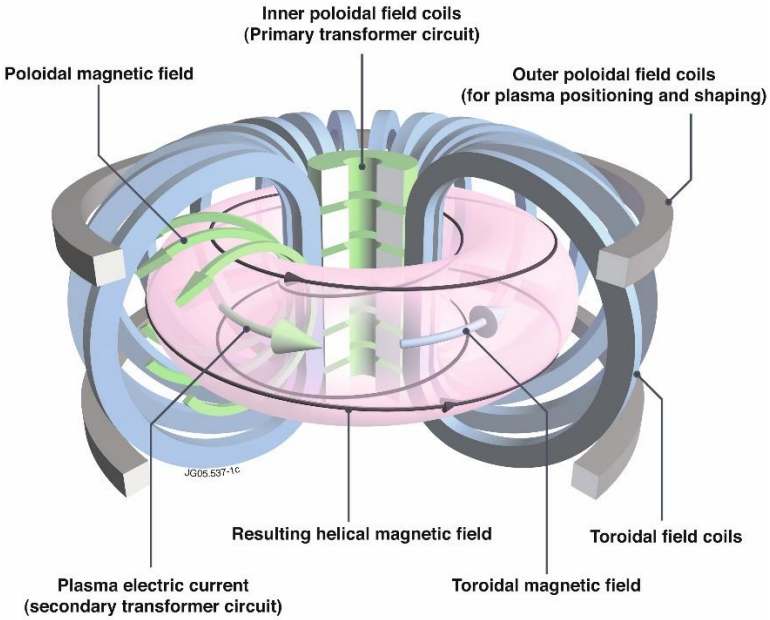

Figure 4: Tokamak Scheme [1].

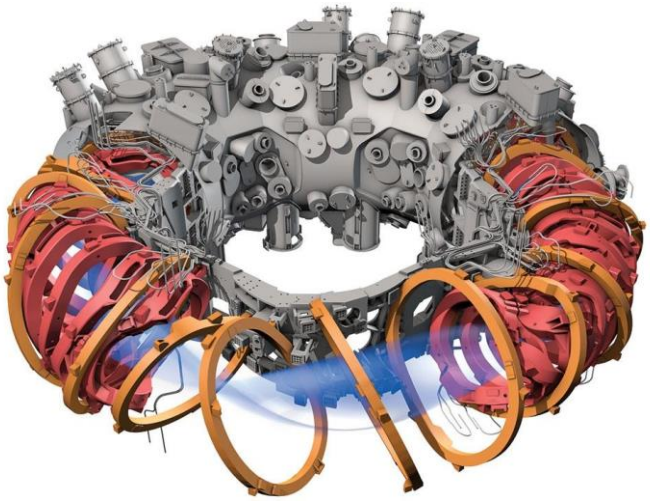

Figure 5: Stellarator Scheme [7].

As previously noted, the Tokamak has become the dominant concept in fusion research due to the achievement of temperature levels and plasma confinement times by means of these machines that had never been attained before 1968 [4]. Tokamak devices multiplied around the globe (more than 200 build) and they have contributed to progress toward fusion energy by means of the achievement of relevant milestones as the world record for fusion power produced in JET (16 MW in 1997), the long-duration plasma pulses record of 6.5 minutes proven by Tore Supra (in 2003) [4] or the achievement of the highest value of fusion triple product (1.53·1021 keV·s·m^{-3}) by Japanese JT-60 [8]. The next steps are called ITER and DEMO, and they will be explained in the following sections.

1.7 The ITER project

In June 1973 Richard Nixon and Leonid Brezhnev met in Washington agreed that cooperating in the field of fusion science was a promising way of easing tensions between their two countries (USA and URSS) [4]. On 23 November 1978, the "Steering Committee of the INTOR Workshop" convened in Vienna but

this project never reached the design phase, and was eventually folded into the next missions [4]. In the late 1970s, the major fusion programmes were run by national laboratories of certain European countries under contract of the EURATOM Treaty and by the governments of Japan, the Soviet Union and the USA [9]. In the mid-1980s, the idea of using a collaborative international project to develop fusion energy for peaceful purposes and to illustrate the east-west knowledge and economic cooperation began to take hold. At the Genova Superpower Summit (1985), Gorbachev, premier of the Soviet Union, proposed to US President Reagan an international project between Europe, Japan, the USA and the URSS which was agreed one year later known as ITER [4][9].

In 1988, conceptual design work gave the go-ahead and several engineering design phases were performed during the following decade until the final ITER design was set in 2001. In addition, The People's Republic of China and the Republic of Korea joined the Project in 2003 and India in 2005. The ITER Organization has also concluded non-Member technical cooperation agreements with Australia and Kazakhstan, as well as over 40 Cooperation Agreements with international organizations, national laboratories, universities and schools. [4].

Clarington (Canada), Rokkasho-Mura (Japan), Vandellós (Spain) and Cadarache (France) were the locations proposed to host ITER. On 28 June 2005, the ITER Members unanimously agreed on Cadarache site as the machine location and that the head of the project would be proposed by Japan. Further negotiations established the ITER Agreement to detail the construction, exploitation and decommissioning phases, as well as the financing, organization and staffing. The ITER Agreement was officially signed at the Elysée Palace in Paris on 21 November 2006 by Ministers from the seven ITER Members [4].

ITER will be the first fusion device to produce net energy, that means that ITER will generate more power than it consumes: for 50 MW of input power, 500 MW of output power will be produced. ITER will try to prove the viability of fusion as an energy source maintaining fusion for long periods of time and to collect the data necessary for the design and subsequent operation of the first electricity-producing fusion power plant.

Its construction began in 2014, the first plasma is expected to be produced in 2025 and the D-T operation will begin in 2035. The next table outlines the main parameters of the future ITER configuration.

ITER PARAMETERS	
Major radius (m)	6.2
Minor radius (m)	2
Toroidal magnetic field (T)	5.3
Plasma Current (MA)	15
Fusion power (MW)	400 - 700
Q	5 - 10

Table 1: ITER dimensions and main parameters.

ITER is not an end in itself: it is the bridge toward a first plant that will demonstrate the large-scale production of electrical power and tritium fuel self-sufficiency. DEMO is this following step. To achieve this in the shortest timescale, studies have shown that aside from the operation of ITER, a parallel program of materials testing would be needed. Development of these materials is the prime purpose of the IFMIF [3]. DEMO conceptual design is currently in progress and providing contributions to the safety analyses of this design is the framework of this document.

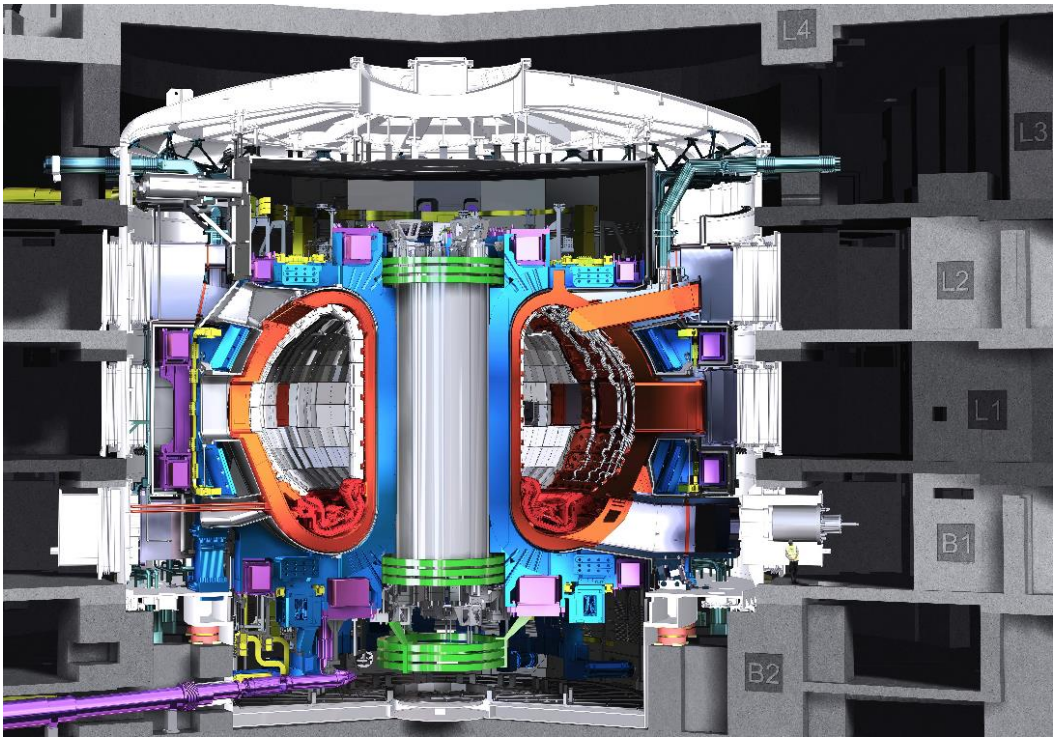

Figure 6: ITER Tokamak [4].

1.8 The DEMO project

The final technology integration consisting of the systems that convert neutron power to electrical power, superconducting magnets, Tritium treatment, Remote Handling and many other technological challenges must take place in a demonstration reactor, DEMO [3][10]. DEMO must become the first prototype of a commercial fusion reactor, the machine that will demonstrate the technological and scientific feasibility of fusion energy [4].

For the moment, different conceptual DEMO projects are under consideration by all ITER Members. For example and inasmuch this document is based on European developments, the European Union is working on four different designs: HCPB, DCLL, HCLL and WCLL concepts. It's too early to say whether DEMO will be an international collaboration, like ITER, or a series of national projects but the shared objective is building DEMO by 2050 [4].

The conceptual designs all sketch out a machine that is larger than ITER. The large radius of the plasma cross-section which determines the size of the machine ranges from 6 to 10 metres, ITER's one measures 6.2 metres and that of the largest tokamak in operation, JET, measures half that. The fusion power generated varies from 500 MW to 1500 MW. Finally, for some Members DEMO will be a pre-industrial demonstration reactor; but for others, it will be a quasi-prototype that requires no further experimental step before the construction of an industrial-scale fusion reactor [4].

China is planning a device called China Fusion Engineering Test Reactor (CFETR) that would bridge the gaps between ITER and DEMO. Its construction could start at around 2020 and be followed by construction of a DEMO in the 2030s [4].

India announced plans to build a device called SST-2 to develop components for a DEMO around 2027, and then start construction of a DEMO in 2037 [4].

South Korea initiated a conceptual design study for a K-DEMO in 2012 targeting the construction by 2037 with potential for electricity generation starting in 2050. In its first phase (2037-2050), K-DEMO will develop and test components and then utilize these components in the second phase after 2050 to demonstrate net electricity generation [4].

Russia plans the development of a fusion-fission hybrid facility called DEMO fusion neutron source (FNS), a reactor that would harvest the fusion-produced neutrons to turn uranium into nuclear fuel and destroy radioactive waste. The DEMO-FNS is planned to be built by 2023, and is part of Russia's fast-track strategy to a fusion power plant by 2050 [4].

The United States of America is considering an intermediate step called Fusion Nuclear Science Facility (FNSF) for the development and testing of fusion materials and components for a DEMO which woulb be built after 2050 [4].

The European Union (that is incumbent upon this document) and Japan are jointly building a powerful tokamak called JT-60SA in Naka, Japan, as a complement to ITER. In addition to constructing the JT-60SA, the International Fusion Materials Irradiation Facility (IFMIF/EVEDA) and the International Fusion Energy Research Centre (IFERC) is in progress as previous projects to a DEMO [4]. The next table outlines the main parameters of the future European DEMO configuration in spite of the permanent review and update [11][12][13].

DEMO PARAMETERS	
Major radius (m)	7.5 - 9.02
Minor radius (m)	2.6 – 2.927
Toroidal magnetic field (T)	5 – 5.667
Plasma Current (MA)	19.6 – 21.6
Fusion power (MW)	400 - 3255
Q	24.33 – 39.86

Table 2: DEMO dimensions and main parameters.

In spite of the presence of all these plans, what seems certain is that the return on experience from ITER operation and the rest of the devices planned will determine the final choices made for DEMO [4]. One of the most relevant criteria to keep in mind for the future DEMO reactor is the safety and this thesis is a contribution to this purpose.

2 AINA 4.0

2.1 Review of the historical AINA versions

2.1.1 Introduction

A conclusion that can be drawn from the historical safety analyses developed for tokamaks fusion reactors is that some of the major risks involve incidents in the vacuum vessel. As noted in previous section, in order to evaluate plasma evolution and in vessel components strains, a safety code called AINA (acronym of Analyses of IN-vessel Accidents) has been developing by the Fusion Energy Engineering Laboratory (FEEL) of the Technical University of Catalonia (UPC) Barcelona-Tech, during the last ten years for different fusion reactors designs as ITER [14][15][16][17][18] and the Japanese DEMO design WCPB [19].

An in-depth critical analysis of the former AINA versions, a new codification and a checking and validation phase have been performed in order to develop a proper, reliable, versatile and flexible tool with the purpose of carrying out safety analyses for the four European DEMO designs (HCPB, DCLL, HCLL and WCLL).

2.1.2 Fusion simulation codes

As previously noted, AINA is a computer code. Computer codes together with the empirical experimentation have been the most important tools applied for the safety analyses of the fusion facilities during the design stages of ITER and DEMO. For this reason, it was necessary a prior research to know the most used codes to perform accident analyses for fusion reactors, in particular for DEMO. The code list and a brief explanation about each one of them is introduced hereunder:

- **MELCOR**: is a fully integrated, engineering-level computer code developed by Sandia National Laboratories for the U.S. Nuclear Regulatory Commission (NRC) to model the progression of severe accidents in nuclear power plants [20]. Because of its capability of thermal-hydraulic response in the primary reactor coolant system, the confinement buildings, the containment, hydrogen production, radionuclide and aerosol transport in nuclear facilities and reactor cooling systems, and predicting structural temperatures (e.g. first wall, blanket, divertor, and vacuum vessel) resulting from energy produced by radioactive decay heat and/or chemical reactions (oxidation), MELCOR was selected to make fusion specific modifications to MELCOR 1.8.2 released in 1992 for fusion safety analyses [21]. The last version of the code, MELCOR 1.8.6 [22] has been applied in the case of a BB module LOCA for the European DEMO configuration accident analyses [23] [24]. In addition, an ex-vessel LOCA in two proposed PHTS (Primary Heat Transfer System) concepts with helium cooling for DEMO HCPB concept was performed with a previous version of the code [25].
- **RELAP5-3D**: is an outgrowth of the one-dimensional RELAP5/MOD3 code developed at the Idaho National Laboratory (INL) for the NRC. The most prominent attribute that distinguishes the RELAP5-3D code from the previous versions is the fully integrated, multi-dimensional thermal-hydraulic and kinetic modelling capability. This removes any restrictions on the applicability of the code to the full range of postulated reactor accidents. Enhancements include a new matrix solver for 3D problems, new thermodynamic properties for water, and improved time advancement for greater robustness [26]. Transient system analysis on the FW of DEMO HCPB

has been carried out for accident scenarios LOFA (Loss Of Flow Accident) and LOCA using RELAP5-3D [27].

- **SIMMER**: is a versatile and flexible tool, applicable for the safety analysis of various reactor types with different neutron spectra and coolants. The code has originally been developed for the severe accident simulation of sodium cooled fast reactors and now is applied also in fusion safety studies [28]. The code used recently in nuclear fusion application is SIMMER-III which consists of three elements: the fluid-dynamics model, the structure model, and the neutronics model [26]. Nowadays, SIMMER-III has just started to be used for DEMO designs [29].
- **PROCESS**: is a reactor systems code that assesses the engineering and economic viability of a hypothetical fusion power station using simple models of all parts of a reactor system, from the basic plasma physics to the generation of electricity [30]. Thus, PROCESS is not really a safety code even though new algorithms towards this aim has been inserted [31]. Its main use is focused on the generation of the operation steady states of DEMO which are the starting point of the safety analyses.
- **ANSYS**: is a comprehensive finite element analysis tool for structural analysis, including linear, nonlinear and dynamic studies. The engineering simulation product provides a complete set of elements behavior, material models and equation solvers for a wide range of mechanical design problems. In addition, ANSYS Mechanical offers thermal analysis and coupled-physics capabilities involving acoustic, piezoelectric, thermal–structural, thermo-electric, and magnetostatic analysis [32]. Structural analysis using ANSYS Mechanical has been performed for DEMO HCPB blanket modules [33] where integrity of FW and caps have been evaluated for a level D condition, which corresponds to an accident scenario. Thermal analysis using ANSYS Mechanical has been performed for DEMO HCPB blanket modules as well [34]. An ex-vessel LOCA analysis with a soft plasma shutdown was done to assess a new cooling scheme with redundancy.
- **AINA**: Up to this project, AINA 3.1 was the last version of the code. It was a proper tool in order to perform a safety analysis for the DEMO WCPB configuration (Japanese concept) [19]. It is important to note that AINA's comparative advantage against the rest of the codes lies in the possibility of simulating the plasma physics and the blanket thermal evolution at the same time and in a short processing time based on simplified and previously validated models.

Furthermore, several codes employed for the ITER design and safety assessment are, at present, on-going phase of modification and improvement to be adapted to the requirements of DEMO scope. These codes are: UFOTRI, GASFLOW, CONSEN, ECOSIMPRO and ASTEC [26]. On the other hand, some codes would be interesting and useful, provided that they suffer the necessary adjustment to be proper for fusion reactor simulations. Such software are: RODOS, WINMACS, STAR-CD/STAR CCM+, ATHLET, TRACE, APROS, ECART, BEST-EST and COCSYS [26]. Finally, it is recommended to keep in mind MEMOS [35] and TOKES [36]; two codes that would be useful to understand, validate and complete the plasma wall interaction model of any other code as AINA.

The next table lists the mentioned simulation codes versus physical phenomena occurring in main DEMO accident analyses:

Code	Thermal-hydraulic	Heat transfer	Plasma transient	Containment	Tritium transport	Tritium permeation	Liquid metal	Chemical reactions (Be, W)	Chemical reactions (LiPb)	Dust mobilization/ release
MELCOR	a	a	-	a	a	-	-	a	-	a
RELAP5-3D	a	a	-	a	-	-	a	-	-	-
UFOTRI & COSYMA	-	-	-	-	-	a	-	-	-	-
RODOS	-	-	-	-	-	-	-	-	a	-
CROM	-	-	-	-	-	-	-	-	a	-
WINMACCS	-	-	-	-	-	-	-	-	a	-
ANSYS Mechanical	-	a	a	-	-	-	-	-	-	-
ANSYS CFX	a	a	-	-	-	-	b	b	-	-
STAR-CD & STAR-CCM+	a	a	-	-	-	-	b	b	-	-
ATHLET&ATHLET-CD	a	a	-	a	-	-	-	-	-	b
TRACE	a	a	-	a	-	-	-	b	-	-
ASTEC	a	a	-	a	a	-	-	a	-	b
CONSEN	a	a	-	a	c	-	-	a	-	-
SIMMER	a	a	-	-	-	-	a	-	-	-
GASFLOW	-	a	-	a	c	-	-	-	-	a
ECOSIMPRO	a	a	-	a	a	a	-	-	-	-
ECART	a	a	-	a	c	-	-	a	-	a
APROS	a	a	-	a	-	-	-	-	-	-
BEST-EST	-	-	-	-	-	-	-	-	-	-
COCOSYS	a	a	-	a	-	-	-	-	-	-
AINA	a	a	a	-	-	-	-	-	-	-

Table 3: Simulation codes versus physical phenomena occurring in main DEMO accident analyses (a – implicit model; b – explicit model; c – adapted model) [26].

2.1.3 AINA 3.0 review

During the first phase of this project, the FEEL research group checked all the models of AINA safety code, specifically the ITER version called AINA 3.0 [14][15][16][17][18] and performed an in-depth critical analysis of the architecture and the functioning of thereof. The original plan was to make the most of the previous work and to minimize the effort to adapt AINA for European DEMO design. AINA 3.0 is the result of the implementation of several improvements to adapt AINA 2.0 to the last design of ITER; AINA 2.0, in turn, is the evolution of a primordial Japanese code called SAFALY.

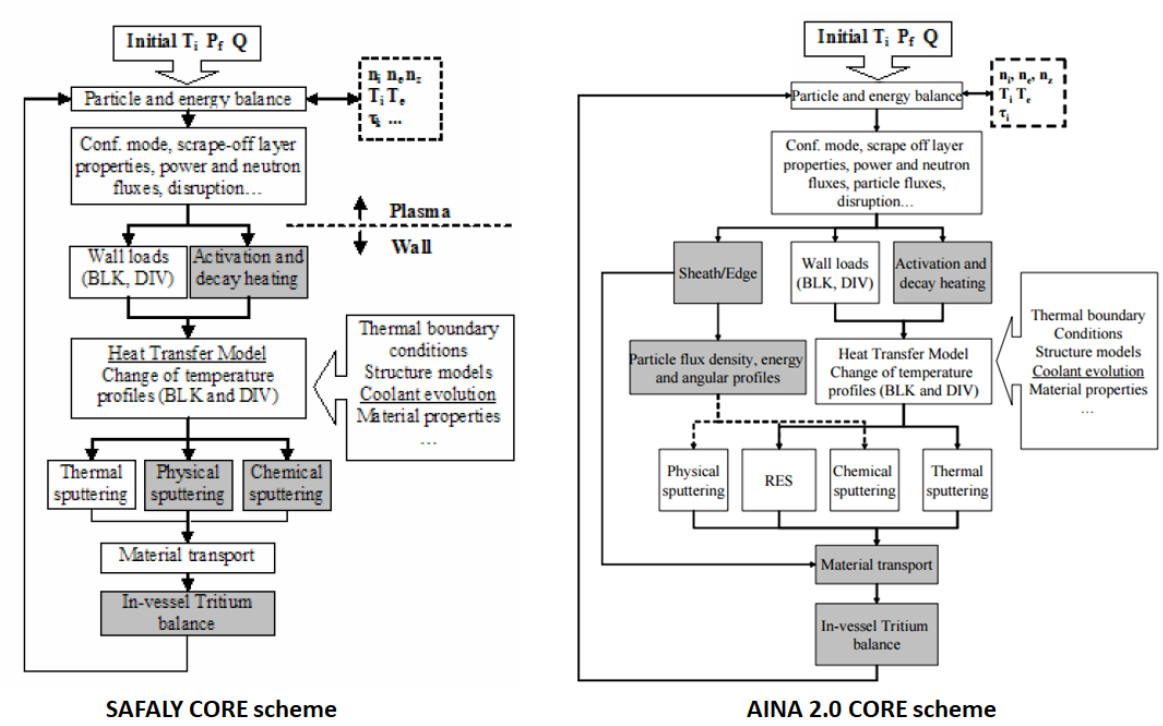

Figure 7: AINA evolution progress.

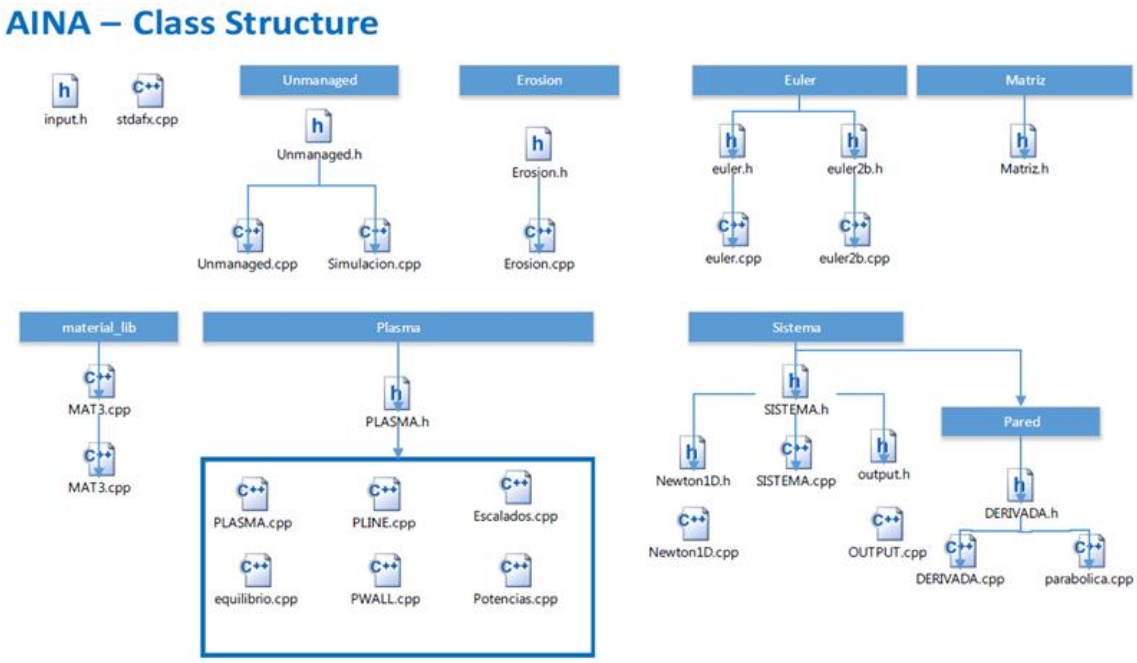

Figure 8: AINA 3.0 class architecture.

This process consisted of tracking line by line of all the code (more than 15.000 lines of code of C++) with the aim of understanding each of them. The following figures show two of the tool-documents used to carry out this arduous task.

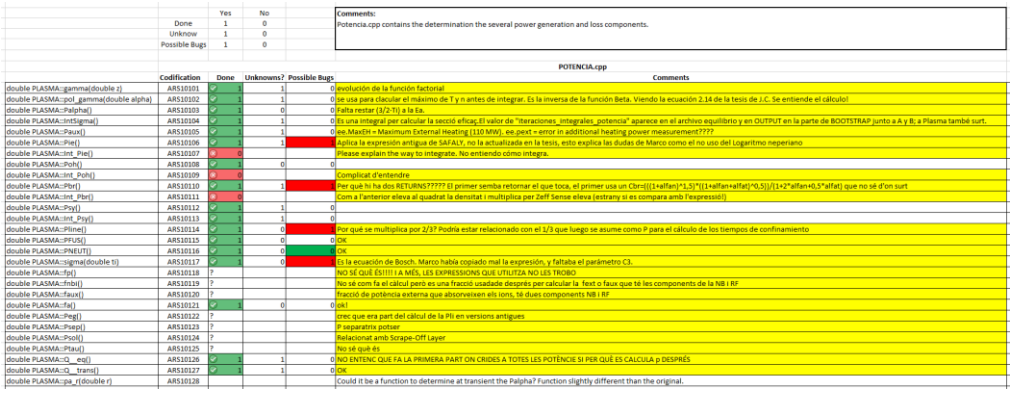

	Yes	No
Done	1	0
Unknow	1	0
Possible Bugs	1	0

Comments:
Potencia.cpp contains the determination the several power generation and loss components.

POTENCIA.cpp

Codification	Done	Unknowns?	Possible Bugs	Comments
double PLASMA::gamma(double z)	AR510101	✓ 1	1	0 evolución de la función factorial
double PLASMA::pol_gamma(double alpha)	AR510102	✓ 1	1	0 se usa para calcular el máximo de T y n antes de integrar. Es la inversa de la función Beta. Viendo la ecuación 2.14 de la tesis de J.C. Se entiende el cálculo!
double PLASMA::Palpha()	AR510103	✓ 1	0	0 Falta restar (3/2·Ti) a la Ea.
double PLASMA::IntSigma()	AR510104	✓ 1	1	0 Es una integral per calcular la secció eficaç.El valor de "iteraciones_integrales_potencia" aparece en el archivo equilibrio y en OUTPUT en la parte de BOOTSTRAP junto a A y B; a Plasma també surt.
double PLASMA::Paux()	AR510105	✓ 1	1	0 ee.MaxEH = Maximum External Heating (110 MW). ee.pext = error in additional heating power measurement????
double PLASMA::Pie()	AR510106	✓ 1	1	Aplica la expresión antigua de SAFALY, no la actualizada en la tesis, esto explica las dudas de Marco como el no uso del Logaritmo neperiano
double PLASMA::Int_Pie()	AR510107	✗ 0		Please explain the way to integrate. No entiendo cómo integra.
double PLASMA::Poh()	AR510108	✓ 1	0	0
double PLASMA::Int_Poh()	AR510109	✗ 0		Complicat d'entendre
double PLASMA::Pbr()	AR510110	✓ 1	1	Per què hi ha dos RETURNS????? El primer semba retornar el que toca, el primer usa un Cbr=(((1+alfan)^1,5)*((1+alfan+alfat)^0,5))/(1+2*alfan+0,5*alfat) que no sé d'on surt
double PLASMA::Int_Pbr()	AR510111	✗ 0		Com a l'anterior eleva al quadrat la densitat i multiplica per 2eff Sense eleva (estranyi si es compara amb l'expressió!)
double PLASMA::Psy()	AR510112	✓ 1	1	0
double PLASMA::Int_Psy()	AR510113	✓ 1	1	0
double PLASMA::Pline()	AR510114	✓ 1	0	Per què se multiplica por 2/3? Podria estar relacionado con el 1/3 que luego se asume como P para el cálculo de los tiempos de confinamiento
double PLASMA::PFUS()	AR510115	✓ 1	0	0 OK
double PLASMA::PNEUTS()	AR510116	✓ 1	0	0 OK
double PLASMA::sigma(double ti)	AR510117	✓ 1	0	Es la ecuación de Bosch. Marco había copiado mal la expresión, y faltaba el parámetro C3.
double PLASMA::fpi()	AR510118	?		NO SÉ QUÉ ÉS!!!! I A MÉS, LES EXPRESSIONS QUE UTILITZA NO LES TROBO
double PLASMA::fnbi()	AR510119	?		No sé com fa el càlcul però es una fracció usadade després per calcular la fext o faux que té les components de la NB i RF
double PLASMA::faux()	AR510120	?		fracció de potència externa que absorveixen els ions, té dues components NB i RF
double PLASMA::fal()	AR510121	✓ 1	0	0 ok!
double PLASMA::Peg()	AR510122	?		crec que era part del càlcul de la Pli en versions antigues
double PLASMA::Psep()	AR510123	?		P separatrix potser
double PLASMA::Psol()	AR510124	?		Relacionat amb Scrape-Off Layer
double PLASMA::Ptau()	AR510125	?		No sé què és
double PLASMA::Q__eq()	AR510126	✓ 1	1	0 NO ENTENC QUE FA LA PRIMERA PART ON CRIDES A TOTES LES POTÈNCIE SI PER QUÈ ES CALCULA p DESPRÉS
double PLASMA::Q__trans()	AR510127	✓ 1	1	0 OK
double PLASMA::pa_r(double r)	AR510128			Could it be a function to determine at transient the Palpha? Function slightly different than the original.

Figure 9: Document to carry out a preliminary analysis of all the functions present inside the AINA 3.0 code. This example summarizes some functions of the Potencias.cpp file.

	Duda o error	Fichero	Codificación	Comentario	Respuesta posible
1		PLASMA.cpp	1PLASMA.cpp	Cuando calculamos la tau un con la función tau_pa() [línea 12 de Escalados.cpp] ya estamos multiplicando ee.Alpha_Elec_Conf, que es la constante para el cálculo de la tau para las alfas, por lo que no se debería volver a multiplicar. n_alfa=1/4*(ni^2)*sigma*C_alfa*tau (línea 110 o línea 63 en AINA 3.0)	
2		Potencias.cpp	2Potencias.cpp	La función fnbi() calcula la fracción de potencia externa de NB que afecta a los iones pero no se de donde salen las expresiones (líneas 407-409)	Línea 45, 125 y 128 del fichero PLINIT.f de SAFALY original!!!!
3		Potencias.cpp	3Potencias.cpp	En la función Palpha() parece que falta la componente: -3Ti/2 y (1-fripple) para que fuera la Ec. 2.28 de la tesis de J.C.	Podrían ser componentes despreciables.
4		Potencias.cpp	4Potencias.cpp	En la línea 347 para el cálculo de Pline, ¿por que multiplicamos por 2/3?	Creo que el comentario del input FRPU del ejecutable (Ratio of line radiation from main plasma to edge plasma (in case of Ar as impurity, the ratio is 1/3)) que nos da la respuesta ya que después para el cálculo de la Pline multiplica por 0,5 que es el valor de esta variable.
5		Potencias.cpp	5Potencias.cpp	En las líneas 174 y 181 falta el factor Co= de la expresión Ec. 4.11 del documento "Estudios de seguridad deterministas de ITER. Contribución al desarrollo del código SAFALY". No es la expresión que parece en la tesis de J.C.	
6		Potencias.cpp	6Potencias.cpp	Pbr() tiene dos "returns".	Lo que viene tras el primer "return" no se ejecuta y debe ser la manera como se calculaba en una versión anterior del código. En AINA 3.0 solo tiene un return!
7		Potencias.cpp	7Potencias.cpp	No llama a Int_Psy. No hace falta multiplicar por el volumen porque la expresión (Ec. 2,34 de la tesis de J.C) usada ya te lo da en MW. Hay varios "returns". Rw un input que ocupa el slot f48 no aparece en el ejecutable de AINA. A la beta toroidal se le da un valor de 2 en la línea 250 de manera directa para el cálculo.	No llama a Int_Psy porque creo que esta expresión, justamente con el componente (1-Rw)^0.5, ya tiene en cuenta el perfilado. Tras el primer "return" deben venir modelos antiguos. En AINA 3.0 solo hay un modelo para Psy.
8		Potencias.cpp	8Potencias.cpp	En el cálculo de Pie() usa la Ec. 10 del documento "Development of Time Dependent Safety Analysis Code for Plasma Anomaly Events in Fusion Reactors" de Honda. No es la que sale en la tesis de J.C; la de J.C difiere en un factor 0.5 y un logaritmo de Coulomb.	Si en la Ec 2.27 de la tesis de J.C. Asume un logaritmod e Coulomb de 20, te queda la Ec. 10 de Honda usada!
9		Potencias.cpp	9Potencias.cpp	En el cálculo de Pie() se acaba llamando a Int_Pie() con la llamada 'p^q'. No entiendo el cálculo de Int_Pie().	
10		equilibrio.cpp	10equilibrio.cpp	La 1ª vez que calculamos la ptau en la línea 65; la Pline no está dividida entre 3 como indica la Ec 2.43 de la tesis de J.C. En los futuros cálculos de la ptau ya si que cumple la expresión y se divide entre 3. Esto supone que si obtenemos un punto de equilibrio se habrá hecho usando esta ptau que sirve para calcular la tau que no es del todo correcta.	Al ser esta Ptau más grande (ya que no divididmo Pline entre 3) al calcular la tau tanto en las expresiones de modo H y L nos da una tau peor porque la componente ptau está dividiendo; por lo que podemos asumir que estamos siendo conservadores.
11		Simulacion.cpp	11Simulacion.cpp	En la línea 570 damos un nuevo valor a la variable cotaeeror pero no la usamos.	Creo que era el valor que tomaba la condición que te permite salir del for (línea 604) en caso de llegar al equilibrio ya que en inicializar la variable cotaerror se le daba valor 1e-12 (línea 566) pero al final no se usó.
12		Escalados.cpp	12Escalados.cpp	En la línea 177 estamos mirando el límite que dicta: Palfa+Paux+Poh-Pbr-Psyn-Plic<0. Pero al ptau.p usada que viene de de la línea 208 de PLASMA.cpp que viene a su vez de 100 de equilibrio.cpp; tiene la componente Pline dividida entre 3.	Como al tener Pline dividida entre 3 y es una componente que resta, como más pequeña sea, más conservadores seremos.
13		OUTPUT.cpp	13OUTPUT.cpp	Las funciones BetaT(), BetaP(),BetaTH(),BetaFt(),BetaNB(),BetaTotal(),B_poloidal no se de dónde salen las expresiones. No están referenciadas.	En AINA 3.0 no aparecen ,BetaTH(),BetaFt(),BetaNB(),BetaTotal(),B_poloidal
14		OUTPUT.cpp	14OUTPUT.cpp	Las funciones BetaT(), BetaP(); calcula la beta toroidal y poloidal con la misma expresión ahora que no se ejecuta la segunda parte de BetaT() tras un "return" y no tiene sentido.	En AINA 3.0 la BETAT() es distinta!
15		Escalados.cpp	15Escalados.cpp	En la función transicion() usa las expresiones de la Ec 3.14 del "AINA SAFETY CODE" de Dapena para el cálculo de las Pthr pero no son las que pone en sus tesis J.C. en la Ec. 2.42!!!	Tal y como explico en el error siguiente, al final no se usan.
16		Escalados.cpp	16Escalados.cpp	En la función transicion() no cuentan los cálculos hechos entre las líneas 118-124 (la duda anterior hace referencia a estos cálculos) y calculamos la Pthr usando SOLAMENTE la Pthr1 de la Ec. 2,42 de la tesis de J.C. Pero sin la componente (Ma^-1).	Como siempre se toma el valor mínimo de todos los Pthrs; quizás este suele ser el menor habitualmente pero no me convence.

Figure 10: Document to collect possible doubts about the code and explanations.

The following are examples of the tracking line by line carried out during this first stage:

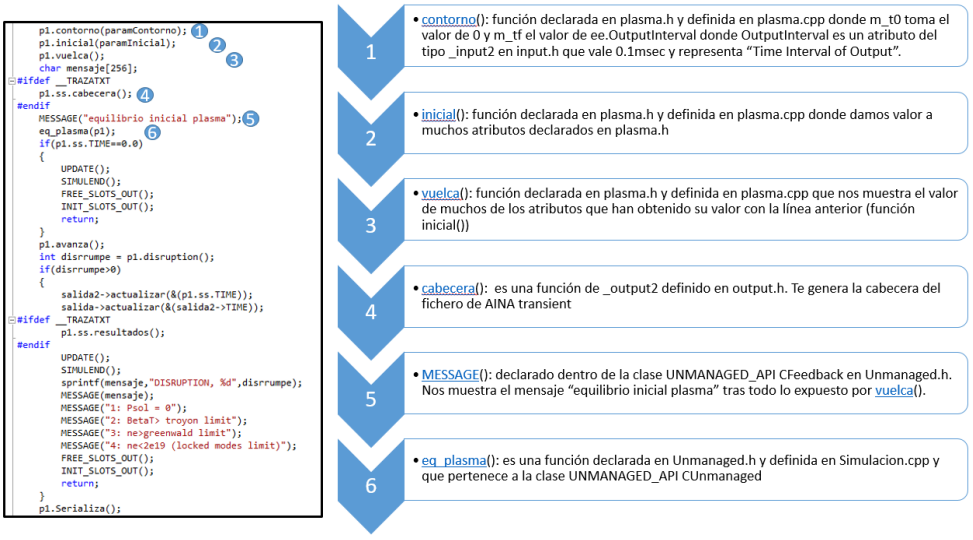

```
    p1.contorno(paramContorno); 1
    p1.inicial(paramInicial);   2
    p1.vuelca();                3
    char mensaje[256];
#ifdef __TRAZATXT
    p1.ss.cabecera(); 4
#endif
    MESSAGE("equilibrio inicial plasma");5
    eq_plasma(p1);  6
    if(p1.ss.TIME==0.0)
    {
        UPDATE();
        SIMULEND();
        FREE_SLOTS_OUT();
        INIT_SLOTS_OUT();
        return;
    }
    p1.avanza();
    int disrrumpe = p1.disruption();
    if(disrrumpe>0)
    {
        salida2->actualizar(&(p1.ss.TIME));
        salida->actualizar(&(salida2->TIME));
#ifdef __TRAZATXT
        p1.ss.resultados();
#endif
        UPDATE();
        SIMULEND();
        sprintf(mensaje,"DISRUPTION, %d",disrrumpe);
        MESSAGE(mensaje);
        MESSAGE("1: Psol = 0");
        MESSAGE("2: BetaT> troyon limit");
        MESSAGE("3: ne>greenwald limit");
        MESSAGE("4: ne<2e19 (locked modes limit)");
        FREE_SLOTS_OUT();
        INIT_SLOTS_OUT();
        return;
    }
    p1.Serializa();
```

1. contorno(): función declarada en plasma.h y definida en plasma.cpp donde m_t0 toma el valor de 0 y m_tf el valor de ee.OutputInterval donde OutputInterval es un atributo del tipo _input2 en input.h que vale 0.1msec y representa "Time Interval of Output".
2. inicial(): función declarada en plasma.h y definida en plasma.cpp donde damos valor a muchos atributos declarados en plasma.h
3. vuelca(): función declarada en plasma.h y definida en plasma.cpp que nos muestra el valor de muchos de los atributos que han obtenido su valor con la línea anterior (función inicial())
4. cabecera(): es una función de _output2 definido en output.h. Te genera la cabecera del fichero de AINA transient
5. MESSAGE(): declarado dentro de la clase UNMANAGED_API CFeedback en Unmanaged.h. Nos muestra el mensaje "equilibrio inicial plasma" tras todo lo expuesto por vuelca().
6. eq_plasma(): es una función declarada en Unmanaged.h y definida en Simulacion.cpp y que pertenece a la clase UNMANAGED_API CUnmanaged

Figure 11: Tracking of the first lines of the AINA 2.0 main file.

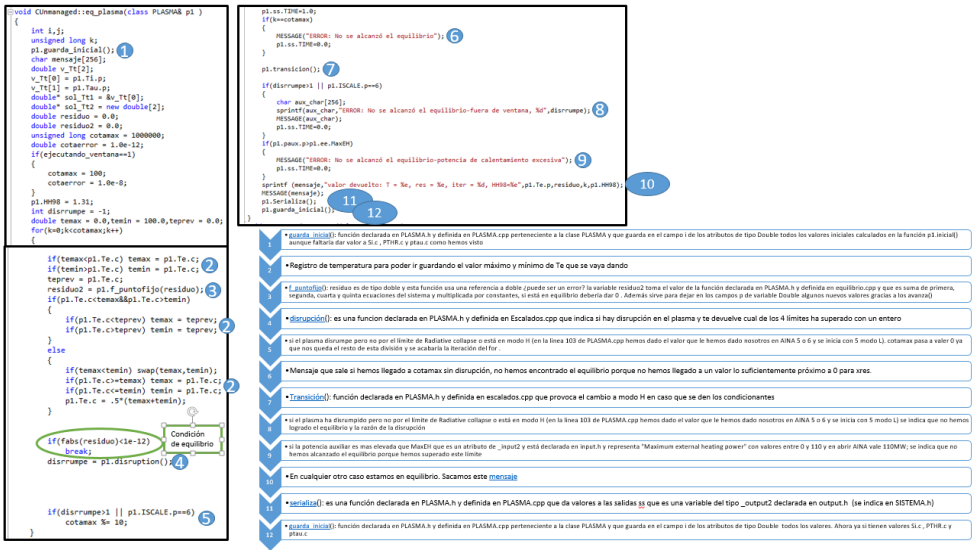

Figure 12: Tracking of the eq_plasma function.

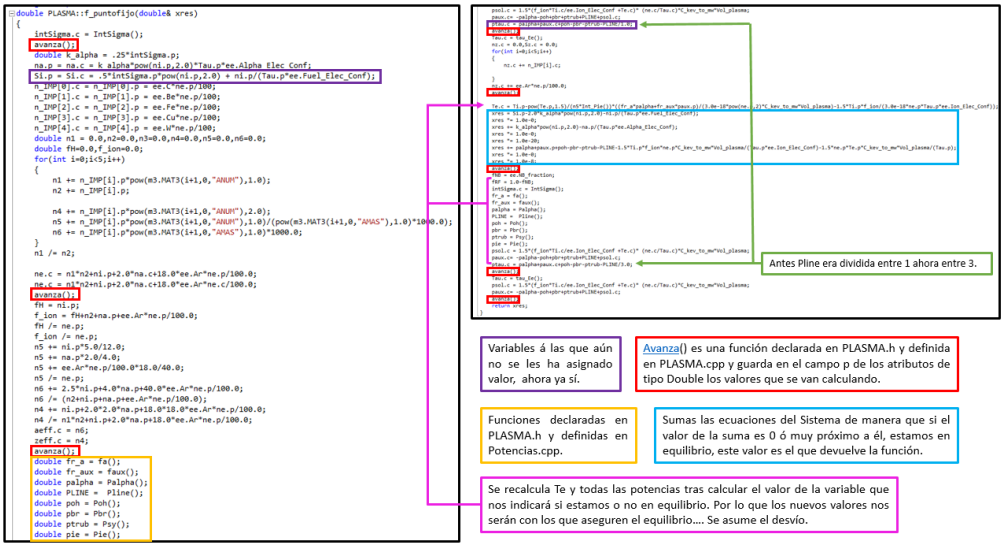

Figure 13: Tracking of the f_puntofijo function.

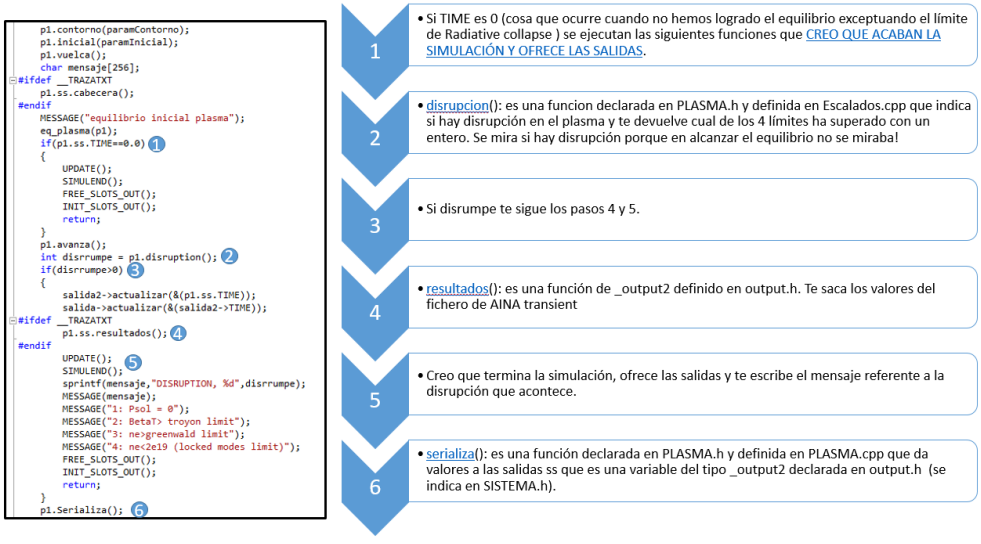

Figure 14: Tracking of first lines of the AINA 2.0 main file (second part).

This effort leaded to detect several deficiencies that should be deal with before the implementation of a new AINA version for the European DEMO safety studies:

- More than 15.000 lines of code of C++ without any comment, which makes it very difficult to modify or understand the code altogether.
- The last version of the AINA 3.0 code (built by the previous AINA development team) is not compilable. For this reason, it is likely that the last version of the executable file does not correspond to the available code version.
- AINA 3.0 does not execute parts of the code while it is running but there is no mention of it (either within the code or throughout the manual).
- There are some substantial inconsistencies between models presented throughout the manual and the final models executed by AINA 3.0. Moreover, it is possible to find inaccurate references or incompletes.
- There are errors in some equations implemented.
- Some numerical methods can be considered as suboptimal, for example, the use of a summation to estimate the Steady State values instead of the Newton method application.
- The use of some factors or strategies that they are not specified throughout the manual.
- It is not possible to modify the nodalization of the thermal model and its final selection is not justified. Therefore, it is not possible to ensure maximum precision during the transients.
- Some models are too hermetic and it is very hard to modify them without altering the global code perspective. In addition, there is a suspicion that the executable file only works properly in anticipated ranges.
- The last version of the executable file shows incoherent results for the temperature of the Blanket and divertor regions and some wrong units of measurement.

Due to these defects and the low level of flexibility, friendliness and reliability detected in AINA 3.0; it was concluded to develop a totally new AINA version for the four European designs of DEMO. AINA 3.0 was not a universal software to be used for a wide range of designs and scenarios. This decision ensured the implementation of the currently most recognized numerical models and the most recent design versions and the creation of a more friendliness tool to be modified and updated.

2.2 Numerical models

2.2.1 Introduction

AINA is a code comprised of a 0D plasma dynamics approach based on a mass and energy balance and a 1D thermal model for the blanket (in the radial direction), specifically for the HCPB configuration, and the divertor. These two blocks feed-back constantly each other by means of the plasma-wall block which estimates the real loads suffered by the in vessel components and the real impurity presence into the plasma core. With this basic concept, AINA is useful to check the integrity of these in-vessel components both when a plasma perturbation induces a Loss Of Plasma Control (LOPC) and a thermo-hydraulic accident takes place in the Plasma Facing Components (PFCs) or in the Vacuum Vessel such as a Loos Of Coolant Accident (LOCA). This chapter describes the new AINA code, specifically the models and the numerical procedures implemented in each block.

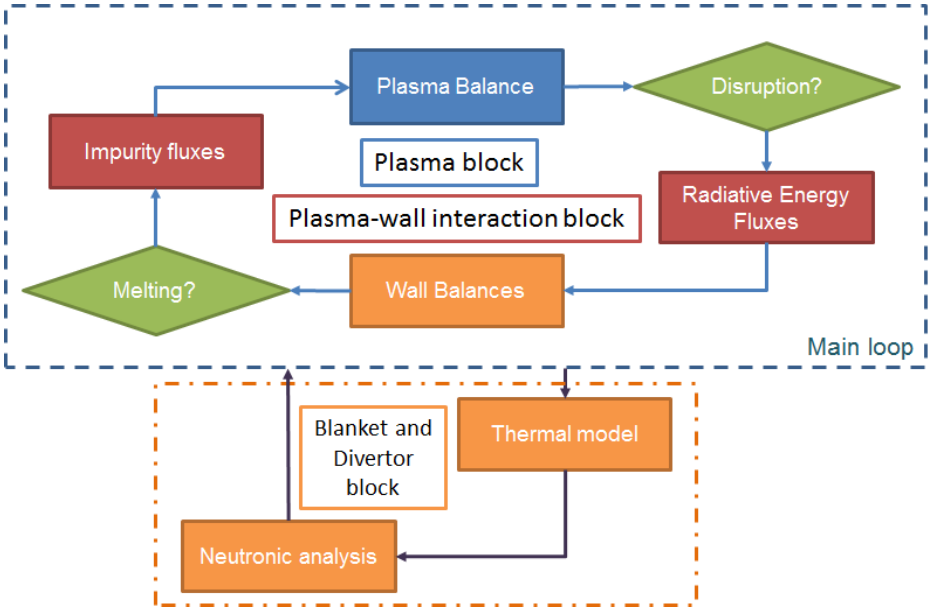

Figure 15: AINA scheme.

2.2.2 Plasma block

This chapter introduces the background of the plasma block on AINA 4.0 and describes the different models that have been implemented in it.

2.2.2.1 Basic Plasma block model

As stated before, the code considers a 0D multi-fluid approach based on the mass and energy balance of the plasma core according to the equations showed below. Particle conservation is considered for fuel ions (n_H) alpha particles (n_α) and every type of impurity (n_{ZXe} and n_{ZW} which are referred to Xenon and Tungsten). On the other hand, the energy conservation expressions considered treat ions and electrons separately. It is important to highlight that all the terms are calculated through volume and radial profiles of plasma density and temperature using the same models as AINA 3.0 [16].

$$\frac{dn_H}{dt} = S_H - 2S_\alpha - \frac{n_H}{\tau_{p,H}}$$

$$\frac{dn_\alpha}{dt} = S_\alpha - \frac{n_\alpha}{\tau_{p,\alpha}}$$

$$\frac{dn_{ZXe}}{dt} = S_{ZXe} - \frac{n_{ZXe}}{\tau_{p,Z}}$$

$$\frac{dn_{ZW}}{dt} = S_{ZW} - \frac{n_{ZW}}{\tau_{p,Z}}$$

$$\frac{3}{2}\frac{d(n_iT_i)}{dt} = f_{ext}P_{ext} + f_\alpha P_\alpha - P_{ie} - \frac{3}{2}\frac{n_iT_i}{\tau_{E,i}}$$

$$\frac{3}{2}\frac{d(n_eT_e)}{dt} = (1-f_{ext})P_{ext} + (1-f_\alpha)P_\alpha + P_{ie} + P_{Ohm} - P_{Br} - P_{sy} - P_{li} - \frac{3}{2}\frac{n_eT_e}{\tau_{E,e}}$$

$$n_e = n_i + 2n_\alpha + \sum_{j=1}^{\infty}(Z_j \cdot n_{Zj}) \quad (3)$$

AINA 4.0 determines a SS (steady state) scenario of the plasma using an average ion temperature and specified power fusion as inputs and solving the system by the Newton method. The initial condition for the first iteration considers an external power (P_{ext}) of 50 MW and the alpha source and ion density estimation as the next expressions show:

$$S_\alpha = \frac{P_{fus}}{E_{fus}} \quad (4)$$

where $E_{fus} = 17.62\ MeV$

$$n_H = \sqrt{\frac{4S_\alpha}{\langle\sigma v\rangle_{DT} \cdot V}} \quad (5)$$

where $\langle\sigma v\rangle_{DT}$ is the velocity averaged cross-section of the deuterium-tritium nuclear fusion reaction.

In this way, S_H (fuelling rate), n_α, n_{ZXe}, n_{ZW}, T_e and P_{ext} will be the unknowns values for the SS resolution. When the SS parameters are calculated, the time evolution of the plasma is estimated by the Euler method.

It is important to point out that the terms of the balance equations are calculated through volume integrals and radial profiles of plasma density and temperature following the AINA 3.0 expressions [37].

2.2.2.2 Cross-section of the Deuterium-Tritium Nuclear Fusion Reaction Model

The velocity averaged cross-section of the deuterium-tritium nuclear fusion reaction is calculated with the Bosch-Hale expression [38]:

$$\langle\sigma v\rangle_{DT} = 10^{-6} \cdot C1 \cdot \theta \cdot e^{-3\xi} \cdot \sqrt{\frac{\xi}{m_r c^2 \cdot T_i^3}} \quad (6)$$

where:

$$\theta = \frac{T_i}{1 - \frac{T_i(C2 + T_i(C4 + T_i C6))}{1 + T_i(C3 + T_i(C5 + T_i C7))}}$$

$$\xi = \left(\frac{B_G^2}{4\theta}\right)^{1/3}$$

$$B_G = 34.3827$$

$$m_r c^2 = 1.124656 \cdot 10^6$$

$$C1 = 1.17302 \cdot 10^{-9}$$

$$C2 = 1.51361 \cdot 10^{-2}$$

$$C3 = 7.51886 \cdot 10^{-2}$$

$$C4 = 4.60643 \cdot 10^{-3}$$

$$C5 = 1.35 \cdot 10^{-2}$$

$$C6 = 1.06750 \cdot 10^{-4}$$

$$C7 = 1.366 \cdot 10^{-5} \qquad (7)$$

2.2.2.3 Alpha Power Fraction Absorbed by Ions and Alpha Power Model

The fraction of alpha power absorbed by ions is estimated using the expression formulated by Honda [39]:

$$f_\alpha = 1 - \left[1 - \left(\frac{T_e}{50}\right) - 0.37\left(\frac{T_e}{50}\right)^{1.75}\right] \qquad (8)$$

From the same reference [39] it is assumed that alpha particles are confined in the plasma until they are thermalized (except the fraction due to the ripple losses):

$$P_\alpha = S_\alpha \left(E_\alpha - \frac{3}{2}T_i\right)(1 - fripple) \qquad (9)$$

where $fripple$ is assumed as an input with a constant value of 0.014 and E_α is alpha's energy (3.52 MeV).

2.2.2.4 Power Exchanged between Ions and Electrons Model

The expression for the power exchanged between ions and electrons is obtained from the same reference as the previous section [39]:

$$P_{ie} = 3 \cdot 10^{-8} \cdot n_e \cdot \sum_k \frac{Z_k n_k}{A_k} \frac{T_i - T_e}{T_i^{1.5}} \qquad (10)$$

where A_k is the atomic mass and Z_k the atomic number for every species.

2.2.2.5 Ohmic Heating Model

The Ohmic heating power is [39]:

$$P_{Ohm} = 1.012 \cdot 10^{19} \cdot C_{oh} \frac{j^2 \cdot Z_{eff} \cdot \ln \Lambda}{T_e^{1.5}} \qquad (11)$$

where:

$$\ln \Lambda = 16.09 - 1.15 log_{10} n_e + 2.30 log_{10} T_e \qquad (12)$$

$$Z_{eff} = \frac{\sum_k Z_k^2 n_k}{\sum_k Z_k n_k} \qquad (13)$$

and j is the plasma current density (MA/m^2).

2.2.2.6 Bremsstrahlung Power Model

The Bremsstrahlung losses are calculated in AINA 4.0 by means of the expression [40]:

$$P_{Br} = 3.34 \cdot 10^{-21} n_e \sum_k Z_k^2 n_k T_e^{0.5} \qquad (14)$$

2.2.2.7 Synchrotron Power Model

Synchrotron power losses are computed through the Albajar equations [41][42]:

$$P_{sy} = 8.2 \cdot 10^{-6} \cdot (1 - R_w)^{0.5} \cdot R \cdot (ak)^{3/2} \cdot n_{e20}^{1.5} \cdot (T_e \cdot B_T)^{2.5} \cdot M_{mcdondald} \cdot G_{heuristic} \qquad (15)$$

where:

$$M_{mcdondald} = \frac{(1 + \frac{1.93030}{\mu})}{(1 - \frac{0.58167}{\mu})} \qquad (16)$$

$$G_{heuristic} = \left(1 + \frac{9}{\frac{R \cdot T_e^{0.5}}{ak}}\right)^{0.5} \qquad (17)$$

$$\mu = \frac{510.902}{T_e} \qquad (18)$$

$$ak = a \cdot k^{1/3} \qquad (19)$$

In addition, a is the minor radius, k the plasma elongation and R_w, with a value of 0.6, represents the wall reflection coefficient of the P_{sy}.

2.2.2.8 Line Power Model

Firstly, it's important to note that the power losses in the plasma core can be summarized as radiation losses and confinement losses. In a simplified way, the total radiation losses due to charged particles acceleration can be divided into three phenomena: the Bremsstrahlung radiation, the Synchrotron radiation and the Line radiation.

- Bremsstrahlung losses are electromagnetic radiation emitted in the range of the X-rays wavelengths mainly due to the deceleration of electrons when deflected by other charge particles. Its numerical model has been defined previously.
- Synchrotron losses are electromagnetic radiation originated by the acceleration suffered for a charged particle inside a magnetic field which undergoes an spiral trajectory. Its numerical model has been defined previously.
- Line radiation is the electromagnetic radiation remainder, the sum of all no covered physical atomic phenomena such as ionization by electron collisions, radiative recombination, charge exchange recombination and excitation.

In contrast to Bremsstrahlung and Synchrotron radiation, Line radiation can not be estimated by means of a reliable and simple model. Historically, AINA has been using models which do not take into account the possible local variations in temperature, density and impurity fraction during a transient. With the

aim of overcoming this deficiency in the 3.0 version of AINA code, the Line power was evaluated following the method exposed by Post and Jensen [43] and proposed to be used in plasma power balance by Sheffield [44].

$$P_{li} = f_{core} \cdot n_e \cdot n_Z \cdot L_z \qquad (20)$$

$$log_{10} L_Z = \sum_i A(i) \cdot [log_{10}(T_i)]^i \qquad (21)$$

Where $A(i)$ are the polynomial fitting coefficients for each of the impurity species [43].

However, this model estimates the radiative losses in the range of short wavelength due to all the physical atomic processes both Line and Bremsstrahlung radiation [43] but this redundancy of Bremsstrahlung contribution will be covered by the method exposed below. It is necessary to note that Line radiation is maximal at low temperatures since at high temperatures as at the plasma core all species are fully ionized and just Bremsstrahlung takes place as shown in Figure 17. For this reason Line radiation will be more important at the plasma edge affecting slightly the global power balance of the plasma core, where radiation losses are dominated by Bremsstrahlung radiation. In addition, in the case of very high Z impurities like Tungsten and medium Z impurities as Xenon or Argon, a fraction of the radiation will be emitted by Line radiation and focused on the plasma edge. However, technically, this contribution is desired to be marginal [45][37]. In summary:

- All light impurities are fully ionized in fusion relevant plasmas due to their small size by which reach the plasma core where the temperatures are maximum without reacting, therefore the loss originating from impurity radiation is purely due to Bremsstrahlung [46][47].
- High and Medium Z impurities contribute to both Bremsstrahlung at the plasma core mainly and, especially, Line at the edge.

In order more easily to remember, Figure 16 shows several impurities and Helium densities and radiation distribution along plasma radius [48].

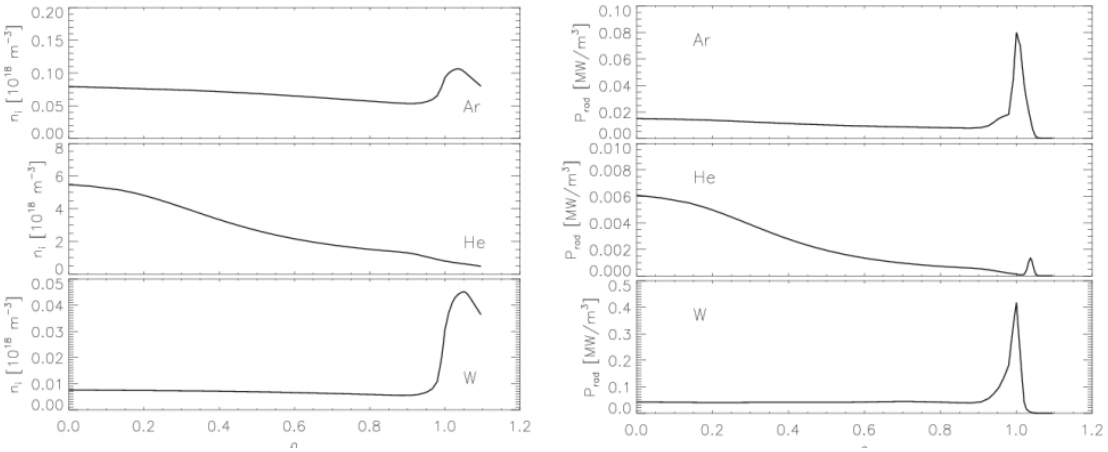

Figure 16: Densities and radiation distribution along plasma radius [48].

With these premises in mind, two factors have been implemented in the AINA code to estimate a numerical value for the Line radiation loses near to the desired one. These factors are:

- f_{core}: represents the fraction of the radiation Line losses which enter into the plasma core due to high and medium Z impurities.
- $f_{P_{li\_ScalingFactor}}$: it is a factor used to adapt the results to the desired operational state conditions.

In short, the final expression used in AINA is the following:

$$P_{li} = f_{core} \cdot f_{P_{li\_ScalingFactor}} \cdot [(n_e \cdot n_Z \cdot L_z) - P_{Br}] \qquad (22)$$

In addition, from the previous statements it is possible to conclude that power in the plasma edge is:

$$P_{edge} = \frac{P_{li}}{f_{core}}(1 - f_{core}) \qquad (23)$$

The final values of these factors will be estimated after a scanning analysis for each of the operational scenarios simulated. The corresponding fixed values must allow to obtain a P_{core_rad} and a P_{edge} slightly higher than the PROCESS simulations results for the purpose of being conservative, not only on plasma model but on thermal blanket model as well.

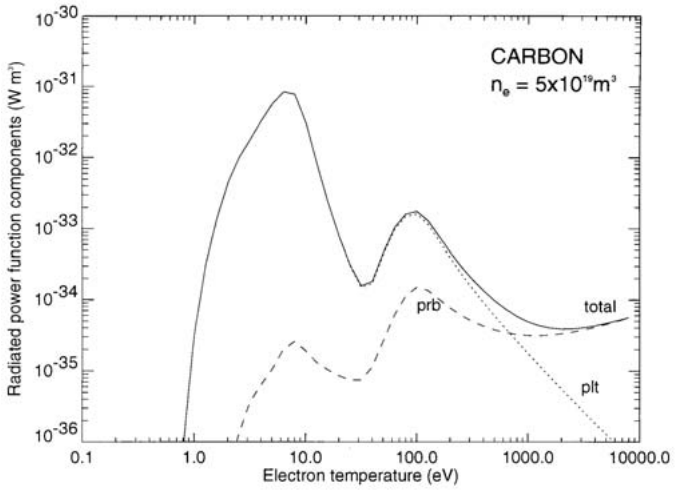

Figure 17: The dependence of the radiative loss function on temperature, for Carbon, at steady ionization balance. The two dominant contributions are Line radiation (plt) and Bremsstrahlung radiation (prb) [49].

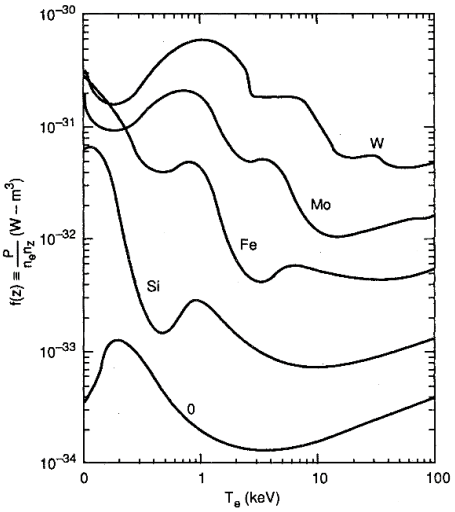

Figure 18: Line radiation factor $f(Z)$ or L_Z as a function of electron temperature for representative impurities Z [44].

After the preliminary in depth and critical analysis of the previous versions of the code used to simulate ITER [14][15][16] and DEMO WCPB [19][37], it was possible to conclude that, the Line power model had not be under consideration the contribution of the Tungsten, for this reason a new model have been developed with the aim of overcoming this deficiency. Furthermore, a fraction of the numerical result was assumed as power in the edge. Unfortunately, this consideration was not explained properly even though an scanning analysis had to be performed to fix the mentioned contribution and to adapt the steady state extracted from AINA to PROCESS conditions for each operational scenario simulated.

Thus, the values of P_{core_rad} and P_{edge} from PROCESS fix the final model used, nevertheless and in spite of PROCESS is the tool used to estimate operational states for DEMO, this code includes a simple and overall radiation model which is not suitable for detailed study of plasma radiation, but since the impurity concentrations are free parameters, it is always possible to find a model with the desired total radiative loss [30]. The model implemented is based on the affirmation that total impurity radiation from the core plasma is mainly due to Bremsstrahlung and Synchrotron:

$$P_{core\_rad} = P_{Br_Z} + P_{sy} \qquad (24)$$

$$P_{Br_Z} = \sum f_{Br_Z} \cdot P_Z \qquad (25)$$

$$P_Z = C_1 \cdot f_Z \cdot \left(\frac{n_e}{7 \cdot 10^{-19}}\right)^{C_2} \cdot V_R \qquad (26)$$

$$f_{Br_{He}} = 0.9\,;\; f_{Br_C} = 0.52\,;\; f_{Br_O} = 0.52\,;\; f_{Br_Z} = 0.35 \qquad (27)$$

Where f_{Br_Z} is the fraction of the total radiation power P_Z of the impurity Z originated by Bremsstrahlung. The remainder is Line radiation and just affects plasma edge. The f_Z represents the thermal ion fraction. This factor and the different model used are the reasons why it is necessary to implement the scaling factor $f_{P_{li\_ScalingFactor}}$.

Other code that uses a similar solution to the power Line estimation is SYMOCORE [50] which assumes that, conversely to Bremsstrahlung and Synchrotron powers which are predominantly located in the plasma core, Line radiation (from Argon or Xenon) occurs near the edge and pedestal. SYMOCORE defines a minor radius ρ_{line} within which the Line radiated power is accounted as a loss. Line radiation power outside this radius is not taken into account in the plasma power balance. This assumption is similar to the f_{core} factor defined by AINA.

In conclusion, codes developers affirm that the treatment of Line radiation will have to be refined in order to reduce uncertainties in system codes in the near future. For this reason, it will be necessary to keep an eye on the possible future strides focused on this field with the goal of implementing them in the AINA code and improving the corresponding model.

2.2.2.9 Energy Confinement Time Model and Scaling Laws

The energy confinement time model is based on a multi-machine empirical database [51]:

$$\tau_{E,e}^{Hmode} = 0.0562 \cdot I_p^{0.93} \cdot R^{1.97} \cdot \left(\frac{a}{R}\right)^{0.58} \cdot k^{0.78} \cdot n_{e19}^{0.41} \cdot B_T^{0.15} \cdot A_i^{0.19} \cdot P^{-0.69} \qquad (28)$$

$$\tau_{E,e}^{Lmode} = \frac{0.023 \cdot I_p^{0.96} \cdot R^{1.83} \cdot k^{0.64} \cdot n_{e19}^{0.4} \cdot B_T^{0.03} \cdot A_i^{0.2}}{\left(\frac{a}{R}\right)^{0.06} \cdot P^{0.73}} \qquad (29)$$

These scaling laws have a limited range of validity, and thus, during the simulation of a plasma transient, can yield physically implausible results. Therefore, they are bounded with a scaling based on theoretical considerations, as prescribed by Uckan [52]:

$$\tau_{E,e} = min\{\tau_{E,e}^{Hmode}, \tau_{E,e}(\Omega)\} \qquad (30)$$

where:

$$\tau_{E,e}(\Omega) = 0.07 \cdot n_{e20} \cdot a \cdot R^2 \cdot q_\Psi \qquad (31)$$

$$q_\Psi = \frac{5 \cdot B_T \cdot a^2 \cdot G1 \cdot G2}{R \cdot I_P} \qquad (32)$$

$$G1 = \frac{1 + (k^2 \cdot (1 + 2d^2 - 1.2d^3))}{2} \qquad (33)$$

$$G2 = \frac{1.17 - 0.65\left(\frac{a}{R}\right)}{\left(1 - \left(\frac{a}{R}\right)^2\right) \cdot \left(1 - \left(\frac{a}{R}\right)^2\right)} \qquad (34)$$

And d is the plasma triangularity.

For transitions from H-mode to L-mode and from L-mode to H-mode, it is assumed the following conditions:

- Transition from mode H to mode L if $P_{sep} < 0.2 \cdot \min(P_{THRi})$
- Transition from mode L to mode H if $P_{sep} > 0.5 \cdot \min(P_{THRi})$

where, from the Polevoi fit [53]:

$$P_{THR0} = 0.1 \cdot n_{e20}^{0.46} \cdot B_T^{0.87} \cdot S_f^{0.84} \cdot A_i^{-1} \qquad (35)$$

$$P_{THR1} = 0.084 \cdot n_{e20}^{0.73} \cdot B_T^{0.74} \cdot S_f^{0.98} \cdot A_i^{-1} \qquad (36)$$

$$P_{THR2} = 0.144 \cdot n_{e20}^{0.7} \cdot B_{OUT}^{0.7} \cdot S_f^{0.9} \cdot A_i^{-1} \cdot \left(\frac{Z_{eff}}{2}\right)^{0.7} \cdot F(A)^\gamma \qquad (37)$$

$$S_f = 4\pi^2 aR\left(\frac{1 + k^2}{2}\right)^{0.5} \qquad (38)$$

$$B_{OUT} = \left(B_{t,OUT}^2 + B_{P,OUT}^2\right)^{0.5} \qquad (39)$$

$$B_{t,OUT} = \frac{B_T \cdot \frac{R}{a}}{\frac{R}{a} + 1} \qquad (40)$$

$$B_{p,OUT} = \left(\frac{\mu I_P}{2\pi a}\right)\left(1 + \frac{a}{R}\right) \qquad (41)$$

$$F(A) = \frac{0.1\frac{R}{a}}{f\left(\frac{R}{a}\right)} \qquad (42)$$

$$f(A) = 1 - \left(\frac{1}{1+A}\right)^{0.5} \qquad (43)$$

In addition, it is assumed an input value of 0.5 for γ.

The power values used not only for the energy confinement time estimation but as the P_{sep} for the transitions boundaries as well is [53]:

$$P = P_{ext} + P_{\alpha} + P_{Ohm} - P_{Br} - P_{sy} - \frac{P_{li} + P_{edge}}{3} \qquad (44)$$

Finally; the rest of energy confinement times are calculated as follows [39]:

$$\tau_{p,H} = C_H \cdot \tau_{E,e} \qquad (45)$$

$$\tau_{p,\alpha} = C_{\alpha} \cdot \tau_{E,e} \qquad (46)$$

$$\tau_{p,Z} = C_Z \cdot \tau_{E,e} \qquad (47)$$

$$\tau_{E,i} = C_i \cdot \tau_{E,e} \qquad (48)$$

where $C_H = 2;\ C_{\alpha} = 5;\ C_Z = 5$ and $C_i = 1$.

2.2.2.10 Other Parameters: Bootstrap Currents

The bootstrap current ratio is calculated using the next equation [54]:

$$f_{bootstrap} = \frac{I_{bootstrap}}{I_P} = C_{bs}\left(\left(\frac{a}{R}\right)^{0.5}\beta_p\right)^{1.3} \qquad (49)$$

where:

$$C_{bs} = 1.32 - 0.235\left(\frac{q_{95}}{q_0}\right) + 0.0185\left(\frac{q_{95}}{q_0}\right)^2 \qquad (50)$$

$$\beta_p = \beta_T \cdot 10^{-2}\left(\frac{B_T \cdot 5 \cdot a \cdot \sqrt{k}}{I_p}\right)^2 \qquad (51)$$

where β_T is the toroidal beta, q_{95} is the safety factor at 95% flux with and q_0 is the safety factor at plasma axis.

2.2.2.11 Plasma Equilibrium Limits

AINA concludes the simulation when the plasma conditions are such that one of the following limits are overcame and; thus, a disruption takes place:

- Beta limit [55]:

$$\beta_T \geq G_{Troyon} \frac{I_p}{aB_T} \qquad (52)$$

where G_{Troyon} it is assumed as an input with a value of 4.5.

- Greenwald limit [56]:

$$n_{e20} \geq \frac{I_p}{\pi a^2} \cdot C \qquad (53)$$

where C it is assumed as an input with a value of 2 since it is conservative enough from the safety point of view.

- P_{sol} limit:

$$P_{ext} + P_{\alpha} + P_{Ohm} - P_{Br} - P_{sy} - P_{li} \leq 0 \qquad (54)$$

- Locked modes limit [51]:

$$n_e \leq 2 \cdot 10^{19} \qquad (55)$$

2.2.3 Thermal Blanket block

The breeding blanket is one of the most challenging and innovative components due to the high strains it suffers. Moreover, several cooling loops embedded inside this component are responsible for maintaining the temperature within reasonable regimes and extracting the undesirable tritium in excess. The determination of 3D detailed temperature distribution by means of analytic method is not feasible thus it requires the usage of Computational Fluid Dynamics (CFD), as ANSYS FLUENT© [57] which are very demanding from a computational point of view; and this matter is not be consistent with the AINA approach about fast processing. For these reasons, flexible thermal-hydraulics routines, based on the finite differences technique, have been developed in order to obtain reliable, approximate and conservative (in comparison with the 3D model) 1D, radial and time-dependent simplified thermal-wall model in a short notice using a standard workstation [58]. In addition, these routines must take into consideration the influence of coolant channels not in line with the 1D segment which are present in the European DEMO designs. The effect of these tubes is considered using a weighted convective negative flux effect in function of the radial distance from the coolant and the poloidal distance from the 1D discretization line. The final expressions modelled are:

$$\rho(T,z)c(T,x)\frac{\delta T(x,T)}{\delta t} = \frac{\delta}{\delta x}\left[\left(1 - f_{COOL_i}\right)k_T(T,x)\frac{\delta T(x,t)}{\delta x} + f_{COOL_i}h_j\left(T(x,t) - T_{j,\infty}(x,t)\right)\right] + f_{WGT,R}f_{WGT,P}h_k\left(T(x,t) - T_{K,\infty}(x,t)\right) + \ddot{q}(x,t) \qquad (56)$$

$$f_{COOL_i}(x) = \sum \delta_j(x)\frac{Surface_{cooled}}{Surface_{Total}} \qquad (57)$$

$$f_{WGT,R}(x) = \sum \delta_k(x) f_{WGT,R} \qquad (58)$$

$$f_{WGT,P}(x) = \sum \delta_k(x) f_{WGT,P} \qquad (59)$$

Where ρ is the material density, c the heat capacity, k_T the thermal conductivity, $\ddot{q}$ the volumetric nuclear heat deposition, h is the heat transfer coefficient, $T(x)$ the material temperature at x, $T_{i,\infty}$ the coolant bulk temperature for the tube i, f_{COOL} the coolant surface for the in line tube which is equal to the relative surface of the coolant tubes to the total surface of the module section, $f_{WGT,R}$ and $f_{WGT,P}$ the coolant factor for the no in lines tubes that are discrete functions which take values only at the specified coolant positions and δ is the Dirac delta function.

The equation is solved considering the total load due to the radiation effect (P_{rad}) in the first node estimated by the plasma block, a Robin boundary condition for the last node by means of a heat transfer coefficient and a bulk temperature condition at the back side of the blanket and a nuclear heating distribution scaled for the Neutron Wall Load (NWL) estimated by the plasma block.

The material properties, the model discretization, the nuclear heating distribution and the boundary conditions associated to the cooling system depend on the blanket design modeled; for this section, the HCPB latest version (HCPB-2015 v3 [59]) has been selected.

2.2.3.1 HCPB-2015 v3 General Architecture

In order to describe the specific peculiarity of the AINA Wall model, the general architecture of the HCPB-2015 v3 "sandwich" concept for an outboard segment is hereinafter described and reported in the following figure.

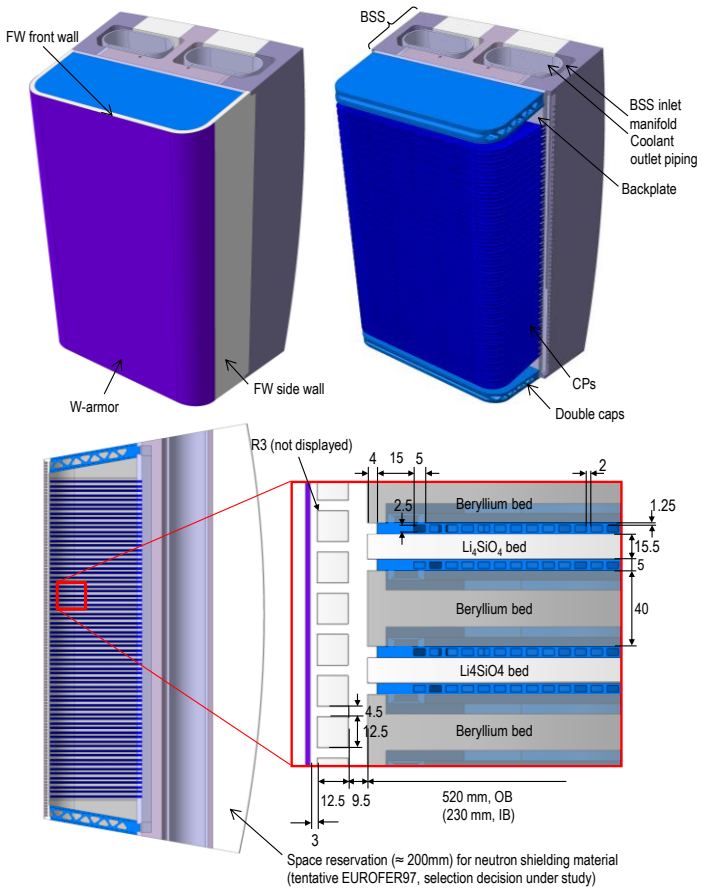

Figure 19: HCPB-2015 BB v3 concept scheme [59].

A 2 mm W-armour layer is assumed for all the modules at the plasma facing side of the FW whereas in the internal part the CP subdivide the Be and the $LiSiO_4$ bed zone which are arranged perpendicularly to the FW and alternated. The double caps are placed on the top and bottom part of the BB, the bed nearby filled by Be pebble. The back part of the BB, BSS, is used as the Helium collecting zone both for input and output. Please for more information refer to reference EFDA_D_2LHS3F [59].

2.2.3.2 HCPB-2015 v3 Cooling Flow Scheme

The HCPB BB is provided by two Helium redundant, fully symmetric, purely counter flow, coolant scheme which each one provide 50% of the cooling performance, see Figure 3 and Figure 4. Beginning from the BSS at 300 °C, the redundant cooling loop A cools the FW (50%) and then the CPs (50%), exiting the BZ and entering again the BSS, where the flow at about 500°C is routed out of the VV. At the same time, the redundant cooling loop B also beginning form the BSS at 300 °C cools the FW (50%) and then the CPs, exiting the BZ at 500 °C to the BSS.

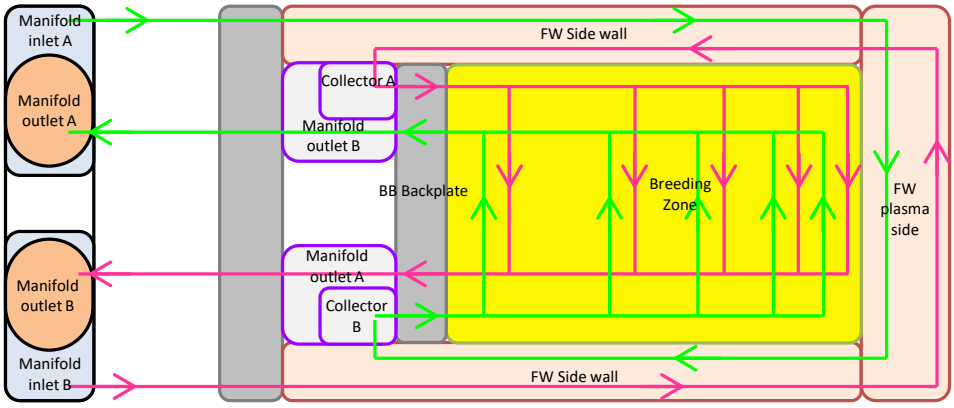

Figure 20: HCPB BB Helium cooling scheme [59].

Even though the distance between nearby coolant channel is fixed, a toroidal cooling channel arrangement has been obtained closing some CH and converting them to “dummy” or “blind”. In this way the thermal behavior of the BB is optimized minimizing at the same time the steel volume fraction in the BZ hence the TBR.

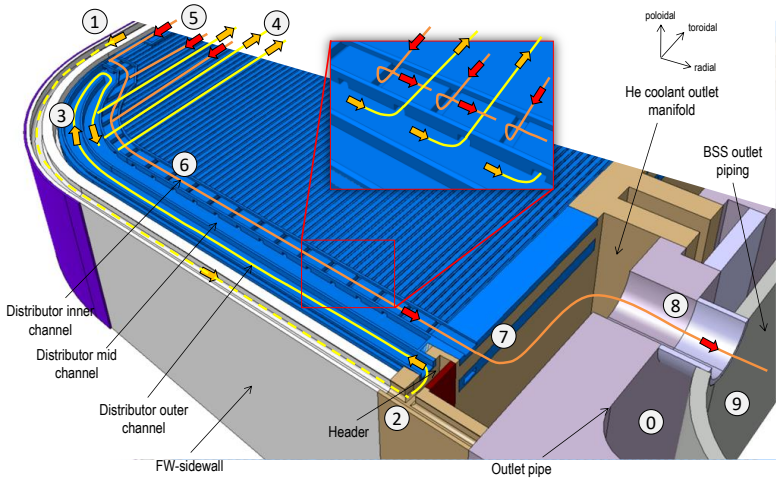

Figure 21: Thermo-hydraulic working principle of the CP [59].

As result of the assessment, the density of the "functional" CH is higher in the front part of the BB where the NHD is higher. In addition to the main BB Helium cooling scheme, a He purge gas system is present. Please for more information refer to EFDA_D_2LHS3F [59].

2.2.3.3 Design HCPB limits

The following material temperature limits are considered:

Material	Temperature Limit
EUROFER	*550*°C
Beryllium	650°C
Tungsten	3422°C
$LiSO_4$	920°C

Table 4: Material Temperature Limits.

2.2.3.4 Materials

In this chapter the material properties employed in the AINA DEMO HCPB code, which are the same used in EFDA_D_2LHS3F [59], are hereinafter reported. When needed the properties have been interpolated.

2.2.3.4.1 Helium

The He properties are extracted from Petersen [60] and the same employed in EFDA_D_2LHS3F [59]. The He is considered as pure because the effect of the purge gas dopant H-2 quantity is too low (1‰) hence considered to do not affect significantly the He properties

Mass density:

$$\rho^{He}(T,\mathrm{p}) = 48.14\frac{p}{T}\left[1+0.4446\frac{p}{T^{1.2}}\right]^{-1}\left[\frac{kg}{m^3}\right], \qquad (60)$$

with the pressure p expressed in [bar] and the absolute temperature T in [K].

Coefficient of dynamic viscosity

$$\mu^{He}(T) = 3.674\cdot 10^{-7}T^{0.7}\left[\frac{kg}{m\,s}\right] \qquad (61)$$

with the absolute temperature T expressed in [K].

Coefficient of thermal conductivity:

$$k^{He}(T,p) = 2.682\cdot 10^{-3}(1+1.123\cdot 10^{-3}p)\cdot T^{\left(0.71(1-2\cdot 10^{-4}p)\right)}\left[\frac{W}{m\,K}\right]. \qquad (62)$$

with the pressure p expressed in [bar] and the absolute temperature T in [K].

The analytical procedure used to compute the heat transfer coefficient is described hereinafter.

The bulk coolant temperature of the CP cooling channels has been extracted from Fig. 50 [61]. Imposing a coolant pressure p, 80 bar [61], and knowing the bulk coolant temperature, T_∞, the Helium coolant density has been obtained in the following way [59][60]:

$$\rho^{He}(T_\infty,\mathrm{p}) = 48.14\frac{p}{T_\infty}\left[1+0.4446\frac{p}{{T_\infty}^{1.2}}\right]^{-1}\left[\frac{kg}{m^3}\right] \qquad (63)$$

The mass flow rate, $\dot{m}$ $\left(\frac{kg}{s}\right)$, of each CP cooling channels has been extracted from [60] and used to compute the Helium coolant velocity, v $\left(\frac{m}{s}\right)$:

$$\dot{m} = \rho\, A\, v \qquad (64)$$

where A is the CP section [m^2].

The Reynolds Number is:

$$Re_D = \frac{\rho\, v\, D}{\mu} \qquad (65)$$

where:

- D is the coolant diameter for circular pipes [m]
- μ is the dynamic viscosity [kg/m/s] obtained as follow [61]:

$$\mu^{He}(T_\infty) = 3.674 \cdot 10^{-7} T_\infty{}^{0.7} \qquad (66)$$

Having a rectangular cross sections, the D is substituted by the hydraulic diameter D_H $[m]$:

$$D_H = 4 * \frac{A}{P} \qquad (67)$$

where P is the wetted perimeter [m].

The Prandlt number, Pr, is obtained as [61]:

$$Pr = \frac{0.7117}{1 + 1.123 * 10^{-3} p * T_\infty{}^{-(0.01 - 1.42 * 10^{-4} * p)}} \qquad (68)$$

Depending on the Reynold Number, the Nusselt Number has been obtained in two different ways:

- Laminar Flow: Re_D<3000

  According to Incropera [62] and assuming a constant heat flux along the pipe length and a CP channel dimension ratio a/b equal to 2, the Nu_d is set to 4.12.

- Turbulent Flow: Re_D≥ 3000

  Following the Gnielinski correlation [63]:

$$Nu_D = \frac{\frac{f}{8}(Re_D - 1000)Pr}{1 + 12.7\sqrt{f/8}(Pr^{2/3} - 1)} \qquad (69)$$

where Re_D is the Reynolds number, Pr is the Prandlt number and f the Darcy-Weisbach friction factor, which can be approximated as:

$$f = (0.79 \ln(Re_D) - 1.64)^{-2} \qquad (70)$$

after the correlation by Petukhov [59][64].

Finally, the Helium heat transfer coefficient for each CP channel is computed as:

$$h = \frac{Nu_D \cdot k}{D} \qquad (71)$$

where k is the Helium thermal conductivity [W/m/k] [60].

$$k^{He}(T_\infty, p) = 2.682 \cdot 10^{-3}(1 + 1.123 \cdot 10^{-3}p) \cdot T_\infty^{\left(0.71(1-2\cdot 10^{-4}p)\right)}. \qquad (72)$$

where:

- p is the pressure expressed in [bar]
- T is the absolute temperature in [K]

2.2.3.4.2 EUROFER97 structural steel

The following table summarizes the thermomechanical properties for the EUROFER97, namely the coefficient of thermal expansion α^{E97}, the density ρ^{E97}, the specific heat capacity c_p^{E97}, the thermal conductivity k^{E97}, which have been extracted from EFDA_D_2LHS3F [59][65].

T $[°C]$	α^{E97} $[10^{-6}/K]$	ρ^{E97} $[kg/m^3]$	c_p^{E97} $[J/kg\ K]$	k^{E97} $[W/m\ K]$
20		7750	448	31,5
100	10.70	7753	460	32,2
150			477	
200	11.20	7713	494	32,7
250			510	
300	11.60	7685	527	33,2
350			544	
400	11.90	7655	565	33,3
450			586	
500	12.20	7625	611	32,8
550			644	
600	12.50	7594	682	32,3
650			728	
700			866	44,8

Table 5: Thermomechanical properties of EUROFER97.

2.2.3.4.3 Tungsten armour

The material properties of the W-armour are taken from the ITER Materials Properties Handbook [66]:

Thermal conductivity,

$$k(T) = 174{,}9274 - 0{,}1067T + 5{,}0067 \cdot 10^{-5}T^2 - 7{,}8349 \cdot 10^{-9}T^3 \left[\frac{W}{m^2K}\right] \qquad (73)$$

heat capacity,

$$c_p(T) = 128{,}308 + 93{,}2797 \cdot 10^{-2}T - 3{,}4097 \cdot 10^{-6}T^2 \left[\frac{J}{kgK}\right], \qquad (74)$$

and density

$$\rho(T) = 19302{,}7 - 2{,}3786 \cdot 10^{-1}T - 2{,}2448 \cdot 10^{-5}T^2 \left[\frac{kg}{m^3}\right], \qquad (75)$$

with T in [°C] in all the cases.

2.2.3.4.4 Li_4SiO_4 pebble bed

The coefficient of thermal expansion α^{LOS}, the density ρ^{LOS} and the specific heat capacity c_p^{LOS} of the Li_4SiO_4 pebble beds has been obtained from Sena [67] and Petukhov [64].The following table summarizes these properties:

T $[°C]$	α^{LOS} $[10^{-6}/K]$	ρ^{LOS} $[kg/m^3]$	c_p^{LOS} $[J/kg\ K]$
0	1.881E-05	1526.4	1392.4
50	1.965E-05		1450
100	2.048E-05		1513.4
150	2.131E-05		1580
200	2.214E-05		1648.5
250	2.298E-05		1718.2
300	2.381E-05		1788.8
350	2.464E-05		1859.9
400	2,548E-05		1931,4
450	2,631E-05		2003.3
500	2.714E-05		2075.3
550	2.798E-05		2147.5
600	2.881E-05		2219.8
650	2.964E-05		2292.3
700	3.048E-05		2364.8
750	3,131E-05		2437,4
800	3,214E-05		2510,1
850	3,298E-05		2582,8
900	3,381E-05		2655,5
950	3.464E-05		2728.3
1000	3.548E-05		2801.1

Table 6: Thermomechanical properties of Li_4SiO_4 pebble beds.

The expression for the effective thermal conductivity of the Li_4SiO_4 pebble beds is given by the following expression [67]:

$$k_{eff}^{Li_4SiO_4}\left(T, \varepsilon_{vol}^{in}\right) = 0.768 + 4.96 \cdot 10^{-4}T + 0.045\varepsilon_{vol}^{in}\left[\frac{W}{mK}\right], \qquad (76)$$

where T is the pebble bed local temperature [°C] and ε_{vol}^{in} is the inelastic volumetric strains in [%], which is the sum of the 3 principal strains. The ε_{vol}^{in} parameter has been considered 0 as a conservative approximation.

2.2.3.4.5 Be pebble bed

The coefficient of thermal expansion α^{Be}, the density ρ^{Be} and the specific heat capacity c_p^{Be} of the Be pebble beds has been obtained from Sena [67] and Petukhov [64]. The following table summarizes these properties:

T $[°C]$	α^{Be} $[10^{-6}/K]$	ρ^{Be} $[kg/m^3]$	c_p^{Be} $[J/kg\ K]$
0	1.134E-05	1166.72	1741.8
50	1.182E-05		1900.97
100	1.229E-05		2045.53
150	1.275E-05		2176.44
200	1.319E-05		2294.66
250	1.361E-05		2401.14
300	1.402E-05		2496.83
350	1.442E-05		2582.71
400	1.480E-05		2659.71
450	1.516E-05		2728.79
500	1.551E-05		2790.93
550	1.585E-05		2847.05
600	1.617E-05		2898.14
650	1.648E-05		2945.13
700	1.667E-05		2988.99
750	1.704E-05		3030.68
800	1.731E-05		3071.14
850	1.755E-05		3111.34
900	1.778E-05		3152.22
950	1.800E-05		3194.76
1000	1.820E-05		3239.9

Table 7: Thermomechanical properties of Be pebble beds.

The expression for the effective thermal conductivity of the Li4SiO4 pebble beds is given by the following expression [59]:

$$k_{eff}^{Be}(T, \varepsilon_{vol}^{in}) = 1.81 + 0.0012 \cdot T - 5 \times 10^{-7} \cdot T^2 + (9.03 - 1.386 \cdot 10^{-3} \cdot T - 7.6 \cdot 10^{-6} \cdot T^2 + 2.1 \cdot 10^{-9} \cdot T^3) \cdot \varepsilon_{vol}^{in} \left[\frac{W}{mK}\right], \quad (77)$$

where T is the pebble bed temperature [°C] and ε_{vol}^{in} is the inelastic volumetric strains in [%], which is the sum of the 3 principal strains.

In the case of the Be pebble beds, the effect of ε_{vol}^{in} in the conductivity of the Be pebble beds is not negligible. This parameter is influenced by thermal expansion between the BB module box and the pebble beds. Thanks to thermomechanical models a correlation between pebble beds temperature and ε_{vol}^{in} has been derived in HCPB TBM BU [59] and applied in AINA models:

$$\varepsilon_{vol}^{in} = \begin{cases} 0.2\%, & T \in [20, 500[°C \\ 0.3\%, & T \in [500, 600[°C \\ 0.5\%, & T \geq 600\ °C \end{cases} \quad (78)$$

2.2.3.5 Nuclear Heating Distribution

At the time of the study, no official nuclear heat data was available for the HCPB-2015 baseline. For this reason as done in EFDA_D_ 2HF7KU_v1.1 [61], the previous data has been adapted scaling proportionally them to a NWL of 0.5 MW/m^2 since according to EFDA_D_ 2HF7KU_v1.1 [61] a heat flux of 0.5 MW/m^2 is assumed and approximated to an exponential function. Due to the diverse macroscopic cross sections and densities, a different nuclear heating density for each material is applied. Depending on the material and the plasma distance the AINA code applies the correspondent value.

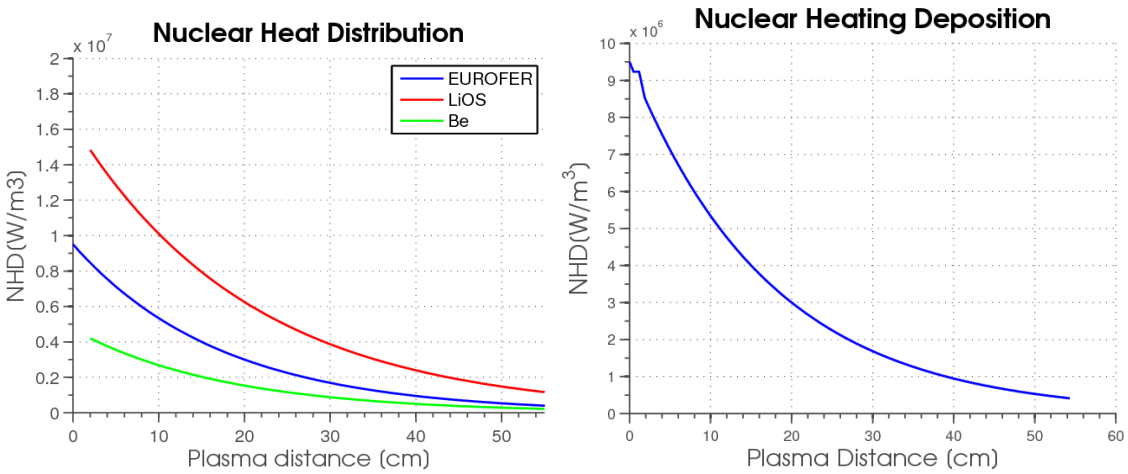

Figure 22: Nuclear Heat Distribution: material and HCPB 1D.

2.2.3.6 Steady state approach

The steady state solver designed by Marco Fabbri follows the process shown by the next figure and requires three main inputs [2]:

- The material thermal properties.
- The nuclear heating distribution.
- The model discretization.

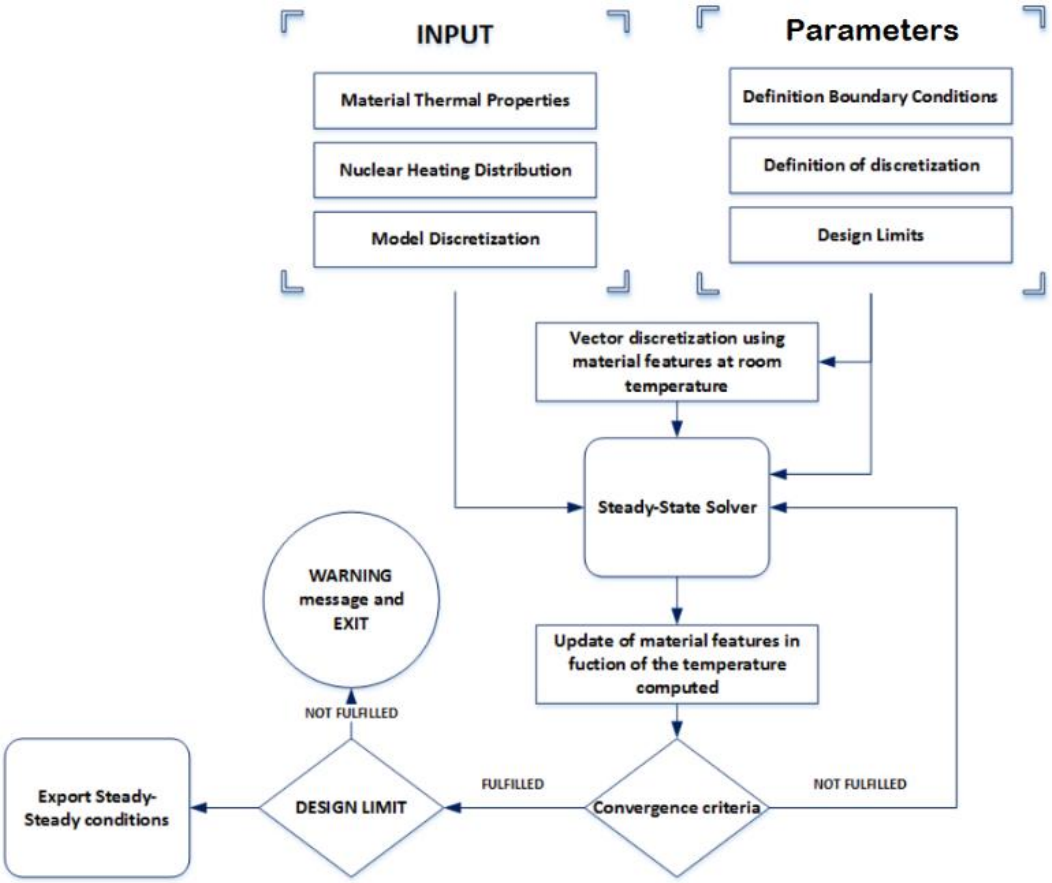

Figure 23: Steady-state solver approach [2].

Fixing these inputs, the boundary conditions and the temperature design limits according to the desired configuration and scenario, the outcomes from the thermal model can be validated by means of a cross-checking with the three-dimensional CFD detailed one. Therefore, the steady state solver computes a tentative solution which allows the update of the material thermal properties. Until the convergence criteria, imposed previously by the user (1ºC is a good selection and this is the default value implemented), is not fulfilled or the maximum number of iteration is achieved (after and in depth analyses, it has been assumed a value of 10 for this limit) the solver continues iterating updating the blanket properties. Once the criteria is passed, the design limits are checked: if they are met, the program will end normally exporting the steady state model solution, if not it will warn the user indicating the affected materials. It could happen that the temperature distribution obtained is not conservative if compared with the three dimensional detailed one. In this case, a scaling function shall be applied to the resulting distribution to achieve at least the same conditions found in the detailed studies.

In addition, it is also important to point out that there are several boundary conditions to apply:

- **First Wall Helium, water or other coolant channel:** for this node is necessary to assume a fixed temperature and a mass flow rate [68].
- **He purge gas system**: In a conservative approach, the He purge gas system has not been taken into account. Hence, the coolant capability decreases and, consequently, the safety factor of the model increases [68].
- **Cooling Plate Helium / Water Channels / Other coolant channels**: it is necessary to assume a fixed mass flow rate for each of them [68].

- **Pebble bed interfaces**: toroidal interfaces between the Pebble bed and the EUROFER have been considered purely conductive [68].
- **Last node**: this node represents the back plate where a Robin boundary condition is assumed by means of a heat transfer coefficient and a bulk temperature [68].
- **First Wall**: in the first node a total load due to the radiation effect against the First Wall is applied.

Specifically, this routine has been slightly modified to be docked in AINA during the Steady Sate estimation. The applied adjustments have been:

- The one-dimensional model and its discretization have been adapted for the desired blanket configuration thanks to the detailed design documents of EUROfusion.
- Necessary inputs and boundary conditions (with the exception of the First Wall boundary condition) have been imposed according to the desired blanket configuration extracted from validated documentation about more detailed studies and properly referenced throughout this document.
- The boundary condition for the First Wall is directly estimated by the plasma block.

It's important to understand that it will be necessary a convergence process to obtain the real steady state since in a first step, the mass and power balance of the plasma block is solved forcing an initial surface temperature. This solution generates a neutron and radiation load on the first wall, so it will be necessary estimate the new temperature reached for the surface of the First Wall due to this load. Then, the mass and power balance will be solved again and all the process will have to be repeated until this surface temperature for the First Wall converges (the convergence criteria is imposed by the user but after an in depth analysis, it concluded that 1ºC is a good selection, so this is the default value implemented).

Layer No.	Material	Thickness [mm]	No. Nodes
1	Tungsten	2	10
2	EUROFER	3	500
3	Helium Coolant	13.5	1
4	EUROFER	8.5	500
5	Be/ Li_4SiO_4/EUR	516	500

Table 8: Specifications of the 1D HCPB blanket AINA model.

2.2.3.7 Transient approach

The transient approach designed by Marco Fabbri [2] and employed by the thermal-hydraulic routine is reported in the following figure. In this case, there are three main inputs:

- The material thermal properties (as in the steady state solver).
- The steady state solution.

The nuclear heating distribution and the coolant conditions updated according to the perturbation imposed by the transient.

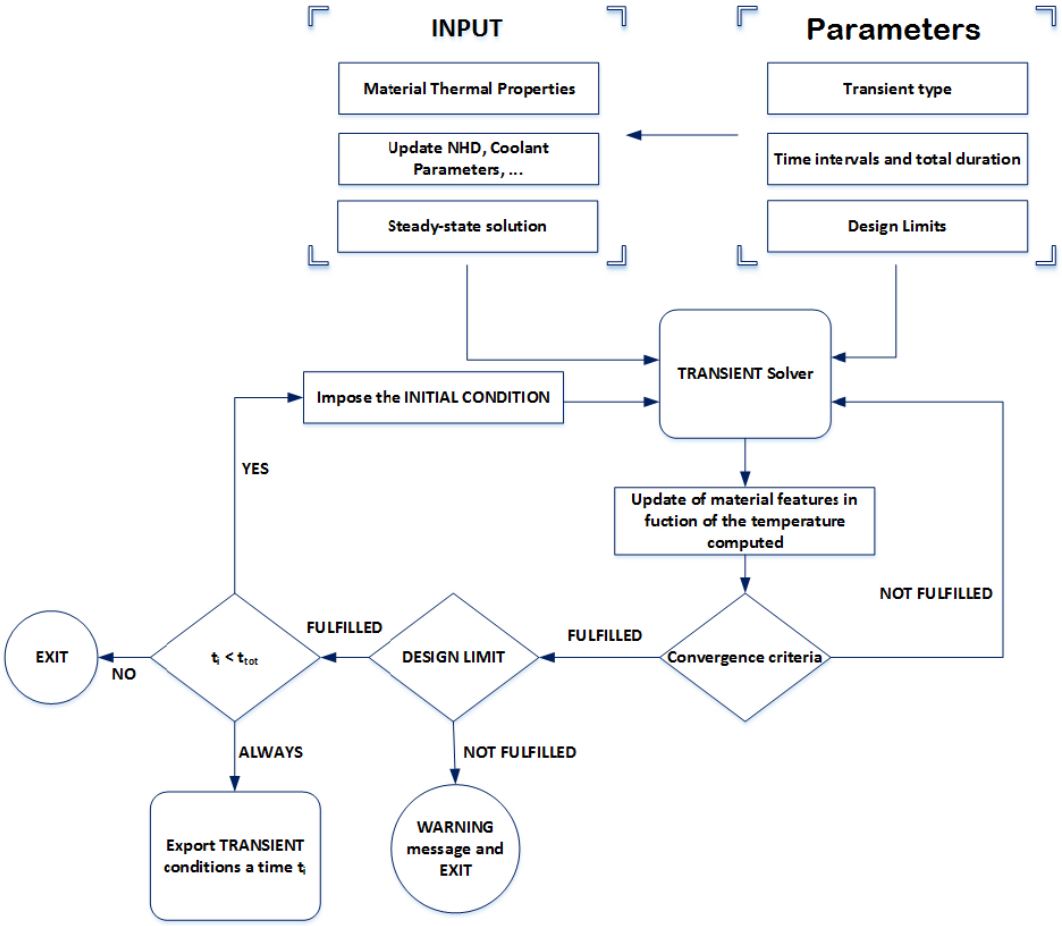

Figure 24: Transient solver approach [2].

Moreover, it is necessary to establish the transient type, the time intervals, the total transient duration and the temperature design limits according to the desired scenario. The process is very similar to the steady state solver. Firstly, the solver computes a tentative transient solution using as initial condition the steady state solution. Then the material thermal properties are updated. Until the convergence criteria is not fulfilled or the maximum number of iteration is achieved the solver continues iterating updating the blanket properties. Once the convergence criteria is passed, the design limits are checked: if they are exceeded it will warn the user indicating the affected materials. Later the routine checks the transient time and exports the solution: if the t_i is within the time interval defined by the user, the solution at t_i is imposed as initial condition for the solution at t_{i+1} entering again in the transient loop solution whereas if it is not the program stops.

As in the steady state case, this routine has been slightly modified to be docked in AINA during the transient simulations. The applied adjustments have been:

- The boundary condition for the First Wall is directly estimated by the plasma block for every simulation time step. Therefore, a plasma perturbation affects the thermal blanket block as well.
- Every simulation time step is equal to 0.1 s since this is the default step time adopted for AINA to solve the transient by means the Euler method. In addition, after an analogous study to the error analysis performed by Marco Fabbri [2], an interval time of one-fifth of the time step has been assumed to solve the thermal system.

A LOCA accident can be forced to simulate this type of transient. The LOCA can affect the FW cooling channel and the internal cooling loops.

2.2.3.8 Other Thermal Blanket block assembly considerations

So far, a general overview about the linkage of the thermal blanket block has been come up with; however, certain fundamental considerations have been applied and must be taken into account:

- To obtain the temperature distribution in the poloidal direction of the blanket for every simulation time step, just the worst region among the 14 poloidal regions which conform the blanket and its associated load flux against the wall $NWL + P_{rad}$ $\left[{}^{MW}/_{m^2}\right]$ is considered. In this way the system maintains its conservatism since even though the radiation between the surface of each poloidal region is not been estimated, the final impurity contribution form the PFC materials is bigger due to the most elevated surface temperature is taken for all the poloidal regions. Thus, it is worth noting that the region OB4 is usually one that suffers the maximum load; however, the region OB5 can be the worst depending on the transient evolution. Fortunately, either OB4 or OB5 have similar radial configurations; for this reason, OB4 is the blanket region modelled. The reason why the temperature distribution cannot be simulated for all the poloidal region is the significant increase in the time processing; moreover, this simplification assumes that the region where the load is maximum must be the critical configuration from the temperature melting limits point of view. This consideration cannot be true but is accepted as a proper approach. If the worst region changes, a notification appears pointing the new worst region and the time when this event happens.
- Despite the fact that the thermal blanket block was designed to stop the simulation if any temperature limit was exceeded, that first approach was modified due to two reasons:
    - Temperature limits are not fully agreed, so the limits assumed in the code are conservatives.
    - It is desirable to be able to obtain the total evolution of the transient and identify when a disruption (passive shutdown) would stop the reactor (this situation is an approximation since the melting consequences are not considered; for example, the positive consequence about the self-shielding phenomena of a plasma-exposed surface during extreme transient heat loads [69]).

  In this way the simulation continues until a disruption takes place or the total simulation time was reached; and a notification appears if any limit has been exceeded indicating the affected material and the time when it happened.

- In the case of the modelled blanket configuration combines several materials for a single layer (it depends on the modelling and the discretization); the thermal solver will be executed as often as different material constitute the layer assuming just one material for each case. It is important to note that the temperature for the first node have to be checked among all the possible cases depending on the material simulated for a mix layer and a difference of 5 % has been assumed as the maximum accepted divergence and the worst value is the adopted one to continue the simulation.
- With the goal of optimizing the processing time, if the boundary condition does not vary significantly (four significant digits $\left[{}^{MW}/_{m^2}\right]$) it is not necessary to execute the thermal solver since the temperature profile remains constant.

The code allows to plot the temperature profile along the one-dimensional segment for all the possible materials.

2.2.4 Thermal Divertor block

A divertor is a device within a tokamak which allows to extract the power conducted in the Scrape-Off Layer (SOL) whilst maintaining the plasma purity removing the great amount of neutral particles and impurities produced by the fusion process. If these particles and impurities went into the core, then the plasma temperature would decrease quickly because of the increased radiation heat loss [70]. This removal process is because in poloidal cross section of vacuum vessel the magnetic field lines generated by the external poloidal coils change locally from their typical configuration due to the superposition of the magnetic field generated by the divertor poloidal coils. The magnetic field lines are circular closed in the core plasma region, while in the so called scrape-off layer they are opened and intersect the divertor target plates [70]. As main interface component between the plasma and the components material, it shall tolerate high heat loads while at the same time contributing in providing neutron shielding for the Vacuum Vessel (VV) and magnet coils, in the vicinity of the divertor region. The divertor design shall provide an engineering solution compatible with today's plasma physics expectations; but, giving the uncertainties in extrapolating the future progress in plasma physics, and thus in component durability, the design shall also provide a mean for rapid replacement and refurbishment [71].

2.2.4.1 Divertor functions

In summary, the most relevant functions which the divertor system must fulfil are [72]:

- To provide magnetic configuration assuring diverted field lines to the outer chamber (where the plasma deposits its energy).
- To exhaust ion particles (alpha, D, T, impurities) thermal power.
- To reduce plasma pollution by controlling impurity density.
- To provide mechanical support for components.
- To allow for assembling sequence.
- To allow for positioning and alignment.
- To provide shielding for system protection.
- To keep operating conditions within range.
- To withstand loads.
- To monitor system status.
- To allow for system components inspection.
- To allow for system maintenance.
- To keep system in safe state in emergency.
- To provide confinement barrier for water coolant.
- To protect torus primary vacuum.

As in thermal blanket case, the thermal divertor block is included in AINA because our scope covers safety studies which intends to provide information for decision making to determine thermal wall profiles checking the integrity of DEMO in-vessel components (melting) and assessing the impurity source when a plasma perturbation or a LOCA takes place [68]. For this reason, a simplified but robust model that estimates the temperature profile evolution along the divertor is required.

2.2.4.2 General Architecture

As can be inferred from the previous section, the divertor design is not an easy task due to the many necessary requirements. For this reason, its architecture has been continuously updated during the last years. The initial design of a single divertor cassette was developed in 2014. This draft was essentially based on the ITER divertor cassette design as plotted in Figure 26. In 2015 the divertor configuration progressed deviating from the ITER design (Figure 27). In particular the size of the cassette has been reduced and a separate cooling loop for the plasma-facing components has been integrated. Compared to the first version, the revised cassette model is characterized by a reduced volume. Both outboard and inboard baffle parts have been removed from the cassette while the breeding blanket has been extended instead. For the time being the dome is not contained in the new CAD model for the sake of design simplification, but equipment of cassette with a dome is still considered as an option [73]. For this reason, the dome has not been modelled for AINA.

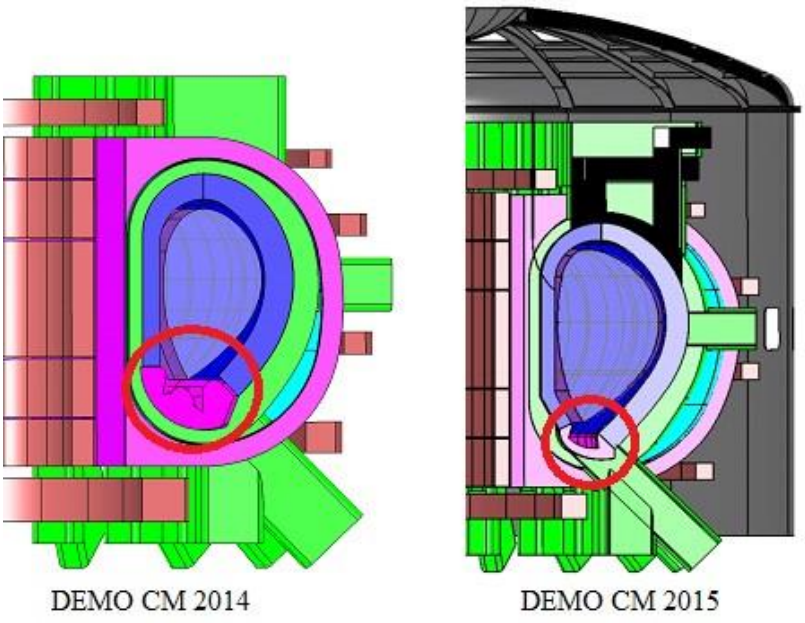

Figure 25: Divertor Configuration model 2014 vs 2015 [73].

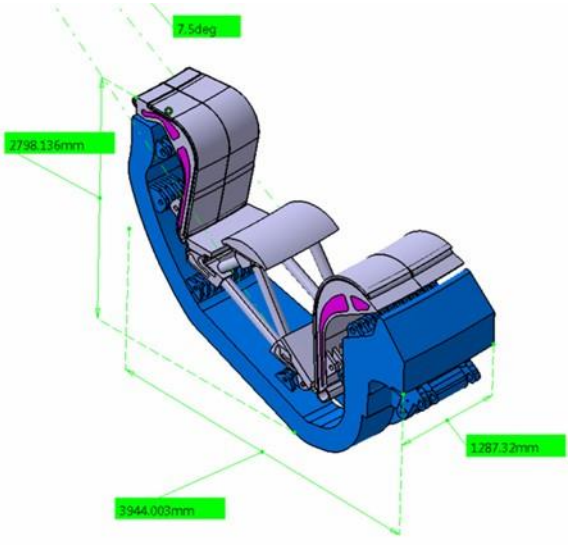

Figure 26: DEMO Divertor cassette 2014 design [73].

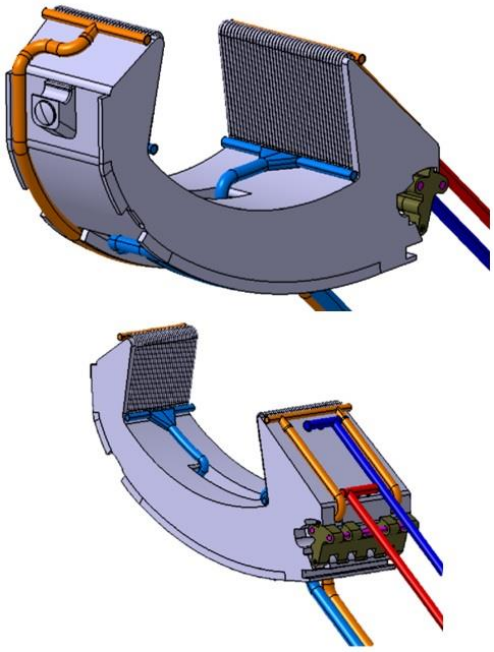

Figure 27: DEMO Divertor cassette 2015 design [74].

The divertor system includes 54 modules. Each divertor module includes the Cassette Body (CB) and the Plasma-Facing Components (PFCs) mounted on the CB, namely the inner vertical target (IVT), outer vertical target (OVT) and a possible dome [71]. The internal layout of the CB is shown in Figure 28. Each divertor CB is connected to the Tokamak Cooling Water System through two pair of radial pipes, one pair for cooling the CB and one pair for cooling the PFC [71]. It is composed by an upper plate, a lower plate, side ribs and internal toroidal and poloidal ribs [75]. The central poloidal rib separates the inlet and outlet coolant fluxes inside the cassette. Ribs thickness was reduced during 2016: 20 mm for internal ribs, 30 mm for cassette shell [74]. Moreover, a central opening is obtained between OVT and IVT to enable the pumping of the exhausted particles from the divertor private region. The opening area of pumping slot is 220 mm (horizontal) x 780 mm (vertical) [75].

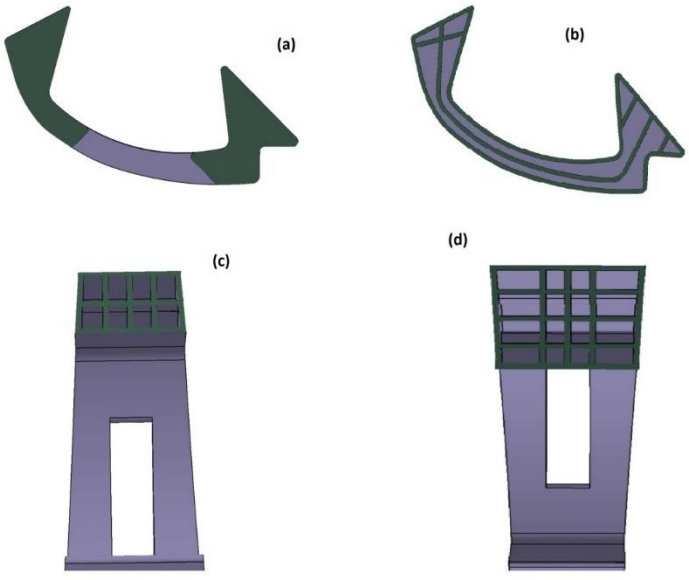

Figure 28: D Section views of the divertor cassette: (a) section on symmetry plane, (b) poloidal section showing toroidal ribs' profiles, (c) inboard toroidal section, (d) outboard toroidal section [75].

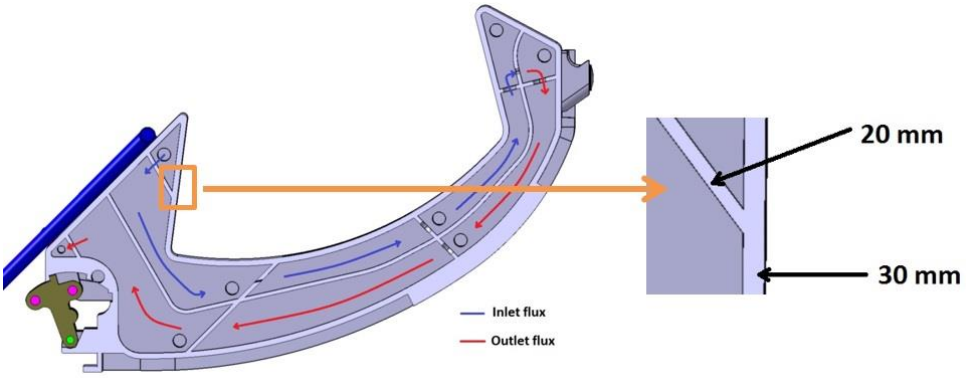

Figure 29: Ribs thickness [74].

he PFCs are cooled in parallel. The IVTs and OVTs are the PFCs that intercept the magnetic field lines, and therefore shall remove the high heat loads coming from plasma via conduction, convection and radiation during the steady state operation and slow transient events as well as during the off-normal events. The IVT has a dimension of ~ 0.6 m high x 0.75 m wide and the OVT has a dimension of ~ 0.65 m high x 0.9 m wide. They include several PFUs (Plasma Facing Units). The nominal toroidal gap between the neighboring PFUs is 0.5 mm. The PFU geometry is based on the so-called “monoblocks” concept, which consists of blocks with a drilled hole. Then, a pipe made of CuCrZr is inserted into these holes, and it is fixed to the blocks through a series of Cu interlayers. Each PFU consists of a W monoblock segment in the lower straight part and a curved W monoblock segment in the upper part. Each monoblock has an axial length of 4 mm (or 4.5 considering the gap) and a constant toroidal width of 23 mm both at OVT and IVT [71].

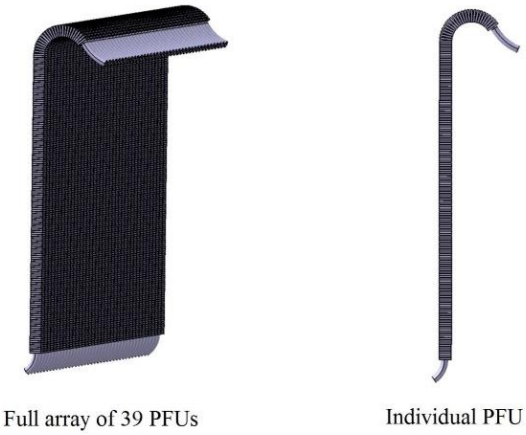

Figure 30: D 3D view of PFUs [71].

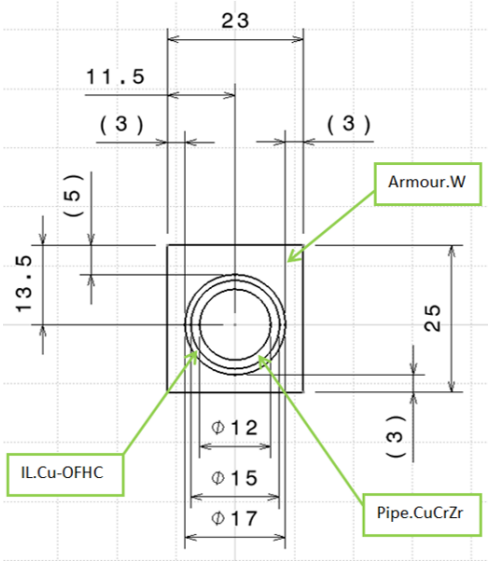

Figure 31: W-monoblock cross section [74].

Two different cooling circuits of water have been adopted as solution after several studies which were carried out to investigate the steady state thermal-hydraulic performances with different temperatures and pressures for CB and PFCs (≈ 300 °C with inlet pressure of 3.5 MPa for CB, ≈ 150 °C with inlet pressure of 5 MPa for PFCs [71][75][70][73][76]). This option is called WCDC (Water Cooled Divertor Cassette) and during 2015 three options were proposed as solution of this cooling layout [75] that are shown in the next two figures. Cooling Option 1 has been selected as the most promising one from the thermal-hydraulic standpoint, while Cooling Option 2, despite of its non-brilliant performances, has been considered as worthy of further investigation being the most interesting from the standpoint of design simplification [73][74]). In this configuration the vacuum pumping hole is crossed by two inlet pipe sections located in the middle of the hole. The inboard outlet feeding pipe goes along the whole CB to connect the inboard outlet manifolds located in the region between divertor and the Blanket [75].

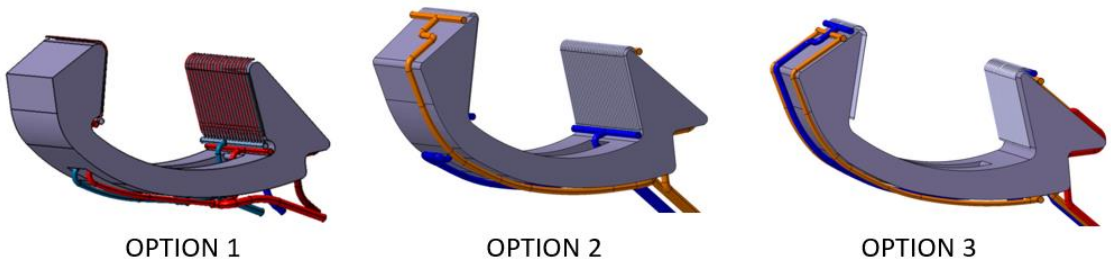

Figure 32: Layout cooling options 1, 2 and 3 [74].

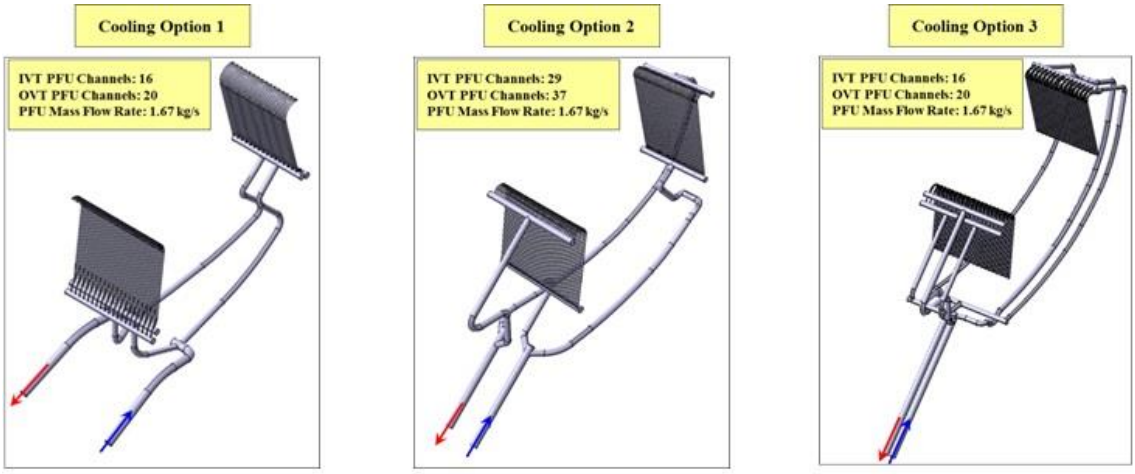

Figure 33: Layout cooling options 1, 2 and 3 [71][73].

2.2.4.3 Design divertor limits

The following material temperature melting limits are considered:

Material	Temperature Limit
Tungsten	3422°C [76]
Cooper	980°C [76]
CuCrZr	1050°C [77]
EUROFER	550°C [78][79]

Table 9: Material Temperature Limits.

Moreover, other limits must be considered and borne in mind as described by MEAP [80] and Domptail [76] documents:

- During normal plasma operations, allowable CuCrZr pipe temperatures are set by a lower bound of 150 °C to avoid loss of ductility caused by irradiation, and an upper bound of 300 °C to avoid excessive creep or irradiation softening (Rule 3).
- Tungsten temperature with a $10\ {}^{MW}/_{m^2}$ heat load was originally set to 1300 °C to avoid recrystallisation however the limit was increased to 1800 °C which allow a certain amount of recrystallisation.
- Since tungsten is a brittle material, the first principal stress is used to assess its integrity and is limited to 500 MPa which is about half its tensile strength at 300 °C. This temperature is the maximum that the tungsten reaches at its inner diameter, where the peak stress is found.
- Peak heat flux at fluid surface: This is the peak heat flux on the inner diameter of the CuCrZr pipe. For water at 150 °C, 5 MPa and 16 m/s the critical heat flux is $44.3\ {}^{MW}/_{m^2}$. Lowering this value is desirable and can be achieved by spreading the flux more evenly around the cooling pipe; this in turns lowers the stress levels.

2.2.4.4 Materials

In this chapter the material properties employed in the divertor model of the AINA DEMO code are hereinafter reported. When needed the properties have been interpolated. The EUROFER and Tungsten have already been introduced in the thermal blanket section.

2.2.4.4.1 Water

The estimation of the mass density ρ is based on the expressions extracted from the IAPWS Industrial formulation 1997 for the Thermodynamic Properties of Water and Steam, September 1997 document [81] which are used to calculate the specific volume. For the first region:

$$\frac{g(p,T)}{RT} = \gamma(\pi,\tau) = \sum_{i=1}^{34} n_i (7.1-\pi)^{I_i} (\tau - 1.222)^{J_i} \qquad (79)$$

$$\vartheta = \left({}^{\delta g}/_{dt}\right)_T \qquad (80)$$

$$\rho = {}^{1}/_{\vartheta} \qquad (81)$$

Where g is the specific Gibbs free energy, ϑ the specific volume, $\pi = {}^{p}/_{p^*}$ and $\tau = {}^{T}/_{T^*}$ with $p^* = 16.53$ MPa and $T^* = 1386$ K; $R = 0.461526\ KJ \cdot Kg^{-1} \cdot K^{-1}$. The coefficients n_i and exponents I_i and J_i are listed in the following table.

i	I_i	J_i	n_i	i	I_i	J_i	n_i
1	0	−2	0.146 329 712 131 67	18	2	3	$-0.441\,418\,453\,308\,46 \times 10^{-5}$
2	0	−1	−0.845 481 871 691 14	19	2	17	$-0.726\,949\,962\,975\,94 \times 10^{-15}$
3	0	0	$-0.375\,636\,036\,720\,40 \times 10^{1}$	20	3	−4	$-0.316\,796\,448\,450\,54 \times 10^{-4}$
4	0	1	$0.338\,551\,691\,683\,85 \times 10^{1}$	21	3	0	$-0.282\,707\,979\,853\,12 \times 10^{-5}$
5	0	2	−0.957 919 633 878 72	22	3	6	$-0.852\,051\,281\,201\,03 \times 10^{-9}$
6	0	3	0.157 720 385 132 28	23	4	−5	$-0.224\,252\,819\,080\,00 \times 10^{-5}$
7	0	4	$-0.166\,164\,171\,995\,01 \times 10^{-1}$	24	4	−2	$-0.651\,712\,228\,956\,01 \times 10^{-6}$
8	0	5	$0.812\,146\,299\,835\,68 \times 10^{-3}$	25	4	10	$-0.143\,417\,299\,379\,24 \times 10^{-12}$
9	1	−9	$0.283\,190\,801\,238\,04 \times 10^{-3}$	26	5	−8	$-0.405\,169\,968\,601\,17 \times 10^{-6}$
10	1	−7	$-0.607\,063\,015\,658\,74 \times 10^{-3}$	27	8	−11	$-0.127\,343\,017\,416\,41 \times 10^{-8}$
11	1	−1	$-0.189\,900\,682\,184\,19 \times 10^{-1}$	28	8	−6	$-0.174\,248\,712\,306\,34 \times 10^{-9}$
12	1	0	$-0.325\,297\,487\,705\,05 \times 10^{-1}$	29	21	−29	$-0.687\,621\,312\,955\,31 \times 10^{-18}$
13	1	1	$-0.218\,417\,171\,754\,14 \times 10^{-1}$	30	23	−31	$0.144\,783\,078\,285\,21 \times 10^{-19}$
14	1	3	$-0.528\,383\,579\,699\,30 \times 10^{-4}$	31	29	−38	$0.263\,357\,816\,627\,95 \times 10^{-22}$
15	2	−3	$-0.471\,843\,210\,732\,67 \times 10^{-3}$	32	30	−39	$-0.119\,476\,226\,400\,71 \times 10^{-22}$
16	2	0	$-0.300\,017\,807\,930\,26 \times 10^{-3}$	33	31	−40	$0.182\,280\,945\,814\,04 \times 10^{-23}$
17	2	1	$0.476\,613\,939\,069\,87 \times 10^{-4}$	34	32	−41	$-0.935\,370\,872\,924\,58 \times 10^{-25}$

Table 10: Numerical values of the coefficients and exponents of the dimensionless Gibbs free energy for region 1 [81].

The coefficient of dynamic viscosity, $\mu^{water}(T)$, is estimated by means of an interpolation using the values extracted from Table 8 of the Heat Exchanger Design Handbook (1986) document [82].

Table 5. Viscosity

P (bar)	t (°C) 0	25	50	75	100	150	200	250	300	350	375
1	1792	890.8	547.1	378.4	12.28	14.19	16.18	18.22	20.29	22.37	23.41
5	1791	890.7	547.1	378.5	282.4	182.0	16.07	18.15	20.25	22.35	23.39
10	1790	890.6	547.2	378.6	282.6	182.1	15.93	18.07	20.20	22.32	23.37
25	1786	890.3	547.5	379.0	283.0	182.5	133.9	17.83	20.06	22.24	23.32
50	1780	889.8	547.9	379.6	283.6	183.2	134.5	106.1	19.86	22.15	23.27
75	1775	889.3	548.3	380.2	284.3	183.8	135.1	106.8	19.74	22.13	23.28
100	1769	888.9	548.7	380.9	284.9	184.4	135.7	107.5	86.42	22.18	23.35
125	1764	888.5	549.1	381.5	285.6	185.1	136.3	108.2	87.40	22.39	23.52
150	1759	888.1	549.5	382.1	286.3	185.7	136.9	108.8	88.32	22.91	23.84
175	1754	887.7	550.0	382.7	286.9	186.3	137.5	109.5	89.21	66.85	24.45
200	1749	887.4	550.4	383.4	287.6	186.9	138.1	110.1	90.06	69.21	25.79
225	1744	887.1	550.9	384.0	288.2	187.6	138.7	110.7	90.88	71.10	47.65
250	1739	886.8	551.3	384.6	288.9	188.2	139.3	111.4	91.67	72.71	58.09
275	1735	886.6	551.8	385.2	289.5	188.8	139.9	112.0	92.43	74.14	61.87
300	1731	886.4	552.3	385.9	290.2	189.4	140.5	112.6	93.18	75.43	64.49
350	1722	886.0	553.3	387.2	291.5	190.6	141.6	113.8	94.61	77.71	68.31
400	1714	885.8	554.3	388.4	292.8	191.8	142.8	114.9	95.98	79.72	71.21
450	1707	885.6	555.3	389.7	294.2	193.1	143.9	116.1	97.28	81.52	73.61
500	1700	885.5	556.4	391.0	295.5	194.3	145.0	117.2	98.55	83.19	75.70
550	1694	885.6	557.5	392.3	296.8	195.5	146.1	118.3	99.76	84.73	77.57
600	1687	885.7	558.6	393.6	298.1	196.7	147.2	119.4	100.9	86.19	79.27
650	1682	885.9	559.7	395.0	299.4	197.9	148.3	120.4	102.1	87.57	80.85
700	1676	886.2	560.9	396.3	300.8	199.0	149.3	121.5	103.2	88.88	82.33
800	1667	887.1	563.3	399.0	303.4	201.4	151.5	123.5	105.4	91.35	85.05
900	1659	888.3	565.8	401.7	306.1	203.8	153.6	125.5	107.4	93.65	87.54
1000	1653	889.9	568.4	404.4	308.7	206.1	155.6	127.5	109.4	95.82	89.84

Table 11: Dynamic viscosity for water [82].

The coefficient of thermal conductivity, $k^{water}(T,p)$, is estimated by means of an interpolation using the values extracted from a website link [83].

The analytical procedure used to compute the heat transfer coefficient for the water is described hereinafter. Firstly, the mass flow rate, $\dot{m}$ $\left(\frac{kg}{s}\right)$, with a value equal to 1.67 [71][73] which has been used to compute the water coolant velocity, v $\left(\frac{m}{s}\right)$:

$$\dot{m} = \rho\, A\, v \qquad (82)$$

where A is the area of the cooling channels [m^2].

The Reynolds Number is:

$$Re_D = \frac{\rho\, v\, D}{\mu^{water}} \qquad (83)$$

where D is the coolant diameter for the circular pipes and the hydraulic diameter for the rectangular ones:

$$D_H = 4\frac{A}{P} \qquad (84)$$

where P is the wetted perimeter $[m^2]$.

The Prandlt number, Pr, is obtained by means of an interpolation using the values extracted from the next table of Heat Exchanger Design Handbook (1986) document [82].

Table 7. Prandtl number

P (bar)	t (°C)										
	0	25	50	75	100	150	200	250	300	350	375
1	13.50	6.137	3.555	2.378	1.000	0.974	0.960	0.950	0.941	0.932	0.928
5	13.48	6.133	3.553	2.377	1.753	1.151	0.984	0.964	0.950	0.939	0.934
10	13.46	6.128	3.551	2.377	1.752	1.150	1.028	0.987	0.965	0.949	0.942
25	13.39	6.113	3.546	2.374	1.751	1.150	0.903	1.096	1.021	0.982	0.969
50	13.27	6.088	3.538	2.371	1.750	1.149	0.902	0.825	1.173	1.057	1.025
75	13.15	6.063	3.529	2.367	1.748	1.148	0.900	0.821	1.466	1.162	1.098
100	13.04	6.039	3.521	2.364	1.746	1.147	0.899	0.817	0.890	1.312	1.191
125	12.93	6.015	3.513	2.360	1.744	1.146	0.897	0.813	0.874	1.545	1.314
150	12.83	5.992	3.505	2.357	1.743	1.145	0.896	0.810	0.860	2.006	1.484
175	12.73	5.970	3.497	2.354	1.741	1.145	0.895	0.806	0.848	1.379	1.753
200	12.63	5.947	3.490	2.350	1.740	1.144	0.894	0.803	0.837	1.216	2.353
225	12.53	5.926	3.482	2.347	1.738	1.143	0.892	0.800	0.827	1.121	8.125
250	12.43	5.904	3.475	2.344	1.736	1.142	0.891	0.798	0.818	1.057	1.937
275	12.34	5.883	3.467	2.341	1.735	1.142	0.890	0.795	0.810	1.009	1.485
300	12.25	5.863	3.460	2.338	1.733	1.141	0.889	0.793	0.803	0.973	1.291
350	12.08	5.823	3.446	2.332	1.731	1.140	0.887	0.788	0.790	0.919	1.103
400	11.92	5.785	3.433	2.326	1.728	1.138	0.885	0.784	0.779	0.880	1.005
450	11.77	5.748	3.420	2.321	1.725	1.137	0.883	0.780	0.769	0.850	0.943
500	11.62	5.713	3.407	2.315	1.723	1.136	0.882	0.777	0.761	0.827	0.899
550	11.48	5.680	3.395	2.310	1.721	1.135	0.880	0.773	0.753	0.807	0.866
600	11.36	5.648	3.384	2.305	1.718	1.134	0.879	0.770	0.747	0.791	0.840
650	11.23	5.617	3.372	2.301	1.716	1.134	0.878	0.768	0.741	0.777	0.818
700	11.12	5.588	3.362	2.296	1.714	1.133	0.876	0.765	0.735	0.765	0.800
800	10.91	5.533	3.342	2.288	1.711	1.131	0.874	0.761	0.726	0.745	0.772
900	10.72	5.483	3.324	2.280	1.707	1.130	0.872	0.757	0.718	0.730	0.750
1000	10.55	5.439	3.307	2.273	1.704	1.129	0.870	0.753	0.712	0.717	0.733

Table 12: Prandlt number for the water [82].

Depending on the Reynold Number the Nusselt No. has been obtained in two different ways:

- Laminar Flow: Re_D<3000

  According to Incropera [62] and assuming a constant heat flux along the pipe length and channel dimension ratio a/b equal to 1 for the CB pipes, the Nu_d is set to 3.61. For the circular pipes of the PFC the value is 4.36.

- Turbulent Flow: Re_D≥ 3000

  Following the Gnielinski correlation [59][63][84]:

$$Nu_D = \frac{\frac{f}{8}(Re_D - 1000)Pr}{1 + 12.7\sqrt{f/8}(Pr^{2/3} - 1)} \qquad (85)$$

where the Darcy-Weisbach friction factor can be approximated as [64][59]:

$$f = (0.79\ln(Re_D) - 1.64)^{-2} \qquad (86)$$

Finally, the water heat transfer coefficient for each cooling channel is computed as [64]:

$$h = \frac{Nu_D \cdot k}{D} \qquad (87)$$

2.2.4.4.2 Cooper

The material properties of the cooper are taken from the ITER Materials Properties Handbook [85][86].

OFHC Copper						
Properties obtained from the ITER Materials Handbook 2004, ITER document number G 74 MA 16 04-05-07 R0.2						
Temperature (C)	Coefficient of Thermal Expansion (C^-1)	Temperature (C)	Young's Modulus (Pa)	Poisson's Ratio	Temperature (C)	Thermal Conductivity (W m^-1 C^-1)
20	1.69E-05	20	1.17E+11	0.330	20	401.00
50	1.70E-05	50	1.16E+11	0.330	50	399.00
100	1.72E-05	100	1.14E+11	0.330	100	395.00
150	1.74E-05	150	1.12E+11	0.330	150	392.00
200	1.77E-05	200	1.10E+11	0.330	200	388.00
250	1.81E-05	250	1.08E+11	0.330	250	385.00
300	1.84E-05	300	1.05E+11	0.330	300	382.00
350	1.88E-05	350	1.02E+11	0.330	350	378.00
400	1.92E-05	400	9.80E+10	0.330	400	375.00
450	1.97E-05				450	371.00
500	2.01E-05				500	368.00
550	2.06E-05				550	364.00
600	2.11E-05				600	361.00
650	2.16E-05				650	358.00
700	2.22E-05				700	354.00
750	2.27E-05				750	351.00
800	2.33E-05				800	347.00
850	2.39E-05				850	344.00
900	2.45E-05				900	341.00
					950	337.00
					1000	334.00

Table 13: Thermomechanical properties of Cooper [85][86].

2.2.4.4.3 CuCrZr

The material properties of the CuCrZr are taken from the ITER Materials Properties Handbook [85][86].

CuCrZr						
Properties obtained for the solution annealed, water quenched and aged material, from the ITER Materials Handbook 2004, ITER document number G 74 MA16 04-02-04 W0.1						
Temperature (C)	Coefficient of Thermal Expansion (C^-1)	Temperature (C)	Young's Modulus (Pa)	Poisson's Ratio	Temperature (C)	Thermal Conductivity (W m^-1 C^-1)
0	1.55E-05	0	1.29E+11	0.340	0	383.26
50	1.59E-05	50	1.27E+11	0.340	50	373.31
100	1.63E-05	100	1.25E+11	0.340	100	365.40
150	1.67E-05	150	1.23E+11	0.340	150	359.36
200	1.70E-05	200	1.21E+11	0.340	200	355.05
250	1.73E-05	250	1.18E+11	0.340	250	352.31
300	1.76E-05	300	1.15E+11	0.340	300	350.97
350	1.79E-05	350	1.12E+11	0.340	350	350.89
400	1.82E-05	400	1.09E+11	0.340	400	351.91
450	1.84E-05	450	1.05E+11	0.340	450	353.88
500	1.86E-05	500	1.02E+11	0.340	500	356.63

Table 14: Thermomechanical properties of CuCrZr [85][86].

2.2.4.5 AINA Divertor Model

As in the BB model [2], in order to obtain the distribution and evolution of temperatures, a one-dimensional model is derived from the three-dimensional divertor design assuming strong simplifications. Once again, it is worth highlighting that these routines do not aim to substitute the three-dimensional CFD studies; however, they can be a great tool for AINA, provided that the conservatism of their outcomes is demonstrated using the results obtained from analyses done by Eurofusion. The AINA

thermal models solver used for BB as well as divertor has been discussed in chapter "Thermal Blanket Block Assembly". This one-dimensional model for the divertor is described in the next section.

2.2.4.5.1 Model Description

As in the BB where the module that suffers the maximum load (OB4) is the blanket region modelled, the one dimensional segment modelled as representative of the divertor will be the most demanded. Assuming that the PFCs are cooled in parallel and the IVTs and OVTs intercept the magnetic field lines, and therefore shall remove the high heat loads coming from plasma via conduction, convection and radiation during the steady state operation and slow transient events as well as during the off-normal events [71], the modelled segment must cross these PFCs, not directly the CB. Moreover, at the IVT strike point local heat flux value can be roughly assumed to be $^1/_2$ that of OVT [74]. Therefore, a segmentation along the OVT and crossing CB was selected. As shown previously, the OVT is a tiled surface in contact with plasma, and a heat sink interlayer made of cooper and CuCrZr with coolant tube inside and the CB has also coolant sections in parallel to the surface. In conclusion, the resulting material layers, the thicknesses and the nodalization assumed are described in the next table and it is based on the truncation error and model discretization method exposed by Fabbri [2] in order to couch a realistic variation of the response functions as the temperature distributions and ensuring an acceptable computational time by means of the refinement of the model nodal mesh fixing time discretization (Δt=0.02 s). Contrary to HCPB blanket, in this case is not necessary scaling factors to compensate unrealistic results.

Layer No.	Material	Thickness [mm]	No. Nodes
1	Tungsten	5	500
2	Cooper	1	500
3	CuCrZr	1.5	500
4	Water Coolant	12	1
5	CuCrZr	1.5	500
6	Cooper	1	500
7	Tungsten	3	500
8	EUROFER	30	500
9	Water Coolant	70	1
10	EUROFER	20	500
11	Water Coolant	70	1
12	EUROFER	20	500
13	Water Coolant	70	1
14	EUROFER	20	500
15	Water Coolant	70	1
16	EUROFER	30	500

Table 15: Material type and thickness for the divertor model.

The following considerations have in particular been taken into account:

- The thickness of the CB water coolant layers (70 mm) have been set to be conservative due its value varies depending on at what height of the OVT is modeled.
- The water coolant layers assumes an f_{COOL}, the coolant surface for the in line tube which is equal to the relative surface of the coolant tubes to the total surface of the module section, equal to 0.54 [87].
- The remaining layers are modeled directly from the design.

2.2.4.5.2 Numerical model

The numerical model is the same as used in the thermal blanket block and based on the research carried out by Marco Fabbri during his thesis development [2]. Likewise, the steady state and transient approaches follow the same structure; for this reason, the necessary boundary conditions and the nuclear heat deposition are presented in the following sections.

2.2.4.5.3 Boundary conditions

- **PFC (OVT and IVT) water coolant channels**: For the PFC water coolant pipes a temperature of 150 ºC , a pressure equal to 5 MPa and a mass flow rate equal to 1.67 kg/s have been assumed [75][70][71][73][76].
- **CB water coolant channels**: For the CB water coolant pipes a temperature of 300 ºC , a pressure equal to 3.5 MPa and a mass flow rate equal to 1.67 kg/s have been assumed [75][70][71][73][76].
- **Last node**: this node represents the back plate Robin BC are assumed: a heat transfer coefficient of $1000\,\frac{W}{m^2}/K$ with a bulk temperature of 200 ºC [74].
- **First node**: in the first node a total load due to the radiation effect against the wall is applied.
- **Heat Load**: As the next section shows the previous checking data analyses has been adapted scaling proportionally them to a NWL of $0.68\,{}^{MW}/_{m^2}$ against the top of the OVT corresponding to an scenario of 2037 MW of fusion power corresponding to $7.232 \cdot 10^{20}\,{}^{n}/_{s}$ [88][87][74] as shown in the following figure has been set. Moreover, other studies with a NWL of $10\,{}^{MW}/_{m^2}$ and $20\,{}^{MW}/_{m^2}$ have been carried out to complete the validation [89][76].

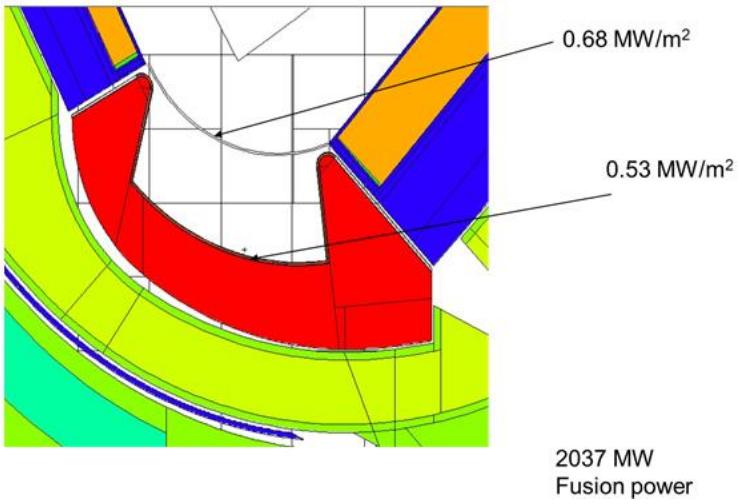

Figure 34: Neutron wall loading in divertor zone [87].

2.2.4.5.4 Nuclear Heat Deposition

At the time of the study, no official nuclear heat data was available for the divertor baseline. For this reason as done in blanket case, three different 3D models with a NWL of $0.68\,{}^{MW}/_{m^2}$ applied have been compared to procure a reasonable approach of the nuclear heat distribution along a one-dimensional representative segment across the OVT and the CB. The three models are shown in the folloeing figures; in addition, the nuclear heat distribution along a one-dimensional representative segment across the OVT and the CB for every model approved after an experts consensus is displayed the fourth figure.

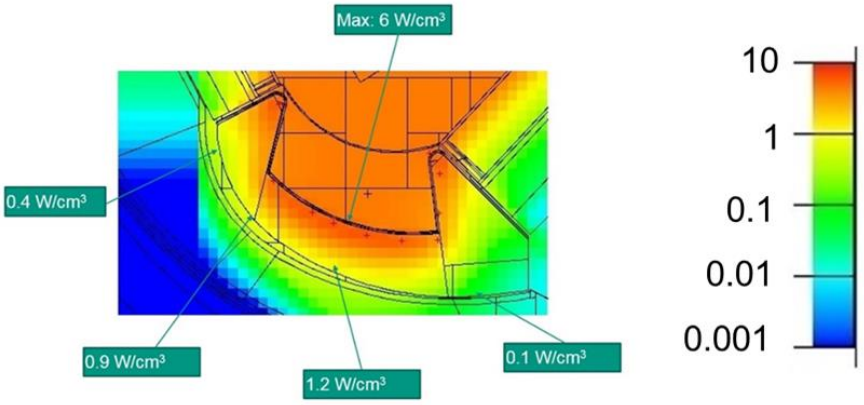

Figure 35: Nuclear thermal power density on divertor [87][70].

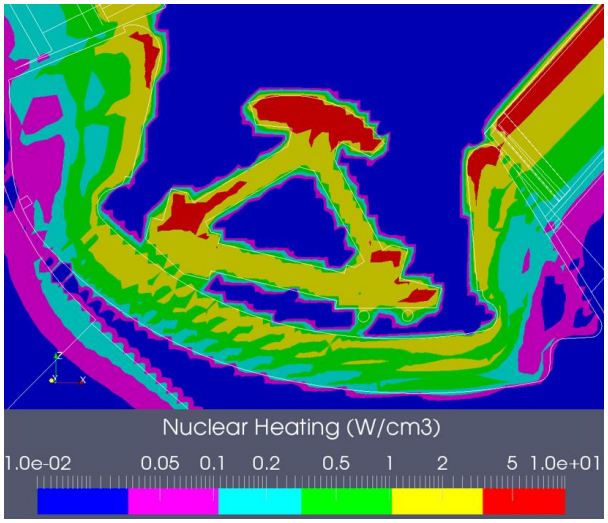

Figure 36: Nuclear thermal power density on divertor [88].

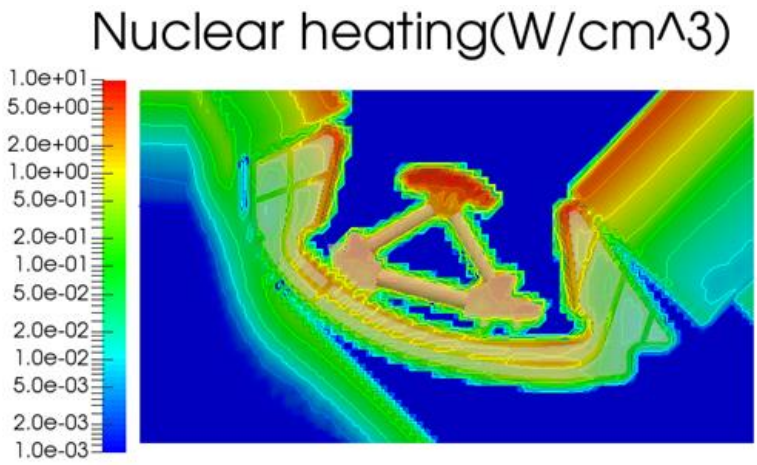

Figure 37: Nuclear thermal power density on Divertor [74].

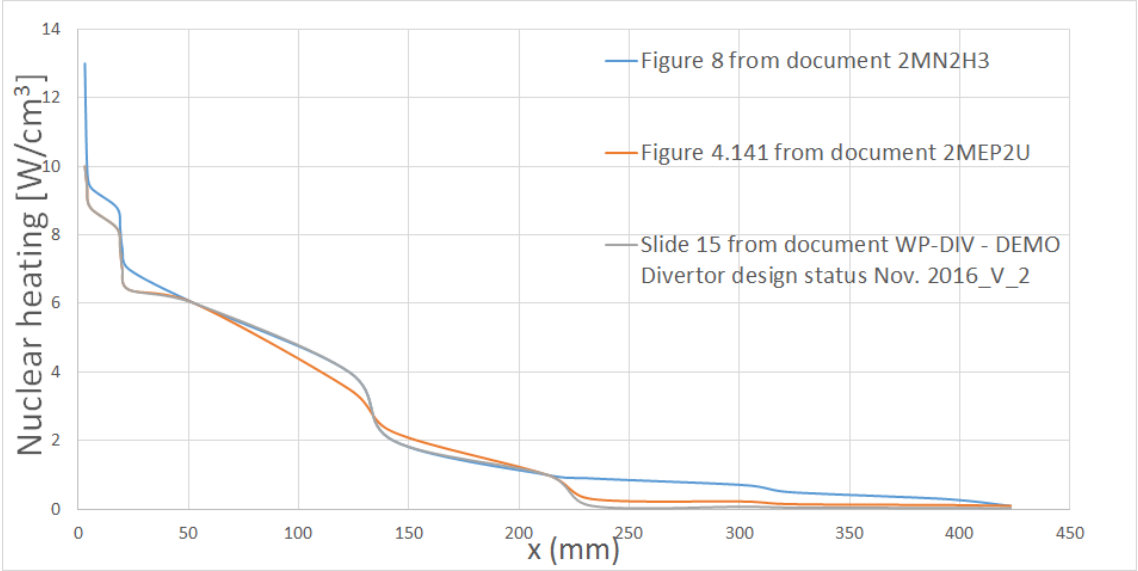

Figure 38: Nuclear heat distribution 1D for every model.

Finally, after an expert consensus and the thermal hydraulic analyses that follows in the next section, the nuclear distribution accepted is composed of the highest values between the three models for the OVT layers and average values for the CB layers. These considerations have been taken up due to it is desirable to be conservative to estimate the divertor surface temperature which lays down the impurity production and for the CB the conservatism have already been assumed with the thickness of its water coolant regions. The final distribution is shown in the next figure:

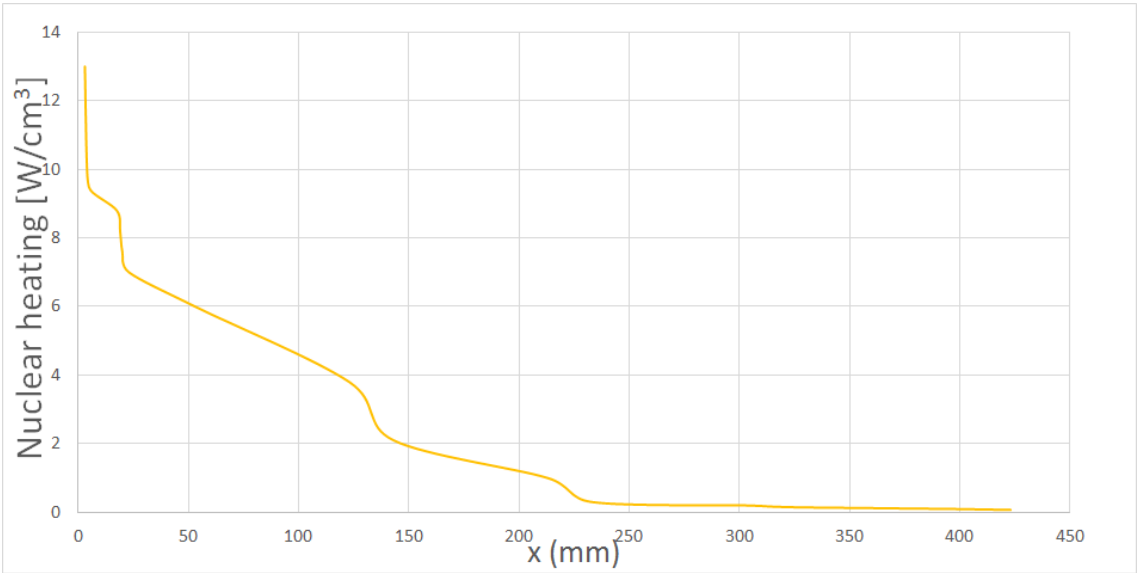

Figure 39: Final nuclear heat distribution 1D.

2.2.4.5.5 Thermal divertor block assembly

Finally, the linkage between the thermal divertor block and the rest of the AINA blocks following the thermal blanket block methodology has been implemented applying and being taken into account the following considerations:

- To obtain the temperature distribution in the poloidal direction of the divertor for every simulation time step, just an unique divertor region is assumed and its associated load flux

against the wall $NWL + P_{rad}$ $\left[MW/m^2\right]$ is considered. In this way, the thermal divertor block is an approach, acceptable from the point of view of impurity production since an average surface temperature is reached over all the divertor wall; however, it will be careful with the material temperature limits because the one-dimensional model is not absolutely conservative along the radial segment.

- As in thermal blanket block, the transient simulation will not stop even though a temperature limit is exceeded although, eventually, a notification will appear if this event takes place.
- With the goal of optimizing the processing time, if the boundary condition does not vary significantly (four significant digits $\left[MW/m^2\right]$) it is not necessary to execute the thermal solver since the temperature profile remains constant.
- The code allows to plot the temperature profile along the one-dimensional segment.

2.2.5 Plasma Wall Interaction block

The plasma wall interaction block implemented in AINA is focused on two aspects:

- Estimation of the loads (P_{rad} and NWL) for the thermal equilibrium calculation.
- Estimation of the impurity fluxes to the plasma core for the plasma mass and energy balance.

2.2.5.1 Wall loads

The neutron wall load is used to scale the nuclear heating distribution in the thermal blocks. Its average value is calculated as:

$$NWL_{Ave} = \frac{S_\alpha \cdot \langle \sigma v \rangle_{DT} \cdot E_n}{S_{wall}} \cdot F_{mult\_BB} \qquad (88)$$

where E_n is the mean energy of neutrons and S_{wall} is the surface of the wall (FW and Divertor). F_{mult_BB} is a multiplication factor embedded due to the incident NWL power will be "multiplied" in the Breeder Blankets, this power multiplication is 1.37, which is a typical value for solid breeder blankets and which has been assumed as a first approximation as well for the initial exploratory studies [59]. The NWL distribution for every module of the wall is derived from the Table 4.6 of the document by Hernandez et a [59].

On the other hand, the radiative heat flux is used as a boundary condition in the first node of the thermal blocks. Its total value is estimated as [37]:

$$P_{rad} = RWL + RDL - \dot{q}_{RadiationReflection} - \dot{q}_{erosion} \qquad (89)$$

In this first milestone, the $\dot{q}_{RadiationReflection}$, radiation reflected for every module of the blanket, and the $\dot{q}_{erosion}$, flux emitted due to due to impurity flux leaving the wall have not been implemented yet. With no $\dot{q}_{erosion}$ consideration, the calculation is more conservative, moreover the $\dot{q}_{RadiationReflection}$ is annulled for the global estimation. Despite this, efforts must be made to implement these models for the future analyses. Its distribution for every module of the wall is derived from the Table 5.2 of the document by Hernandez et a [59].

The RWL_{Ave} is the average radiation load on the first wall, its distribution for every module of the wall is derived from the Table 5.2 of the document by Hernandez et a [59] and its calculation is made using the following expression [37]:

$$RWL_{Ave} = \frac{P_{Br} + P_{sy} + P_{li} + P_{edge}}{S_{wall}} + \frac{P_{\alpha} \cdot 2 \cdot fripple}{S_{wall}} \qquad (90)$$

The RDL_{Ave} is the radiation load on the Divertor and its calculation is made using the following expression [37]:

$$RDL_{Ave} = \frac{P_{SOL} - P_{edge} - P_{div\_rad}}{S_{wall}} \qquad (91)$$

where [52]:

$$P_{SOL} = P_{ext} + P_{\alpha} - P_{Br} - P_{sy} - P_{li} \qquad (92)$$

And P_{div_rad} is the radiation from the divertor region [52] and due to it is not possible to estimate this magnitude, AINA estimates RDL_{Ave} using the following lineal regression [90]:

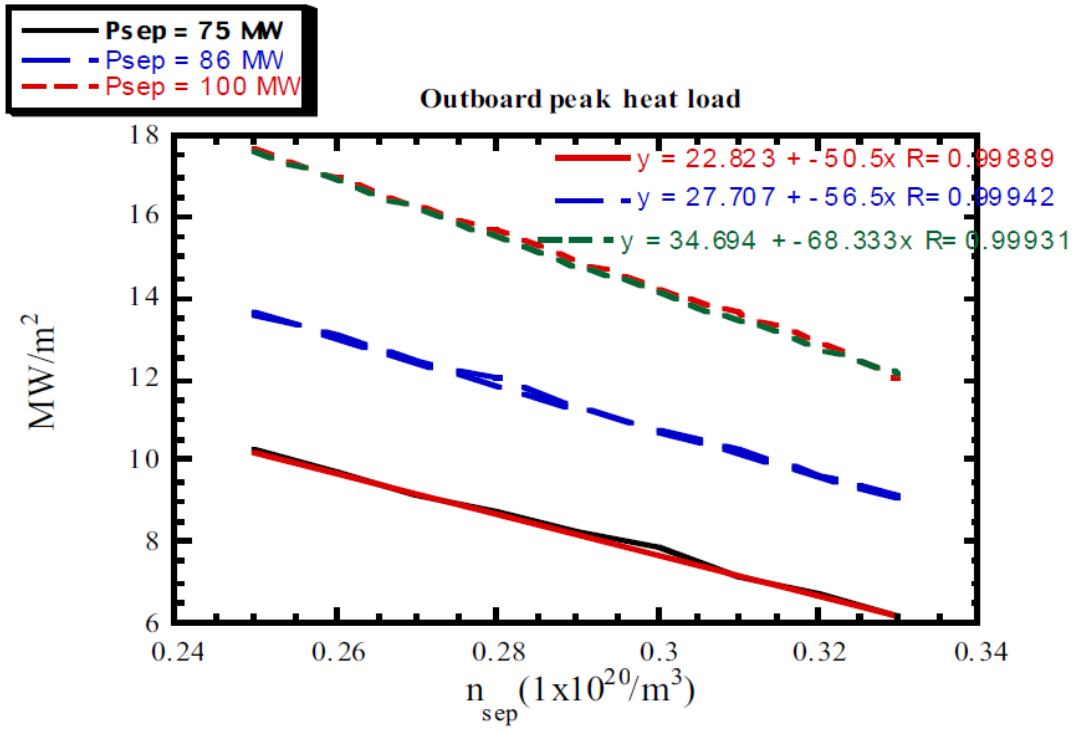

Figure 40: Divertor target heat load [90].

If this value is unduly low ($< 1e^{-10}$), it is desirable to assume:

$$RDL_{Ave} = \frac{P_{SOL} - P_{edge}}{S_{wall}} \qquad (93)$$

Moreover, if the estimation of the radiation load on the Divertor results in a negative value, its value will be null in order to be conservative.

2.2.5.2 Impurity sources

The PFCs (Plasma Facing Components) of the FW (First Wall) and the divertor are designed to withstand severe conditions such as high temperatures, radiation and particle fluxes which degrade and erode the PFC tiles. Moreover, these erosion processes cool the plasma due to Bremsstrahlung and Line radiation

emitted by the eroded impurities [91]. In this sense, erosion processes have another benefit, impurities inside the plasma can shut down the fusion, becoming a passive safety mechanism, for example, when a LOCA takes place since the overheating of the wall increases the impurity production. Furthermore, some impurities, as impurity seeding gases or plasma enhancement gases (PEGs), for example Xenon or Argon; can affect positively the fusion power plant as well since these species allow a significant proportion of heat to be isotropically radiated, via Line radiation, which would otherwise be incident on the PFCs (in this way, a part of this heat flux is not focused on the strike point of the divertor) and, in addition, improve the confinement time of the plasma [92].

2.2.5.2.1 Description model

It is important to note that the operational states fixed for DEMO (DEMO1 and DEMO2 [11][12]) just assume the presence of two impurity species: Xenon (Xe) and Tungsten (W). The behaviour and the presence of these species inside the plasma core will be governed by the following assumptions:

- **Regarding Xenon**: a constant fraction of Xenon is desired inside the plasma core.
- **Regarding Tungsten**: its production model is composed by two main sources:
  - *Thermal Sublimation*: it is a mechanism of impurity emission from PFCs due to thermal vaporization that only depends on PFC temperature [39].
  - *Physical Sputtering*: this process is due to elastic energy transfer from incident particles to target atoms. Surface atoms can be ejected if they receive enough energy to overcome the surface binding energy [93]. It depends only the ion or neutral fluxes which reach the PFC surface and their corresponding energy.

Other erosion sources, have been historically considered in AINA; however, for DEMO, chemical erosion is not included since for Tungsten would be also possible only if Oxygen was present [94]. Something similar occurs for Radiation Enhanced Sublimation source that it is a process unique for Carbon [93][95]. Finally, as showed in Figure 41, it is important to remember that the assumptions adopted are useful to model a simplified version from a more complex scenario composed of many several processes.

It is necessary to note that extreme power loads due to disruptions and Edge Localized Modes (ELMs) can lead to severe melting [96]. This process is not purely modelled but it is under consideration by means of temperature melting limits included in the thermal blanket block of AINA.

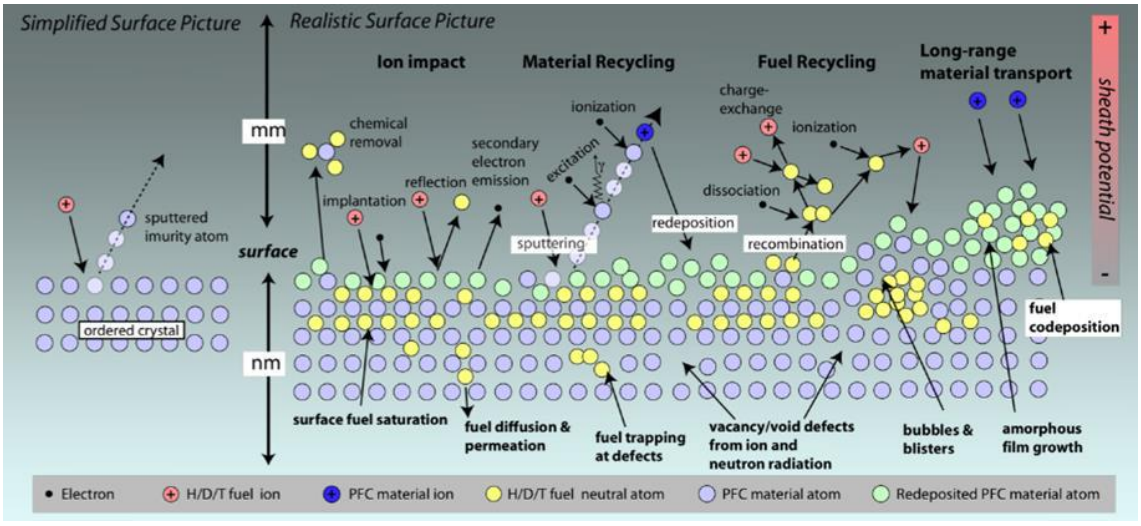

Figure 41: Simplified and realistic model of the processes which take place by Plasma-Wall interactions [97].

2.2.5.2.1.1 Thermal sublimation

As mentioned above, thermal sublimation source is calculated as a function of the PFC temperature by means of the following model exposed by Uckan [52]:

$$\Gamma_{Subli_i} = \frac{2.6 \cdot 10^{14}}{\sqrt{M_i \cdot T}} 10^{\frac{B_i - A_i}{T}} \qquad (94)$$

Where T is the PFC surface temperature in $[K]$, M_i is the atomic mass of the PFC material in $^{g}/_{mol}$, A_i and B_i are fixed coefficients. In the case of Tungsten:

$$[M_i, A_i, B_i] = [183.8, 44485, 12.74]$$

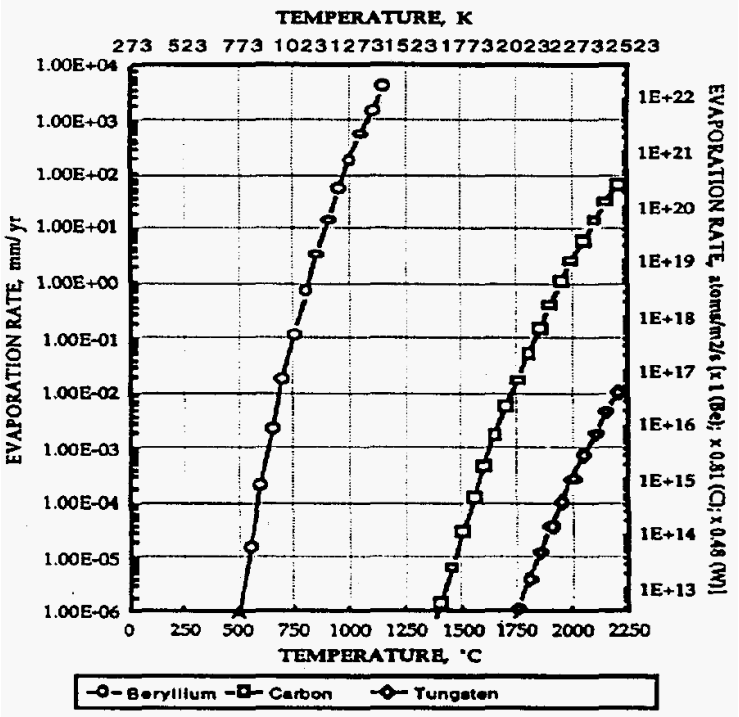

Figure 42: Thermal sublimation data $\left[^{mm}/_{year} \text{ or } ^{atoms}/_{m^2 \cdot s}\right]$ for Be, C, and W as a function of the target T [52].

2.2.5.2.1.2 Physical Sputtering

As previously stated, the sputtering process can be described as a momentum transport in a collision cascade initiated by the incident particle in the surface layer of the solid. A surface atom is ejected if its energy is higher than the surface binding energy [98]. The physical sputtering model used in AINA is based on empirical formulas where the sputtering yield is described as a function of the projectile energy (E_0) at normal incidence. This model was formulated by Bohdansky in 1984 [99] and improved by Wilson [100][101]:

$$Y_{PhysSput}(E_0) = Q \cdot S_n \cdot \left(1 - \left(\frac{E_{th}}{E_0}\right)^{2/3}\right) \cdot \left(1 - \frac{E_{th}}{E_0}\right)^2 \qquad (95)$$

Where E_0 is the projectile energy in [eV], S_n is the nuclear stopping cross section:

$$S_n(\varepsilon) = \frac{0.5 \cdot ln(1 + 1.2288\varepsilon)}{\varepsilon + 0.1728\varepsilon^{1/2} + 0.008\varepsilon^{0.01504}} \qquad (96)$$

ε is the reduced energy:

$$\varepsilon = \frac{E_0}{E_{TF}} \qquad (97)$$

E_{th} is the threshold energy [eV]:

$$E_{th} = E_s \cdot \left[7 \cdot \left(\frac{M_2}{M_1}\right)^{-0.54} + 0.15 \cdot \left(\frac{M_2}{M_1}\right)^{1.12}\right] \qquad (98)$$

M_1 and M_2 are the masses of the projectile and the target atom, respectively; and E_s is the surface binding energy [eV]:

$$E_s = \frac{HEVA \cdot M_2}{Avogadro \cdot e} \qquad (99)$$

Where $HEVA$ is the heat of evaporation $[J/g]$, $Avogadro$ is $6.0221367e^{23}[particles/mol]$ and e is $1.602176462e^{-19}$.

Q is a fitting parameter estimated as:

$$Q = 1.633 \cdot E_s^{-2/3} \cdot (Z_1 \cdot Z_2)^{2/3} \cdot \left(Z_1^{2/3} \cdot Z_2^{2/3}\right)^{1/3} \cdot \frac{M_1^{5/6} \cdot M_2^{1/6}}{M_1 + M_2} \cdot \frac{0.15 + 0.05 \cdot \frac{M_2}{M_1}}{1 + 0.05 \cdot \left(\frac{M_2}{M_1}\right)^{1/6}} \qquad (100)$$

Where Z_1 and Z_2 are the atomic numbers of the projectile and the target atom, respectively; and, finally, E_{TF} is the Thomas-Fermi energy [eV]:

$$E_{TF} = 30.74 \cdot \frac{M_1 + M_2}{M_2} \cdot Z_1 \cdot Z_2 \cdot \left(Z_1^{2/3} + Z_2^{2/3}\right)^{1/2} \qquad (101)$$

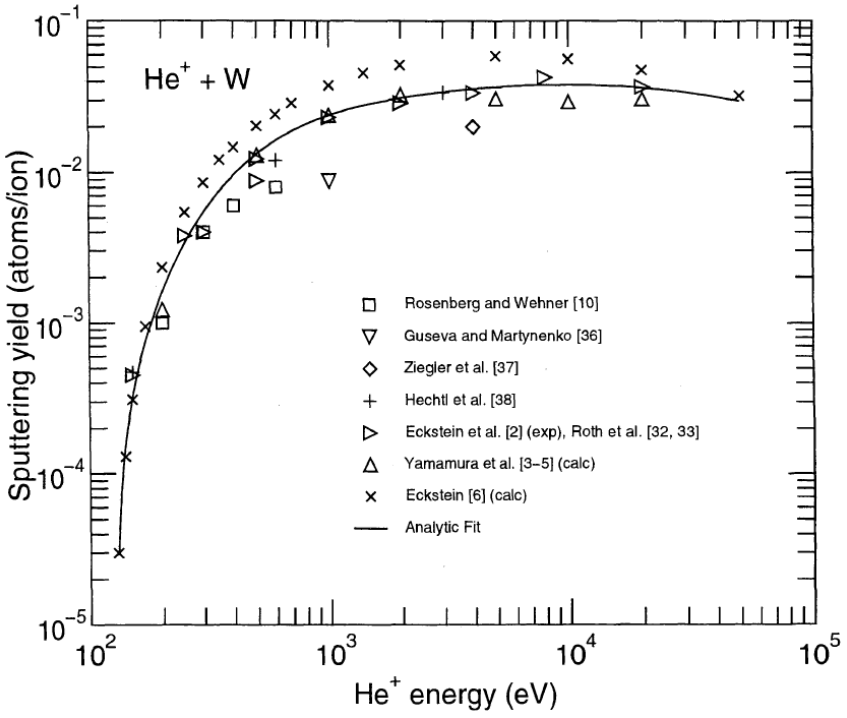

Figure 43: Energy dependence of the Tungsten self-sputtering yield when Helium ions are incident [94].

Eventually, as the sublimation model, it is necessary to get the impurity flux from the physical sputtering process. Hence, the final expression modeled is:

$$\Gamma_{PhysSput} = Y_{PhysSput} \cdot \Gamma_{incident\ ions\ or\ neutral\ particles} \qquad (102)$$

Where $\Gamma_{incident\ ions\ or\ neutral\ particles}$ is the ions or neutral particles flux against the PFC $\left[\frac{incident\ ions\ or\ neutral\ particles}{m^2 \cdot s}\right]$.

To sum up, the total impurity generation is:

$$\Gamma_{Total} = \Gamma_{PhysSput} + \Gamma_{Subli} \qquad (103)$$

2.2.5.2.1.3 Transport model

The final aim is to use real impurities sources on the mass balance of the plasma block. Thus, first of all, it is necessary to adapt the impurity generation data as follows:

$$S_{Geeration\ Z_i} = \Gamma_{Total_{Z_i}} \cdot \frac{Sup_{PFC}}{V_{plasma}} \qquad (104)$$

Where Sup_{PFC} is the PFC surface $[m^2]$ and V_{plasma} is the plasma volume $[m^3]$.

However, as historically several experiments and documents have introduced, not all the impurity generation reach the core plasma and a major fraction of the eroded Tungsten migrates predominantly through direct transport channels in the outer plasma scrape-off layer without entering the confined plasma [37][39][52][102][103]. This phenomena is related through a complicated transport process, involving ionization of the atoms, their streaming along magnetic field lines, and their diffusion perpendicular to the field lines [52]. Therefore AINA uses a screening factor which is calculated for the steady state estimation to fit the impurity content of plasma in reference scenarios: DEMO1 and DEMO2 [11][12]; and this factor remains constant during transient simulations. It is also important to highlight the checking suffered for this value which is compared with historical estimations carried out. A transport probability of 10^{-3} means that 1 out of 1000 particles leaving the wall will enter the core plasma was assumed by Uckan [39]. From experimental results [104][105][106] it is possible to assume that a probability of a Beryllium atom produced at the wall to penetrate into the main plasma is in the range of 0.1 to 0.01. A similar probability for a Beryllium atom produced at the divertor neutralizer plate to penetrate into the main plasma is in the range of 10^{-2} to 10^{-3}. Moreover, from ASDEX experiments [102][103] it is acceptable that the dominance of W migration paths in the edge plasma can be explained by the comparatively short ionization length of eroded tungsten atoms, which leads to a good shielding by the edge plasma and is in agreement with spectroscopic measurements of Tungsten penetration probability in the range of 1%. Taking all these reference into account, it is appropriate to conclude that the screening factor adapted by AINA must be within a range between [0.1% - 10%].

On the other hand, a time delay of transport should be considered since the impurities do not reach the plasma core instantly. It is known that a laser ablation experiment [107][108][109] shows a fast transport of impurities into the plasma. Therefore, a time delay of one energy confinement time could be judged as conservative from a safety point of view [39].

$$S_{Z_i}(t) = C_{screen_{Z_i}} \cdot \left(t - \tau_{E,e}\right) \qquad (105)$$

Where S_{Z_i} is the impurity i source $\left[\frac{atoms}{m^3 \cdot s}\right]$, $C_{screen_{Z_i}}$ is the screening factor for the impurity i and $\tau_{E,e}$ is the energy confinement time [s].

In spite of the accepted assumptions introduced above, scanning analyses will be carried out when the transients are simulated with the goal of understanding how a variation of the screening factor or the transport time delay could affect the evolution of the behavior plasma.

2.2.5.2.1.4 Inputs Data for the Physical Sputtering Model

As stated earlier ion fluxes, neutral particle fluxes and their corresponding energies on the surface of the PFCs are necessary to calculate the erosion on it. Nowadays, there are no sufficient documents and information for DEMO. For this reason, an extrapolation from ITER values have been carried out.

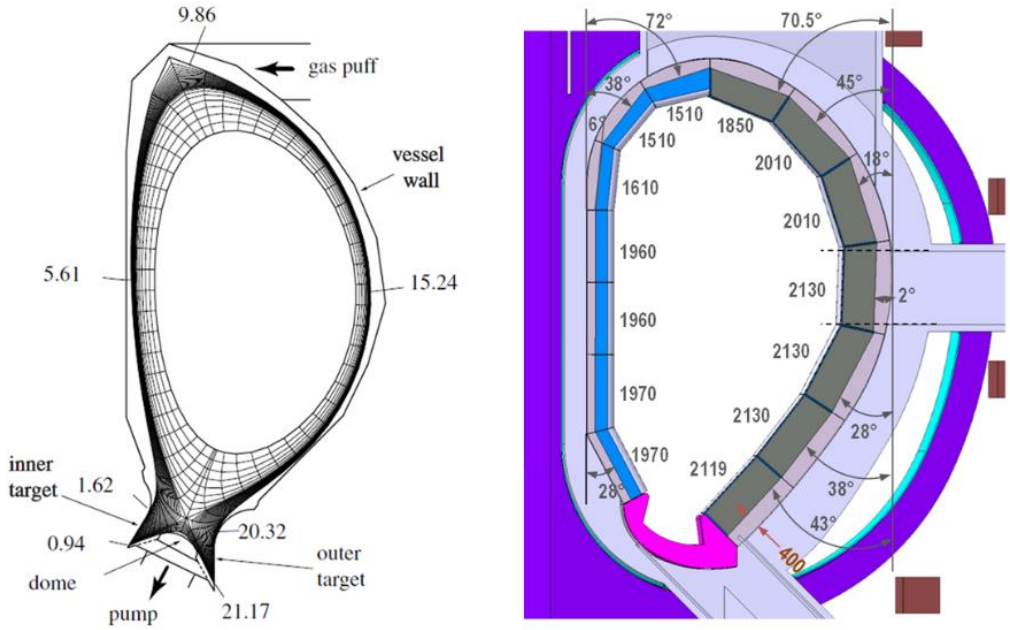

Figure 44: ITER design modeled for the document from which extrapolate data (left) [110] **and DEMO configuration used in the current version of AINA (right)** [59]**.**

The following table shows a central point for each poloidal section of DEMO which has been fixed based on the ITER configuration.

Section	Central point (m)
OB1	11.4
OB2	12.6
OB3	14
OB4	15.24
OB5	17
OB6	18.4
OB7	19.8
IB1	2
IB2	3.3
IB3	4.61
IB4	6.6
IB5	8
IB6	9.4
IB7	10.2
Divertor	0

Table 16: Central point for each poloidal section of DEMO based on the ITER configuration.

The data used is extracted from the Behrisch, Federici, Kukushkin and Reiter document [110]. The graphs used are shown in the next figure.

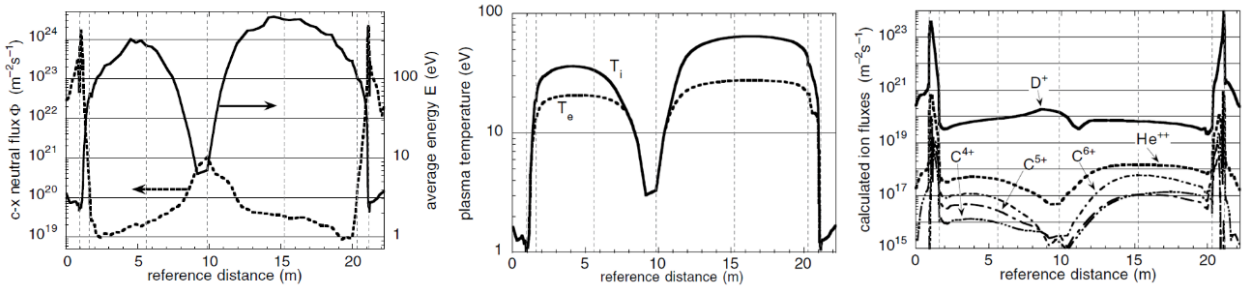

Figure 45: Calculated profile of the total neutral flux and of their mean energy along edge (left), profiles of ion and electron temperatures along the edge (center) and calculated profiles of the total flux of the various ions onto the vessel walls (right) [110].

Using these data and comparing the two similar configurations, average input values in the presheath region have been defined for each poloidal section of DEMO as shown in the following table. It is important to note that divertor is assumed as a unique section with the maximum temperature, energy and ion and neutral particle fluxes of all the divertor surface with the aim to be conservative:

Section	T_e $[eV]$	T_i $[eV]$	$n^{+}_{D_{19}}$ $[m^{-2}s^{-1}]$	$n^{++}_{He_{19}}$ $[m^{-2}s^{-1}]$	E_n $[eV]$	$n_{n_{19}}$ $[m^{-2}s^{-1}]$
OB1	20	29	4.5	0.04	150	20
OB2	23	49	7	0.1	400	5
OB3	25	60	5.5	0.12	550	4.5
OB4	26	64	5	0.14	540	4
OB5	27	62	4.5	0.13	490	3
OB6	27	61	3.5	0.11	350	2
OB7	25	52	2.5	0.09	180	1
IB1	17	34	2.5	0.035	80	2
IB2	20	35	6	0.055	180	1.3
IB3	20	34	7.5	0.06	300	2.2
IB4	19	28	10	0.03	200	3.5
IB5	14	14	15	0.012	60	8
IB6	3	3	14	0.007	7	17
IB7	6	6	12	0.01	18	18
Divertor	0.7	0.7	100000	70	3.8	100000

Table 17: Data extracted from ITER simulation adapting the poloidal configuration to DEMO design.

Unfortunately, these assumed values are extracted from ITER simulation. Hence, a method to extrapolate to DEMO will be modeled. With this objective in mind, the following two figures extracted from Militello document [111] have been used to estimate necessary scaling factors.

	Core	Edge		SOL		Detached Divertor
		Pedestal Top	Separatrix	Near SOL	Far SOL	
ALCATOR C-MOD	3	0.4	0.1	0.02	0.01	0.001
ASDEX U	2.8	0.45	0.09	0.03	0.01	0.001
JET	3.6	1	0.12	0.04	0.03	0.001
ITER	20	5.3	0.2	0.05	0.04	0.001
DEMO	50	5	0.16	0.04	0.03	0.001
MAST	1.3	0.1	0.06	0.015	0.01	0.001

Table 18: Electron temperature $[keV]$ in the six regions of the machines investigated (H-mode) by Militello [111].

	Core	Edge		SOL		Detached Divertor
		Pedestal Top	Separatrix	Near SOL	Far SOL	
ALCATOR C-MOD	29	20	1.75	2	1	20
ASDEX U	8.5	5	2.5	0.8	0.3	5
JET	7.5	4.85	2.25	1.1	0.4	7
ITER	12	7	5	1.6	0.6	7
DEMO	14	9	4.5	1.4	0.5	9
MAST	3.8	4.2	0.5	0.45	0.3	4

Table 19: Plasma density $[10^{19}m^{-3}]$ in the six regions of the machines investigated (H-mode) by Militello [111].

With the corresponding values in the core region and in the far SOL region (ending at 105% of the minor radius) for ITER and DEMO showed in the two previous tables; it is possible to adopt the following factors:

$$factor\_ITER\_T_e = {}^{20}/_{0.04}\left[{}^{T_{e\,core}}/_{T_{e\,FarSOL}}\right] \quad (106)$$

$$factor\_DEMO\_T_e = {}^{50}/_{0.03}\left[{}^{T_{e\,core}}/_{T_{e\,FarSOL}}\right] \quad (107)$$

$$factor\_ITER\_n_e = {}^{12}/_{0.6}\left[{}^{n_{e\,core}}/_{n_{e\,FarSOL}}\right] \quad (108)$$

$$factor\_DEMO\_n_e = {}^{14}/_{0.5}\left[{}^{n_{e\,core}}/_{n_{e\,FarSOL}}\right] \quad (109)$$

Simultaneously, new factors are calculated from the values estimated by Behrisch, Federici, Kukushkin and Reiter [110] and showed in Table 17:

$$New\_factor\_ITER\_T_e(i) = {}^{T_{e\,ref_{core}}\cdot 1000}/_{T_{e\,presheath(i)}} \quad (110)$$

Where $T_e\_ref\_core = 8.8\ keV$ is the electron temperature in the core used for the ITER simulation [110] and $T_e\_presheath(i)$ is the electron temperature in the pre-sheath region extracted from Table 17 for each poloidal section i.

$$New\_factor\_ITER\_T_i(i) = {}^{T_{e\,ref_{core}}\cdot 1000}/_{T_{i\,presheath(i)}} \quad (111)$$

Where $T_e\_ref\_core = 8.8\ keV$ is the electron temperature in the core used for the ITER simulation [110] and $T_i\_presheath(i)$ is the ion temperature in the pre-sheath region extracted from Table 17 for each poloidal section i.

$$New\_factor\_ITER\_E_n(i) = {}^{T_{e\,ref_{core}}\cdot 1000}/_{E_{n\,presheath(i)}} \quad (112)$$

Where $T_e\_ref\_core = 8.8\ keV$ is the electron temperature in the core used for the ITER simulation [110] and $E_n\_presheath(i)$ is the neutral energy in the pre-sheath region extracted from Table 17 for each poloidal section i.

$$New\_factor\_ITER\_n_{i_D}(i) = {n_{e\,ref_{core}} \cdot 1000}\Big/{n_{i_D\,wall(i)}} \quad (113)$$

Where $n_e\_ref\_core$ is the electron density used in the core for the ITER simulation [110] and $n_{i_D}\_wall(i)$ is the deuterium ion flux on the wall extracted from Table 17 for each poloidal section i.

$$New\_factor\_ITER\_n_{i_{He}}(i) = {n_{e\,ref_{core}} \cdot 1000}\Big/{n_{i_{He}\,wall(i)}} \quad (114)$$

Where $n_e\_ref\_core$ is the electron density used in the core for the ITER simulation [110] and $n_{i_{He}}\_wall(i)$ is the helium ion flux on the wall extracted from Table 17 for each poloidal section i.

$$New\_factor\_ITER\_n_n(i) = {n_{e\,ref_{core}} \cdot 1000}\Big/{n_{n_{wall(i)}}} \quad (115)$$

Where $n_e\_ref\_core$ is the electron density used in the core for the ITER simulation [110] and $n_n\_wall(i)$ is the neutral particles flux on the wall extracted from Table 17 for each poloidal section i.

Taking these factors into account, it is possible to obtain an scaling factor for DEMO using the following expressions:

$$New\_factor\_DEMO\_T_e(i) = \frac{New_{factor_{ITER_{T_e(i)}}}}{{factor_{DEMO_{T_e}}}\Big/{factor_{ITER_{T_e}}}} \quad (116)$$

$$New\_factor\_DEMO\_T_i(i) = \frac{New_{factor_{ITER_{T_i(i)}}}}{{factor_{DEMO_{T_e}}}\Big/{factor_{ITER_{T_e}}}} \quad (117)$$

$$New\_factor\_DEMO\_E_n(i) = \frac{New_{factor_{ITER_{E_n(i)}}}}{{factor_{DEMO_{T_e}}}\Big/{factor_{ITER_{T_e}}}} \quad (118)$$

$$New\_factor\_DEMO\_n_{i_D}(i) = \frac{New_{factor_{ITER_{n_{i_D}(i)}}}}{{factor_{DEMO_{n_e}}}\Big/{factor_{ITER_{n_e}}}} \quad (119)$$

$$New\_factor\_DEMO\_n_{i_{He}}(i) = \frac{New_{factor_{ITER_{n_{i_{He}}(i)}}}}{{factor_{DEMO_{n_e}}}\Big/{factor_{ITER_{n_e}}}} \quad (120)$$

$$New\_factor\_DEMO\_n_n(i) = \frac{New_{factor_{ITER_{nn(i)}}}}{{factor_{DEMO_{n_e}}}\Big/{factor_{ITER_{n_e}}}} \quad (121)$$

Finally, the accepted values for DEMO are estimated as follows:

$$T_e\_presheath\_DEMO(i) = \frac{T_e \cdot 1000}{New_{factor_{DEMO_{T_e(i)}}}} \quad (122)$$

Where $T_e\_presheath\_DEMO(i)$ is the electron temperature in the pre-sheath region for each poloidal section i of DEMO and T_e is the electron temperature in the core region.

$$T_i\_presheath\_DEMO(i) = \frac{T_e \cdot 1000}{New_{factor_{DEMO_{T_i(i)}}}} \quad (123)$$

Where $T_i\_presheath\_DEMO(i)$ is the ion temperature in the pre-sheath region for each poloidal section i of DEMO and T_e is the electron temperature in the core region.

$$E_n\_presheath\_DEMO(i) = \frac{T_e \cdot 1000}{New_{factor_{DEMO_{E_n(i)}}}} \quad (124)$$

Where $E_n\_presheath\_DEMO(i)$ is the neutral energy in the pre-sheath region for each poloidal section i of DEMO and T_e is the electron temperature in the core region.

$$n_{i_D}\_wall\_DEMO(i) = \frac{n_e}{New_{factor_{DEMO_{n_{i_D}(i)}}}} \quad (125)$$

Where $n_{i_D}\_wall\_DEMO(i)$ is the deuterium ion flux on the wall for each poloidal section i of DEMO and n_e is the electron density in the core region.

$$n_{i_{He}}\_wall\_DEMO(i) = \frac{n_e}{New_{factor_{DEMO_{n_{i_{He}}(i)}}}} \quad (126)$$

Where $n_{i_{He}}\_wall\_DEMO(i)$ is the helium ion flux on the wall for each poloidal section i of DEMO and n_e is the electron density in the core region.

$$n_n\_wall\_DEMO(i) = \frac{n_e}{New_{factor_{DEMO_{n_n(i)}}}} \quad (127)$$

Where $n_n\_wall\_DEMO(i)$ is the neutral particles flux on the wall for each poloidal section i of DEMO and n_e is the electron density in the core region.

To check the adequacy of the method, the values shown in Table 17 have been extrapolated to the following conditions of the DEMO1 scenario [11]:

- $T_e = 13.065\ keV$
- $n_e = 7.98e19\ m^{-3}$

The results are shown in the following table:

Section	T_e [eV]	T_i [eV]	$n^+_{D_{19}}$ $[m^{-2}s^{-1}]$	$n^{++}_{He_{19}}$ $[m^{-2}s^{-1}]$	E_n [eV]	$n_{n_{19}}$ $[m^{-2}s^{-1}]$
OB1	8.9	12.9	2.6	0.02	66.8	11.4
OB2	10.2	21.8	4	0.06	178.2	2.9
OB3	11.1	26.7	3.1	0.07	245	2.6
OB4	11.6	28.5	2.9	0.08	240.5	2.28
OB5	12	27.6	2.6	0.07	218.2	1.7
OB6	12	27.2	2	0.06	155.9	1.1
OB7	11.1	23.2	1.4	0.05	80.2	0.6
IB1	7.6	15.1	1.4	0.02	35.6	1.1
IB2	8.9	15.6	3.4	0.03	80.2	0.7
IB3	8.9	15.1	4.2	0.03	133.6	1.3
IB4	8.5	12.5	5.7	0.02	89.1	2
IB5	6.2	6.2	8.6	0.007	26.7	4.6
IB6	1.3	1.3	8	0.004	3.1	9.7
IB7	2.7	2.7	6.8	0.006	8	10.3
Divertor	0.3	0.3	57000	39.9	1.7	57000

Table 20: Data in the pre-sheath region for each poloidal section of DEMO.

Several references have been consulted in order to validate the final values. For example, Asakura [112] fixes the electron temperature on the PFCs surface about 1-20 eV for DEMO. Similarly, a CELLSOR simulation [113] predicts a $E^+_{D_{wall}} = 100\ eV$ (energy of the incident deuterium ions on the wall) fixing a $T_e = 24.9\ keV$ in the region core. Following the sheath model explained subsequent; the energy of the incident deuterium ions estimated by the AINA method is about 10-70 eV for a $T_e = 13.065\ keV$ which is according to the CELLSOR simulation. In the case of the divertor, the Wischmeier document [114] fixes a limit electron temperature on the target of 2-5 eV and the average electron temperature of the divertor surface extracted from the AINA method is lower than it and coherent. Moreover, the ion flux to the target surface estimated by Wischmeier is $5 \cdot 10^{23} m^{-2} s^{-1}$. For AINA this parameter reaches $5.7 \cdot 10^{23} m^{-2} s^{-1}$ and this value can be assumed as valid despite of it is an average value for all the divertor surface and not only represents the peak value for the target section as the Wischmeier document adopts [114]. In the same vein, a SONIC simulation [115], a SOLPS 5.1 simulation [116] and a B2.5-EIRENE simulation [117] forecast electron temperatures on the target lower than 10 eV, as well. Similar conclusions can be extracted from experiments and modelling carried out in ASDEX Upgrade and DIII-D [118] where similar ions fluxes are estimated on the divertor target.

Unfortunately, this extrapolation from ITER values to DEMO is a weak point of the code and should be further studied in the future. It would be desirable to obtain directly the necessary inputs from, for example, a B2-EIRENE simulation for DEMO1 scenario [11].

2.2.5.2.1.5 Sheath model

The sheath is a region of net charge, usually in a thin region adjacent to a solid surface and where $n_e < n_i$ [49]. This region is due to the difference between the electron thermal velocity to the absorbing surface of the PFCs and the ion thermal velocity by the square root of the mass ratio. This discrepancy generates an electric field which brings the two flows to equality by decreasing the electron flow and enhancing the ion flow. This electric field is located in a narrow sheath near the surface, its width being several Debye lengths. A small electric field, the pre-sheath, extend more deeply into the plasma [47].

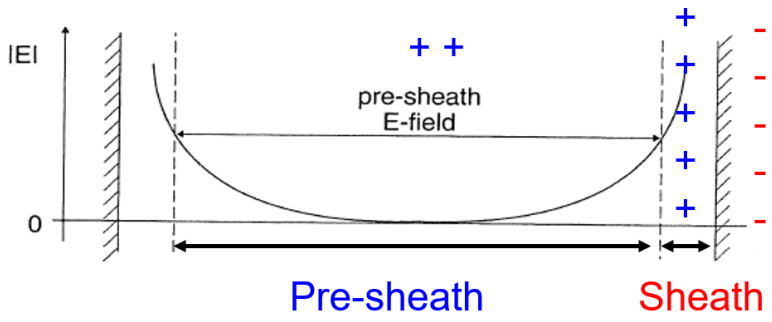

Figure 46: Electric fields which establish the sheath and pre-sheath [119].

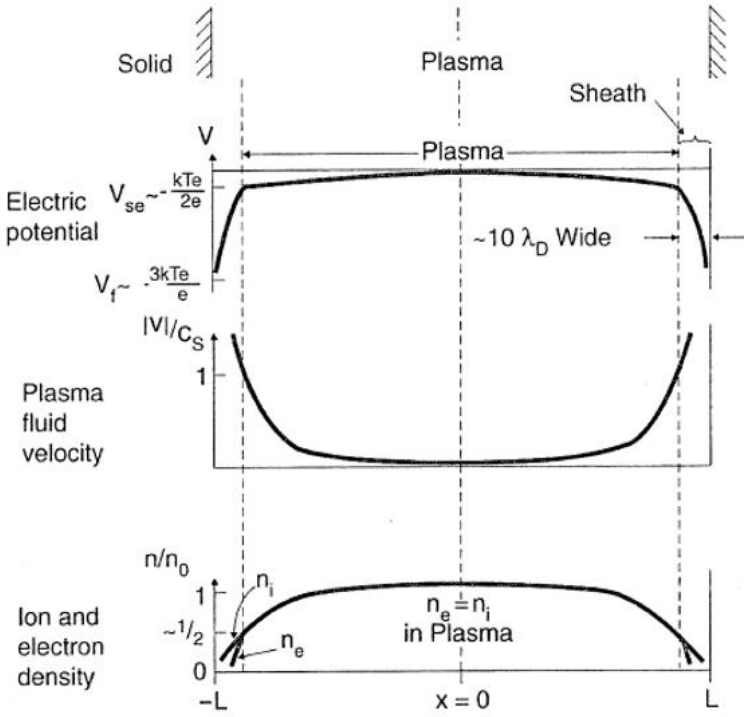

Figure 47: Spatial variation of the electric potential, plasma velocity and the ion and electron densities across the sheath, the pre-sheath and the plasma [119].

The incident energy of ions on the surface is equal to the sum of the energy with which ions enter the pre-sheath, the energy gained in the pre-sheath and the energy gained in the assumed collision-less sheath [47]:

$$E_{i_{wall}} = T_{e_{presheath}} + \left(\frac{3}{2} + \gamma\right) \cdot T_{i_{presheath}} + Z_i \cdot \phi \quad (128)$$

Where $T_{e_{presheath}}$ and $T_{i_{presheath}}$ are the temperatures of the projectile electrons and ions, respectively; γ is known as the sheath heat transmission coefficient and it represents the transfer energy from electrons to ions for each charged pair lost to the solid along the sheath and the pre-sheath, AINA fixes its value to $^5/_3$ since it is assumed an adiabatic flow with isotropic pressure [119][49]; Z_i is the ions formed and ϕ [49]:

$$\phi = \frac{1}{2} \cdot T_{e_{presheath}} \cdot ln\left(\left(2\pi \cdot \frac{m_e}{m_i}\right)\left(1 + \frac{T_{i_{presheath}}}{T_{e_{presheath}}}\right)\right) \quad (129)$$

Where m_e and m_i are the mas of the electron and the projectile ion, respectively $[uma]$.

Finally, it is important to note that the incident ion flux on the surface is the same as the ion flux entering the sheath from the pre-sheath [119].

2.2.5.2.1.6 Transients Assumptions

Ions and neutral particles fluxes against the PFC are used as inputs to estimate the total impurities sources due to, in the Tungsten case, physical sputtering processes. For transient calculations the model assumes that these magnitudes may vary; therefore, a weighting coefficient is applied over the initial value of ion and neutral particle fluxes to obtain the value at some instant of the transient [37]:

$$\Gamma_{incident\ ions\ or\ neutral\ particles}(t) = \Gamma_{incident\ ions\ or\ neutral\ particles}(0) \cdot \frac{n_i(t)}{n_i(0)} \cdot \frac{\tau_{E,e}(0)}{\tau_{E,e}(t)} \quad (130)$$

A similar requirement exists in the temperature weighting used to estimate the incident energy of these fluxes by means of sheath model:

$$T_{i,surface}(t) = T_{i,surface}(0) \cdot \frac{T_i(t)}{T_i(0)} \quad (131)$$

$$T_{e,surface}(t) = T_{e,surface}(0) \cdot \frac{T_e(t)}{T_e(0)} \quad (132)$$

Finally, for the case of neutral energy flux, the coefficient applied is a composition of the two previous:

$$E_{neutral}(t) = E_{neutral}(0) \cdot \frac{n_i(t)}{n_i(0)} \cdot \frac{\tau_{E,e}(0)}{\tau_{E,e}(t)} \cdot \frac{T_e(t)}{T_e(0)} \quad (133)$$

2.3 AINA 4.0 development

2.3.1 Methodology

It is important to remember that one of the objectives of this project was to develop a new version of the AINA code focused to the simulations of the European DEMO configurations. Following the AINA historical philosophy, AINA must be split out in three blocks: the plasma block, the plasma wall interaction block and thermal blanket block. Every block had to be built, checked and validated separately, especially the thermal blanket block since its development is vastly different depending on the modelled configuration. Subsequently, these three blocks were linked, thereby obtaining a new version of AINA (AINA 4.0).

The next step consisted of an evaluation through benchmarking. PROCESS code, which was already explained in a previous section, was the tool used for this purpose. In this stage was possible to check if the new version of AINA is able to simulate the SS scenarios fixed by EUROfusion. These scenarios are the starting point from which several transients due to plasma perturbations or thermohydraulic accidents can be simulated. Because of this, it is feasible to identify that events lead to critical and most negative consequences and, thereafter, outline safety contributions.

The next figure gives an idea of the followed procedure.

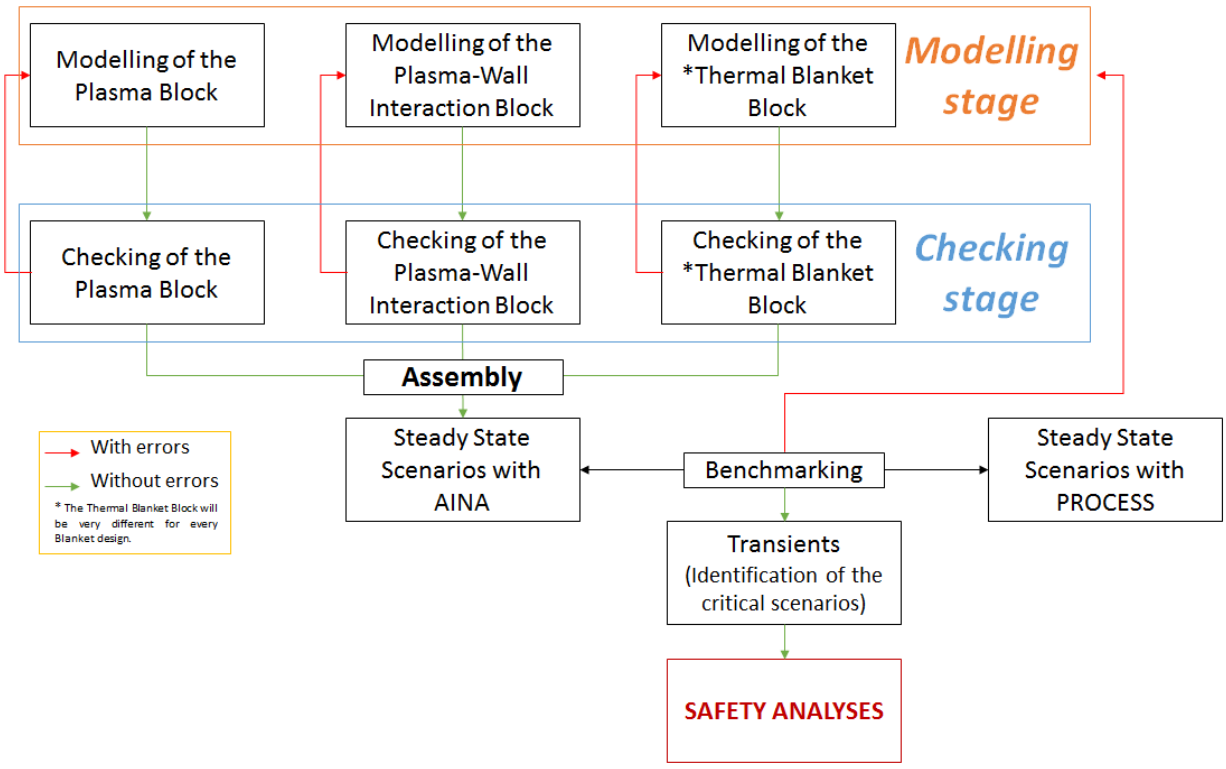

Figure 48: Scheme of the methodology.

2.3.2 AINA 4.0 structure

The structure of this new version of AINA was geared toward a user-friendly and intuitive code not only to be run but to be modified or updated as well. Moreover, it is important to remember that MATLAB has been the framework used. With these characteristics in mind and the three-blocks philosophy AINA 4.0 is structured as shown the following figure. The first row shows the files corresponding to each block and the rest of the levels show files or Matlab functions (namefile.m) depending on the branching degree. With this branching design it is possible to modify or update specific parts of the code without affecting or adapting the rest of the code. In addition, the functionality of each of these files or functions is easily identifying thanks to its name, its position inside the general structure of the code and brief explanations and comments which functions incorporate throughout the code.

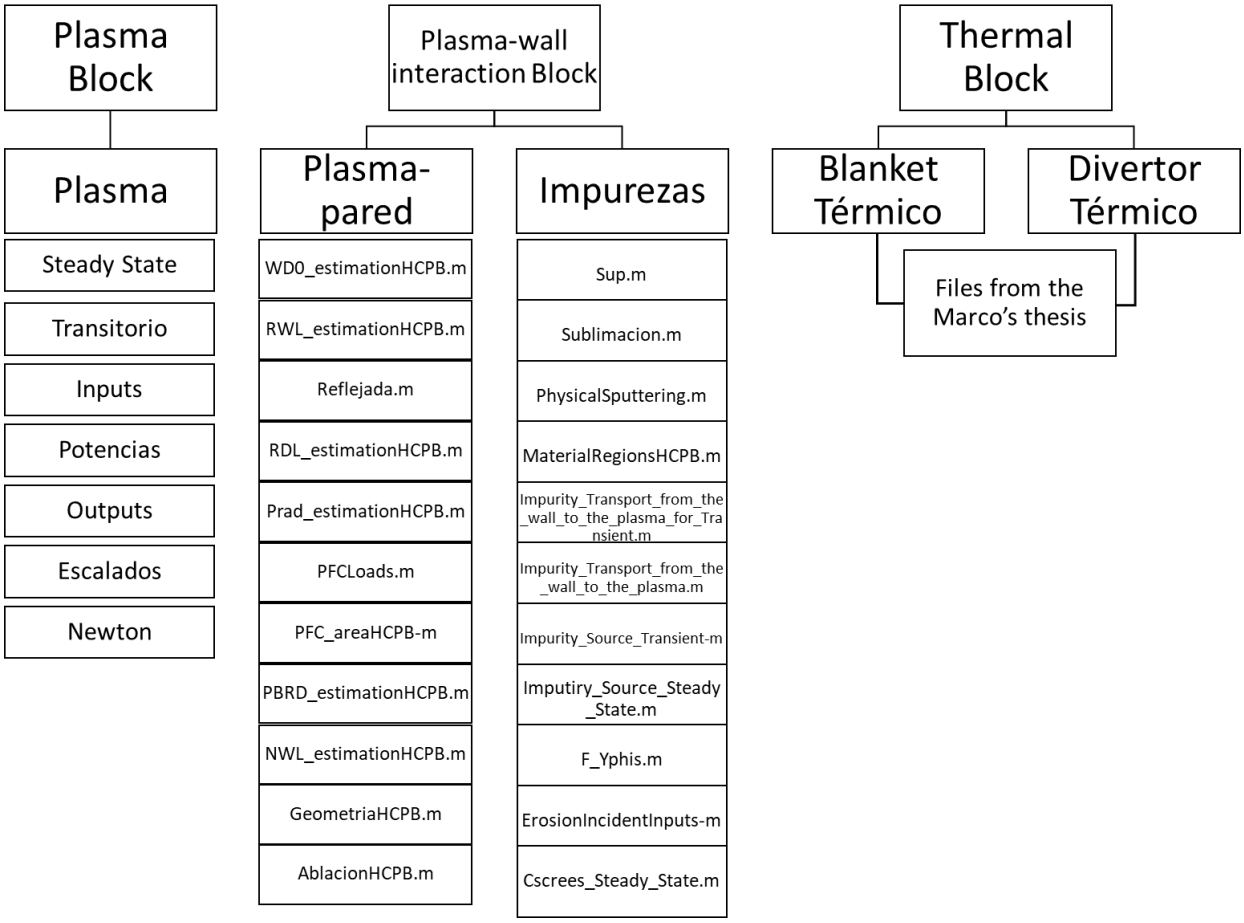

Figure 49: AINA 4.0 files structure.

The following is a brief explanation of most important files of the code (a more detailed explanations are thorough the comment inside the code). With respect to the plasma bloc:

- ***Steady State***: file containing the function with the mass and power balance and the codification to estimate a steady state scenario. It is possible to safe the values for a specific steady state scenario as DEMO1 [11] or DEMO2 [12] when it has been estimated in order to jump over this process in future simulations.
- ***Transitorio***: this is the main file. File containing the function where all the sequence based on the Euler method to estimate a steady state scenario (the Steady State file is included) and its evolution depending on the transient applied is codified.
- ***Inputs***: File containing several functions where all the inputs parameters to set the reactor, the desired steady state to be simulated and the perturbation to be applied can be modified. The name of the function shows the kind of variables included; for example the PlasmaGeometry.m ot the LOCAs.m functions.
- ***Potencias***: File containing all the functions to calculate the powers which appear throughout the mass and power balances of the one-dimensional plasma model. Some of the most important functions are the CyclotronPowerLossesNuevoImpurezas.m or the OhmicPowerNuevoImpurezas functions.
- ***Outputs***: Functions containing parameter which are interested to know after the scenario estimation as the Beta_estimation.m or the PlasmaIntensity.m functions.

- ***Escalados***: This file contains all the functions related to calculate the confinement time parameter and the possible mode leaps (H mode to L).
- ***Newton***: File containing the function with the Newton method codification used in the mass and power balance to estimate the steady state scenario.

In terms of plasma-wall interaction block, it consists of two files:

- ***Plasma-pared***: containing all the necessary functions to estimate the loads suffered by the walls (the Prad and the NWL) in each of its regions. These values are boundary conditions for the thermal model. The name of each function provides an insight into its utility, for example the NWL_estimationHCPB.m estimates the NWL for each Blanket region. Some functions are in charge of providing the geometric characteristics of the wall regions as the GeometriaHCPB.m function and some of them are portions of the code aimed to improve these models in the future but are not currently implemented, for example the Reflejada.m and the AblaciónHCPB.m functions.
- ***Impurezas***: containing all the required functions to estimate the impurities production from the wall and its transport to the plasma. Some of these functions are specifically built to the Steady State estimation process as the Impurity_Source_Steady_State.m function and other of them are codified for the transient evolutions as the Impurity_Source_Transient.m function. Even so, mostly all the functions are used both for Steady State scenarios and for transients and, as their names suggest, encode physics phenomena as the Sublimacion.m or the PhysicalSputtering.m functions..

Finally, the thermal block is split out in two files. Both use the same kind of functions derived from the Fabbri's thesis [2], however one of them is adapted to each blanket design and the other one is focused on the divertor. These functions are responsible to estimate the thermal behavior along a representative one-dimensional segment which passes through the internal layers of the blanket or the divertor by means of the numerical model codified by Fabbri [2].

3 AINA Study as a Contribution to Safety Analyses of HCPB DEMO

Firstly, it is important to highlight that the tool used to carry out this safety study has been AINA 4.0, the design of the modeled Blanket is the HCPB-2015 v3 [59], the reference scenario is DEMO1 [11] and all the data and assumptions are based on DEMO BB Safety Data List document [120]; as has already advanced throughout this project.

3.1 Introduction

The safety and environmental goals of a fusion power plant design are to protect workers from radiation, electromagnetic fields, chemical and other hazards; the public from radioactive and toxic materials and the environment from pollutants and waste [121]. In particular, the general safety principals document for DEMO [122] establishes that the top-level safety objectives for DEMO are:

- To protect workers, the public and the environment from harm.
- To ensure in normal operation that exposure to hazards within the facility and due to release of hazardous material from the facility is controlled, kept below prescribed limits and minimized to be as low as reasonably achievable.
- To ensure that the likelihood of accidents is minimized and that their consequences are bounded.
- To ensure that the consequences of more frequent incidents, if any, are minor.
- To apply a safety approach that limits the hazards from accidents such that in any event there is no need for public evacuation on technical grounds.
- To minimize radioactive waste hazards and volumes and ensure that they are as low as reasonably achievable.

In addition, the four DEMO Fundamental Safety Functions are therefore identified as [122][123]:

- Confinement of radioactive and hazardous materials.
- Limitation of exposure to ionizing and electromagnetic radiation.
- Limitation of the non-radiological consequences of conventional hazards.
- Limitation of Environmental Legacy.

A conclusion that can be drawn from the historical safety analyses developed for tokamaks fusion reactors is that some of the major risks involve incidents in the vacuum vessel and during the last ten years AINA has become a great tool in order to evaluate plasma evolution and these in-vessel components strains. The Blanket is a safety relevant component since its failure could impact the operation of other components, most notably the vacuum vessel. Moreover, the Blanket is credited for some interlock functions such as neutron shielding to the magnets that may affect the dose to the workers during maintenance operations, and hence its design could impact the overall safety of the machine [121]. For this reason, as the Propose Safety Importance Classification Scheme for DEMO Systems, Structures and Components document [124] set, all the in vessel components are assigned SIC 1 or SIC 2, as figure Table 21 shows, because they must provide confinement and management of heat removal and long term temperatures in order to protect the population [122]. Thus, this safety study is faced to figure out on one hand if the in vessel components fulfil the following safety functions in support of confinement and on the other hand the possible consequences if these functions are not satisfied:

- Control of plasma energy.
- Control of thermal energy.
- Control of coolant energy.

System	Subsystem	Safety function provided	SIC class
Fueling and Wall Conditioning	Gas injection	Components providing the 1st confinement barrier	SIC-1
	Pellet Injection	Components providing the 1st confinement barrier	SIC-1
	Glow discharge cleaning	Components providing the 1st confinement barrier	SIC-1
	Fusion plasma termination	Components providing the 1st confinement barrier	SIC-1
Cooling Systems	Primary VV HTS	Management of chemical energy in case of ex VV cooling failure	SIC-2
		Components providing confinement function	SIC-2
	Primary Blanket HTS	Management of heat removal and long term temperatures	SIC-2
	Primary Divertor HTS	Provide confinement	SIC-1
	Draining and refilling	Provide confinement	SIC-1
Neutral Beam H&CD DNB	Beam source vessel	Confinement	SIC-2
	Beam Line Vessel	Confinement function	SIC-1
	Transmission Lines and High Voltage Decks	Confinement function	SIC-1
	HV Bushing	Confinement function	SIC-1

Table 21: List of Safety Functions and SIC Class for the in vessel components [124].

3.2 Types of Accidents

Common objective of the FFMEAs done for the various DEMO systems [125][126][127][128] was, at first, to provide a complete list of potential accident initiating events (IEs). Among those, the Selection of reference accident scenarios for the DEMO plant document [129] has identified 21 PIEs (Postulated Initiating Events) as the most representative for the deterministic assessments to be performed in the first phase of the DEMO design activities both to check the compliance with safety limits and to give rationales for the selection of the reference DEMO reactor model. The vast majority of these 21 PIEs could induce the following load or accident scenarios which AINA is able to simulate:

- Plasma disruption or structural material melting due to a LOPC: disruptions represent the highest risk for DEMO integrity and it is assumed that they are only caused by instabilities induced by failures in the systems operating to confine, diagnose and feed the plasma or by accidental events leading to the entrance of undesired elements [130]. By means of AINA, it is possible to identify those failures which can lead to the maximum wall damage due to the electromagnetic and thermal load [131]. Likewise, some failures cannot lead the plasma to a disruption event, however this perturbation can affect the plasma physics and damage the materials which make up the in vessel structure and containment. The perturbations that AINA can simulate are:
    - a failure in the external power supply system.
    - a failure in the fuel source system.
    - a variation in the confinement system.
    - an entrance of an undesired quantity of impurities.

- In-vessel melt either of FW, blanket structure and/or divertor modules because of thermal stresses due to a LOCA: the Blanket is designed with sufficient cooling ability under normal operational conditions, however, it is necessary to study the temperature evolution in the Blanket structure when a LOCA takes place [132]. AINA is able to replicate this phenomena by means of the variation of the coolant mass flow rate through the cooling sections. They can affect the cooling loops in the BB, the cooling channel of the FW, the cooling regions in the CB of the divertor and the cooling channel of the PFCs of the divertor. It is necessary to remember that AINA cannot simulate consequences of this kind of accident as a leakage, a release nor a penetration of coolant or radioactive products into other structure regions.

Moreover, peak heat loads can be simulated using the thermal divertor block of AINA independently. In this way, it will be possible to study the real divertor behaviour since the load AINA applies against the divertor is an average value; however, important peaks will be suffered by this component in the reality, $6.23\ {}^{MW}/_{m^2}$ [11].

3.3 Steady State Scenario DEMO1

First of all, it is important to remember the characteristics of the steady state scenario used to develop the safety study. Thus, AINA 4.0 steady state simulation of DEMO1 scenario is presented in this section. The basic tokamak reactor parameters used both as inputs and to compare the AINA values have been based on the output data from the DEMO1 reference reactor configuration released on April 2015 by PROCESS (or document: DEMO1_Reference_Design_-_2015_April_(_EU_2MDKFH_v1_0.dat) [11][133].

INPUTS	**DEMO1**	
Major Radius (m)	9.072	
Minor Radius (m)	2.927	
Toroidal Field (T)	5.667	
q95	3.247	
Vp (m^3)	2502	
Sp (m^2)	1428	
P_{fus} (MW)	2037	
T_i (keV)	13.065	
OUTPUTS	**AINA 4.0**	**PROCESS**
T_e (keV)	13.04	13.065
S_H ($m^{-3}s^{-1}$)	8.95e18	2.82e18
n_e (m^{-3})	8.35e19	7.98e19
n_e (m^{-3})	7.55e19	6.99e19
n_H (m^{-3})	6.94e19	6.144e19
n_α (m^{-3})	5.98e18	7.98e18
n_{Ztotal} (m^{-3})	3.66e16	3.51e16
n_{ZXe} (m^{-3})	3.25e16	-
n_{ZW} (m^{-3})	4.17e15	-
f_{Xe} (%)	0.0389	0.0389
f_W (%)	0.005	0.005
P_{ext} (MW)	66.4	50
Q	30.68	39.86
P_α (MW)	399	407
P_{ie} (MW)	1.76	0

P_{Ohm} (MW)	0.95	1.1
P_{Br} (MW)	80.98	87.9
P_{syn} (MW)	30.2	25.9
P_{li} (MW)	54.31 (f_{core} fraction) / 226.3	191
P_{edge} (MW)	172	172.9
P_{core_rad} (MW)	165.6	132.6
P_{rad_total} (MW)	337.6	305.5
P_{SOL} (MW)	300	-
β_{total} (%)	3.26	3.1
β_t (%)	2.81	3.2
β_p (%)	0.96	1.1
$\tau_{E,e}$ (s)	4.15	4.23
Plasma Current (MA)	20.3	19.6
$f_{bootstrap}$	0.25	0.32
NWL (MW/m^2)	1.07	1.05
P_{rad_FW} (MW/m^2)	0.17	0.22

Table 22: Main global parameters of the DEMO1 computed by means of AINA 4.0 and compared with PROCESS results.

These values obtained from the AINA 4.0 simulation are similar to those achieved from the PROCESS simulation and no meaningful discrepancies have been found. Nevertheless, AINA 4.0 is unable to converge in a steady state scenario for a P_{ext} of 50 MW with these conditions imposed. However due to the P_{core_rad} and P_{edge} values, AINA estimates a conservative scenario, not only on plasma model but on thermal blanket model as well. Therefore, it can be concluded that AINA 4.0 is a suitable and fast tool to analyse the time evolution behaviour of theses parameters assuming this starting point.

Notwithstanding, it is necessary to highlight that for the DEMO1 scenario certain functional temperature limits [59][79][120] (EUROFER, Beryllium and Li_4SiO_4) for the HCPB BB design are slightly exceeded in the worst poloidal region (OB4) as envisaged by thermo-hydraulic analyses [68][59][61]:

Material	**Temperature Limit** $[^{o}C]$	**T** $[^{o}C]$
Tungsten	3422	483.5
EUROFER	550	563
Beryllium	650	677
Li_4SiO_4	920	956

Table 23: HCPB AINA DEMO1 SS maximum temperature.

The infringement of these functional temperature limits will be treated as possible melting scenarios throughout this document despite the fact they are not the materials melting limits. However it is important to note that this limits infringement may be explained by the intrinsic deviation due to the simplification of the thermal blanket model which was studied during the thermal HCPB blanket validation. The greater overtaking amounts to 4% while that deviation is around 5% [2]. Accordingly, it would be advisable to undertake a design review focused on ensuring a suitable operating temperature range with a bigger safety margin for all the materials which make up the HCPB BB.

All figures extracted from AINA and used in the following analysis are contained in Annex A.

3.4 LOPC Accidents

3.4.1 Failure in the External Power Supply System

Currently, external power input is required for the fusion technologies not only to achieve an operational state but also to keep the plasma hot since most of the energy produced by fusion is carried away by the neutrons and, nowadays, it is not clear yet whether ignition will be the optimum operating regime, at which the production of hot Helium is enough to sustain the plasma and the external energy sources can be turned off. Tokamaks use as this external heating supply a neutral beam injection and sources of high-frequency electromagnetic waves which are sensible technologies, for this reason the consequences of their possible failures must be studied.

3.4.1.1 Auxiliary heating cut-off

Accident description: An unexpected and instantaneous auxiliary heating cut-off takes place at second $t = 0.1\ s$ while the HCPB DEMO reactor is operating on DEMO1 SS.

Event sequence: This failure produces a fast decrease of ion and electron temperatures but confinement time rises leading to fusion power increase and P_{SOL} reduction. The average electromagnetic power P_{rad} radiated from the plasma core to the PFC of the divertor decreases, consequently the temperature of the PFC surface in the divertor is lower than the DEMO1 state one forcing a slight impurity percentage decline of Tungsten inside the plasma core. All of this converges at a new steady state which produces a higher fusion power of 2420 MW. So, apparently the ignition point has been achieved, however the increase of neutronic heat flux (NWL) through the blanket induces the overtaking of the functional temperature limits wider than in the DEMO1 state. This event is observed before 20 seconds (Li_4SiO_4: 1031 ºC, Beryllium: 700 ºC and EUROFER: 565 ºC) when NWL has increased by 18%. For this reason it is necessary to conclude that it is really important to detect rapidly an external power cut-off in order to proceed with a fast plasma shutdown (FPSS) [132] (by means of the control of the confinement system) during the first seconds for the purpose of preventing blanket melting, specifically for the Li_4SiO_4 and Beryllium regions. It is remarkable how Tungsten temperature of the FW remains practically unchanged because of the small P_{rad} variation.

3.4.1.2 Auxiliary heating decrease

Accident description: An unexpected and sudden decrease of auxiliary heating takes place at second $t = 0.1\ s$ while the HCPB DEMO reactor is operating on DEMO1 SS.

Event sequence: An analogous and scaled sequence to the previous one takes place when this accident occurs. When a multiplication factor of 0.5 is applied, 2197 MW of fusion power is reached forcing, once again, an increase of the operating temperatures for the BB materials (Li_4SiO_4: 985 ºC and Beryllium: 686 ºC). In short, any auxiliary heating reduction must be detected instantly in order to proceed with a fast plasma shutdown (FPSS) and thereby avoiding the BB material collapse.

3.4.1.3 Auxiliary heating increase

Accident description: An unexpected and sudden increase of auxiliary heating up to a multiplication factor of 6.3 takes place at second 0.1 while HCPB DEMO reactor is operating on DEMO1 SS.

Event sequence: First of all it is important to note that OB5 region becomes the worst (it receives the maximum load flux $NWL + P_{rad}$ between the second 0.3-0.5 s depending on the multiplication factor

which affect external power. As soon as the incident takes place ion and electron temperatures increase and all the species densities fall; except the impurity percentage of Tungsten which rise due to the increase of the average electromagnetic power P_{rad} against the divertor. This leads to an initial and abrupt fusion power increment although it finally decreases rapidly achieving a new state which produces less fusion power than DEMO1. For this reason this kind of scenarios could be interesting only with the aim of reaching instantaneous fusion power peaks (2116 MW). On the other hand, a controlled auxiliary heating increase can conduce to a steady state where the functional temperature limits of the BB materials are not exceeded, for example a multiplication factor of 6.3 leads to an steady state where the Li_4SiO_4 temperature is 815 ºC (below the acceptable value). Ideally, these incidents should be detected for the purpose of foreseeing an important power fusion decrease. Once the plasma has stabilized, the new scenario does not represent a risk scenario unless the external power keeps increasing and it reaches the following kind of accident.

Accident description: An unexpected and sudden increase of auxiliary heating with a multiplication factor larger than 6.3 takes place at second 0.1 while HCPB DEMO reactor is operating on DEMO1 SS.

Event sequence: This perturbation leads plasma to terminate due to the beta limit infringement. The higher multiplication factor is, the faster plasma collapse is. Fusion power and densities quickly diminish, except the impurity percentage of Tungsten which rise due to the increase of the average electromagnetic power P_{rad} against the divertor; however, mainly ion temperature increases reaching more than 22 keV. At the time of the disruption, the plasma thermal energy (U) estimated by Paknezhad expression [134] and exposed hereunder, is 1.5 GJ for a multiplication factor of 6.4, consequently the EUROFER limit of 550 ºC would be significantly exceeded [135] as well as the rest of the temperature limits, including Tungsten.

$$U = \frac{3}{2}\sum_{Z} n_Z T_Z V \qquad (134)$$

Where subscript Z indicates the plasma species, n_Z is the specie density, T_Z is the temperature of every specie and V is, as always, the plasma volume. For this reason it is necessary to conclude that it is really important to detect rapidly an excessive auxiliary heating increase since the plasma termination could be very fast as the following table shows:

Multiplication factor	Plasma termination time $[s]$	Plasma Thermal energy U $[GJ]$
6.4	88.5	1.5
7	12.8	1.5
8	3.6	1.5
9	2	1.5

Table 24: Disruption time and plasma thermal energy for an excessive auxiliary heating increase.

Nevertheless and in spite of these severe consequences, it is highly unlikely to achieve auxiliary heating as high as those which can lead to this type of accident due to the installed external power capacity would not exceed 150 MW.

3.4.1.4 Auxiliary heating perturbation summary

Mult. factor	Plasma termination	Plasma termination time $[s]$	Consequences	Mitigation	Observations
0 (cut-off)	Stabilized	-	Fusion power increase. Several temperature limits exceeded.	External power variation detection. A controlled fast plasma shutdown.	In DEMO1 temperature limits are already slightly exceeded; however, this conditions worsen the scenario.
0.5	Stabilized	-	Fusion power increase. Several temperature limits exceeded.	External power variation detection. A controlled fast plasma shutdown.	In DEMO1 temperature limits are already slightly exceeded; however, this conditions worsen the scenario.
2	Stabilized	-	Fusion power decrease. BB temperature decrease.	Not necessary.	Increasing the external power leads to closer to the BB operating temperatures.
3	Stabilized	-	Fusion power decrease. BB temperature decrease.	Not necessary.	Increasing the external power leads to closer to the BB operating temperatures.
4	Stabilized	-	Fusion power decrease. BB temperature decrease.	Not necessary.	Increasing the external power leads to closer to the BB operating temperatures.
5	Stabilized	-	Fusion power decrease. BB temperature decrease.	Not necessary.	Increasing the external power leads to closer to the BB operating temperatures.
6.4	Beta Limit	88.5	Excessive plasma thermal energy. All temperature limits exceeded	External power variation detection.	In principle, it is not possible to reach such high external power.
7	Beta Limit	12.8	Excessive plasma thermal energy. All temperature limits exceeded	External power variation detection.	In principle, it is not possible to reach such high external power.
8	Beta Limit	3.6	Excessive plasma thermal energy. All temperature limits exceeded	External power variation detection.	In principle, it is not possible to reach such high external power.
9	Beta Limit	2	Excessive plasma thermal energy.		

			All temperature limits exceeded	External power variation detection.	In principle, it is not possible to reach such high external power.

Table 25: Auxiliary heating perturbation summary

3.4.2 Failure in the Fuel Source System

The fueling system must provide the required D-T fuel mixture to maintain the plasma as foreseen by the plasma scenarios [136]. This system in DEMO is composed of two types of equipment, the pellet injection system which will deposit material in the plasma core and the gas injection which will supply the material needed for pre-fill, ramp up and plasma enhancement gases [136]. For AINA simulations, only the pellet injection system is considered for the steady operational scenario DEMO1 where almost 100 % of particles injected arrive into the plasma core. Therefore the fueling of DEMO can be only ensured by pellets injected from the HFS (High Field Side) [137][138][139]. This complex system is necessary in order to maintain the equilibrium of the plasma, for this reason the consequences of its possible failures must be studied.

3.4.2.1 Fueling rate cut-off

Accident description: An unexpected and instantaneous fueling rate cut-off takes place at second t $t = 0.1\ s$ while the HCPB DEMO reactor is operating on DEMO1 SS.

Event sequence: In case fueling is stopped, it is possible to observe how fusion power quickly diminish as well as densities, except the impurities percentages due to physical sputtering driven by the increase in ion and electron temperatures. This growth takes place basically as a result of auxiliary heating injection, reaching more than 25 keV. Moreover, the lower the impurities percentages, the lesser the power losses; for this reason the confinement time increases to 18.1 s. All of this leads to a reduction in BB temperatures reaching acceptable values far below the melting limits, including the surface temperature of the Tungsten, and from the second 0.4, the region OB5 becomes the worst. A transition mode is detected after 22.9 seconds and, finally, plasma collapses at 25.5 s by an overshoot beta limit disruption. Despite this, at the time of the collapse, the plasma thermal energy (U) achieves values of up to 0.5 GJ, and this disruption could be mitigated by a disruption mitigation system [135] and, thereby, the BB material would be safeguarded. Nevertheless, it would be useful to detect a fueling cut off instantaneously for the purpose of conducing the plasma to a better and controlled plasma shutdown if it is possible.

3.4.2.2 Fueling rate decrease

Accident description: An unexpected and sudden decrease of fueling rate takes place at second $t = 0.1\ s$ while the HCPB DEMO reactor is operating on DEMO1 SS.

Event sequence: Firstly it is important to note that OB5 becomes the worst region after 0.6 s. As in the previous case, a fueling reduction leads to a fusion power decrease, specifically half of fueling provides just over half the initial fusion power (from 2037 MW to 1141 MW). Initially, there is an increase of ion and electron temperatures but these magnitudes are rapidly stabilized around the initial value ($T_e = 13.06$ and $T_i = 13.45$). Similarly, densities diminish in the first instance with the exception of Xenon due to the Xenon source is constant and Tungsten which decreases much more as a result of the radiation load reduction against PFCs making get down notably the surface temperature. The confinement time gets stabilized at a rate of 6.1 s and the temperature of the BB and divertor materials are greatly reduced even almost below the functional temperature limits (Li_4SiO_4: 768 ºC, Beryllium: 615 ºC, EUROFER: 556

ºC and Tungsten: 472.2 ºC). In conclusion, beyond this failure does not cause a dangerous scenario, the new steady state obtained could be a better candidate for DEMO operation from the point of view of temperature limits no exceedance and despite the generation of lower fusion power and, consequently, less gain ($Q = 17.2$).

3.4.2.3 Fueling rate increase up to 25%

Accident description: An unexpected and sudden increase of fueling rate up to 25% takes place at second $t = 0.1\ s$ while the HCPB DEMO reactor is operating on DEMO1 SS.

Event sequence: As in the above case, a new steady state scenario is achieved, however this one is not positive and several risks are derived from this kind of perturbation as discussed hereafter. The fusion power expands reaching a rate of 3472 MW ($Q = 52.3$), while ion and electron temperatures get stabilized around their initial values and after an initial drop; in contrast, the confinement time achieves a higher constant rate of 6.4 s and densities grow, mainly Tungsten due to the radiation and neutron load increase against PFCs. All of this leads to a scenario in which OB5 becomes the worst region after 5.5 s and where functional temperature limits are widely exceeded in less than 50 s (except in Tungsten case) and the melting is unmitigated (Li_4SiO_4: 1212 ºC, Beryllium: 764 ºC, EUROFER: 572.5 ºC and Tungsten: 509.5 ºC). In addition, a new fueling rate increase could induce the scenario analyzed in the following case. For these reasons, it is essential to be able to guarantee a quick detection and actuation of a fueling increase in order to stop the excessive warming

3.4.2.4 Fueling rate increase above 25%

Accident description: An unexpected and sudden increase of fueling rate above 25% takes place at second $t = 0.1\ s$ while the HCPB DEMO reactor is operating on DEMO1 SS.

Event sequence: In this case; fusion power, densities and confinement time are continuously growing until a Greenwald limit disruption takes place. The higher fueling rate multiplication factor is, the earlier collapse happens. Therefore, for a fueling rate of 50% the crucial risk involves an initial melting scenario and a subsequent high energetic disruption whilst for a higher fueling rate the crucial risk involves an instantaneous and very energetic plasma termination. In short, it is necessary to detect an increase of fueling rapidly and activate a fast plasma shutdown (FPSS) since all these perturbations cause structural damage. It is important to note that, for example, for ITER the fueling rate capacity can cover up to $7.8 \cdot 10^{19}\ {}^{}/_{m^3 s}$ (above a multiplication factor of 10 for DEMO1) [16] and hence the dealt scenarios may occur.

Multiplication factor	Plasma termination time $[s]$	Plasma Thermal energy $U\ [GJ]$	Max. T Li_4SiO_4 $[ºC]$
1.5	74.7	2.1	1614
2	19.4	1.95	1566
3	5	1.5	1200
6	1.7	1.3	1034

Table 26: Disruption time and plasma thermal energy for an excessive fueling rate increase.

3.4.2.5 Fueling rate perturbation summary

Mult. factor	Plasma termination	Plasma termination time $[s]$	Consequences	Mitigation	Observations
0 (cut-off)	Beta Limit	25.5	A plasma thermal energy with a rate of 0.5 GJ.	Disruption mitigation system.	-
0.5	Stabilized	-	Fusion power decrease.	Not necessary.	New steady state with lower material temperatures.
1.25	Stabilized	-	Fusion power increase. All temperature limits exceeded.	Fueling rate variation detection.	Melting in less than 20 s.
1.5	Greenwald Limit	74.7	Fusion power increase. Excessive plasma thermal energy (2.1 GJ). All temperature limits widely exceeded.	Fueling rate variation detection and a FPSS activation.	This is the worst scenario due to the high temperatures and the high plasma thermal energy.
2	Greenwald Limit	19.4	All temperature limits widely exceeded. Excessive plasma thermal energy (1.95 GJ). Fusion power increase.	Fueling rate variation detection and a FPSS activation.	-
3	Greenwald Limit	5	All temperature limits widely exceeded. Excessive plasma thermal energy (1.5 GJ). Fusion power increase.	Fueling rate variation detection and a FPSS activation.	-
6	Greenwald Limit	1.7	All temperature limits widely exceeded. Excessive plasma thermal energy (1.3 GJ). Fusion power increase.	Fueling rate variation detection and a FPSS activation.	-

Table 27: Fueling rate perturbation summary.

3.4.3 Improvement in the Confinement System

Historically, AINA has been used in safety analyses to scan the influence of an increase in confinement time [16][19][37] owing, among other reasons, to the H mode discovery occurred on 4 February 1982. Following this path, at first, the behaviour of plasma parameters in case of a permanent increase of confinement time will be simulated and discussed.

Accident description: An unexpected and sudden permanent increase of confinement time takes place at second $t = 0.1\ s$ while the HCPB DEMO reactor is operating on DEMO1 SS.

Event sequence: Confinement time improvement produces a fast increase of ion and electron temperatures as well as densities, which drive to an overall raise of fusion power until plasma terminates disruptively due to the beta limit infringement. In general, PFCs surface temperatures quickly grow, the region OB5 becomes the worst in the first few seconds (~ 0.3 s) and the rest of material temperatures reach very high values which lead to a global melting scenario. The lower the multiplication factor is the grater maximum temperatures are achieved due to the plasma collapse takes place later. Nevertheless, the plasma thermal energy discharged during the disruption cause structural damage and melting in any case, hence, it is necessary to detect instantaneously an unexpected variation in confinement time with the aim of conducing the reactor to a controlled plasma shutdown. On the other hand, this kind of scenarios may be useful to obtain fusion power peaks if the disruption effects could be controlled or a safe state recovered rapidly.

Multiplication factor	Plasma termination time $[s]$	Plasma Thermal energy $U\ [GJ]$	Max. T Li_4SiO_4 $[^{o}C]$	Max. $P_{fus}\ [MW]$
1.5	31.7	2.4	1475	4708
2	5.5	2.4	1432	4905
3	3.7	2.4	1408	5332
5	3	2.4	1388	5565

Table 28: Disruption time and plasma thermal energy for a confinement time improvement.

It is important to note that any confinement time reduction induces a loss of plasma confinement during the first seconds after the perturbation ($< 5\ s$) with a fusion power drop; however, it is not possible to extract the precise consequences of these events from AINA owing to the numerical restrictions derived from the confinement law expressions implemented in the code. Therefore, it must be necessary to detect rapidly a failure in the confinement system which could lead to this kind of situation.

3.4.4 Occasional Variation of Confinement Time

In line with the previous cases, a punctual confinement time variation may happen due to an unexpected behaviour during the operation time. Despite the fact these events might not take place, it was concluded, after an experts' discussion, that analysing the evolution of this kind of phenomena may be useful.

As shown in figures contained in Annex A, the impact of these events is highly dependent on the duration of the confinement time variation and it does not depend so much on the variation factor suffered. Therefore, when the confinement time rises abruptly but decreases after 0.1 seconds, the effects are not severe since both a multiplication factor of 3 and 10 excites the plasma but the steady state is recovered in less than 20 seconds. During this transition an instantaneous fusion power peak is reached due to a fast increase of ion and electron temperatures, as well as the BB materials temperatures rise

slightly but they are stabilized rapidly. On the other hand, in case the duration of the confinement time variation is longer, the operations steady state is recovered whilst the perturbation disappears before the corresponding termination time tracked down in the previous section. For instance, an increase of the confinement time due to a multiplication factor with a value of 3 leads the plasma to a transitional state which can be intrinsically recovered as long as the perturbation lasts less than 3.7 seconds as Table 43 shows. Nevertheless and in spite of the recovery, the longer the duration of the perturbation is the grater maximum temperatures are achieved and it is highly probable that the reactor suffers a melting situation. In view of these circumstances, as in the previous case, it is necessary to detect instantaneously an unexpected variation in confinement time with the aim of conducing the reactor to a controlled plasma shutdown since, for example, as the following table illustrates how a perturbation duration of 1 second leads to high temperatures.

Moreover, in all the cases the region OB5 becomes the most demanded after 0.3 seconds.

Multiplication factor	Perturbation duration $[s]$	Li_4SiO_4 ΔT $[^{o}C]$	Be ΔT $[^{o}C]$	EUROFER ΔT $[^{o}C]$	Max. P_{fus} $[MW]$
3	0.1	13	2.2	0.2	2096
3	0.5	49	7.3	0.9	2423
3	1	102	14.5	1.7	2803
3	3	384	51	6	4790
10	0.1	16	3	0.3	2117

Table 29: Maximum temperature increase and fusion power peak for an occasional confinement time improvement.

3.4.5 Entrance of an Undesired Quantity of Impurities

As already stated, when the reactor is operating, a flux of particles enter the plasma as impurities due to the erosion phenomena which is inherent to the nature of plasma wall interaction. It can be cause of several undesirable effects as a PFC damage or beneficial effects as shutting down the fusion due to an increase of Bremsstrahlung and line radiation, becoming a passive safety mechanism, for instance, if a LOCA takes place. Therefore, the consequences of an undesired quantity of impurities must be studied.

3.4.5.1 Punctual impurity increase up to 300%

Accident description: A punctual increase of the impurities presence (Xe and W) up to 300% takes place at second $t = 0.1\ s$ while the HCPB DEMO reactor is operating on DEMO1 SS. This kind of perturbation can recreate the consequences of a leakage.

Event sequence: This event produces a sudden rise of confinement time, fusion power, power losses (Bremsstrahlung and line radiation); a decrease of the ions and electrons temperatures and, after a few seconds, the achievement of dangerous melting temperatures on the BB materials. A recovery of the initial steady state takes place after 20 seconds; however, the detection of this kind of perturbation and a controlled plasma shutdown must be fast since, as noted, the material temperatures rise rapidly.

Multiplication factor	Li_4SiO_4 ΔT $[^{o}C]$	Be ΔT $[^{o}C]$	EUROFER ΔT $[^{o}C]$	Max. P_{fus} $[MW]$
1.5	51	14.5	1.3	2299
2	130	33.6	3.6	2739
2.5	282	73.5	7	3486
2.9	417	113	11	4196

Table 30: Maximum temperature increase and fusion power peak for a punctual impurity increase.

3.4.5.2 Punctual impurity increase equal or above 300%

Accident description: A punctual increase of the impurities presence (Xe and W) equal to 300% takes place at second $t = 0.1\ s$ while the HCPB DEMO reactor is operating on DEMO1 SS. This kind of perturbation can recreate the consequences of a leakage.

Event sequence: Differing from the previous case, the plasma equilibrium is not recovered after a perturbation of this magnitude. Firstly, the plasma skips instantaneous to the L mode where the fusion power grows (until a peak of 4365 MW), as well as the power losses linked to the greater impurities presence. Consequently, the temperature in the BB rises rapidly (Li_4SiO_4: 1395 ºC, Beryllium: 771 ºC, EUROFER: 572 ºC and Tungsten: 534.8 ºC). Densities are continuously growing until a Greenwald limit disruption takes place at 12 seconds releasing a thermal energy of 1.8 GJ which can damage the reactor structure. Therefore, it is necessary to detect an important leakage instantly and leading the reactor to a controlled plasma shutdown in order to mitigate or prevent these possible an undesirable consequences.

3.4.5.3 Tungsten permanent entrance increase

Accident description: An increase of the Tungsten impurity production takes place from second $t = 0.1\ s$ while the HCPB DEMO reactor is operating on DEMO1 SS. The previous cases could recreate the consequences of a leakage, however, in this case the simulation recreates a variation of the production rate and, consequently, the number of impurities which arrive to the plasma core permanently. These phenomena might occur due to the deterioration of the PFCs.

Event sequence: In this case; fusion power, densities and confinement time are continuously and slowly growing. Depending on the new impurity production rate the plasma may reach a new steady state or it might collapse by mean of the infringement of the Greenwald limit. Nevertheless, any alternative is not instantaneous, so the incident detection must be previous to the endpoint in order to prevent a melting scenario which could take place for any case.

3.4.6 Load Peak against the Divertor

Certain regions of the DEMO divertor may suffer important load peaks in the reality that differ from the average value used during AINA simulations. This peak can grow up to $6.23\ {}^{MW}/_{m^2}$ [11], hence the importance of simulating and procuring the temperature profile along the 1D divertor segmentation in order to ensure the not exceeding of the melting limits. As shown in Figure 50 the temperatures in normal operation conditions without any LOCA do not outperform the specified limits. The Tungsten reaches a temperature of up to 483°C, significantly lower than the limit 3422ºC. Likewise, the Cooper and the CuCrZr temperatures belonging to the internal structure are far below the respective constrains as well. Therefore and unlike the HCPB BB design, the DEMO divertor design seems to be supporting the operational conditions with some margin. Despite this substantial safety margin, possible negative consequences will have to be beard in mind in the future accident studies referring to LOCAs covered in the next section. Moreover, it is important to remember that the divertor modeling used in AINA is a preliminary configuration which shall be updated and improved.

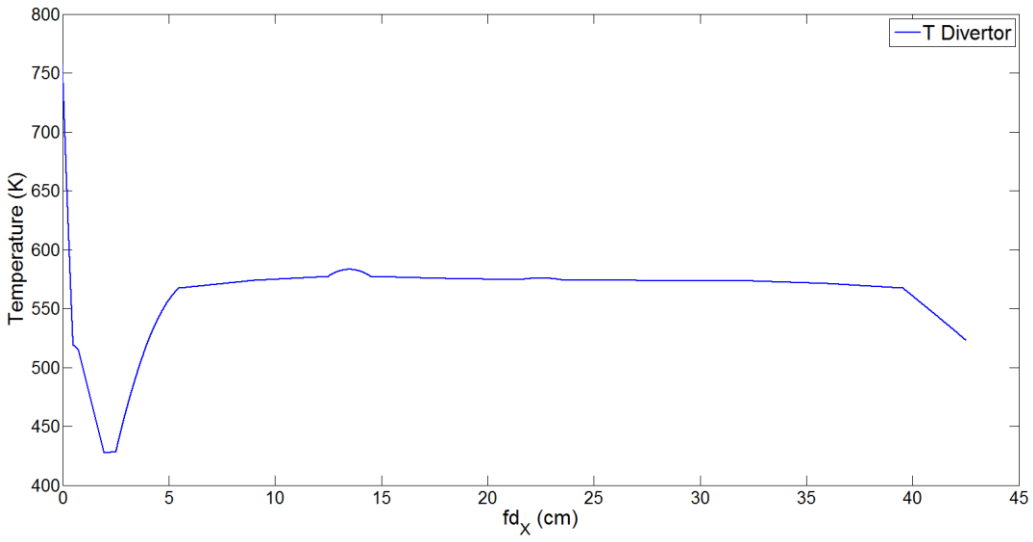

Figure 50: Temperature profile along the 1D segmentation of the divertor when a $P_{rad} = 6.23\ {}^{MW}/_{m^2}$ takes place.

3.5 LOCA Accidents

First of all, it should be underlined that Annex A shows all figures extracted from AINA LOCA simulations used in this section. Only for the first case (BB LOCA 30% in all the cooling loops) has been attached all the historical graphs (fusion power, densities, ion and electron temperatures, betas, NWL...) and which refer to the plasma conditions. This is due directly to LOCA perturbations only affect the temperature profile along the BB and the divertor materials; however, the production rate of Tungsten by sublimation process (depending on material temperature) is greatly lower than physical sputtering process (virtually independent of temperature). Consequently since the entrance of impurity is not affected by this kind of perturbations, conditions inside the plasma remain practically unchanged. In the end, those absent figures in Annex A for any case which is not the first one would be the same as in this first case. On the other hand, it is important to remember that the divertor modeling used in AINA is a preliminary configuration which would be advisable to improve and update when a more detailed thermo-hydraulic assessment for the final design of the divertor carries out; for this reason, the conclusions drawn from the LOCA simulations for the divertor must be taken with a grain of salt. Nevertheless, a preliminary overview of its behaviour may be emanated from these analyses and initial lessons may be learned.

Moreover, it is important to note that as it was introduced throughout M. Fabbri's thesis [2] the conclusions which are drawn from the thermal transients are indicative and may vary with a more accurate model as Figure 51 demonstrates. Because this study is the first accident evaluation of the HCPB transient behaviour, no direct comparison is possible. More optimistic and realistic results could be obtained increasing the No. of discretization for the last layer (from 500 nodes to 3000; it is worth reminding that the cooling parameters $f_{WGT,R}$ and $f_{WGT,P}$ must be tuned to match the solution function in shape and magnitude.) due to its big thickness but the total computational time would be enormous. For this reason and as Fabbri [2] suggested, scaling factors to compensate unrealistic results will be used to estimate the maximum temperatures for the last layer of the blanket when a LOCA takes place. In overloads transient cases (LOPC accidents) has not been necessary to adapt the results since the temperature peaks and distributions were very similar between a more accurate model and the reduced computational time model implemented in AINA. Nevertheless, the conclusions extracted from the LOCA

accident analysis are unlikely to vary significantly since the temperature peak of the last layer largely surpasses the melting limits in the first instants (10 - 20 s) for all the materials even though the thermal blanket model in AINA was more refined. The results extracted from the study used to estimate the scaling factors to compensate unrealistic results and the expression used to calculate more optimistic temperatures are shown hereafter:

LOCA 50%	$\Delta T_{3000nodes}$	$\Delta T_{500nodes}$	Mult. Factor f_{opt}
Li_4SiO_4	64	272.7	0.23
Be	21	78.4	0.27
EUROFER	1	5.4	0.19

Table 31: Scaling factors for converting last layer temperatures into more accurate values.

$$T_{accurateTransient} = T_{SteadyState} + \left(f_{opt} \cdot \Delta T_{500nodes}\right)$$

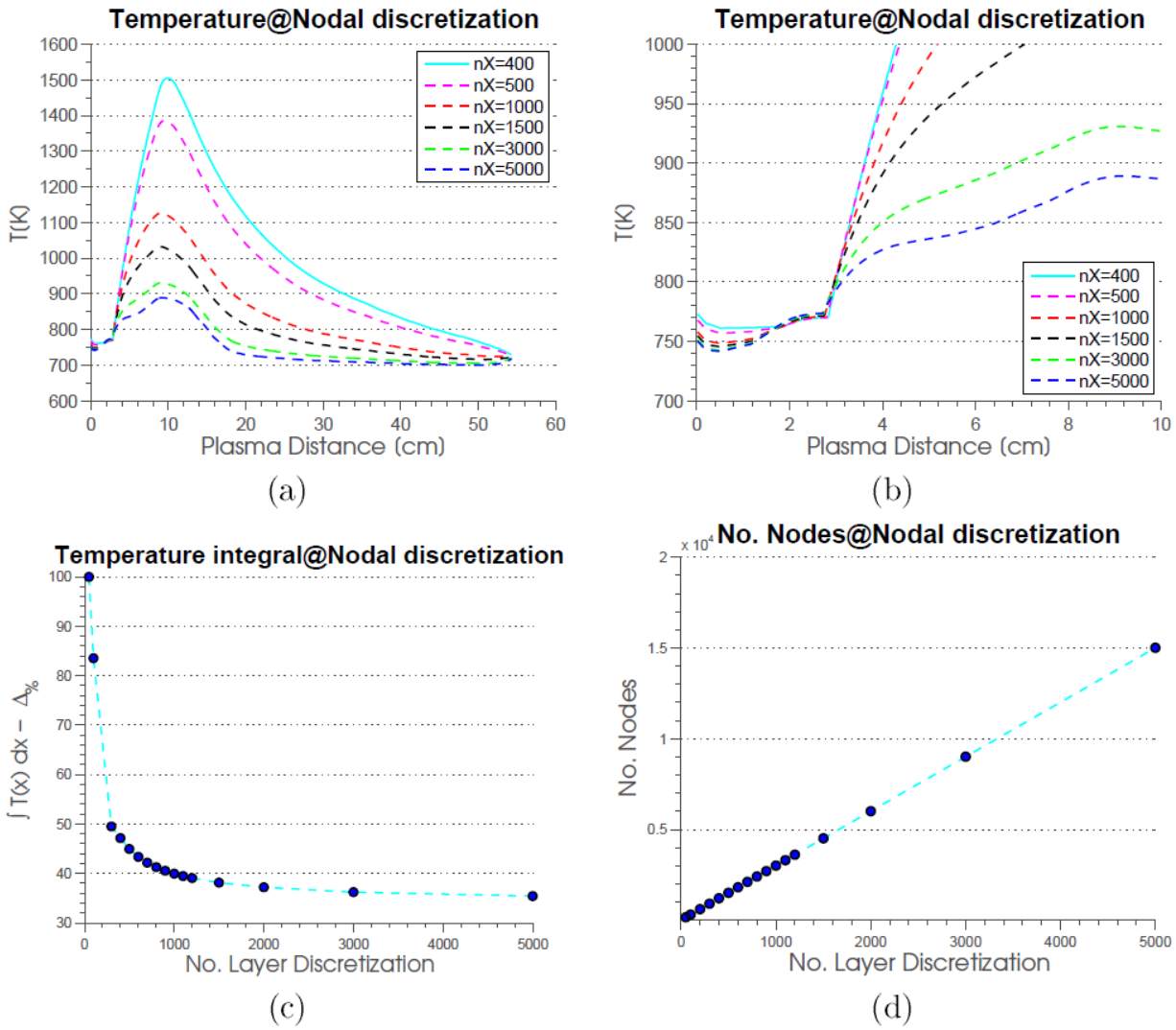

Figure 51: Meh sensibility.

3.5.1 BB LOCA 30%

Accident description: an small LOCA simulation where the He loop No.1, the He loop No. 2 and the FW channel of the BB architecture loses 30% of the mass flow rate at second $t = 0.1\ s$ while the HCPB DEMO

reactor is operating on DEMO1 SS. The perturbation is applied using a step function and hence the progressive decrease of the mass flow rate has not been taken into account.

Event sequence: As indicated above, only the material temperatures of the BB structure change; the plasma parameters remain virtually unchanged. This temperature distribution is affected both in magnitude and in shape due to the modification of the cooling features and, as logic, enhanced variations are placed in most loaded areas. At 40 s a new steady state is found even though some maximum material temperatures reached are far greater than design limits (Li_4SiO_4: 1079 ºC, Beryllium: 716 ºC and EUROFER: 566 ºC / more accurate: Li_4SiO_4: 979 ºC, Beryllium: 687 ºC and EUROFER: 563.6 ºC). The spatial position of these material temperature peaks is unchanged and around 9 cm due to the proximity to the internal coolant loops affected. Moreover, Li_4SiO_4 is more sensitive than other material due to the lower thermal conductivity and, as observed in the steady state, the Beryllium and Li_4SiO_4 suffers higher temperature since the effect of the convention is less effective due to a bigger distance from the cooling channel lines. EUROFER distribution is almost unchanged. The Tungsten FW suffers a slight temperature increase (Tungsten: 491.8 ºC) as well; but it is kept far below its melting limit. It is important to note that if just the internal loops (the He loop No.1, the He loop No. 2) suffer this level of LOCA, the temperature of the FW is not susceptible to change. On the other hand, if just the FW channel suffers this level of LOCA the maximum temperature of the Li_4SiO_4 rises by 0.5 ºC for the most conservative case (500 nodes). In summary, it is essential to be able to guarantee a very quick detection if the LOCA takes place in the internal loops (the He loop No.1, the He loop No. 2) in order to proceed to a proper mitigation action such as a fast plasma shutdown (FPSS) injecting impurity gases (e.g. Ne, Ar, etc.) as in ITER. Thus, it would be possible to prevent a melting damage inside the internal structure of the BB. On the other hand, from the AINA results, it might be concluded as well that a small rupture in the FW cooling channel is less dangerous and the reaction time margin is much longer.

3.5.2 BB LOCA 60%

Accident description: a medium LOCA simulation where the He loop No.1, the He loop No. 2 and the FW channel of the BB architecture loses 60% of the mass flow rate at second $t = 0.1\ s$ while the HCPB DEMO reactor is operating on DEMO1 SS. The perturbation is applied using a step function and hence the progressive decrease of the mass flow rate has not been taken into account.

Event sequence: Once again, only the material temperatures of the BB structure change; the plasma parameters remain virtually unchanged. A new steady state is found at 50 s even though, as in the previous case, some maximum material temperatures reached are far greater than design limits (Li_4SiO_4: 1359 ºC, Beryllium: 805 ºC and EUROFER: 574 ºC / more accurate: Li_4SiO_4: 1032.6 ºC, Beryllium: 711.6 ºC and EUROFER: 565 ºC). The spatial position of these material temperature peaks remains unchanged (9 cm) and it is validated the fact that Li_4SiO_4 is more sensitive than other material due to the lower thermal conductivity and the Beryllium and Li_4SiO_4 suffers higher temperature since the effect of the convention is less effective due to a bigger distance from the cooling channel lines. The Tungsten FW temperature is slight higher than in the previous case (Tungsten: 509.6 ºC) however it is kept far below its melting limit. It is important to note that if just the internal loops (the He loop No.1, the He loop No. 2) suffer this level of LOCA, the temperature of the FW is not susceptible to change. On the other hand, if just the FW channel suffers this level of LOCA the maximum temperature of the Li_4SiO_4 rises by 1 ºC for the most conservative case (500 nodes). Therefore, the temperature along the profile is strongly linked with its particular principal cooling channel for every region. As previously, with the objective of proceeding to a proper mitigation action it is essential to be able to guarantee a very quick detection if the LOCA takes

place in the internal loops (the He loop No.1, the He loop No. 2). Thus, it would be possible to prevent a melting damage inside the internal structure of the BB. On the other hand, a medium rupture in the FW cooling channel may be bearable by the HCPB design.

3.5.3 BB LOCA 90%

Accident description: a big LOCA simulation where the He loop No.1, the He loop No. 2 and the FW channel of the BB architecture loses 90% of the mass flow rate at second $t = 0.1\ s$ while the HCPB DEMO reactor is operating on DEMO1 SS. The perturbation is applied using a step function and hence the progressive decrease of the mass flow rate has not been taken into account.

Event sequence: The overall behaviour of the reactor is analogous to the previous cases although it causes a greater and faster temperature impact since bigger temperature increase in the first time-steps despite the new steady state is found at 160 s. In this simulation and getting worse the previous cases, the design limits are excessively surpassed and thus a global melting would be nearly instantaneous (Li_4SiO_4: 4342 ºC, Beryllium: 1425 ºC and EUROFER: 647.7 ºC / more accurate: Li_4SiO_4: 1599.3 ºC, Beryllium: 879 ºC and EUROFER: 579 ºC). In addition, the temperature distribution shape is deeply affected. Likewise, the Tungsten FW reaches a higher temperature than in the earlier cases (Tungsten: 600.9 ºC) and despite the fact that the melting limit is not surpassed, the liberation rate of Tungsten by sublimation processes is slightly rising in the long term. If just the internal loops (the He loop No.1, the He loop No. 2) suffer this level of LOCA, the temperature of the FW is not susceptible to change; likewise, if just the FW channel suffers this LOCA the maximum temperature of the Li_4SiO_4 rises just by 2 ºC for the most conservative case (500 nodes). Therefore, once again, the temperature along the profile is strongly linked with its particular principal cooling channel for every region. As above, a very quick detection if the LOCA takes place in the internal loops (the He loop No.1, the He loop No. 2) is extremely necessary as well as a proper and fast mitigation action such as a fast plasma shutdown (FPSS) injecting impurity gases (e.g. Ne, Ar, etc.) as in ITER which may stop the reactor in less than 3 s [132]. As in the medium and small LOCA cases, a big rupture in the FW cooling channel may be bearable by the HCPB design; even so, its detection is necessary to prevent other negative impacts such as long term damages.

3.5.4 Divertor LOCA 30%

Accident description: an small LOCA simulation where the CB and the PFC cooling loops of the divertor architecture loses 30% of the mass flow rate at second $t = 0.1\ s$ while the HCPB DEMO reactor is operating on DEMO1 SS. The perturbation is applied using a step function and hence the progressive decrease of the mass flow rate has not been taken into account.

Event sequence: As in the BB LOCA cases, only the material temperatures of the divertor structure changes; the plasma parameters remain virtually unchanged. Specifically, when an small LOCA takes place in the divertor, the temperature along the divertor is affected however this increase is very mild; in the order of 5 ºC for the Tungsten of the PFC (from 181.8 ºC to 186.9 ºC), 5 ºC for the Cooper and the CuCrZr of the PFC and 2 ºC for the EUROFER of the CB. In this case, the behaviour of all the materials used in the divertor design have a similar level of thermal sensitivity due to their thermal conductivity and the architecture of the cooling circuits. If just the CB loops suffers the LOCA, the temperatures of the PFC materials remain almost unchanged and something similar takes place when the LOCA concerns the PFC loop since the temperature in the CB does not vary. In summary, a small LOCA in the divertor may be bearable by the divertor configuration, however a detection of the problem would be desirable in order to prevent other negative consequences such as any other simultaneous failure. On the other

hand, as already noted, certain regions of the DEMO divertor may suffer important load peaks $6.23\ {}^{MW}/_{m^2}$ that differ from the average value used during AINA simulations; nevertheless, due to the substantial margin the melting limits and the divertor temperatures extracted from AINA, it might suggest that this kind of accident could be tolerable for these demanded regions as well.

3.5.5 Divertor LOCA 60%

Accident description: a medium LOCA simulation where the CB and the PFC cooling loops of the divertor architecture loses 60% of the mass flow rate at second $t = 0.1\ s$ while the HCPB DEMO reactor is operating on DEMO1 SS. The perturbation is applied using a step function and hence the progressive decrease of the mass flow rate has not been taken into account.

Event sequence: When a medium LOCA takes place in the divertor, the temperature increases 16 ºC in the Tungsten of the PFC (from 181.8 ºC to 198.2 ºC), 16 ºC in the Cooper and the CuCrZr of the PFC and 6 ºC in the EUROFER of the CB. This temperature rise is stabilized after 100 s. Logically, the temperature increase is higher than in the previous case; nevertheless, it still remains mild and far below the melting limits. On the other hand, it is validated the fact that the behaviour of all the materials used in the divertor design have a similar level of thermal sensitivity due to their thermal conductivity and the architecture of the cooling circuits. As in previous case, the temperature along the profile is strongly linked with its particular principal cooling channel for every region (PFC and CB cooling behaviours are very independent each other). As before, a medium LOCA in the divertor may be bearable by the divertor configuration not only for the average value used during AINA simulations and for the real load peaks $6.23\ {}^{MW}/_{m^2}$ as well, however a detection of the problem would be desirable in order to prevent other negative consequences.

3.5.6 Divertor LOCA 90%

Accident description: a big LOCA simulation where the CB and the PFC cooling loops of the divertor architecture loses 90% of the mass flow rate at second $t = 0.1\ s$ while the HCPB DEMO reactor is operating on DEMO1 SS. The perturbation is applied using a step function and hence the progressive decrease of the mass flow rate has not been taken into account.

Event sequence: When a big LOCA takes place in the divertor the temperature stabilization occurs after 200 s suffering a Tungsten temperature increase of the PFC of 76 ºC (from 181.8 ºC to 258.2 ºC), a Cooper and CuCrZr temperature increase of the PFC of 74 ºC and a EUROFER temperature increase of the CB of 35 ºC. The most demanded spatial position of the CB is around 13.5 cm. It is evident that this level of LOCA causes a higher temperature impact along the divertor although, once again, the melting temperature restrictions are not exceeded. As earlier cases, with the objective of preventing other negative consequences a fast detection of the accident would be necessary.

3.5.7 Divertor and BB LOCA 30% or 60% or 90%

Accident description: a LOCA simulation where the CB and the PFC cooling loops of the divertor architecture and the He loop No.1, the He loop No. 2 and the FW channel of the BB architecture loses 30% or 60% or 90% of the mass flow rate at second $t = 0.1\ s$ while the HCPB DEMO reactor is operating on DEMO1 SS. The perturbation is applied using a step function and hence the progressive decrease of the mass flow rate has not been taken into account. This kind of accident may be due to a loss of the

cooling mass flow in the Primary Heat Transfer System (PHTS) which might affect the overall cooling system.

Event sequence: In summary, the consequences of this kind of accident are the sum of both phenomena discussed previously separately (the BB LOCA and the divertor LOCA). As has been pointed previously, the most relevant effect is a melting global scenario, specifically the internal BB materials would be the most demanded; for this reason, it would be necessary to assure a proper detection system in order to identify rapidly a loss of the cooling mass flow in the Primary Heat Transfer System (PHTS) and to lead the reactor to a safe shutdown as it has been agreed in the earlier cases.

3.6 Conclusions

First and foremost, it is necessary to recall the fact that, on the basis of the information drawn from AINA simulations, certain temperatures reached during an operational scenario according to the steady state DEMO1 permanently and slightly exceed the design melting limits (an excess of 4%). Specifically, this transgression affects the BB architecture. For this reason and even though it may be explained by the intrinsic deviation of the thermal HCPB blanket model (a temperature deviation of 5% [2]) which was extracted from its validation phase, all the outcomes and all the conclusions which may be derived from the HCPB AINA safety analysis must be judged according to this tenet and keeping in mind a possible design review focused on ensuring a suitable operating temperature range with a bigger safety margin for all the materials which make up the HCPB BB. Likewise, all the information drawn from the divertor thermal model has to be taken with a grain of salt since this modeling is preliminary and subjected to possible improvements and updates.

With regard to LOCAs to the BB, from AINA outcomes, it concludes that this kind of failure inside the cooling system does not affect the internal plasma conditions but, undoubtedly, even a slight loss of the mass flow (about 30%), leads the reactor to an overall melting scenario rapidly since the material temperatures increase drastically during the first seconds after the cooling channel rupture. Specifically, the most demanded area is the Li_4SiO_4 layer due to its lower thermal conductivity and a big distance from the cooling channel lines, consequently, the effect of the convention is less effective than in the other layers. For this reason, it is indispensable the installation of a quick response system capable of detecting a cooling anomaly rapidly and activating a proper mitigation action such as a fast plasma shutdown FPSS injecting impurity gases (e.g. Ne, Ar, etc.) as in ITER.

On the other hand and broadly speaking, there are three possible scenarios when a LOPC takes place. At best, a new steady state with a fusion power decrease and lower temperatures along the HCPB and divertor structure may be achieved. This case would be safe and a mitigation system or action would not be necessary. Further, it could be considered that the new steady states achieved in these cases could be better candidates for DEMO operation from the point of view of temperature limits no exceedance and despite the generation of lower fusion power and, consequently, less gain. An increase of the external power injection between 200% and 630% and a decrease of the fueling injection rate are those anomalies may lead the reactor to this kind of non-dangerous situation. Another potential consequence would involve a risk of structural damage due to a very energetic plasma termination which may discharge a great amount of thermal energy against the internal reactor walls. From AINA outcomes, an increase of the external power injection above 630% would disrupt within a short period of time (89 s at best) and transferring 1.5 GJ of thermal energy against the walls that damages and melts the structure. Notwithstanding the foregoing, this situation would be highly unlikely since, in principle, it would not be

possible to reach such high external power. Likewise, a cut-off of the fueling injection may induce to a plasma collapse in 25 s; however the thermal power released and around 0.5 GJ could be mitigated by a proper disruption mitigation system and, thereby, safeguarding the BB material. Finally, the third potential consequence arisen from a LOPC is the same as the impacts emerged when a LOCA takes place, a melting process. From the analysis of the AINA simulations, this situation might occur due to a decrease or a cut-off of the external power injection, a fueling rate injection increase up to 25%, an occasional variation of confinement time beneath the corresponding termination time and a punctual impurity increase up to 300%. All these situations may be highly dangerous since temperatures rise extremely rapid. In contrast to LOCA detection system which must identify a failure in the cooling system, in this case it is essential to be able to guarantee a quick detection and actuation by means of a proper system depending on the affected equipment because just an increase temperature detection system must not be fast enough. For example, a monitoring failure system for the external power injection equipment or the fueling injection equipment is necessary as well as an impurity detection system. A system to monitor the confinement time is more complex, therefore, in this case, it would be essential the aforementioned increase temperature detection system. The mitigation action would be the activation of a fast plasma shutdown (FPSS) for all the cases. Last but not least, there are certain incidents which may drive the reactor to suffer not only a melting scenario and a very energetic plasma disruption at the same time. These triggers are an increase of fueling injection above 50%, a permanent improvement in the confinement time and a punctual impurity increase above 300%. Therefore and owing to the double effect, there are the most critical failures and a special attention in order to avoid them will be necessary. The measures to be taken are the mitigation systems and actions for the particular cases explained previously.

4 AINA DCLL, HCLL, WCLL

4.1 Short Introduction and Objectives of Work

During 2018, safety analyses contributions, similar to the HCPB one, were carried out for the DCLL, HCLL and WCLL DEMO designs and they and their relevant findings will be presented throughout the current chapter.

Eventually the final section summarizes the overall conclusions presented in the previous chapters.

4.2 DCLL Blanket

4.2.1 Introduction

The DCLL Blanket System is based on the use of:

- The Reduced Activation Ferritic/Martensitic (RAFM) steel EUROFER as structural material.
- The eutectic Pb–15.7Li enriched at 90% in ^{6}Li as main coolant (power extraction), tritium breeder and neutron multiplier.
- The He gas as secondary coolant for the wall exposed to plasma and supporting structures [140].

In 2016, the DCLL design has been adapted to the current DEMO 2015. The evolution of the BB segments from DEMO 2014 to DEMO 2015 was mainly characterized by the increase of the poloidal size. The current OB segments have the same number of modules than in DEMO 2014 (8) but with a new distribution (several modules with a FW length larger than 2 m), whereas the number of modules in the IB segments has been increased from 7 to 8 [141]. Nevertheless, the BB model of AINA maintains the organization in multi-module segment (MMS) arrangement with 7 OB and 7 IB BB modules per segment [59] used for the HCPB-2015 v3 model in order to benefit from the code already implemented (NWL distribution, segments areas…). As seen in the following figure, the NWL distribution is almost equal regardless of the segmentation applied.

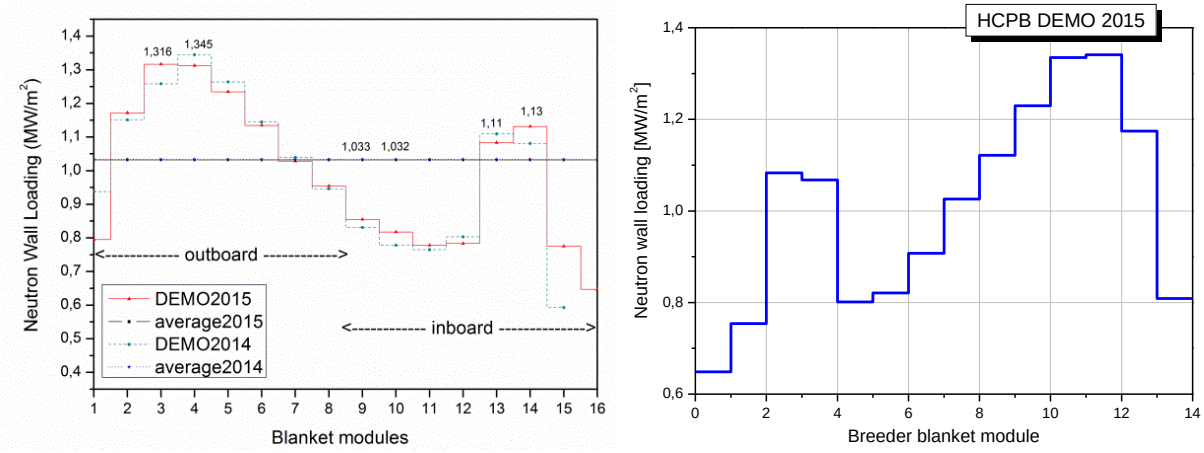

Figure 52: NWL poloidal distributions on the FW for the DCLL DEMO2015 model (left) [141] and Neutron Wall Loading poloidal distributions on the FW for the HCPB-2015 v3 model (right) [59].

For AINA, the OBC (Outboard Central Segment) equatorial module (OB4) design has been studied for the purpose of modelling a thermal DCLL BB. The current design is called v3.1 and is the update from the previous design version 2.0 [140][142].

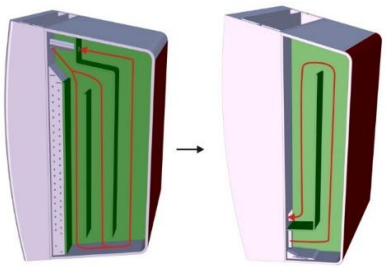

Figure 53: Comparison of the v2.0 (left) and the current v3.1 (right) [143].

4.2.2 General Architecture

The general features of the modules are:

- They are composed of these radial layers: the Tungsten armor, the FW, the breeding zone, the backwall and the BSS (Back Supporting Structure). This composition will be described in more detail in the next sections as in Figure 59.
- Regarding the breeder zone (BZ):
  - Each module is toroidally divided into 7 PbLi circuits by radial stiffening plates.
  - PbLi flows in parallel through channels with rectangular cross-section.
  - PbLi flows mainly in poloidal direction (counter-flow in channels separated by a toroidal stiffening plate).
- There is an internal manifold to feed Helium to the different box structures, including the FW.
- Regarding the BSS: There are several long poloidal ducts for distribution and collection of the coolants (2 PbLi + 4 He) and contains the radial distribution of high/low temperature streams.
- DCLL modules are cooled in parallel in order to reduce the pressure loss [144].

4.2.3 PbLi Circuits

At the release date of the v2.0, all the BB pipes were required to be routed through the VV upper ports to make easier the remote maintenance procedure and gravity draining was not contemplated. For that reason, the v2.0 routing did not allow to drain the modules. Therefore, the locations of both the inlet and the outlet channels were moved from the top to the bottom of the module, so that PbLi circulates upwards near the FW, turns at the top and goes downwards along the rear channel in the current v3.1. This scheme allows the total or partial draining of the module, depending on its inclination [141].

Besides, as stated before, the coaxial inlet/outlet pipes with circular cross-section, which involved potential MHD and thermal problems, were substituted by rectangular cross-section openings placed at different poloidal positions [141].

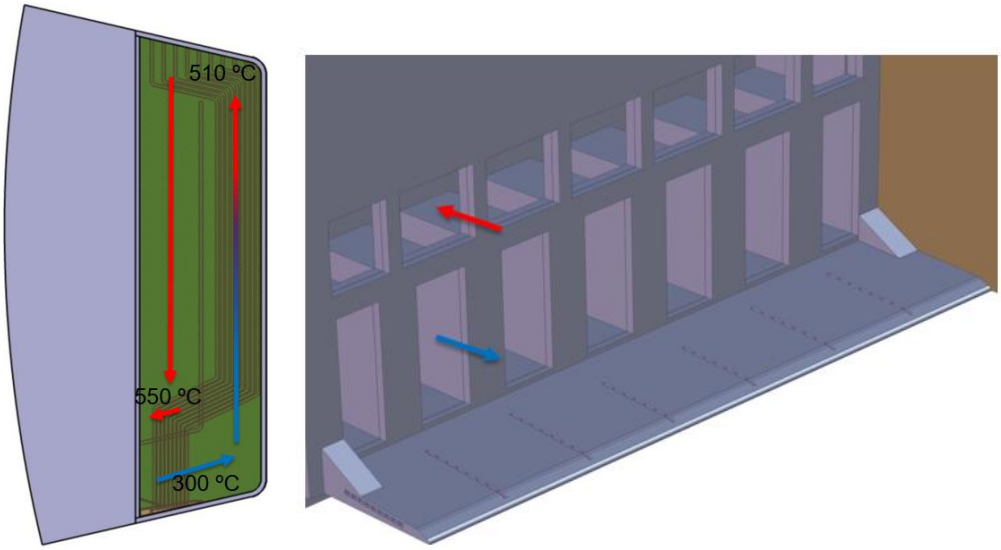

Figure 54: PbLi routing in the current v3.1 (left) and PbLi inlet/outlet connections in the current v3.1 [144].

Moreover, the v3.1 CAD [145][146] model includes a complete set of FCIs (Flow channel inserts) which is made up of an alumina sandwich FCI (0.1 mm thick Al2O3 layer between 2 plates of 0.5 mm thick EUROFER) with a gap of 2 mm between the FCI and the structure walls [141].

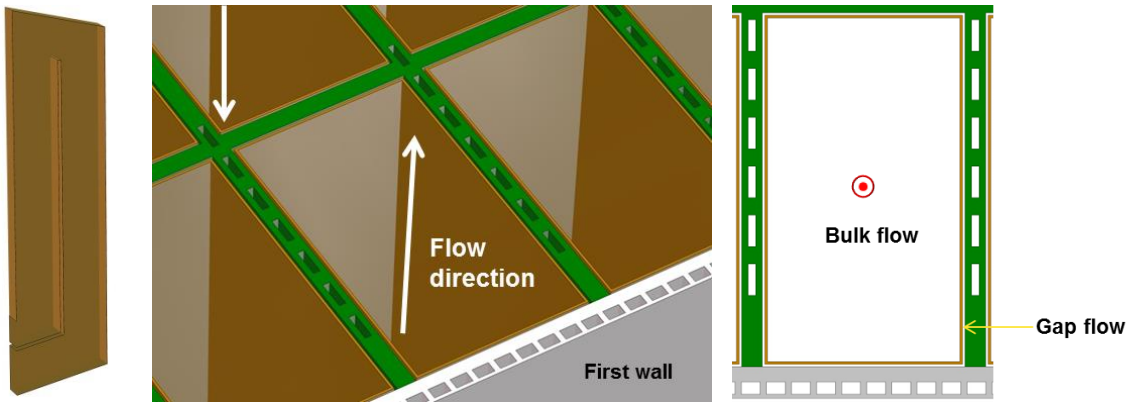

Figure 55: Flow channel inserts. Toroidal cut view of FCI covering a whole channel (left), detailed poloidal cut view (central) and schematic top view (right) [141].

4.2.4 Helium Circuits

Previously, Helium circulated twice along the FW in order to increase the outlet temperature. In the current v3.1 there is just one pass in poloidal direction along the FW, which is longer than the previous one; leading to less velocity and a pressure drop [141][143].

Another important difference is that now the radial walls (side walls and radial stiffening plates) are cooled in parallel between them but in series with the FW (including top and bottom walls). There is a direct feeding from the FW channels to the radial walls channels (cooling in series), which simplifies the mass flow distribution according to requirements and maximizes the Helium outlet temperature [141][144].

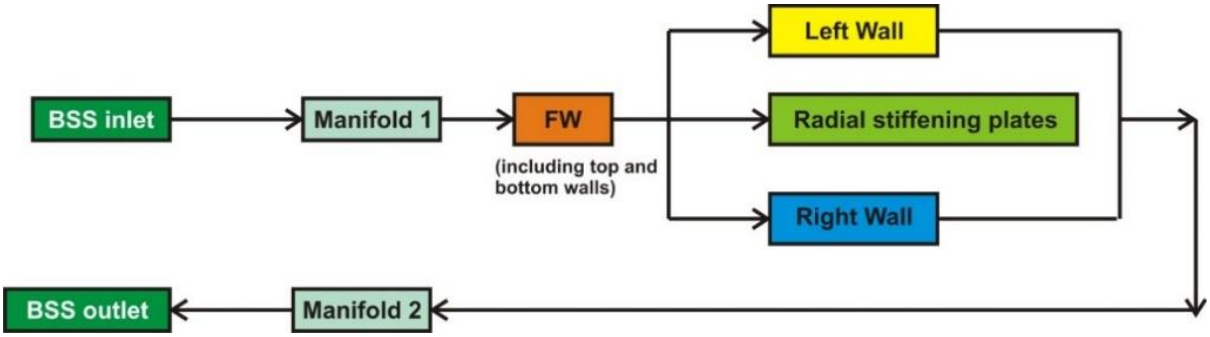

Figure 56: He flow diagram [141][143][144].

The dimensions of the Helium channels are 20x8 mm^2 with a distance between the Helium channels and the interface W-EUROFER of 1.5 mm.

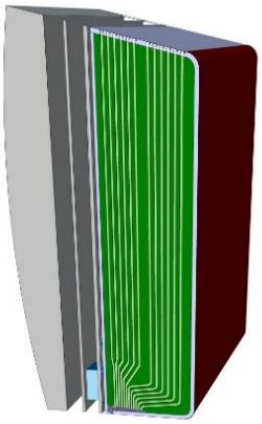

Figure 57: Cut view of a radial stiffening plate for the OBC [141].

4.2.5 Back Supporting Structure

The DCLL BSS integrates the service connections for all the modules. Besides, it must accomplish shielding and supporting functions. It consists in a long 'C-shape' (OB segments) or 'cane-shape' (IB segments) structure with a series of poloidal ducts covering the whole length of the segment. Such ducts, combined with small radial channels which connect the BSS and the modules, are used for distributing the PbLi and Helium flows to the different modules in a segment as well as to collect the outlet flow and to extract it towards the auxiliary systems. The rationale for the definition of the PbLi channels has been to minimize the corrosion, the pressure drop and the MHD effects. Thus, a low and constant flow velocity has to be maintained varying the cross-section area of the PbLi/He channels. [141]

4.2.6 Design Evolution

In summary, the evolution of the OB4 from v2.0 to v3.1 is characterized by:

- One of the main differences with the previous design is that the backwall of the modules is now separated 2 cm from the BSS front wall [141].
- Larger poloidal dimension. Smaller radial dimension of the breeding zone but larger space allocated for the BSS.
- Reduction of poloidal PbLi channels (from 3 to 2).
- Increase in the number of parallel channels in toroidal direction (from 6 to 7).

- Substitution of the coaxial inlet/outlet pipes with circular cross-section (potential MHD and thermal problems) by rectangular cross-section openings placed at different poloidal positions.
- The dimensions of the FW channels have changed from 15x10 mm^2 to 20x8 mm^2.

Please for more information about the DCLL v3.1 refer to EFDA_D_2N7G6D [141].

4.2.7 Material Properties: Lead-Lithium

Most of the material properties employed in the AINA DEMO DCLL has already outlined throughout the analogous chapter for the AINA DEMO HCPB. For this reason, only properties of Lead-Lithium must be described.

The properties of Lead-Lithium at the eutectic composition (Pb15.7Li) have been taken from [147]. It is important to remember the double function in the DCLL as main coolant and as tritium breeder, tritium carrier and neutron multiplier. The PbLi melting point is set in 235 ºC, therefore defining one of the operational limits for this breeder. The expressions presented in following equations have been assumed for the density, specific heat, thermal conductivity and dynamic viscosity, respectively:

$$\rho\left[\frac{kg}{m^3}\right] = 10520 \cdot (1 - 1.13 \cdot 10^{-4}T) \qquad (135)$$

$$Cp\left[\frac{J}{kg \cdot K}\right] = 195 - 9.116 \cdot 10^{-3}T \qquad (136)$$

$$k\left[\frac{W}{m \cdot K}\right] = 1.95 + 19.6 \cdot 10^{-3}T \qquad (137)$$

$$\mu\,[Pa \cdot s] = 1.87 \cdot 10^{-4} \cdot e^{\frac{11640}{RT}} \qquad (138)$$

4.2.7.1 Methodology to Compute the PbLi Heat Transfer Coefficient

A similar procedure to that used for the He and W cooling channels for the HCPB [2] and divertor model has been followed for the purpose of computing the PbLi heat transfer coefficient which is described hereinafter.

The PbLi heat transfer coefficient is computed as:

$$h = \frac{Nu \cdot k}{D} \qquad (139)$$

where Nu is the Nusselt number, k is the PbLi thermal conductivity $[W/m/k]$ which has been dealt in Lead-Lithium properties section; $D\,[m]$ is the hydraulic diameter which, having a rectangular cross sections, is estimated as:

$$D = 4 * \frac{A}{P} \qquad (140)$$

where A is the channel section $[m^2]$ and P is the wetted perimeter $[m]$.

In the case of Nusselt number, the Ji and Gardener correlation has been used [142][148]:

$$Nu = 7 + \frac{0.00782 \cdot Pe^{0.811}}{1 + 4 \cdot 10^{-4} \cdot Ha^{1.5} \cdot f(Pe)} \qquad (141)$$

Where Pe is the Péclet number and Ha is the Hartmann number.

$$Pe = Re_D \cdot Pr \qquad (142)$$

$$f(Pe) = 0.3 + 4.75 \cdot 10^{-5} \qquad (143)$$

where the Reynolds Number is:

$$Re_D = \frac{\rho\, v\, D}{\mu} \qquad (144)$$

Where ρ is the fluid density $[kg/m^3]$ and μ is the dynamic viscosity $[kg/m/s]$ which have been dealt in Lead-Lithium properties section and v is the PbLi velocity $[m/s]$.

$$v = \frac{\dot{m}}{\rho \cdot A} \qquad (145)$$

where $\dot{m}$ is the mass flow $[kg/s]$.

The Prandlt number, Pr, is:

$$Pr = \frac{C_p \cdot \mu}{k} \qquad (146)$$

where C_p is the heat capacity $[J/kg \cdot K]$ which has been dealt in Lead-Lithium properties section.

The Hartmann number is estimated as:

$$Ha = \frac{Re_D}{200} \qquad (147)$$

The preceding expression is derived from the following figure assuming a PbLi turbulent flow for the DCLL design [149]. Moreover, it has been selected after a scanning study with the aim of ensuring that the heat transfer coefficient decreases with the mass flow along the scale of values that this magnitude may take.

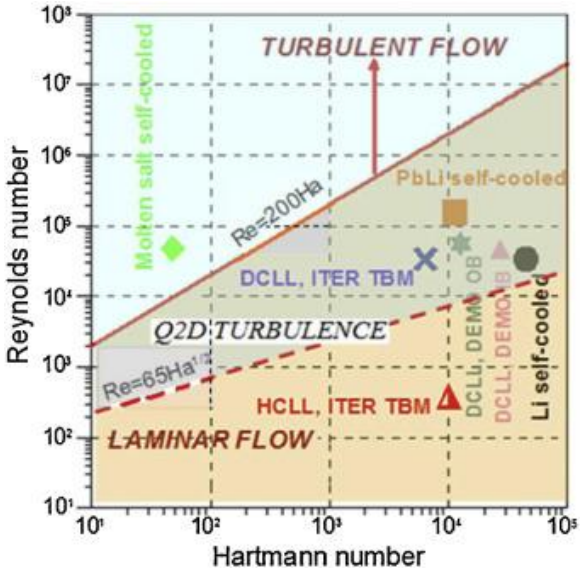

Figure 58: Hartmann–Reynolds number diagram [149].

4.2.8 AINA DCLL Wall model

The 1D AINA DCLL thermal blanket model is based on the methodology used to develop the 1D AINA HCPB thermal model [2] doomed to represent the behaviour of the more complex 3D CFD models. Therefore, a 1D simplified model has been built and consolidated using the results extracted from the thermal-hydraulic analysis performed by Fernández et al [141].

4.2.8.1 Model Description

The AINA DCLL thermal blanket model shall aim to represent the most conservative thermal behaviour of the whole DCLL BB in the simplest possible way in order to check if EUROFER exceeds its melting limit (550 ºC) in the worst case. Currently, the most accurate thermal-hydraulic study of the DCLL v3.1 has been created in the PLATOON code [141][150] (PLAtform for Thermal-hydraulic One-dimensional OutliNe is a steady-state code written in MATLAB Simulink which is currently being adapted to perform transient analyses) in order to determine the key parameters affecting the performance of the primary heat transfer system and the power conversion system (mass flows, inlet and outlet temperatures, pressure drop in the PbLi and He circuits, etc.) [141]. The maximum EUROFER temperatures drawn from this study will be used to recreate a 1D segmentation along the blanket composed of the worst case for each layer depth.

The model will be based on the OBC equatorial module (OB4) which has been historically selected as the most demanded region. Its design and its components composition is described in following figure and tables.

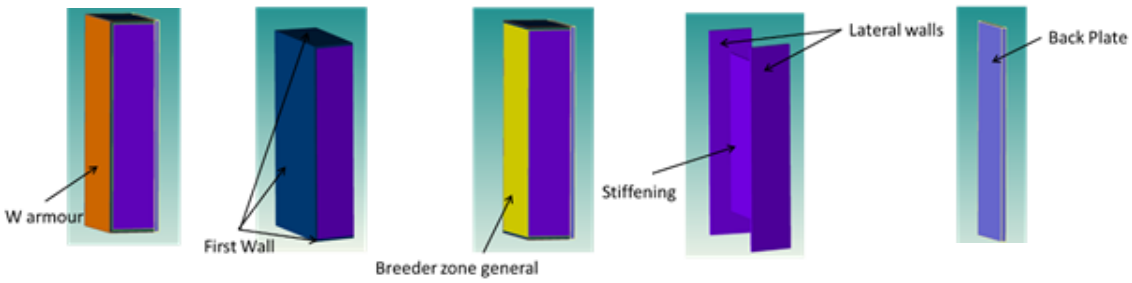

Figure 59: Components of the blanket modules in the DCLL v3.1 design [151].

equatorial OBC module*		Thickness (cm)	Partial thicknesses (cm)	Total thickness (cm)
				65
FW	FW coating	2 (mm)	2.7	2.7
	FW EUROFER	25 (mm)		
Breeder zone*	PbLi gap	2 (mm)	29	60.3
	FCI layer	2 (mm)		
	PbLi bulk 1	28.2		
	FCI layer	2 (mm)		

	PbLi gap	2 (mm)		
	Stiffening	1.65 (cm)	1.65	
	PbLi gap	2 (mm)		
	FCI layer	2 (mm)		
	PbLi bulk 2	28.85	29.65	
	FCI layer	2 (mm)		
	PbLi gap	2 (mm)		
	Back wall	2	2	2
walls	Top wall	2		-
	Bottom wall	2		-
	Side walls	3		-
BSS	variable thickness: 66 cm in the OB mid-plane EUROFER-PbLi1- EUROFER-PbLi2-EUROFERr= 2.5/22/2/7/32.5 cm thickness zones			

Table 32: Radial build for the BB and BSS component for OB sides [141].

DCLL OB (DEMO 2015)							
Radial Subdivision (%)	0,16%	1,96%	45,74%		3,14%	49,00%	100,00%
Material	**Armour (2mm)**	**FW**	**Breeding module**	**Side walls (Left&Right)**	**Backplate Gap**	**BSS**	**Vol. (%)**
EUROFER [%]		73,397	11,322	91,539	50,999	66,900	41,001
PbLi (90% Li_6) [%]			86,906		8,963	30,163	54,813
Tungsten [%]	100						0,157
Al2O3 [%]			0,178				0,081
Void (Helium @ 80bar) [%]		26,603	1,594	8,461	40,037	2,937	3,946
Total	**100,0**	**100,0**	**100,0**	**100,0**	**100,0**	**100,0**	**100,0**

Table 33: Blanket material composition for the OBC [152].

Moreover, considering that the BZ back zone temperatures are mainly driven by the coolant outlet conditions and the BSS temperatures are very low the 1D AINA DCLL thermal blanket model domain ends at the backwall. On the other hand, the Helium channel along the breeding zone is not modeled due to constraints derived from the 1D simplifications which causes a more conservative results. The resulting material layers, the thicknesses and the nodalization assumed are described in Table 48Table 48: and it is based on the truncation error and model discretization method exposed by Fabbri [2] in order to couch a realistic variation of the response functions as the temperature distributions and ensuring an acceptable computational time by means of the refinement of the model nodal mesh fixing time

discretization ($\Delta t = 0.02\ s$). Contrary to HCPB blanket, in this case is not necessary scaling factors to compensate unrealistic results.

The Helium coolant layer assumes a f_{COOL} which is equal to the relative surface of the coolant tubes to the total surface of the module section, with an approximately value of 0.71 based on the DCLL CAD model [141][145][146]. Likewise, the f_{COOL} for the PbLi bulks is equal to 0.86. Besides, the material emissivity used for irradiation during 100% LOCA is equal to 0.3 as in the HCPB model [2].

Layer No.	Material	Thickness [mm]	No. Nodes
1	Tungsten	2	500
2	EUROFER	1.5	500
3	Helium Coolant	8	1
4	EUROFER	15.5	500
5	PbLi	2	1
6	EUROFER	2	500
7	PbLi	282	1
8	EUROFER	2	500
9	PbLi	2	1
10	EUROFER	16.5	500
11	PbLi	2	1
12	EUROFER	2	500
13	PbLi	288.5	1
14	EUROFER	2	500
15	PbLi	2	1
16	EUROFER	20	500

Table 34: Material Type, thickness and nodalization.

4.2.8.2 Numerical Model

The numerical model is the same as used in the thermal HCPB blanket block and the thermal divertor blocks based on the research carried out by Marco Fabbri during his thesis development [2]. Likewise, the steady state and transient approaches follow the same structure; for this reason, the necessary boundary conditions and the nuclear heat deposition are presented in the following sections.

4.2.8.3 Boundary Conditions

- **FW Helium Channel**: For the FW Helium channels, it is dealt an inlet temperature of 300 ºC and an outlet temperature ranges from 420 to 465 ºC [141][143][144]; thus, a temperature of 400 ºC is assumed. Besides, the mass flow rate ranges from 1.56 to 3.4 kg/s [141][143][144]; hence the FW mass flow per cooling channel (the OBC FW is now cooled by 46 channels [141]) is set at 0.06 kg/s. The Helium inlet pressure is equal to 80 bar [141].
- **Helium side walls and radial stiffening plates channels and Helium purge gas system**: In a conservative approach, these cooling channels have not been modeled decreasing the coolant capability of the BB hence increasing the safety factor of the model.
- **PbLi Channels**: For the PbLi coolant pipes are accepted an inlet temperature of 300 ºC and an average outlet temperature of 550 ºC [141][143][144]. Hence, for the PbLi bulk 1 a temperature of 438 ºC and for the PbLi bulk 2 a temperature of 545 ºC are fixed from a conservative point of view. Besides, the mass flow rate ranges from 52.87 to 55 kg/s [141][143][144]; hence the PbLi mass flow per cooling channel (it is recalled that there are 7 PbLi parallel channels [141]) is set at 7.6 kg/s.

- **Last node**: For the last node which represents the back plate, a Robin BC with a heat transfer coefficient of 1000 W/m^2/K and a bulk temperature of 550 ºC is assumed [141].
- **FW/first node**: in the first node a total load due to the radiation effect against the wall is applied. For the validation phase a heat flux on the FW of 0.22 MW/m^2 is assumed [141]. In addition, the power density for the first node (Tungsten) which is extrapolated for new NWL values when AINA runs is equal to 22.51 W/cm^3 [141].
- **Power deposition**: For the validation phase it is applied a mean NWL of 1.03 MW/m^2 [2]. The corresponding power density profiles for both the EUROFER and PbLi regions are also depicted in the following figure.

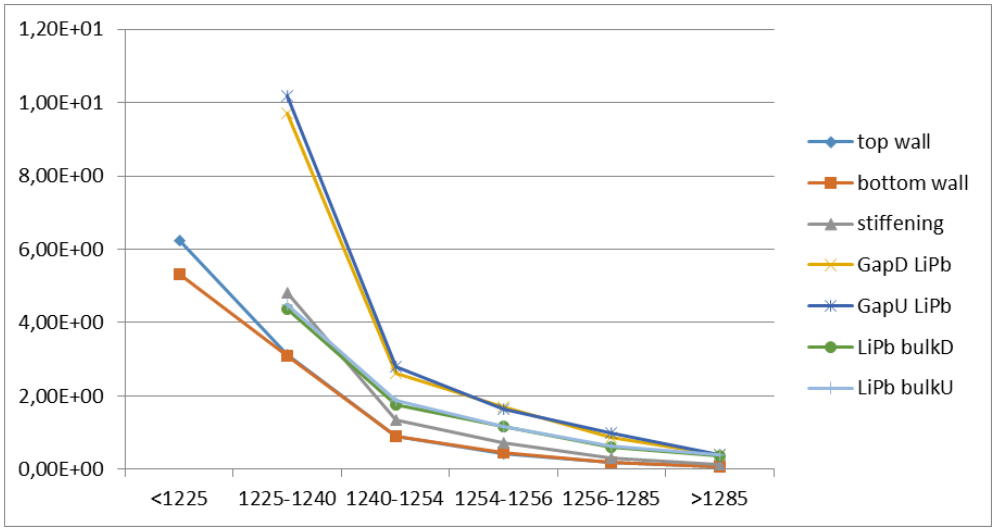

Figure 60: Radial distributions of the power density (W/cm³) along the OB equatorial BB module for PbLi and EUROFER components in 6 radial regions. A quasi exponential decrease is observed [141].

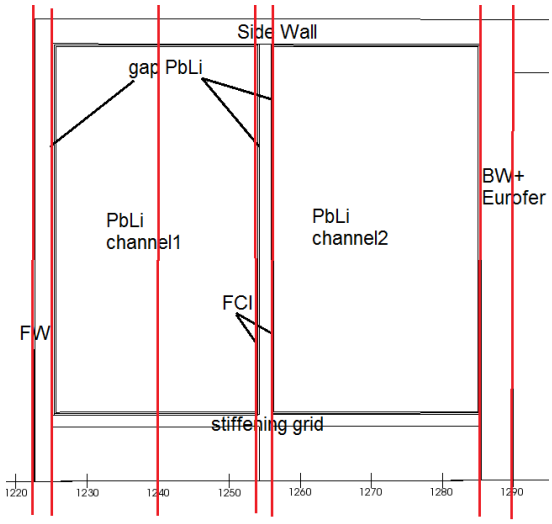

Figure 61: The six radial regions used in the previous figure to the first assessment of the power and power density in PbLi and Steel components for the OBC equatorial module [141].

Based on this data and after an expert consensus where the most demanded curve has been selected, the nuclear distributions accepted for both the EUROFER and PbLi and which are extrapolated for new NWL values when AINA runs are shown in the next table:

Radial regions (cm)	EUROFER power density (W/cm³)	PbLi power density (W/cm³)

<1225 (FW)	6.23	-
1225-1240 (PbLi bulk 1)	4.82	10.2
1240-1254 (PbLi bulk 1)	1.35	2.79
1254-1256 (Stiffening)	0.72	1.71
1256-1285 (PbLi bulk 2)	0.3	0.98
>1285 (Backwall)	0.1	0.4

Table 35: Power density (W/cm^3) radial distribution along the EUROFER and the PbLi.

It is important to remember that the power density for the first Tungsten nodes is equal to 22.51 W/cm^3 [141].

4.2.8.4 Model Validation

With the goal of validating the one-dimensional DCLL blanket AINA thermal-hydraulic behaviour it would be desirable to cross-check its corresponding outcomes with results extracted from a more detailed (three-dimensional) thermal hydraulic analysis. A thermal-hydraulic model of the OBC equatorial module has been created in the PLATOON code [141][150]. The model couples thermally the different PbLi and He circuits, as well as the structure walls and the FW Tungsten layer, and allows a fast evaluation of the thermal-hydraulic behaviour with enough accuracy to improve the operational and geometry parameters, to identify possible thermal issues and to obtain input data for successive more detailed analyses [141].

The following table (Table 50) summarizes the highest temperatures obtained in different types of walls included in the model. Most of them are found in the external surface of those parts of the left wall which are located at certain distance from the Helium channels (so they are assumed to be non-cooled). Those temperatures are mainly concentrated there because of the large total thickness of the left wall (35 mm). They cannot be considered realistic since just one-dimensional heat diffusion is assumed in the solid elements of the model. However, they can involve thermal issues and must be carefully taken in consideration for future analyses [141].

Type	Tmax (ºC)	Position
LW	556.9	Exterior surface of the non-cooled part contacting enclosure 6
LW	587.3	Exterior surface of the non-cooled part contacting enclosure 2
LW	637.4	Exterior surface of the non-cooled part contacting enclosure 3
LW	714.2	Exterior surface of the non-cooled part contacting enclosure 4
LW	561.5	Exterior surface of the non-cooled part contacting enclosure 7
LW	567.5	Exterior surface of the non-cooled part contacting enclosure 8
LW	733.3	Exterior surface of the non-cooled part contacting enclosure 5
Top wall	548.9	Exterior surface of the non-cooled part contacting enclosure 6
FW	525.8	Interface between W and EUROFER of the part contacting enclosure 5

Radial SP	554.6	Exterior surface of the non-cooled part contacting enclosure 5	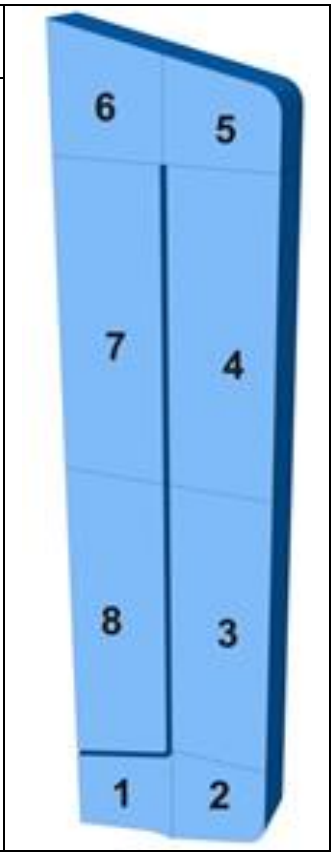
Radial SP	549.5	Exterior surface of the non-cooled part contacting enclosure 8	

Table 36: Possible hot spots in the EUROFER walls and enclosures [141].

On the basis of previous data and the temperature value for the Tungsten FW, extracted from a preliminary CFD study for the former DCLL model (v2.0) [140], which was 538 ºC when EUROFER reaches 530 ºC; the following table used to validate our model has been accepted after an experts' discussion:

Zone	T_{max} (ºC)	Observations and references
Tungsten in the FW	533.8	Extrapolation of data from [140] for a new maximum temperature in the FW.
EUROFER in the FW	525.8	From the previous table. [141]
EUROFER in the stiffening layer	554.6	From the previous table. [141]
EUROFER in the last FCI layer	549.5	From the previous table. [141]

Table 37: Temperatures for the AINA 1D thermal DCLL blanket model validation.

In general, the EUROFER temperatures are very close to the limits. Indeed, the limit of 550 ºC is definitely exceeded in the stiffening layer.

4.2.8.5 Cross-checks

The temperature DCLL 1D radial profile are computed by AINA and is reported in the following figure. These results refers to the thermal blanket block not coupled with the plasma model and, as already stated, forcing a mean NWL of 1.03 MW/m^2 and a heat flux on the FW of 0.22 MW/m^2.

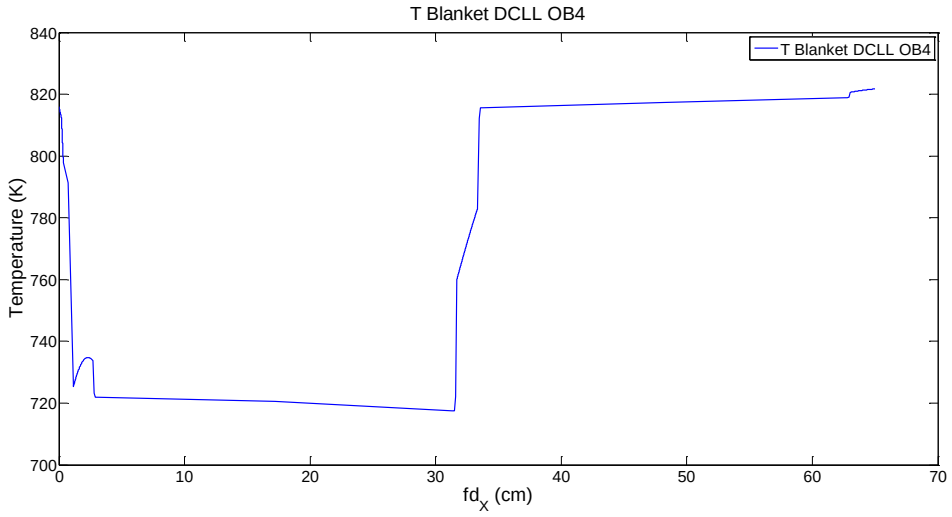

Figure 62: DCLL AINA 1D Temperature profile.

To validate the 1D DCLL AINA thermal-hydraulic behaviour the following outcomes have been cross-checked with the 3D CFD detailed ones (referenced in the section above) and reported in the next table:

	3D DCLL CFD	AINA DCLL	Relative difference (%)
Tungsten Temperature in the FW (ºC)	533.8	542.9	+1.7
EUROFER Temperature in the FW (ºC)	525.8	539.1	+2.5
EUROFER Temperature in the stiffening (ºC)	554.6	542.5*	-2.2
EUROFER Temperature in the last FCI (ºC)	549.5	545.6	-0.7
Mean Bulk PbLi Channels velocity (m/s)	0.017-0.0195 [141] 0.02 [144]	0.0172-0.0173	-

Table 38: AINA 1D DCLL results cross-check. *This value does not correspond to the stiffening layer exactly. It is the next FCI layer but it is valid since the enclosure model do not distinguish these layers.

4.2.9 Conclusions

The 1D DCLL AINA thermal-hydraulic behaviour has resulted coherent and representative of the DCLL BB global behaviour analysed by means of 3D detailed CFD. No meaningful discrepancies have been found. Indeed, the maximum temperature relative difference is less than 2.5 %. In spite of this, the EUROFER limit of 550 ºC is not exceeded, as in 3D CFD case, but in these imposed conditions all the hot spots are very close to the limit. Taking into account, all the simplifications done, the results and the development stage, the model fulfils the current work proposal.

Furthermore, in principle and in agreement with previous studies, the DCLL concept justifies those appealing characteristics on which supposedly is based.

Unfortunately and as was the HCPB case, the 1:1 temperature distribution along X-axis comparison has not been carried out because the data is unavailable and so the verification has been only limited to specific hot spots. However and due to the model resulted coherent, conservative, representative and the run time is extremely short, a more complex model is not needed.

4.3 AINA Study as a Contribution to Safety Analyses of DCLL DEMO

Firstly, it is important to highlight that, as in the HCPB case, the tool used to carry out this safety study has been AINA 4.0, the reference scenario is DEMO1 [11] and all the data and assumptions are based on DEMO BB Safety Data List document [120]. The difference to that case is the design of the BB implemented in AINA, the modelled design is known as DCLL v3.1 [141].

4.3.1 Types of Accidents

According to the criterion and the process of the HCPB safety analysis where, the most representative 21 PIEs [129] for the deterministic assessments are kept in mind in order to check the compliance with safety limits and to give rationales for the selection of the reference DEMO reactor model, the following load or accident scenarios have been simulated by AINA for the DCLL case as well:

- Plasma disruption or structural material melting due to a LOPC. The perturbations that AINA may simulate and induce to this kind of scenario are: a failure in the external power supply system, a failure in the fuel injection system, a variation in the confinement system and an entrance of an undesired quantity of impurities.
- In-vessel melt either of FW, blanket structure and/or divertor modules because of thermal stresses due to a LOCA. It is necessary to remember that AINA cannot simulate consequences of this kind of accident as a leakage, a release or a penetration of coolant or radioactive products into other structure regions.

4.3.2 Steady State Scenario DEMO1

First of all, it is important to remember the characteristics of the steady state scenario used to develop the safety study. Thus, AINA 4.0 steady state simulation of DEMO1 scenario is presented in this section. The basic tokamak reactor parameters used both as inputs and to compare the AINA values have been based on the output data from the DEMO1 reference reactor configuration released on April 2015 by PROCESS (or document: DEMO1_Reference_Design_-_2015_April_(_EU_2MDKFH_v1_0.dat) [11][133].

The characteristics of the steady state scenario used to develop the safety study are the same as those used in the HCPB case; the DEMO1 scenario ones [11][133]. Inputs and the relevant PROCESS crosschecking have been exposed in the HCPB case where no meaningful discrepancies have been found between AINA and PROCESS outputs.

Unlike for the HCPB case where certain functional temperature limits are slightly exceeded in the worst poloidal region (OB4) at the DEMO1 scenario, there is no temperatures infringement for the DCLL steady state case as the following table summarizes. For this reason, it would not be necessary to undertake a design review focused on ensuring a bigger safety margin for the material temperatures; notwithstanding, owing to the limit closeness of the EUROFER, it should be advisable to keep an eye on EUROFER regions throughout the safety analysis when any perturbation takes place.

Material	Temperature Limit $[^{o}C]$	T $[^{o}C]$
Tungsten	3422	508.6
EUROFER	550	548.9

Table 39: DCLL AINA DEMO1 SS maximum temperature.

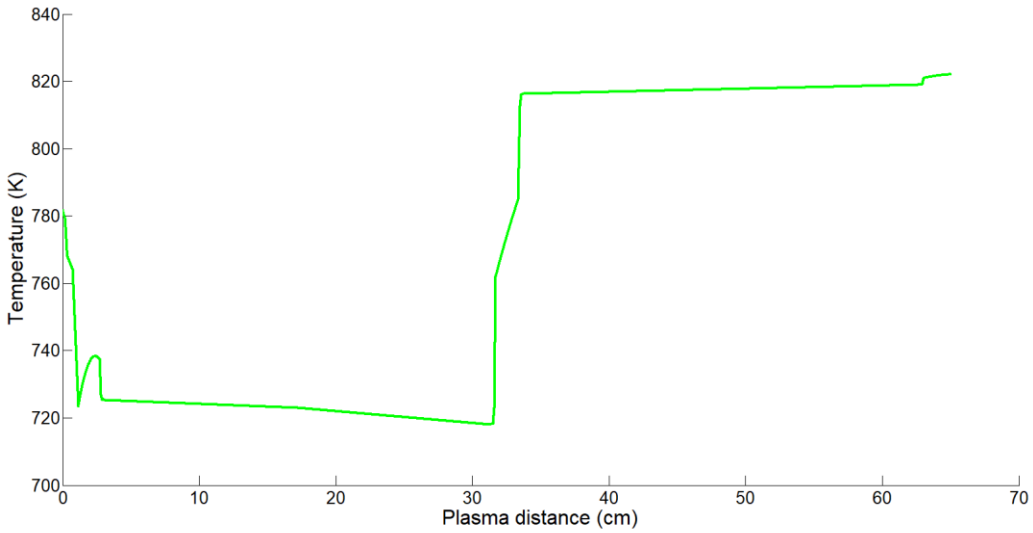

Figure 63: DCLL AINA 1D Temperature profile for DEMO1.

All figures extracted from AINA and used in the following analysis are contained in Annex B.

4.3.3 LOPC Accidents

The behavior of the plasma physics for this kind of anomalies is the same as in the HCPB cases. That means that only the temperatures reached by the BB materials require a particular attention since regarding the other conclusions are shared. Moreover, certain differences are observed in the FW temperatures in relation to HCPB analysis due to the more sensible thermal and power density model implemented in this BB configuration.

4.3.3.1 Failure in the External Power Supply System

It is important to remember that external power input is required for the fusion technologies not only to achieve an operational state but also to keep the plasma hot since most of the energy produced by fusion is carried away by the neutrons and, nowadays, it is not clear yet whether ignition will be the optimum operating regime. For this reason the consequences of possible failures from the external power supply system must be studied. Three different scenarios may occur which are outlined hereunder.

4.3.3.1.1 Auxiliary heating cut-off or decrease

Accident description: An unexpected and sudden auxiliary heating cut-off or decrease takes place at second t=0.1 s while the DCLL DEMO reactor is operating on DEMO1 steady state.

Event sequence: This failure produces a fast decrease of ion and electron temperatures but confinement time rises leading to fusion power increase and P_{SOL} reduction. The average electromagnetic power (P_{RAD}) radiated from the plasma core to the PFC of the divertor decreases, consequently the temperature of the PFC surface in the divertor is lower than the DEMO1 state one forcing, with the ion and electron temperature decrease, a slight impurity percentage decline of Tungsten inside the plasma core. All of this converges at a new steady state which produces a higher fusion power of 2420 MW for the cut-off case and 2197 MW for a 50% external power decrease case. So, the ignition point can be achieved theoretically despite the increase of neutronic heat flux (NWL) through the blanket which induces a temperature increase for the BB materials, specially in the FW, but within the allowed range

(Tungsten: 529.7 ºC and EUROFER: 526.3 ºC for the cut-off case, the most demanded). In summary, the DCLL design would be capable of withstanding an ignition scenario due to the BB configuration, specifically its cooling specifications; and this scenario does not induce any risk apparently.

4.3.3.1.2 Auxiliary heating increase up to a multiplication factor of 6.3

Accident description: An unexpected and sudden increase of auxiliary heating up to a multiplication factor of 6.3 takes place at second 0.1 while DCLL DEMO reactor is operating on DEMO1 steady state.

Event sequence: First of all it is important to note that OB5 region becomes the worst (it receives the maximum load flux $NWL + P_{RAD}$) between the second 0.3-0.5 s depending on the multiplication factor which affect external power. As soon as the incident takes place, ion and electron temperatures increase and all the species densities fall; except the impurity percentage of Tungsten which rises due to the increase of the internal temperatures. This leads to an initial and abrupt fusion power increment although it finally decreases rapidly achieving a new state which produces less fusion power than DEMO1 and where the FW temperatures initially increase (Tungsten: 525.7 ºC and EUROFER: 522.3 ºC for a multiplication factor of 6) due to the P_{RAD} effect while the rest of the BB temperature decrease. Ideally, these incidents should be detected for the purpose of foreseeing an important power fusion decrease. Once the plasma has stabilized, the new scenario does not represent a risk scenario unless the external power keeps increasing and it reaches the following level of accident.

4.3.3.1.3 Auxiliary heating increase with a multiplication factor larger than 6.3

Accident description: An unexpected and sudden increase of auxiliary heating with a multiplication factor larger than 6.3 takes place at second 0.1 while DCLL DEMO reactor is operating on DEMO1 steady state.

Event sequence: This perturbation leads plasma to terminate due to the beta limit infringement. The higher multiplication factor is, the faster plasma collapse is. Fusion power and densities quickly diminish, except the impurity percentage of Tungsten which rise due to the increase of the temperatures and the average wall loads; mainly ion temperature increases reaching more than 22 keV. At the time of the disruption, the plasma thermal energy (U) is 1.5 GJ for a multiplication factor of 6.4, consequently the EUROFER limit of 550 ºC would be significantly exceeded [135] as well as the rest of the temperature limits, including Tungsten. Nevertheless and in spite of these severe consequences, it is highly unlikely to achieve auxiliary heating as high as those which can lead to this type of accident due to the installed external power capacity would not exceed 150 MW.

4.3.3.1.4 Auxiliary heating perturbation summary

Mult. factor	Plasma termination	Plasma termination time $[s]$	Consequences	Mitigation	Observations
0 (cut-off)	Stabilized	-	Fusion power increase.	Not necessary.	Ignition scenario is achieved.

0.5	Stabilized	-	Fusion power increase.	Not necessary.	New SS more energetic.
2	Stabilized	-	Fusion power decrease. BB temperature decrease except in the FW.	Not necessary.	New SS less energetic.
5	Stabilized	-	Fusion power decrease. BB temperature decrease except in the FW.	Not necessary.	New SS less energetic.
6.4	Beta Limit	88.5	Excessive plasma thermal energy (1.5 GJ).	External power variation detection.	In principle, it is not possible to reach such high external power.
7	Beta Limit	12.8	Excessive plasma thermal energy (1.5 GJ).	External power variation detection.	In principle, it is not possible to reach such high external power.
8	Beta Limit	3.6	Excessive plasma thermal energy (1.5 GJ).	External power variation detection.	In principle, it is not possible to reach such high external power.
9	Beta Limit	2	Excessive plasma thermal energy (1.5 GJ).	External power variation detection.	In principle, it is not possible to reach such high external power.

Table 40: Auxiliary heating perturbation summary

4.3.3.2 Failure in the Fuel Source System

The fueling system must provide the required D-T fuel mixture to maintain the equilibrium of the plasma, for this reason the consequences of its possible failures must be studied. Four different scenarios analogous to the HCPB cases may occur and they are outlined hereunder.

4.3.3.2.1 Fueling rate cut-off

Accident description: An unexpected and instantaneous fueling rate cut-off takes place at second t=0.1 s while the DCLL DEMO reactor is operating on DEMO1 steady state.

Event sequence: A fueling source stop induces a fusion power and densities decrease, except the impurities percentages due to physical sputtering driven by the increase in ion and electron temperatures. Ion temperature reaches more than 25 keV owing to the auxiliary heating permanent injection. Moreover, the lower the impurities percentages, the lesser the power losses; for this reason the confinement time increases up to a maximum value of 18.1 s. With regard to structural conditions, all of this leads the reactor to a reduction in BB temperatures reaching values far below the melting limits, including the FW regions. On the other hand, it is important to highlight that the region OB5

becomes the worst from the second 0.4. Therefore and as a drastic outcome, a transition mode is detected after 22.9 s and, finally, plasma collapses at 25.5 s by an overshoot beta limit disruption. Despite this and as in the HCPB case, at the time of the collapse, the plasma thermal energy (U) achieves values of up to 0.5 GJ, and this disruption could be mitigated by a disruption mitigation system [135] and, thereby, the BB material would be safeguarded. Nevertheless, it would be useful to detect a fueling cut off instantaneously for the purpose of conducing the plasma to a better and controlled plasma shutdown if it is possible.

4.3.3.2.2 Fueling rate decrease

Accident description: An unexpected and sudden decrease of fueling rate takes place at second t=0.1 s while the DCLL DEMO reactor is operating on DEMO1 steady state.

Event sequence: Firstly it is important to note that OB5 becomes the worst region after 0.6 s. As in the previous case, a fueling reduction leads to a fusion power decrease, specifically half of fueling provides just over half the initial fusion power (from 2037 MW to 1130-1140 MW). Initially, there is an increase of ion and electron temperatures but these magnitudes are rapidly stabilized around the initial value ($T_e = 13.08$ and $T_i = 13.48$). Similarly, densities diminish in the first instance with the exception of the impurities source due to the Xenon entrance is constant and Tungsten which decreases much more as a result of the radiation load reduction against PFCs making get down notably the surface temperature. The confinement time gets stabilized at a rate of 6.1 s and the temperature of the BB and divertor materials are greatly reduced (EUROFER in the FW region: 488 ºC and Tungsten: 490.6 ºC). In conclusion, beyond this failure does not cause a dangerous scenario, in fact, the safety temperature margins are wider in comparison with DEMO1.

4.3.3.2.3 Fueling rate increase up to 25%

Accident description: An unexpected and sudden increase of fueling rate up to 25% takes place at second t=0.1 s while the DCLL DEMO reactor is operating on DEMO1 steady state.

Event sequence: As in the previous case, a new steady state scenario is achieved, however this one is not positive and several risks are derived from this kind of perturbation as discussed hereafter. The fusion power expands reaching a rate of 3472 MW ($Q = 52.3$), while ion and electron temperatures get stabilized around their initial values and after an initial drop; in contrast, the confinement time achieves a higher constant rate of 6.4 s and densities grow, mainly Tungsten due to the radiation and neutron load increase against PFCs. All of this leads to an analogous scenario to the HCPB case in which OB5 becomes the worst region after 5.5 s. With regard to materials stresses, the temperatures rise, specifically in the FW region where the EUROFER functional temperature limit is widely exceeded at 50.6 s reaching 636 ºC. Likewise the Tungsten temperature amounts to maximally 642 °C; however, its melting limit is not reached. For these reasons, it is essential to be able to guarantee a quick detection and actuation of a fueling increase in order to stop the excessive EUROFER melting warming. In addition, a new fueling rate increase could induce the scenario analyzed in the following case which would make the situation worse.

4.3.3.2.4 Fueling rate increase above 25%

Accident description: An unexpected and sudden increase of fueling rate above 25% takes place at second t=0.1 s while the DCLL DEMO reactor is operating on DEMO1 steady state.

Event sequence: This kind of perturbation leads the reactor to a transient state where fusion power, densities and confinement time are continuously growing until a Greenwald limit disruption takes place.

Logically, the higher fueling rate multiplication factor is, the earlier collapse happens. Moreover prior this very energetic plasma disruption, for a fueling rate of 50%, an initial melting scenario takes place for the EUROFER FW region at 27.3 s. Likewise, the Tungsten temperatures reaches 770 °C; well below its melting limit, even so, substantial. Therefore, it is necessary to detect an increase of fueling rapidly and activate a FPSS since all these perturbations cause structural damage. It is important to remember once again that ITER the fueling rate capacity can cover up to $7.8 \cdot 10^{19}$ $/_{m^3 s}$ (above a multiplication factor of 10 for DEMO1) [16] and hence the dealt scenarios may occur.

Multiplication factor	Plasma termination time $[s]$	Plasma Thermal energy U $[GJ]$	Max. Tungsten T $[^{o}C]$	Max. EUROFER T $[^{o}C]$ in the FW
1.5	74.7	2.1	770	756
6	1.7	1.3	513.5	509

Table 41: Disruption time and plasma thermal energy for an excessive fueling rate increase.

4.3.3.2.5 Fueling rate perturbation summary

Mult. factor	Plasma termination	Plasma termination time $[s]$	Consequences	Mitigation	Observations
0 (cut-off)	Beta Limit	25.5	A plasma thermal energy with a rate of 0.5 GJ.	Disruption mitigation system.	-
0.5	Stabilized	-	Fusion power decrease.	Not necessary.	New steady state with lower material temperatures.
1.25	Stabilized	-	Fusion power increase. EUROFER limit exceeded at 50.6 s.	Fueling rate variation detection.	Melting in less than 20-50 s.
1.5	Greenwald Limit	74.7	Fusion power increase. Excessive plasma thermal energy (2.1 GJ). EUROFER limit exceeded at 27.3 s.	Fueling rate variation detection and a FPSS activation.	This is the worst scenario due to the high temperatures and the high plasma thermal energy.
6	Greenwald Limit	1.7	Excessive plasma thermal energy (1.3 GJ). Fusion power increase.	Fueling rate variation detection and a FPSS activation.	-

Table 42: Fueling rate perturbation summary.

4.3.3.3 Improvement in the Confinement System

It is important to remember that the behavior of plasma parameters in case of a permanent increase of confinement time will be simulated and discussed due to, among other reasons, the H mode discovery.

Accident description: An unexpected and sudden permanent increase of confinement time takes place at second t=0.1 s while the DCLL DEMO reactor is operating on DEMO1 steady state.

Event sequence: Equally to the analogous HCPB case, this kind of perturbation produces fast ion and electron temperatures increase as well as densities. This transient drives the reactor to an overall raise of fusion power until plasma terminates disruptively on account of the beta limit infringement. The region OB5 becomes the most demanded region promptly (~ 0.3 s) and, in general, PFCs surface temperatures quickly grow. Moreover, if the confinement increment is based on a multiplication factor of 1.5 the disruption takes more than 30 s, which means the EUROFER melting limit is surpassed at 27 s and the Tungsten temperature reaches 576.5 ºC. That is not the case if the confinement time increase is greater owing to the early plasma collapse. In summary, the lower the multiplication factor is the grater maximum temperatures are achieved due to the plasma collapse takes place later. Nevertheless, the plasma thermal energy discharged during the disruption causes structural damage and melting in any case, hence, it is necessary to detect instantaneously an unexpected variation in confinement time with the aim of conducing the reactor to a controlled plasma shutdown. On the other hand, this kind of scenarios may be useful to obtain fusion power peaks if the disruption effects could be controlled or a safe state recovered rapidly.

Multiplication factor	Plasma termination time $[s]$	Plasma Thermal energy U $[GJ]$	Max. EUROFER T $[ºC]$	Max. P_{fus} $[MW]$
1.5	31.7	2.4	571	4708
5	3	2.4	507	5565

Table 43: Disruption time and plasma thermal energy for a confinement time improvement.

Moving on to other issues, it is important to remember, once again, that it is foreseeable that any confinement time reduction induces a loss of plasma confinement during the first seconds after the perturbation (< 5 s) with a fusion power drop; however, it is not possible to extract the precise consequences of these events from AINA owing to the numerical restrictions derived from the confinement law expressions implemented in the code. Therefore, it might be advisable to detect rapidly a failure in the confinement system which could lead to this kind of no discussed situation.

4.3.3.4 Occasional Variation of Confinement Time

As it was already outlined, it is possible that a punctual confinement time variation may or may not take place due to an unexpected behavior during the operation time; so after an experts' discussion, it has concluded that analysing the evolution of this kind of phenomena may be useful and interesting.

The impact of these events is highly dependent on the duration of the confinement time variation but it does not depend so much on the variation factor suffered as the following table suggests. Therefore, when the confinement time rises abruptly but decreases after 0.1 seconds, the effects are not severe since both a multiplication factor of 3 and 10 excites the plasma but the steady state is recovered in less than 20 seconds. During this transition, an instantaneous fusion power peak is reached due to a fast and short increase of ion and electron temperatures. In case the duration of the confinement time variation is longer, the operations steady state is supposedly recovered as long as the perturbation disappears before the corresponding termination time tracked down in the previous section. For instance, an increase of the confinement time due to a multiplication factor with a value of 3 leads the plasma to a transitional state which can be intrinsically recovered as long as the perturbation lasts less than 3.7 s. However, it has been detected an unpredictable episode where the plasma collapses due to the Greenwald limit violation in less than 22 s. This transient takes place when the occasional variation of confinement time lasts more than 3 s. Finally, it is necessary to highlight that the reactor suffers a melting situation (without taking the possible disruption into account) when the duration of the confinement

time variation lasts more than 2 s. In view of these circumstances, as in the previous case, it is necessary to detect instantaneously an unexpected variation in confinement time with the aim of conducing the reactor to a controlled plasma shutdown.

Multiplication factor	Perturbation duration $[s]$	Max. EUROFER T $[^{o}C]$ in the FW	Max. P_{fus} $[MW]$
3	0.1	506	2096
3	0.5	509	2423
3	1	516	2803
3	3	634 (melting at 15.1 s)	4790
10	0.1	506	2117

Table 44: Maximum temperature increase and fusion power peak for an occasional confinement time improvement.

Moreover, in all the cases the region OB5 becomes the most demanded after 0.3 s.

4.3.3.5 Entrance of an Undesired Quantity of Impurities

Several undesirable effects as a PFC damage or beneficial effects as shutting down the fusion due to an increase of Bremsstrahlung and line radiation may be caused by a flux of particles enter the plasma as impurities due to the erosion phenomena which is inherent to the nature of plasma wall interaction. This is why, this kind of perturbations must be studied and discussed.

4.3.3.5.1 Punctual impurity increase up to 300%

Accident description: A punctual increase of the impurities presence (Xe and W) up to 300% takes place at second t=0.1 s while the DCLL DEMO reactor is operating on DEMO1 steady state. This kind of perturbation can recreate the consequences of a leakage.

Event sequence: This perturbation drives the reactor to a sudden rise of confinement time, fusion power, power losses (Bremsstrahlung and line radiation); a drop of the internal plasma temperatures and, after a few seconds, an increase of the BB temperatures exceeding, for example, the EUROFER melting limit at 6.3 s when the increase of the impurities presence is 290% (the melting occurs when the increase of the impurities presence is above 200%). Finally, a recovery of the initial steady state takes place after a short time; however, it is necessary to detect this kind of perturbation in order to carry out a controlled plasma shutdown fast enough. Thus, the possible melting scenario may be prevent.

Multiplication factor	Melting time $[s]$	Max. EUROFER T $[^{o}C]$ in the FW	Max. P_{fus} $[MW]$
1.5	No melting	526	2299
2.9	6.3	654	4196

Table 45: Maximum temperature increase and fusion power peak for a punctual impurity increase.

4.3.3.5.2 Punctual impurity increase equal or above 300%

Accident description: A punctual increase of the impurities presence (Xe and W) equal to 300% takes place at second t=0.1 s while the DCLL DEMO reactor is operating on DEMO1 steady state. This kind of perturbation can recreate the consequences of a leakage.

Event sequence: In this case, the steady state is not recovered after the perturbation takes place in contrast with the previous one. Firstly, the plasma skips instantaneous (at 0.1 s) to the L mode where the fusion power grows (until a peak of 4365 MW). Likewise, the power losses linked to the greater impurities presence suffer an exceptional increase. Consequently, the temperature in the BB rises rapidly

exceeding the EUROFER melting limit at 5.8 s and reaching 622 ºC for the EUROFER in the FW and 634 ºC for the Tungsten (in the impurity increase equal to 300% case). Finally and due to densities are continuously growing, the Greenwald limit is infringed, so a disruption takes place at 12 s and it releases 1.8 GJ of thermal energy which can damage the reactor structure. Therefore, it is necessary to detect an important leakage instantly and leading the reactor to a controlled plasma shutdown in order to mitigate or prevent these possible undesirable consequences.

4.3.3.5.3 Tungsten permanent entrance increase

Accident description: An increase of the Tungsten impurity production takes place from second t=0.1 s while the DCLL DEMO reactor is operating on DEMO1 steady state. The previous cases could recreate the consequences of a leakage, however, in this case the simulation recreates a variation of the production rate and, consequently, the number of impurities which arrive to the plasma core permanently. These phenomena might occur due to the deterioration of the PFCs.

Event sequence: After this perturbation occurs, several plasma physics conditions increases slowly but continuously as fusion power, densities and confinement time. In addition, the plasma may reach a new steady state or it might collapse by mean of the infringement of the Greenwald limit depending on the new impurity production rate although it is necessary a huge Tungsten source so that the second case takes place. Nevertheless, any alternative is not instantaneous; for example, a fourfold of tungsten entrance causes an EUROFER limit infringement after 63.2 s; consequently the detection system has enough time to act and physical phenomena which may be identified easily and rapidly.

4.3.4 LOCA Accidents

First of all, it should be underlined that, as in the HCPB cases, LOCA perturbations only affect the temperature profile along the BB and the divertor materials; however, the production rate of Tungsten by sublimation process (depending on material temperature) is greatly lower than physical sputtering process (virtually independent of temperature). Consequently since the entrance of impurity is not affected by this kind of perturbations, conditions inside the plasma remain practically unchanged. On the other hand, it is important to remember that the divertor modeling used in AINA is a preliminary configuration which would be advisable to improve and update when a more detailed thermo-hydraulic assessment for the final design of the divertor carries out; for this reason, the conclusions drawn from the LOCA simulations where the divertor is affected must be taken with a grain of salt. LOCAs where just the divertor is affected have already been studied throughout the HCPB safety analysis.

For the DCLL BB configuration specifically, it will be noted throughout the study that the internal LOCAs do not affect virtually the temperature of the internal layers. This fact can be explained by the numerical expressions based on experimental regressions to compute the PbLi heat transfer coefficient where the mass flow perturbations of the coolant (in this scale of values) do not vary severely the heat transfer coefficient of the SS. For this reason, the conclusion extracted from the internal layers must be taken with a grain of salt even though the global conclusions would not be affected significantly since, as will be seen, an small LOCA is already critical for the FW. Consequently, the FW results may be extrapolated from a conservative point of view and any level of LOCA and irrespective of the coolant affected (He or PbLi) will have to be properly detected and the corresponding mitigation action activated.

4.3.4.1 BB LOCA 30%

Accident description: an small LOCA simulation where the Helium FW channel and all the PbLi coolant channels of the BB architecture loses 30% of the mass flow rate at second t=0.1 s while the DCLL DEMO reactor is operating on DEMO1 steady state. The perturbation is applied using a step function and hence the progressive decrease of the mass flow rate has not been taken into account.

Event sequence: As noted previously, only the material temperatures of the BB structure are affected materially since the plasma parameters remain virtually unchanged. Both temperature magnitude and shape vary on account of the modification of the cooling features. The largest changes are placed in most demanded areas and, indeed, due to DCLL configuration where the internal BB has huge coolant gaps, the FW is the most loaded region. In this case, at 100 s a new steady state for the thermal system is found where the temperatures of the FW have increased considerably despite the fact that the melting limits are not exceeded (Tungsten: 537 ºC and EUROFER: 534 ºC). It is certain that this incident does not induce a critical scenario; however, it is advisable to be able to guarantee a quick detection if the LOCA takes place in the Helium FW loop in order to proceed to a proper mitigation action since, as will be pointed in the following cases, if the LOCA is worse, the melting scenario occurs. On the other hand, from the AINA results, it might be concluded that ruptures in the PbLi coolant channels are less dangerous due to the numerical expressions used, as already discussed. Even then, AINA may not be conservative enough for these cases due to the slow response observed and a complementary study made by other more detailed thermal-hydraulic code as MELCOR would be recommended to verify these conclusions. Meanwhile, the FW results may be extrapolated from a conservative point of view for the BB, so the small LOCA in the PbLi channels is advisable to be detected.

4.3.4.2 BB LOCA 60%

Accident description: a medium LOCA simulation where the Helium FW channel and all the PbLi coolant channels of the BB architecture loses 60% of the mass flow rate at second t=0.1 s while the DCLL DEMO reactor is operating on DEMO1 steady state. The perturbation is applied using a step function and hence the progressive decrease of the mass flow rate has not been taken into account.

Event sequence: Obviously and following the trend of the previous case, only the material temperatures of the BB structure change. The new steady state for the thermal conditions is found at 160 s even though and in contrast to the previous case, the EUROFER temperature in the FW region is greater than design limit from the second 39.5 and reaches 594 ºC. Likewise, the Tungsten reaches 597 ºC. Therefore if a quick detection and a proper mitigation has already recommended for the small LOCA case (30%); it is clear that these responses are extremely necessary to prevent a melting damage in the FW region when the LOCA is bigger. Once again, the behavior of those regions cooled by the PbLi channel will have to be studied with greater stringency to verify the outputs of AINA and meanwhile the conclusions extracted from the FW region may be extrapolated for the internal layers.

4.3.4.3 BB LOCA 90%

Accident description: a big LOCA simulation where the Helium FW channel and all the PbLi coolant channels of the BB architecture loses 90% of the mass flow rate at second t=0.1 s while the DCLL DEMO reactor is operating on DEMO1 steady state. The perturbation is applied using a step function and hence the progressive decrease of the mass flow rate has not been taken into account.

Event sequence: The overall behavior of the reactor is analogous to the previous case although the current one causes a greater and faster temperature impact. The new thermal equilibrium is achieved after 300 s and the EUROFER melting scenario is exceeded at 18.1 s in the FW region. Specifically, the EUROFER area reaches more than 847 ºC and the tungsten layer more than 851 ºC. Once again, the regions cooled by the large PbLi channels seem to be supporting this kind of perturbations due to the numerical expressions used to compute the PbLi heat transfer coefficient the; however, the complementary analysis is still recommended and the conclusions extracted for the FW region are extrapolated for the regions cooled by PbLi.. As above, a very quick detection if the LOCA takes place in the Helium FW loop is extremely necessary as well as a proper and fast mitigation action such as a FPSS injecting impurity gases (e.g. Ne, Ar, etc.) as in ITER which may stop the reactor in less than 3 s [132].

4.3.4.4 Divertor and BB LOCA 30% or 60% or 90%

Accident description: a LOCA simulation where the CB and the PFC cooling loops of the divertor architecture and the Helium FW channel and all the PbLi coolant channels of the BB architecture loses 30% or 60% or 90% of the mass flow rate at second t=0.1 s while the DCLL DEMO reactor is operating on DEMO1 steady state. The perturbation is applied using a step function and hence the progressive decrease of the mass flow rate has not been taken into account. This kind of accident may be due to a loss of the cooling mass flow in the Primary Heat Transfer System (PHTS) which might affect the overall cooling system.

Event sequence: In summary, the consequences of this kind of accident are the sum of both phenomena discussed previously separately (the BB LOCA and the divertor LOCA). As has been pointed previously, the most relevant effect is a melting global scenario, specifically the BB materials in the FW region would be the most demanded; for this reason, it would be necessary to assure a proper detection system in order to identify rapidly a loss of the cooling mass flow and to lead the reactor to a safe shutdown as it has been agreed in the earlier cases.

4.3.5 Conclusions

First of all, it is important to highlight the fact that, unlike for the HCPB case where certain functional temperature limits are slightly exceeded in the worst poloidal region (OB4) at the DEMO1 scenario, there is no temperatures infringement for the DCLL steady state case. For this reason, it would not be necessary to undertake a DCLL design review.

With regard to LOCAs, it is necessary to remember that as according to the HCPB findings as well, it concludes that this kind of failure inside the cooling system does not affect the internal plasma conditions. Turning to substance, it has been observed that there comes a turning point when a rupture in the Helium FW channel leads the reactor to a melting scenario. This breaking point is around 35% losses of the mass flow which passes through the channel. Specifically, the EUROFER layer of the FW is the most demanded area from the thermal point of view for the AINA models. Consequently, it is indispensable the installation of a quick response system capable of detecting a cooling anomaly rapidly and activating a proper mitigation action such as a FPSS. With regard to internal LOCAs which affect the PbLi channels, it is important to remember that these perturbations do not affect virtually the temperature of the EUROFER internal layers during the AINA simulations due to, possibly, the numerical expressions used to compute the PbLi heat transfer coefficient. However, the conclusion extracted from the FW LOCAs are restrictive enough to safeguard the internal layers since the most critical thermal physics characteristics and design specifications of the Helium channels (coolant of the FW) in contrast

to large PbLi channels (coolant of the internal layers). Consequently, the FW results may be extrapolated from a conservative point of view and any level of LOCA and irrespective of the coolant affected (He or PbLi) will have to be properly detected and the corresponding mitigation action activated.

Concerning LOPC cases there is a wide variability of situations depending on the perturbation simulated. For example, when the injected external power is reduced it is possible to achieve, theoretically, a more energetic steady state or even the ignition point with no melting or disruption risk. In contrast, if the injected external power rises, the reactor is driven to no risks scenarios (new steady states less energetic) or impossible situation due to technological limitations (the injected external power system has constraints). The fueling rate perturbations cover practically all possible consequences; a low thermal energy disruption which can be mitigated by a typical mitigation system takes place when the fueling rate is cut-off, a new steady state with no risk is achieved if the fueling injection is reduced but not disappear, a melting scenario occurs when the fueling rate increases 25%, a high thermal energy disruption takes place when the increase is equal or over 600% and a melting and disruption scenario happens if the increase is between the two prior cases. The last situation is the worst one, so it summarizes the strategy in order to safeguard the reactor for all the cases which consists in implementing a fueling rate variation detection system and a FPSS activation equipment. With respect to a permanent confinement time improvement, a plasma collapse scenario which discharges a great amount of energy against the reactor structure is the most relevant consequence and it is necessary to detect instantaneously this perturbation with the aim of conducing the reactor to a controlled plasma shutdown. On the other hand, if the confinement time improvement is punctual (the perturbation lasts less than a value that causes a disruption) it is possible to reach melting values for the EUROFER if the improvement is sufficiently high and lasts long enough. Finally, a punctual impurity increase above 200% induces a melting scenario and for an increase above 300% the plasma collapses releasing a lot of thermal energy. Therefore, it is necessary to detect an important leakage instantly and, once again, leading the reactor to a controlled plasma shutdown.

Last but not least, it is really important to summarize several differences observed in contrast with the rest of the blankets. The DCLL 1D modeled is able to withstand important NWL gains due to the internal layers are essentially coolant channels. For this reason the ignition state is achieve despite the possible and slight EUROFER melting limit exceedance scenario forecast [141]. Hence, all that situations where the NWL rises would be critical although AINA, due to the DCLL configuration and its thermal modeling, does not reflect strongly this conclusion. As regards the FW, the model is highly sensitive due to the P_{RAD} used for checking the steady state is equal to 0.22; in contrast, the rest of the blankets used a 0.5 value. For this reason, the simulations lead the reactor to a melting scenario when the P_{RAD} rises widely, for example, the fueling rate increase up to 25% case.

4.4 HCLL Blanket

4.4.1 Introduction

The HCLL DEMO (Helium Cooled Lithium Lead) model was developed by CEA. The TRIPOLI-4 Monte Carlo code has been used to perform the nuclear analyses focused on analyzing three different variants of the HCLL blanket design:

- Optimized-Conservative concept: beer box concept (Horizontal Stiffening Plates plus Vertical Stiffening Plates), two cooling plates per breeding unit. This concept is similar to the TBM (Test Blanket Module) concept foreseen in ITER.
- Advanced concept: Horizontal Stiffening Plates only and two cooling plates per slices.
- Advanced-Plus concept: Horizontal Stiffening Plates only.

As result of the pertinent analyses, the Advanced-plus option has been established as the new DEMO HCLL reference design solution [153][154][155]. This concept takes the maximum advantage in term of TBR (Tritium Breeding Ratio), the cooling plate function and stiffening plate function are merged in only one type of plate this enable the suppression of an extra helium manifold and result in more space for the breeding zone [154].

Concepts	**Optimized conservative**	**Advanced**	**Advanced-Plus (DDD)**
	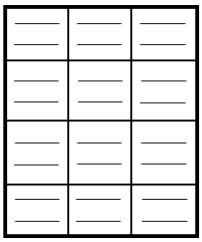	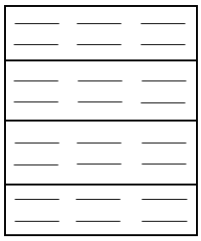	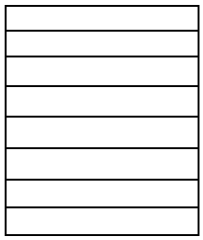
	hSP, vSP, 2CP	hSP, 2CP	hSP
TBR	+	-	+ (MMS) ++ (SMS)
PP	+	-	+ or -
Shielding (Manifold simplification)	-	+	++
Risk not to achieve high requirements	High	Medium	Low
Risk not to fulfill design criteria	Low	High	Very High

Figure 64: *DEMO HCLL Breeding Zones layout concepts and risk analyses* [153][154].

4.4.2 General Architecture

The HCLL Blanket System is based on the use of:

- The structural material of the HCLL module is a Reduced Activation Ferritic / Martensitic steel (RAFM) developed and produced in Europe, the EUROFER (designated EUROFER97) [153].

- Helium is chosen as coolant at 8 MPa pressure. Inlet temperature is set at 300 °C in order to provide a minimum temperature to melt the PbLi before plasma operation. The outlet temperature is set at a minimum of 500 °C [153][156].
- The eutectic Pb-15.7Li enriched at 90% in 6Li is chosen as breeder, neutron multiplier and carrier [153][156]. Moreover, it soothes the structural material temperatures as well due to its flow.

As has already been stated, the latest Breeding Blanket System is divided into 18 identical sectors. Each sector is formed by two Inboard (IB) and three Outboard (OB) segments. For AINA, the OBC (Outboard Central Segment) equatorial module (OB4) design has been studied for the purpose of modeling a thermal HCLL blanket block since it is supposed to be the module that has to withstand the highest loads.

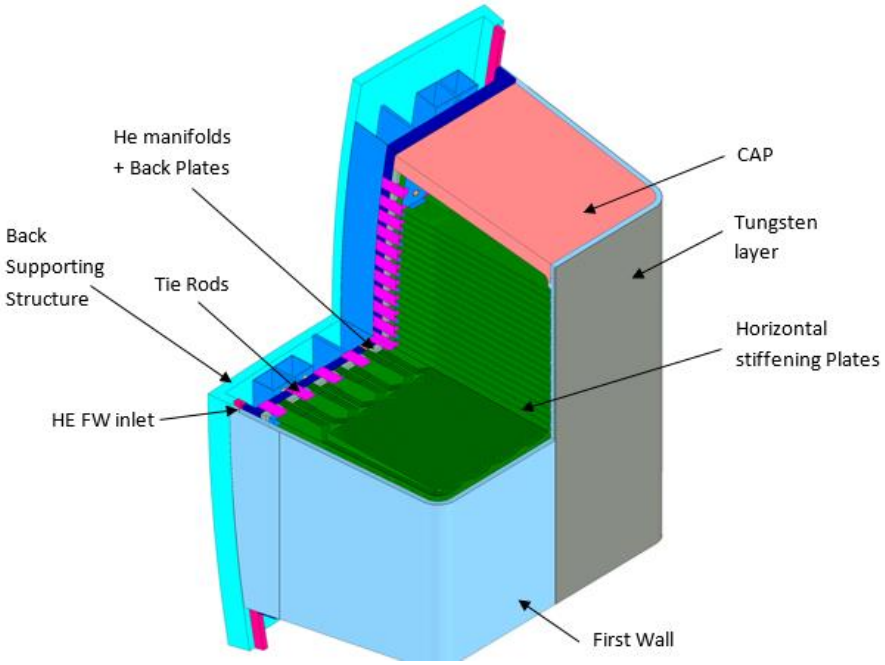

Figure 65: *Isometric view of 3/4 equatorial outboard module* [153].

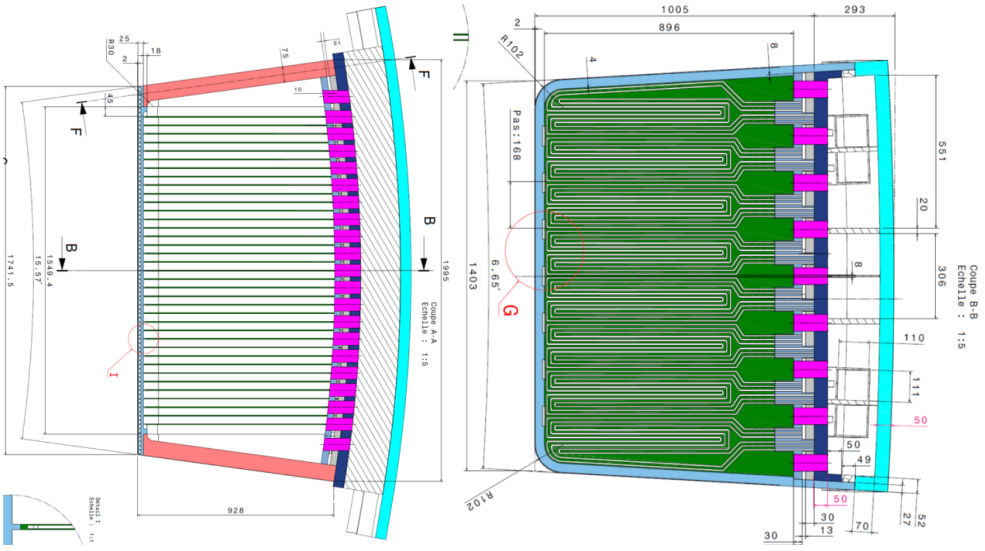

Figure 66: *Radial – poloidal cut and radial – toroidal cut BB of the module* [153].

Each HCLL BB segment, including the OB4 modeled, consists of several box modules with the following components [153]:

- The armour which consists of a Tungsten protective layer of 2 mm in front of the boxes in order to prevent plasma erosion.
- The U-shaped integrated FW forming the front of the boxes which consists of a structure in EUROFER where are integrated the cooling channels.
- The Breeder Zone (BZ) which consists of:
    - The eutectic Pb–15.7Li enriched at 90% in 6Li as breeder, neutron multiplier and tritium carrier.
    - Upper and lower CAPS to form the modules boxes on top and bottom.
    - Back Plate (BP) on the back to close the modules boxes.
    - Actively cooled horizontal Stiffening Plates (hSP) with the function:
        - to stiff the box delimitated by the FW, CAPS and BP in case of in-box LOCA
        - to route the breeder/multiplier
        - to remove the heat from the breeder/multiplier via integrated cooling channels
    - Potentially Cooling Plates (CP) to remove the heat from the breeder/multiplier via integrated cooling channels
- The Back Supporting Structure (BSS) which distributes and collects the Helium coolant and PbLi breeder to/from blanket modules as a manifold system.
- Feeding Piping through the upper/lower ports

In summary, the HCLL blanket module consists of a EUROFER steel box formed by a U-shaped plate sealed on its sides by cover plates, all of which are Helium-cooled. The rear of the module is divided into several flat cavities by back plates, which serve to distribute the Helium and PbLi flow to the various parts of the BB. The box is reinforced by hSP only in order to withstand the 8 MPa Helium pressure in case of accidental pressurization, and in order to guide and cool the PbLi [23].

4.4.3 Helium Circuit

As already stated, Helium is chosen in HCLL as coolant at 8 MPa pressure and its inlet temperature is set at 300 °C [153][154][23][157]. It comes from the BSS and enter directly into the FW cooling channels. A radial/toroidal/radial (i.e. “horizontal”) cooling scheme has been retained for the FW using an alternate (or counter-current) flow. After flowing through the FW, Helium is collected in a distribution chamber in the back of the module and distributed in the cooling channels of the hSP and Caps and then exit into the BSS where it is collected. [153]

The dimensions of the Helium tubes for the FW are 10x15 mm^2 with a distance between them of 5.2 mm and the dimensions of Helium channels of the hSP which flow through the BZ are 6x3 mm^2 with a distance between them of 8 mm. [153]

Hence, owing to the Helium circuit configuration, the cooling modelization of the FW will be similar to that implemented for the rest of the BBs designs, but the BZ will have to consider the effect of Helium which flows through the hSP by means of the method to estimate the lateral cooling effect which was developed for the HCPB BB [2].

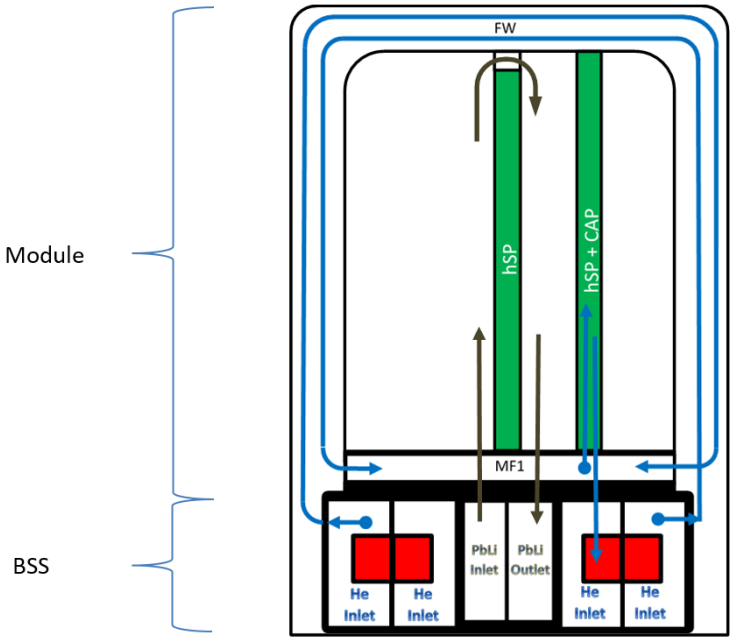

Figure 67: Helium distribution scheme [153].

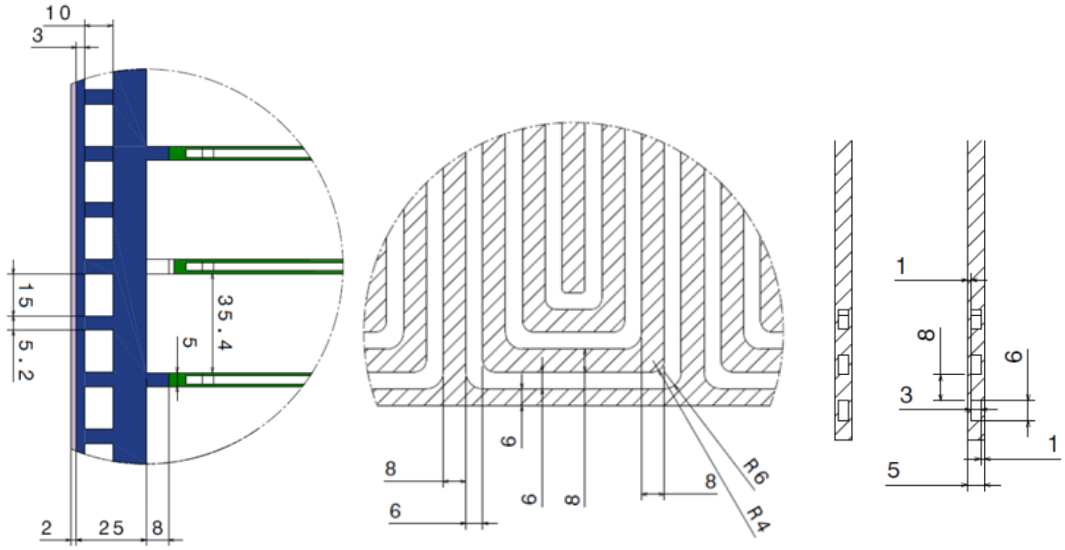

Figure 68: Detail and geometry of the FW channels and the hSP channels [153][158].

4.4.4 PbLi Circuits

The PbLi breeder enters from BSS and is routed to half of the slices in parallel. PbLi flows between two hSP frontward (radially), and goes to the slice above through the holes designed one other two hSP, on the back of the FW, and then radially flows backwards until it is collected by the BSS.

The PbLi along the BZ is not considered when the 1D segmentation is modeled and just a layer which represents the PbLi manifold tube is implemented and is treated as a coolant layer. This criteria has been assumed since the most demanded area is the hSP composed of EUROFER and cooled by Helium and where a melting limit may be analyzed. It is even possible that the PbLi produces a soothing thermal effect due its flow but it has not been assumed either (conservative assumption).

4.4.5 Back Supporting Structure

Regarding the BSS which serves as both an attachment point and to feed Helium and LiPb into the BB [23], a new design has been proposed on the DEMO 2015 baseline and it has been optimized in 2016 in order to have the best compromised between the targeted TBR, the required shielding performance while reducing pressure drops and keeping the temperature as low as possible with the aim of reducing thermo-mechanical stresses. Modules are attached to the BSS following the Multi Module Segment (MMS) design in order to form a blanket segment which can be removed from the upper port. [153]

Its architecture is constituted by a poloidal banana-shaped structure where two independent Helium Inlet and 2 independent Helium Outlet volumes are designed on both sides, plus two volumes of PbLi for inlet and outlet in the middle of the structure [153]. It is important to note that as will be shown, two manifold layers (one for the PbLi and one for the Helium) has been implemented in parallel for the 1D segmentation modeled in AINA following the thickness characteristics as shown in table 7 of the Aubert document [154]. This modelization does not affect the conclusions extracted and enable to justify the thickness values adopted despite its differences from the real design where the Helium and the PbLi would share the same layer.

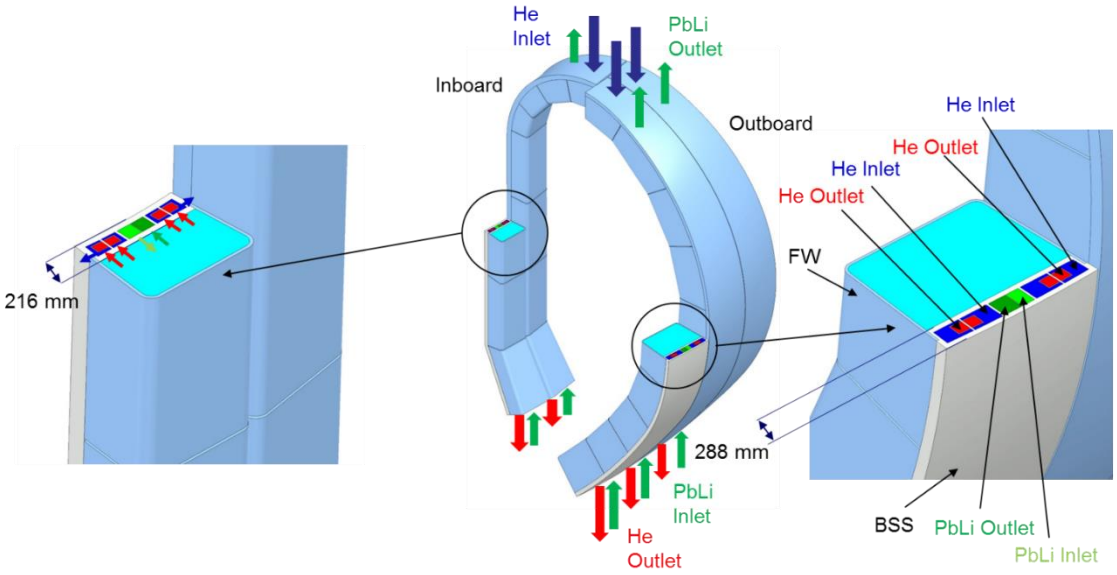

Figure 69: CAD model of the Inboard and outboard BSS [153].

4.4.6 Material Properties

All materials properties employed in the AINA DEMO HCLL has already outlined throughout the analogous chapter/documents for the AINA DEMO HCPB and DCLL.

4.4.7 Methodology to compute the lateral cooling

It should be recalled that the former AINA thermal wall model solver was not suitable to adapt to the most of DEMO designs because it was not able to take into consideration the influence of coolant channels not in line with the 1D segment. For this reason, a similar procedure to that used for the HCPB model and based on the Fabbri's methodology [2] has been followed in order to implement the lateral cooling effect as a weighted convective negative flux as:

$$\dot{q} = h\,(T - T_{\infty}) \qquad (148)$$

where:

- $\dot{q}$ is the convective negative flux $[W/m^2]$
- h is the heat transfer coefficient $[W/m^2/K]$
- T is the material temperature $[K]$
- T_∞ is the bulk coolant temperature $[K]$

Likewise, it is important to remember that $f_{WGT,R}$ and $f_{WGT,P}$ are the coolant factors for the no in lines tubes. They are discrete functions which take values only at the specified coolant positions and after a steady state crosscheck analysis. They have been outlined thorough Thermal Blanket Block Assembly section.

As already stated, owing to the Helium circuit configuration the effect of Helium which flows through the hSP (horizontal Stiffening Plate) will be modeled as a single lateral cooling channel modeled by means of the Fabbri's methodology [2] and the specifications set out in Boundary Conditions section.

4.4.8 AINA HCLL Wall model

The 1D AINA HCLL thermal blanket model is based on the methodology used to develop the 1D AINA HCPB and DCLL thermal model [2] doomed to represent the behavior of the more complex 3D CFD models. Therefore, a 1D simplified model has been built and consolidated using the results extracted from the thermal-hydraulic analysis performed by Aubert et al [153].

4.4.8.1 Model Description

The AINA HCLL thermal blanket model shall aim to represent the most conservative thermal behavior of the whole HCLL BB in the simplest possible way in order to check if EUROFER exceeds its melting limit (550 °C) in the worst case. Currently, the most accurate thermal-hydraulic study of the Advanced-Plus concept has been carried out with Cast3M [159] FEM code. The maximum EUROFER temperatures drawn from this study will be used to recreate a 1D segmentation along the blanket composed of the worst case for each layer depth.

As already stated, the model will be based on the OBC equatorial module (OB4) which has been historically selected as the most demanded region. The 1D model dimensions have been taken from the following tables and the configuration described previously.

Name	Thichness (cm)	Composition
Equatorial Inboard/Outboard Module (FW+BZ+MF)	51.4/94.5	-
Equatorial Inboard/Outboard Module breeder Zone (BZ)	**36.7/79.8**	-
W armor	0.2	100% W
First Wall and Side Wall	2.5	71% Eurofer - 29% He
Caps	**7.5**	**97% Eurofer - 3% He**
Horizontal stiffining / cooling plates	**0.5**	**60% Eurofer - 40% He**
Internal module manifold (MF)	**12.0**	-
Back plate between the breeding zone and the LiPb manifold	1	100% Eurofer
LiPb manifold	3.6	13.6% Eurofer – 83.8% LiPb – 2.6% He

Back plate between the LiPb manifold and 1st He manifold	3	100% Eurofer
He manifold	1.3	100% He
Back plate between the module and the back supporting structure	3.1	100% Eurofer
BSS wall and side wall	5.0	100% Eurofer
He LiPb separator in BSS	2.25	100% Eurofer

Table 46: Advanced-Plus HCLL breeding blanket characteristics [154].

HCLL OB (DEMO 2016)							
Radial Subdivision (%)	0,16%	2,03%	42,21%		6,90%	48,70 %	100,00 %
Material	**Armour (2mm)**	**FW (25mm)**	**Breeding Module (520mm)**	**Caps**	**Backplates/ Internal Manifolds (85mm)**	**BSS (600 mm)**	**Vol. (%)**
EUROFER [%]		64,910	9,850	67,200	41,390	60,61	37,848
Be [%]			36,635				15,463
Li_4SiO_4 [%]	100		14,906				6,291
Tungsten [%]							0,162
Void (Helium @ 80bar) [%]		35,090	38,610	32,800	58,610	39,39	40,236
Total	**100,0**	**100,0**	**100,0**	**100,0**	**100,0**	**100,0**	**100,0**

Table 47: Blanket material composition for the OBC [152].

Considering that the BZ back zone temperatures are mainly driven by the coolant outlet conditions and the BSS temperatures are very low the 1D AINA HCLL thermal blanket model domain ends at the BSS wall. The 1D segmentation selected passes through the hSP along the BZ and assuming the lateral cooling of the Helium tubes. This choice causes more conservative results. The resulting material layers, the thicknesses and the nodalization assumed are described in the next table and it is based on the truncation error and model discretization method exposed by Fabbri [2] in order to couch a realistic variation of the response functions as the temperature distributions and ensuring an acceptable computational time by means of the refinement of the model nodal mesh fixing time discretization (Δt=0.02 s). Contrary to HCPB blanket, in this case is not necessary scaling factors to compensate unrealistic results.

Layer No.	Material	Thickness [mm]	No. Nodes
1	Tungsten	2	52
2	EUROFER	3	500
3	Helium Coolant	10	1
4	EUROFER	12	500
5	EUROFER	6	500
6	Helium Coolant	6	1
7	EUROFER	8	500
8	Helium Coolant	6	1
9	EUROFER	8	500
10	Helium Coolant	6	1
11	EUROFER	150	500

12	EUROFER	150	500
13	EUROFER	150	500
14	EUROFER	150	500
15	Helium Coolant	6	1
16	EUROFER	8	500
17	Helium Coolant	6	1
18	EUROFER	8	500
19	Helium Coolant	6	1
20	EUROFER	124	500
21	EUROFER	10	500
22	PbLi	36	1
23	EUROFER	30	500
24	Helium Coolant	13	1
25	EUROFER	31	500
26	EUROFER	50	500

Table 48: Material Type, thickness and nodalization.

The Helium coolant layer for the FW assumes a f_{COOL} which is equal to the relative surface of the coolant tubes to the total surface of the module section, with an approximately value of 0.74 based on the HCLL 3D model [153]; and 0.67, 1.83 and 0.84 for the internal Helium BZ channels respectively. In addition, as the previous table shows, the 1D segmentation straddles these three tubes two times with what an accurate temperatures selections of the Helium allows a more realistic model. Likewise, the f_{COOL} for the PbLi and the Helium manifolds have been fixed with low values due to the geometry (0.22 and 0.18 respectively). Besides, the material emissivity used for irradiation during 100% LOCA is equal to 0.3 as in the HCPB and DCLL models [2]. On the other hand, a huge EUROFER layer has been split out into four layers (from layer 11 to 14) with the aim of accomplishing realistic results keeping in mind the truncation error and model discretization method exposed by Fabbri [2].

4.4.8.2 Numerical Model

The numerical model is the same as used in the thermal HCPB and DCLL blanket block and the thermal divertor blocks based on the research carried out by Marco Fabbri during his thesis development [2]. Likewise, the steady state and transient approaches follow the same structure; for this reason, the necessary boundary conditions and the nuclear heat deposition are presented in the following sections.

4.4.8.3 Boundary Conditions

- **FW Helium Channel**: For the FW Helium channels, it is dealt an inlet temperature of 300 °C and an outlet temperature ranges of 500 °C [153][154][23]; thus, a temperature of 415 °C is assumed in conjunction with the thermal results of the Aubert's study [153][154]. Besides, the mass flow per cooling channel is set at 0.053 kg/s [153][154] and the Helium inlet pressure is equal to 80 bar [153][154][156][23].
- **BZ Helium Channels:** As stated above, the Helium coolant channels in the BZ has been modeled not only as coolant layers, but also lateral cooling. Based on Aubert's thermal hydraulic analysis, a range from 529 °C to 420 °C has been set out. Besides, the mass flow per cooling channel is set at 0.0049 kg/s [153][154] and the Helium inlet pressure is equal to 80 bar [153][154][156][23].

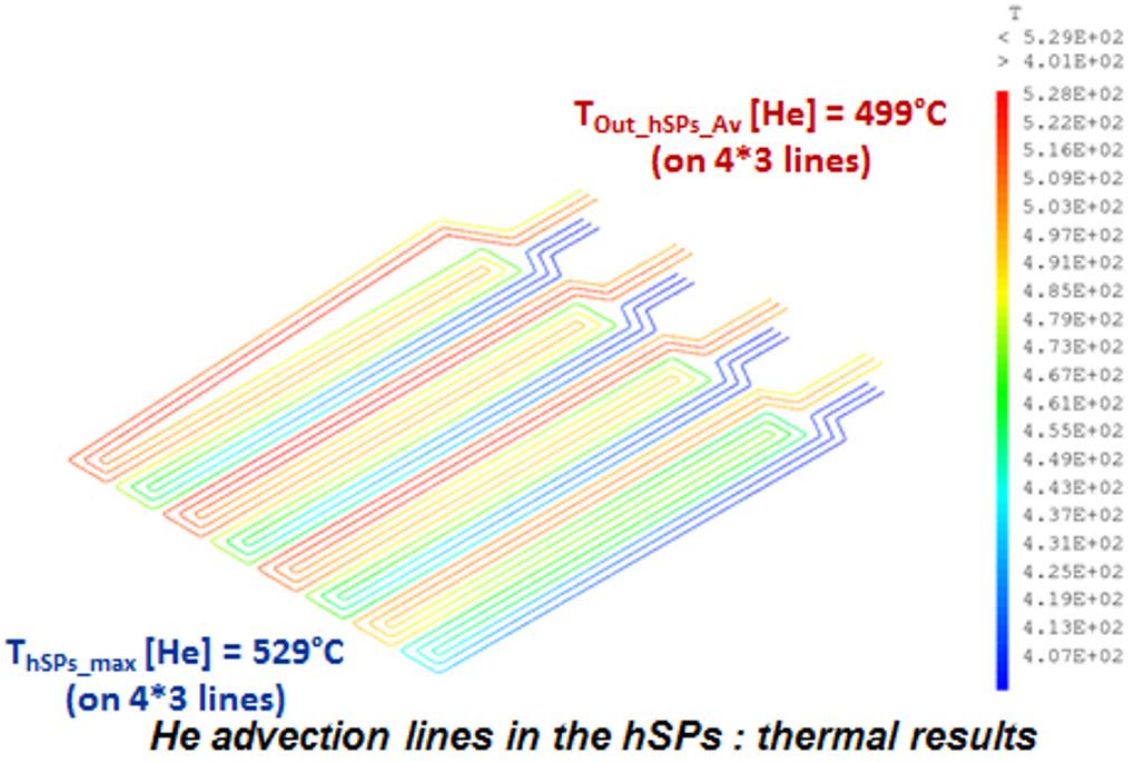

Figure 70: He thermal results in the hSP [153][154].

- **Helium Manifold:** The temperature is fixed at 300 °C and the mass flow at 6x0.0049 kg/s since 6 BZ Helium tubes are piped with this manifold [153][154].
- **PbLi Manifold**: The temperature is fixed at 300 °C and the mass flow at 0.375 kg/s since the total PbLi mass flow is equal to 810 kg/s which has to be divided into 18 toroidal coils, into 15 segments and into 8 manifolds per segment [153]. The final value is in the range 10% up to 100% of the total mass flow rate of the Tritium Extraction and Removal system [153].
- **Last node:** For the last node which represents the BSS wall a temperature of 440 °C is assumed [153][154].
- **FW/first node**: in the first node a total load due to the radiation effect against the wall is applied. For the validation phase a heat flux on the FW of 0.5 MW/m^2 is assumed [153][154]. In addition, the power density for the first node (Tungsten) which is extrapolated for new NWL values when AINA runs is equal to 21.6 W/cm^3 [153].
- **Power deposition**: For the validation phase it is applied a mean neutron wall loading (NWL) of 1.01 MW/m^2 [153][154]. The corresponding power density profiles are also depicted in the following figure and table.

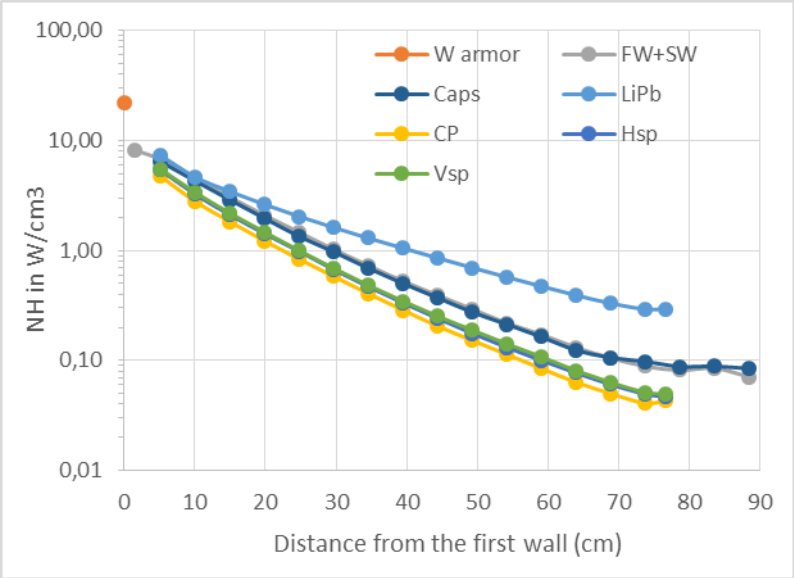

Figure 71: Radial distributions of the power density (W/cm³) along the OB equatorial in the different part of the HCLL breeding blanket design [153].

Distance from the plasma (cm)	comment	NH W/cm³	stat. err.	NH W/cm³	stat. err.
0,1	W armor	21,6	0,1%		
1,45	FWall	8,2	0,1%		
		LiPb		hSP	
5,2	1	7,3	0,0%	4,8	0,1%
10,1	2	4,6	0,1%	2,9	0,2%
15,0	3	3,4	0,1%	1,9	0,3%
19,9	4	2,6	0,1%	1,3	0,3%
24,8	5	2,1	0,1%	0,9	0,4%
29,7	6	1,6	0,1%	0,6	0,4%
34,6	7	1,3	0,1%	0,4	0,5%
39,5	8	1,1	0,1%	0,3	0,5%
44,4	9	0,9	0,1%	0,2	0,6%
49,3	10	0,7	0,1%	0,2	0,7%
54,2	11	0,6	0,1%	0,1	0,8%
59,1	12	0,5	0,2%	0,1	0,8%
64,0	13	0,4	0,2%	0,1	0,9%
68,9	14	0,3	0,2%	0,1	1,0%
73,8	15	0,3	0,2%	0,0	1,1%
76,7	16	0,3	0,4%	0,0	2,4%
77,7	BP1	0,04	1,0%		
80,0	MF1	0,25	0,3%		
83,3	BP2	0,06	0,6%		
86,4	BP3	0,06	1,1%		
89,5	BP4	0,06	0,5%		
92,4	BSS	0,08	0,2%		

Table 49: Outboard equatorial module radial nuclear heating profile in the different part of the HCLL BB [153].

Therefore, the nuclear distribution accepted for the EUROFER along the hSP slice, manifolds layers and BSS region and which is extrapolated for new NWL values when AINA runs is extracted from the previous table.

It is important to remember that the power density for the first Tungsten nodes is equal to 21.6 W/cm^3 [153].

4.4.8.4 Model Validation

With the goal of validating the one-dimensional thermal-hydraulic behavior of the HCLL blanket AINA it would be desirable to cross-check its corresponding outcomes with results extracted from a more detailed (three-dimensional) thermal hydraulic analysis. A thermal-hydraulic model of the OBC equatorial module was performed with Cast3M [159] FEM code by Aubert [153] with which to assess temperature distribution on the equatorial outboard module under steady state condition and based on the geometry and the specifications exposed above.

From this analysis it was concluded that the maximum EUROFER temperature in the models is reached in the hSP and is around 562 °C and the maximum EUROFER temperature in the FW is below 550 °C. The following table summarizes the highest temperatures obtained in different regions of the wall.

Component	Parameter	Value
Tungsten	Maximum W temperature	500 °C
FW	Maximum EUROFER temperature	493 °C
Equatorial Outboard Module	Maximum EUROFER temperature	562 °C

Table 50: HCLL hot spots [153].

In general, the EUROFER temperatures along the FW is far below to the limit but not for the internal BZ. Indeed, the limit of 550 °C is definitely exceeded.

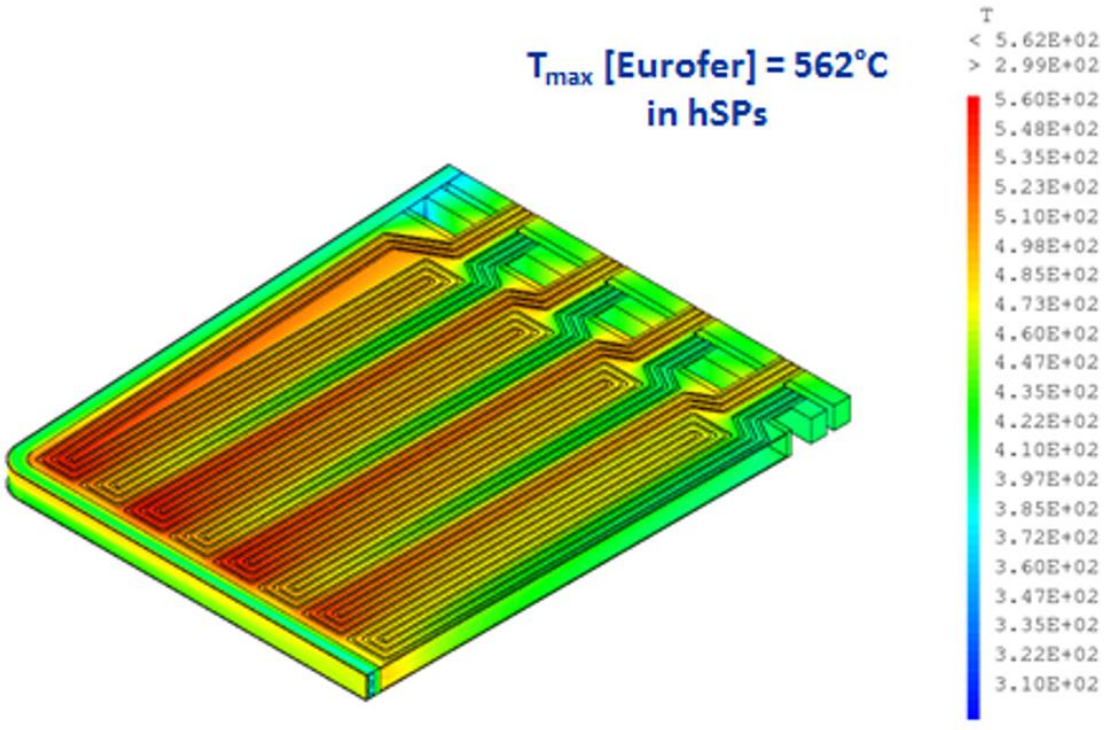

Figure 72: Thermal results on EUROFER and Tungsten components [153][154].

4.4.8.5 Cross-checks

The temperature HCLL 1D radial profile are computed by AINA and is reported in the following figure. These results refers to the thermal blanket block not coupled with the plasma model and, as already stated, forcing a mean neutron wall loading (NWL) of 1.01 MW/m^2 and a heat flux on the FW of 0.5 MW/m^2.

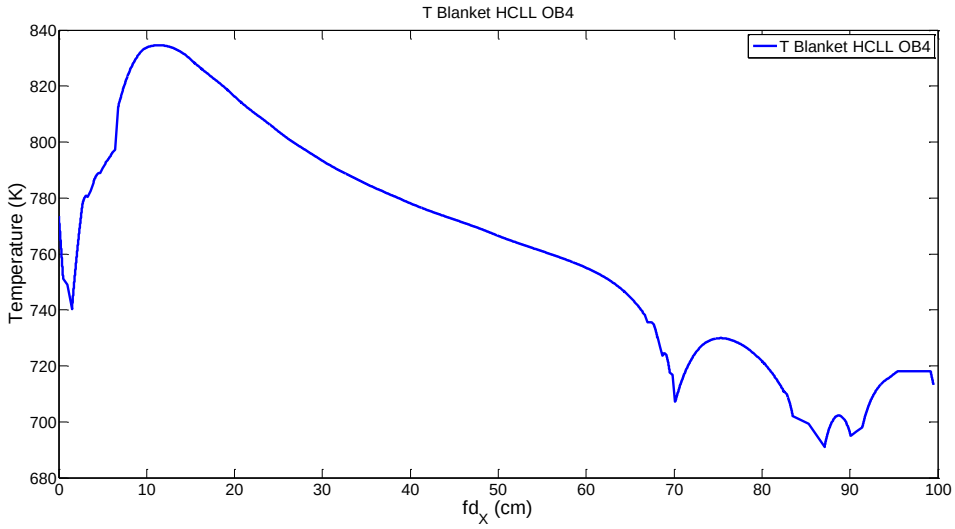

Figure 73: HCLL AINA 1D Temperature profile.

To validate the 1D HCLL AINA thermal-hydraulic behavior the following outcomes have been cross-checked with the 3D Finite Element (FE) detailed ones (referenced in the section above) and reported in the following table:

	3D HCLL FE	AINA HCLL	Relative difference (%)
Tungsten Temperature in the FW (°C)	500	500.4	+0.08
EUROFER Temperature in the FW (°C)	493	492.3	-0.14
Maximum EUROFER Temperature in the BZ (°C)	562	561.6	-0.07

Table 51: AINA 1D HCLL results cross-check.

4.4.9 Conclusions

The 1D HCLL AINA thermal behavior has resulted coherent and representative of the HCLL BB global behavior analyzed by means of 3D detailed FE. No meaningful discrepancies have been found. Indeed, the maximum temperature relative difference is less than 0.2%.

On the other hand, as shown in previous table, the EUROFER limit of 550 °C is exceeded, both in 3D case and AINA simulation, it therefore follows that for the most demanding conditions estimated for DEMO1 by AINA this limit will be even more surpassed. Thus, it will be advisable a design review since the HCLL concept may not justify those appealing characteristics on which supposedly is based.

Taking all these conclusions into account, all the simplifications done, the results and the development stage, the model fulfils the current work proposal. Unfortunately and as were the HCPB and DCLL

cases, the 1:1 temperature distribution along X-axis comparison has not been carried out because the data is not unavailable and so the verification has been only limited to specific hot spots. However and due to the model resulted coherent, conservative, representative and the run time is extremely short, a more complex model is not needed.

4.5 AINA Study as a Contribution to Safety Analyses of HCLL DEMO

As in the HCPB and DCLL cases, AINA 4.0 has been the tool used to carry out the following safety study, DEMO1 is the reference scenario [11] and all the data and assumptions are based on DEMO BB Safety Data List document [120]. The difference to the previous cases is the design of the BB implemented in AINA, the modeled design is known as HCLL Advanced-plus option [153].

4.5.1 Types of Accidents

According to the criterion and the process of the HCPB and DCLL safety analyses where, the most representative 21 PIEs [129] for the deterministic assessments are kept in mind in order to check the compliance with safety limits and to give rationales for the selection of the reference DEMO reactor model, the following load or accident scenarios have been simulated by AINA for the HCLL case as well:

- Plasma disruption or structural material melting due to a LOPC. The perturbations that AINA may simulate and induce to this kind of scenario are: a failure in the external power supply system, a failure in the fuel source system, a variation in the confinement system and an entrance of an undesired quantity of impurities.
- In-vessel melt either of FW, blanket structure and/or divertor modules because of thermal stresses due to a LOCA. It is necessary to remember that AINA cannot simulate consequences of this kind of accident as a leakage, a release or a penetration of coolant or radioactive products into other structure regions.

4.5.2 Steady State Scenario DEMO1

The characteristics of the steady state scenario used to develop the safety study are the same as those used in the HCPB and DCLL cases; the DEMO1 scenario ones [11][133]. Inputs and the relevant PROCESS crosschecking have been exposed in the HCPB case where no meaningful discrepancies have been found between AINA and PROCESS outputs.

Unlike for the DCLL case and in the same way as the HCPB case, certain functional temperature limits are slightly exceeded in the worst poloidal region (OB4) at the DEMO1 scenario as the following table summarizes. Specifically, EUROFER suffers this problem. For this reason, it would be necessary to undertake a design review focused on ensuring a bigger safety margin for the EUROFER temperatures.

Material	Temperature Limit $[^{o}C]$	T $[^{o}C]$
Tungsten	3422	550.1
EUROFER	550	577.6

Table 52: HCLL AINA DEMO1 SS maximum temperature.

All figures extracted from AINA and used in the following analysis are contained in Annex C.

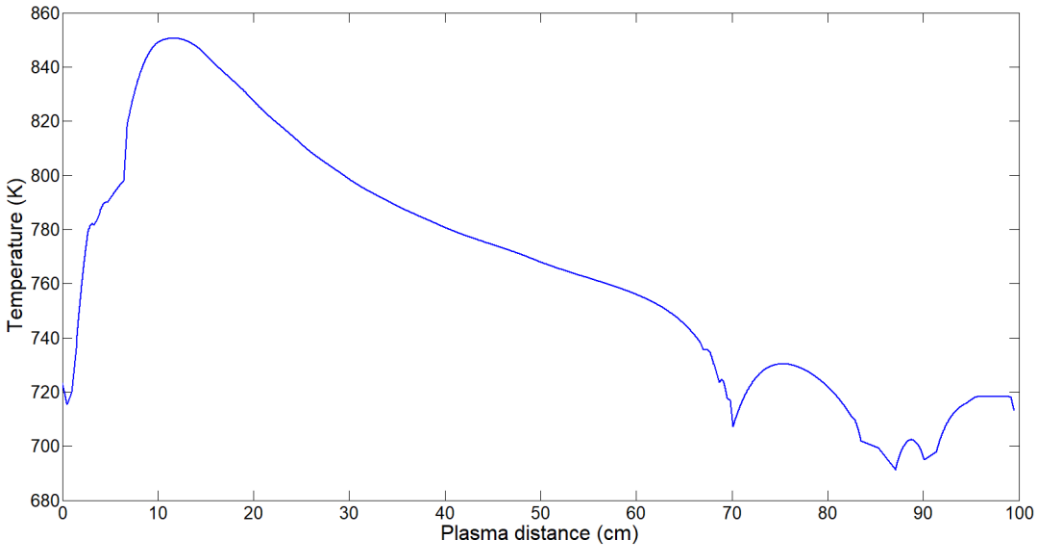

Figure 74: HCLL AINA 1D Temperature profile for DEMO1.

4.5.3 LOPC Accidents

The behavior of the plasma physics for this kind of anomalies is the same as the HCPB and DCLL simulations. Therefore and once again only the temperatures reached by the BB materials require a particular attention since regarding the other conclusions are shared. Moreover, certain differences are observed in the FW temperatures in relation to the previous safety analyses due to the thermal and power density model implemented in this BB configuration which is based on the steady state checking with the corresponding 3D model.

4.5.3.1 Failure in the External Power Supply System

As stated in the preceding safety analyses, the external power input is required for the fusion technologies not only to achieve an operational state but also to keep the plasma hot since most of the energy produced by fusion is carried away by the neutrons. In addition, currently, it is not clear yet whether ignition will be the optimum operating regime. For this reason the possible consequences of failures from the external power supply system should be studied. These failures are classified into three different scenarios which are outlined hereunder.

4.5.3.1.1 Auxiliary heating cut-off or decrease

Accident description: An unexpected and sudden auxiliary heating cut-off or decrease takes place at second t=0.1 s while the HCLL DEMO reactor is operating on DEMO1 steady state.

Event sequence: As in the previous cases, this failure leads the reactor to a new steady state which produces a higher fusion power of 2420 MW for the cut-off case and 2197 MW for a 50% external power decrease case. So, apparently the ignition point has been achieved, however the increase of neutronic heat flux (NWL) through the blanket induces the overtaking of the EUROFER functional temperature limit wider than in the DEMO1 state rapidly. The maximum EUROFER temperature reached is equal to 582 ºC. Likewise, the Tungsten temperature rises up to 458ºC due to the P_{RAD} slight increase. For a 50% external power decrease case the temperatures reached are 579.5 ºC and 452.8 ºC, respectively. For this reason it is necessary to conclude that it is really important to detect rapidly an external power cut-off in order

to proceed with a fast plasma shutdown (FPSS) [132] (by means of the control of the confinement system) during the first seconds for the purpose of preventing blanket melting.

4.5.3.1.2 Auxiliary heating increase up to a multiplication factor of 6.3

Accident description: An unexpected and sudden increase of auxiliary heating up to a multiplication factor of 6.3 takes place at second 0.1 while HCLL DEMO reactor is operating on DEMO1 steady state.

Event sequence: First of all it is important to note that OB5 region becomes the worst (it receives the maximum load flux $NWL + P_{RAD}$) between the second 0.3-0.5 s depending on the multiplication factor which affect external power. Plasma temperatures increase and all the species densities fall; except the impurity percentage of Tungsten which rise due to the increase of the internal temperatures. An initial and abrupt fusion power increment takes place although it finally decreases rapidly achieving a new state which produces less fusion power than DEMO1. For this reason this kind of scenarios could be interesting with the aim of reaching instantaneous fusion power peaks and, on the other hand, a controlled auxiliary heating increase can conduce to a steady state where the functional EUROFER temperature is closer to the acceptable limit. Ideally, these incidents should be detected for the purpose of foreseeing an important power fusion decrease. Once the plasma has stabilized, the new scenario does not represent a risk scenario unless the external power keeps increasing and it reaches the following level of accident.

4.5.3.1.3 Auxiliary heating increase with a multiplication factor larger than 6.3

Accident description: An unexpected and sudden increase of auxiliary heating with a multiplication factor larger than 6.3 takes place at second 0.1 while HCLL DEMO reactor is operating on DEMO1 steady state.

Event sequence: As in the previous safety analyses, this level of auxiliary heating perturbation causes a plasma disruption due to the beta limit infringement. As would be expected, the higher multiplication factor is, the faster plasma collapse is. Once again, fusion power and densities quickly diminish, except the impurity percentage of Tungsten which rise due to the increase of the temperatures, mainly ion temperature increases reaching more than 22 keV. When the disruption takes place, the plasma thermal energy (U) reaches 1.5 GJ for a multiplication factor of 6.4. This level of energy release brings about the overcoming of the EUROFER limit [135]. Nevertheless and in spite of these severe consequences, it is important to stress that it is highly unlikely to achieve auxiliary heating as high as those which can lead to this type of accident due to the installed external power capacity would not exceed 150 MW.

4.5.3.1.4 Auxiliary heating perturbation summary

Mult. factor	Plasma termination	Plasma termination time $[s]$	Consequences	Mitigation	Observations
0 (cut-off)	Stabilized	-	Fusion power increase.	External power variation detection.	In DEMO1 EUROFER temperature limit is already slightly exceeded; however, this conditions worsen the scenario.
			EUROFER temperature limit exceeded.	A controlled fast plasma shutdown.	
0.5	Stabilized	-	Fusion power increase.	External power variation detection.	In DEMO1 EUROFER temperature limit is already slightly

			EUROFER temperature limit exceeded.	A controlled fast plasma shutdown.	exceeded; however, this conditions worsen the scenario.
2	Stabilized	-	Fusion power decrease. BB temperature decrease.	Not necessary.	Increasing the external power leads to closer to the acceptable EUROFER BB operating temperature.
3	Stabilized	-	Fusion power decrease. BB temperature decrease.	Not necessary.	Increasing the external power leads to closer to the acceptable EUROFER BB operating temperature.
4	Stabilized	-	Fusion power decrease. BB temperature decrease.	Not necessary.	Increasing the external power leads to closer to the acceptable EUROFER BB operating temperature.
5	Stabilized	-	Fusion power decrease. BB temperature decrease.	Not necessary.	Increasing the external power leads to closer to the acceptable EUROFER BB operating temperature.
6.4	Beta Limit	88.5	Excessive plasma thermal energy. All temperature limits exceeded by the thermal energy released.	External power variation detection.	In principle, it is not possible to reach such high external power.
7	Beta Limit	12.8	Excessive plasma thermal energy. All temperature limits exceeded by the thermal energy released.	External power variation detection.	In principle, it is not possible to reach such high external power.
8	Beta Limit	3.6	Excessive plasma thermal energy. All temperature limits exceeded by the thermal energy released.	External power variation detection.	In principle, it is not possible to reach such high external power.
9	Beta Limit	2	Excessive plasma thermal energy. All temperature limits exceeded by the thermal energy released.	External power variation detection.	In principle, it is not possible to reach such high external power.

Table 53: Auxiliary heating perturbation summary

4.5.3.2 Failure in the Fuel Source System

The fueling system provides the required D-T fuel mixture to maintain the equilibrium of the plasma as foreseen by the operating scenarios [136], therefore the consequences of its possible failures have to be analyzed. Four different scenarios analogous to the HCPB and DCLL cases may take place.

4.5.3.2.1 Fueling rate cut-off

Accident description: An unexpected and instantaneous fueling rate cut-off takes place at second t=0.1 s while the HCLL DEMO reactor is operating on DEMO1 steady state.

Event sequence: An case fueling is stopped, fusion power and densities decrease, except the impurities percentages due to physical sputtering driven by the ion and electron temperatures increase, the first one reaches more than 25 keV. Moreover, the confinement time increases up to a maximum value of 18.1 s due to the power losses fall. With regard to structural conditions, a reduction in BB temperatures happens reaching values closer than the acceptable EUROFER melting limit, the maximum EUROFER temperature decreases to 565.4 ºC. On the other hand and as in the previous analyses, it is important to highlight that the region OB5 becomes the worst from the second 0.4. Finally, a transition mode is detected after 22.9 s which leads to a plasma collapses at 25.5 s by an overshoot beta limit disruption. Despite this, at the time of the collapse the plasma thermal energy (U) achieves values of up to 0.5 GJ; consequently this disruption could be mitigated by a disruption mitigation system [135] and, thereby, the BB material would be safeguarded from this energy release. Nevertheless and as concluded in the HCPB and DCLL cases it would be useful to detect a fueling cut off instantaneously for the purpose of conducing the plasma to a better and controlled plasma shutdown if it is possible.

4.5.3.2.2 Fueling rate decrease

Accident description: An unexpected and sudden decrease of fueling rate takes place at second t=0.1 s while the HCLL DEMO reactor is operating on DEMO1 steady state.

Event sequence: OB5 becomes the worst region after 0.6 s. As in the fueling cut-off case, a feed reduction leads to a fusion power decrease. As discussed at the previous blankets nalyses, initially there is an increase of ion and electron temperatures but these magnitudes are rapidly stabilized around the initial value. Similarly, densities diminish in the first instance with the exception of the impurities source due to the Xenon entrance is constant and Tungsten which decreases much more as a result of the radiation load reduction against PFCs making get down notably the surface temperature, for example, the Tungsten temperature for the BB is reduced to 442 ºC. The confinement time gets stabilized at a rate of 6.1 s and the temperature of the BB and divertor materials are greatly reduced but not below the functional EUROFER temperature limit (EUROFER: 565 ºC). In conclusion, beyond this failure does not cause a new dangerous scenario since, as has repeatedly been pointed out, the melting limit of the EUROFER is already infringed during DEMO1 SS, the new steady state obtained could be a better candidate for DEMO operation from the point of view of temperature limits no exceedance and despite the generation of lower fusion power and, consequently, less gain ($Q = 17.2$).

4.5.3.2.3 Fueling rate increase up to 25%

Accident description: An unexpected and sudden increase of fueling rate up to 25% takes place at second t=0.1 s while the HCLL DEMO reactor is operating on DEMO1 steady state.

Event sequence: Due to this perturbation a new steady state scenario is achieved, however this one is not positive and several risks take place. The fusion power expands greatly reaching a rate of 3472 MW

($Q = 52.3$), ion and electron temperatures get stabilized around their initial values and after an initial drop, the confinement time achieves a higher constant rate of 6.4 s and densities grow, mainly Tungsten due to the radiation and neutron load increase against PFCs. All of this leads the reactor to an analogous scenario to the HCPB and DCLL cases in which OB5 becomes the worst region after 5.5 s. With regard to materials stresses, the temperatures rise, Tungsten reaches 495 ºC after 250s and EUROFER functional temperature limit is widely exceeded in less than 50 s and the melting is unmitigated (EUROFER: 610 ºC). Consequently, it is essential to be able to guarantee a quick detection and actuation of a fueling increase in order to stop the excessive EUROFER melting warming. In addition, a new fueling rate increase could induce the scenario analyzed in the following case which would make the situation worse.

4.5.3.2.4 Fueling rate increase above 25%

Accident description: An unexpected and sudden increase of fueling rate above 25% takes place at second t=0.1 s while the HCLL DEMO reactor is operating on DEMO1 steady state.

Event sequence: DEMO suffers a transient state where fusion power, densities and confinement time are continuously growing until plasma collapses due to a Greenwald limit disruption. Logically, the higher fueling rate multiplication factor is, the earlier collapse takes place. For a fueling rate of 50% the crucial risk involves an initial EUROFER melting scenario (620 ºC) and the subsequent high energetic disruption whilst for a higher fueling rate the crucial risk involves an instantaneous and very energetic plasma termination. Likewise, for the first situation the Tungsten temperature reaches 550 °C; well below its melting limit, even so, substantial. All these perturbations cause structural damage, hence it is necessary to detect an increase of fueling rapidly and activate a FPSS. It is important to remember once again that in ITER, the fueling rate capacity can cover up to $7.8 \cdot 10^{19}$ $/_{m^3 s}$ (above a multiplication factor of 10 for DEMO1) [16] and hence this kind of dramatic scenarios might come about.

Multiplication factor	Plasma termination time $[s]$	Plasma Thermal energy U $[GJ]$	Max. Tungsten T $[ºC]$	Max. EUROFER T $[ºC]$
1.5	74.7	2.1	550	620
6	1.7	1.3	454.5	578

Table 54: Disruption time and plasma thermal energy for an excessive fueling rate increase.

4.5.3.2.5 Fueling rate perturbation summary

Mult. factor	Plasma termination	Plasma termination time $[s]$	Consequences	Mitigation	Observations
0 (cut-off)	Beta Limit	25.5	A plasma thermal energy with a rate of 0.5 GJ.	Disruption mitigation system.	-
0.5	Stabilized	-	Fusion power decrease.	Not necessary.	New steady state with lower material temperatures.
1.25	Stabilized	-	Fusion power increase. EUROFER limit widely exceeded at 50.6 s.	Fueling rate variation detection.	Melting.

1.5	Greenwald Limit	74.7	Fusion power increase. Excessive plasma thermal energy (2.1 GJ). EUROFER limit widely exceeded at 27.3 s.	Fueling rate variation detection and a FPSS activation.	This is the worst scenario due to the high temperatures and the high plasma thermal energy.
6	Greenwald Limit	1.7	Excessive plasma thermal energy (1.3 GJ). Fusion power increase.	Fueling rate variation detection and a FPSS activation.	-

Table 55: Fueling rate perturbation summary.

4.5.3.3 Improvement in the Confinement System

It is important to remember that, historically, AINA has been used in safety analyses to scan the influence of an increase in confinement time [16][19][37] due to, among other reasons, the H mode discovery.

Accident description: An unexpected and sudden permanent increase of confinement time takes place at second t=0.1 s while the HCLL DEMO reactor is operating on DEMO1 steady state.

Event sequence: Equally to the analogous HCPB and DCLL cases, this kind of perturbation produces fast plasma temperatures and densities increase which drive the reactor to an overall raise of fusion power until plasma terminates disruptively due to the beta limit infringement. The region OB5 becomes the most demanded region promptly (~0.3 s) and, in general, PFCs surface temperatures quickly grow due to the load flux $NWL + P_{RAD}$ rise. If the confinement increment is based on a multiplication factor of 1.5, the BB Tungsten temperature reaches 491.2 ºC. Moreover, the disruption takes more than 30 s, long enough to the EUROFER melting limit is surpassed in wider way at 27 s (600 ºC). That is not the case if the confinement time increase is greater owing to the early plasma collapse. In summary, the lower the multiplication factor is the grater maximum temperatures are achieved due to the plasma collapse takes place later. Nevertheless, the plasma thermal energy release during the beta disruption causes structural damage and melting in any case (for a multiplication factor of 5 with an almost instantly collapse too). Consequently, it is necessary, once again, to detect instantaneously an unexpected variation in confinement time with the aim of conducing the reactor to a controlled plasma shutdown. On the other hand, as mentioned in the previous safety analyses, this kind of scenarios might be useful to obtain fusion power peaks if the disruption effects could be controlled or a safe state recovered rapidly.

Moving on to other issues, it is important to remember, once again, that it is foreseeable that any confinement time reduction induces a loss of plasma confinement during the first seconds after the perturbation (< 5 s) with a fusion power drop; however, it is not possible to extract the precise consequences of these events from AINA owing to the numerical restrictions derived from the confinement law expressions implemented in the code. Therefore, it might be advisable to detect rapidly a failure in the confinement system which could lead to this kind of no discussed situation.

Multiplication factor	Plasma termination time $[s]$	Plasma Thermal energy U $[GJ]$	Max. EUROFER T $[^{o}C]$	Max. P_{fus} $[MW]$
1.5	31.7	2.4	600	4708
5	3	2.4	579.3	5565

Table 56: Disruption time and plasma thermal energy for a confinement time improvement.

4.5.3.4 Occasional Variation of Confinement Time

In line with the previous cases, it is possible that a punctual confinement time variation may or may not take place due to an unexpected behavior during the operation time, hence it has concluded that analyzing the evolution of this kind of phenomena may be necessary.

Firstly, it is important to point out that in all the cases the region OB5 becomes the most demanded after 0.3 s. As it was outlined in the HCPB and DCLL safety analyses, the impact of these events is highly dependent on the duration of the confinement time variation. In contrast, it does not depend so much on the variation factor suffered. Therefore, when the confinement time rises abruptly but decreases after 0.1 seconds, the effects are not severe and the steady state is recovered in less than 20 seconds not only for a low multiplication factor of 3 but also a high multiplication factor of 10. During this transition, an instantaneous fusion power peak is reached due to a fast and short increase of plasma temperatures. Consequently, the BB temperatures remain practically unchanged. In case the duration of the confinement time variation is longer, the operations steady state is supposedly recovered as long as the perturbation disappears before the corresponding termination time tracked down in the previous section. For instance, an increase of the confinement time due to a multiplication factor with a value of 3 leads the plasma to a transitional state which can be intrinsically recovered as long as the perturbation lasts less than 3.7 s. However, it has been detected an unpredictable episode where the plasma collapses due to the Greenwald limit violation in less than 22 s and where the FW and internal BB temperatures rise sharply. This transient takes place when the occasional variation of confinement time lasts equal to or more than 3 s. In view of these circumstances, it is necessary to detect instantaneously an unexpected variation in confinement time with the aim of conducing the reactor to a controlled plasma shutdown if this variation is long enough to be critical.

Multiplication factor	Perturbation duration $[s]$	Max. EUROFER T $[^{o}C]$	Max. Tungsten T $[^{o}C]$	Max. P_{fus} $[MW]$
3	0.1	577.8	450	2096
3	0.5	578.3	451.3	2423
3	1	579.2	451.6	2803
3	3	589.8	538.4	4790
10	0.1	577.8	450	2117

Table 57: Maximum temperature increase and fusion power peak for an occasional confinement time improvement.

4.5.3.5 Entrance of an Undesired Quantity of Impurities

A flux of particles enter the plasma may induce several undesirable effects as a PFC damage or beneficial effects as shutting down the fusion due to an increase of Bremsstrahlung and line radiation. For this reason, this kind of perturbations must be studied and discussed.

4.5.3.5.1 Punctual impurity increase up to 300%

Accident description: A punctual increase of the impurities presence (Xe and W) up to 300% takes place at second t=0.1 s while the HCLL DEMO reactor is operating on DEMO1 steady state. This kind of perturbation can recreate the consequences of a leakage.

Event sequence: As seen in HCPB and DCLL cases, the reactor suffers a sudden rise of confinement time, fusion power, power losses (Bremsstrahlung and line radiation); a drop of the internal plasma temperatures and an increase of the BB temperatures. Finally, a recovery of the initial steady state takes place, accordingly the steady state temperatures are also recovered after 60 s for the 1.5 multiplication factor case and 100 s for the 2.9 multiplication factor case, the worst one. In conclusion, it is necessary to detect this kind of perturbation in order to carry out a controlled plasma shutdown fast enough to avoid the abrupt temperatures rise.

Multiplication factor	Max. Tungsten T $[ºC]$	Max. EUROFER T $[ºC]$	Max. P_{fus} $[MW]$
1.5	459	579.5	2299
2.9	511	596.6	4196

Table 58: Maximum temperature increase and fusion power peak for a punctual impurity increase.

4.5.3.5.2 Punctual impurity increase equal or above 300%

Accident description: A punctual increase of the impurities presence (Xe and W) equal to 300% takes place at second t=0.1 s while the HCLL DEMO reactor is operating on DEMO1 steady state. This kind of perturbation can recreate the consequences of a leakage.

Event sequence: In this case and in contrast with the previous one, the steady state is not recovered after the perturbation takes place in a short period of time depending on the level of perturbation. The plasma skips instantaneous (at 0.1 s) to the L mode, the fusion power grows (until a peak of 4365 MW) and the power losses linked to the greater impurities presence suffer an exceptional increase. Consequently, the temperature in the BB rises rapidly exceeding, by a a wider margin, the EUROFER melting limit reaching 583.5 ºC for the EUROFER and 525.5 ºC for the Tungsten (in the impurity increase equal to 300% case). Finally, densities are continuously growing, therefore, the Greenwald limit is infringed. A disruption takes place at 12 s and it releases 1.8 GJ of thermal energy which would damage the reactor structure. On account of all the dangerous consequences exposed, it is necessary to detect this kind of perturbation instantly and leading the reactor to a controlled plasma shutdown in order to mitigate or prevent the structure damage.

4.5.3.5.3 Tungsten permanent entrance increase

Accident description: An increase of the Tungsten impurity production takes place from second t=0.1 s while the HCLL DEMO reactor is operating on DEMO1 steady state. The previous cases could recreate the consequences of a leakage, however, in this case the simulation recreates a variation of the production rate and, consequently, the number of impurities which arrive to the plasma core permanently. These phenomena might occur due to the deterioration of the PFCs.

Event sequence: After this perturbation occurs, several plasma physics conditions grows slowly but continuously as fusion power, densities and confinement time. Depending on the new impurity production rate the plasma may reach a new steady state or it might collapse by mean of the Greenwald limit infringement. It should be noted that a huge Tungsten source is necessary in order to the second case takes place. For example, a fourfold of tungsten entrance does not cause a plasma collapse but the temperature EUROFER reaches 593 ºC and Tungsten reaches 479 ºC. Nevertheless, any alternative is not instantaneous; consequently the detection system has enough time to act. Moreover, the physical phenomena which must be detected would be identified easily and rapidly.

4.5.4 LOCA Accidents

Firstly, it should be underlined once again that, as in the HCPB and DCLL cases, LOCA perturbations only affect the temperature profile along the BB and the divertor; however, the production rate of Tungsten by sublimation process (depending on surface material temperature) is greatly lower than physical sputtering process (independent of surface material temperature). Therefore, conditions inside the plasma remain practically unchanged. On the other hand, it is important to remember once again that the divertor modeling used in AINA is a preliminary configuration which would be advisable to improve and update when a more detailed thermo-hydraulic assessment for the final design of the divertor carries out; for this reason, the conclusions drawn from the LOCA simulations where the divertor is affected must be taken with a grain of salt. Moreover, LOCAs where just the divertor is affected have already been studied throughout the HCPB safety analysis.

4.5.4.1 BB LOCA 30%

Accident description: an small LOCA simulation where the Helium FW channel and the Helium and PbLi coolant loops of the BB architecture loses 30% of the mass flow rate at second t=0.1 s while the HCLL DEMO reactor is operating on DEMO1 steady state. The perturbation is applied using a step function and hence the progressive decrease of the mass flow rate has not been taken into account.

Event sequence: As it is well known, only the material temperatures of the BB structure changes; the plasma parameters remain virtually unchanged. This temperature distribution is affected in magnitude due to the modification of the cooling features and, as logic, enhanced variations are placed in most loaded areas where the coolant effect is lower. In this case, a new steady state for the thermal system is found at 50 s. The Tungsten temperatures of the FW have increased to 459 ºC and the maximum EUROFER temperatures reaches 586 ºC which is far greater than the design limit. It is certain that this incident does not induce a much more dramatic scenario than the DEMO1; however, it is advisable to be able to guarantee a quick detection if the LOCA takes place in the Helium coolant loops of the BB in order to proceed to a proper mitigation action since, as will be pointed in the following cases, if the LOCA is greater, the melting scenario will be far worse. On the other hand, from the AINA results, it might be concluded that an small rupture in the FW cooling channel is not dangerous.

4.5.4.2 BB LOCA 60%

Accident description: a medium LOCA simulation the Helium FW channel and the Helium and PbLi coolant loops of the BB architecture loses 60% of the mass flow rate at second t=0.1 s while the HCLL DEMO reactor is operating on DEMO1 steady state. The perturbation is applied using a step function and hence the progressive decrease of the mass flow rate has not been taken into account.

Event sequence: Obviously and following the trend of the previous case, the infringement of the EUROFER temperature limit is greater. The new steady state is found at 80 s. The Tungsten temperature reaches 477 ºC which is kept far below its melting limit and EUROFER temperature rises to 598 ºC. As previously, it is essential to be able to guarantee a very quick detection if the LOCA takes place in the Helium coolant loops of the BB with the objective of proceeding to a proper mitigation action. As in the previous case, a medium rupture in the Helium FW cooling channel may be bearable by the HCLL design.

4.5.4.3 BB LOCA 90%

Accident description: a big LOCA simulation where the Helium FW channel and the Helium and PbLi coolant loops of the BB architecture loses 90% of the mass flow rate at second t=0.1 s while the HCLL

DEMO reactor is operating on DEMO1 steady state. The perturbation is applied using a step function and hence the progressive decrease of the mass flow rate has not been taken into account.

Event sequence: The overall behavior of the reactor is analogous to the previous cases although the current one causes a greater and faster temperature impact and the melting damage is much more dramatical. The new thermal equilibrium is achieved after 200 s and the Tungsten temperature reaches 565.4 ºC and the EUROFER rises to 663 ºC. Moreover and in contrast to the milder cases, the EUROFER in the FW exceeds the design limit as well (555 ºC). Thus, if this level of LOCA takes place either in the Helium coolant loops of the BB or in the Helium FW as well, a very quick detection is extremely necessary as well as a proper and fast mitigation action such as a fast plasma shutdown (FPSS).

4.5.4.4 Divertor and BB LOCA 30% or 60% or 90%

Accident description: a LOCA simulation where the CB and the PFC cooling loops of the divertor architecture and the Helium FW channel and the Helium and PbLi coolant loops of the BB architecture loses 30% or 60% or 90% of the mass flow rate at second t=0.1 s while the HCLL DEMO reactor is operating on DEMO1 steady state. The perturbation is applied using a step function and hence the progressive decrease of the mass flow rate has not been taken into account. This kind of accident may be due to a loss of the cooling mass flow in the Primary Heat Transfer System (PHTS) which might affect the overall cooling system.

Event sequence: In summary, the consequences of this kind of accident are the sum of both phenomena discussed previously separately throughout the BB HCLL LOCA study and throughout the divertor HCPB LOCA study. As has been pointed previously, the most relevant effect is a melting global scenario, specifically the BB EUROFER it would be necessary to assure a proper detection system in order to identify rapidly a loss of the cooling mass flow and to lead the reactor to a safe shutdown as it has been agreed in the earlier cases.

4.5.5 Conclusions

First of all, it is important to highlight the fact that, as in the HCPB case where certain functional temperature limits were slightly exceeded in the worst poloidal region (OB4) at the DEMO1 scenario, the EUROFER, in the most demanded areas of the internal layers of the BB, suffers this problem for the HCLL DEMO design. For this reason, it would be necessary to undertake a design review focused on ensuring a bigger safety margin for the EUROFER temperatures.

With regard to LOCAs, it is necessary to remember, once again, that this kind of failure does not affect the internal plasma conditions from AINA outcomes. However, even a slight loss of the mass flow (about 30%), leads the reactor to a more tangible melting scenario since the EUROFER exceeds more widely its melting limit. This critical scenario is intensified not only for the quick response but the magnitude of the temperature reached if the mass flow loss inside the cooling channels is greater. So much so that, a big LOCA simulation where the Helium FW channel and the Helium and PbLi coolant loops of the BB architecture loses 90% of the mass flow rate causes a melting scenario in the FW area, which does not take place if the mass flow loss is less intense.

On the other hand and concerning LOPC cases, broadly speaking, there are three possible scenarios as in the HCPB study when a LOPC takes place. At best, a new steady state with a fusion power decrease and lower EUROFER temperatures may be achieved. This case would be safe and a mitigation system or action would not be necessary; moreover, the final scenarios could be better candidates for DEMO

operation from the point of view of temperature limits no exceedance despite the generation of lower fusion power and, consequently, less gain. Those perturbations which induce to this option are: an increase of the external power injection between 200% and 630% and a decrease of the fueling injection rate (not fueling cut-off). In contrast, another potential consequence would involve a risk of structural damage due to a very energetic plasma termination which may discharge a great amount of thermal energy against the internal reactor walls. From AINA outcomes, an increase of the external power injection above 630% would disrupt within a short period of time (89 s at best) and transferring 1.5 GJ of thermal energy against the walls that damages and melts the structure. Notwithstanding, this situation would be highly unlikely since, in principle, it would not be possible to reach such high external power. Likewise, a cut-off of the fueling injection may induce to a plasma collapse in 25 s; however the thermal power released and around 0.5 GJ could be mitigated by a proper disruption mitigation system and, thereby, safeguarding the BB material. Finally, the third potential consequence arisen from a LOPC is the same as the impacts emerged when a LOCA takes place, a more critical melting scenario than the DEMO1 steady state. This situation might occur due to a decrease or a cut-off of the external power injection, a fueling rate injection increase up to 25%, an occasional variation of confinement time beneath the corresponding termination time and a punctual impurity increase up to 300%. All these situations may be highly dangerous since temperatures rise extremely rapid. In these cases it is essential to be able to guarantee a quick detection and actuation by means of a proper system depending on the affected equipment; for example, a failure monitoring system for the external power injection, the fueling injection and the impurity entrance. It is likely that just a temperature variation detection system must not be fast enough to ensure this requirement; even if the confinement time varies which its monitoring is more complex but there is no alternative. The mitigation action would be the activation of a fast plasma shutdown (FPSS) for all the cases. Last but not least, there are certain incidents which may drive the reactor to suffer both a melting scenario and a very energetic plasma disruption at the same time. These triggers are an increase of fueling injection above 50%, a permanent improvement in the confinement time and a punctual impurity increase above 300%. Therefore and owing to the double effect, these are the most critical failures and a special attention in order to avoid them will be necessary. The measures to be taken are the mitigation systems and actions for the particular cases explained previously.

4.6 WCLL Blanket

4.6.1 Introduction

The WCLL DEMO (Water Cooled Lithium Lead) model was developed by ENEA, KIT and ASIPP [160]. The present work is based on a specifically developed WCLL DEMO 2016 MCNP model which is designed using a Single Module Segment approach (ID. WCLL2016.v0.1, SMS approach) [160][161].

The layout proposed for WCLL BB design 2015 based on Multi Module Segment (MMS) approach showed positive features; however, drawbacks have been identified on segmentation which has been improved with the current SMS approach where main geometries of the modules are simplified to face, as much as possible, manufacturing issues [162].

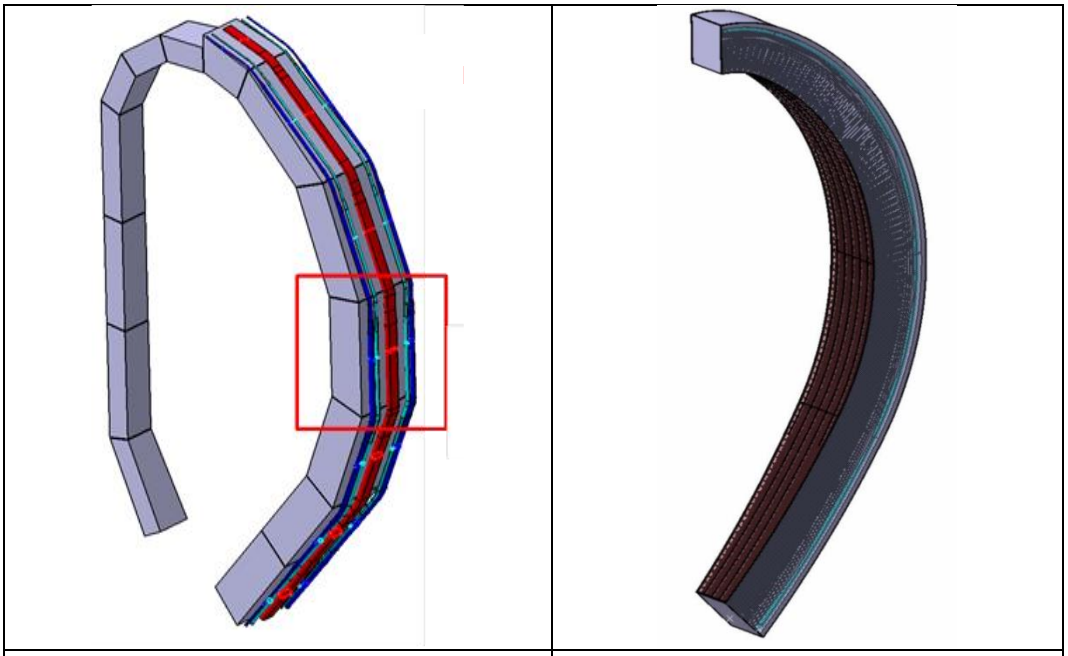

a) WCLL2015v0.2 | b) WCLL2016v1.0

Figure 75: *Comparison of WCLL BB 2015 and 2016 designs* [162].

4.6.2 General Architecture

The WCLL BB uses reduced activation ferritic-martensitic steel EUROFER as structural material filled with Lithium-Lead (PbLi) as breeder, neutron multiplier and tritium carrier, and water at typical Pressurized Water Reactor (PWR) conditions (Tin = 295 °C, Tout = 328°C at 15.5 MPa) as coolant [160][161][162][163][164][165].

As has already been stated, the WCLL BB 2016 is designed as SMS concept which is divided into 18 identical sectors. Each sector is formed by two Inboard (IB) and three Outboard (OB) segments [161][162]. For AINA is maintained the same poloidal segmentation used in the 2015 concept with 14 segments where the OBC (Outboard Central Segment) of the 2016 concept is analogous to the equatorial module (OB4) of the 2015 concept which will be modeled and studied for the purpose of replicating a thermal WCLL blanket block based on the module that has to withstand the highest loads.

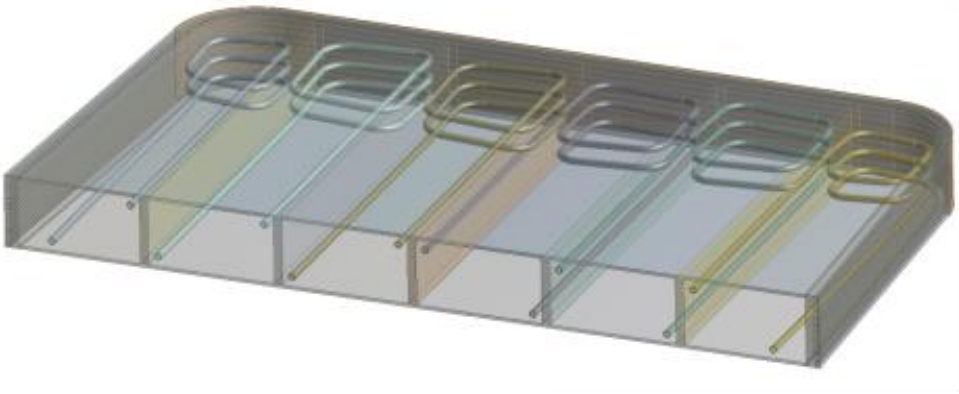

Figure 76: *Single breeding unit of an Outboard segment* [160].

The single BB module is composed by the following components:

- First Wall (FW) and Sidewalls (SW)
- Top and bottom walls
- Internal Stiffening and Baffle plates
- Back Supporting Structure
- Breeding Zone cooling pipes
- Lithium Lead (Pb Li) internal manifold
- Inlet and Outlet Breeding Zone (BZ) Cooling Water Manifolds
- Inlet and Outlet manifolds of First Walls (FW) cooling Water

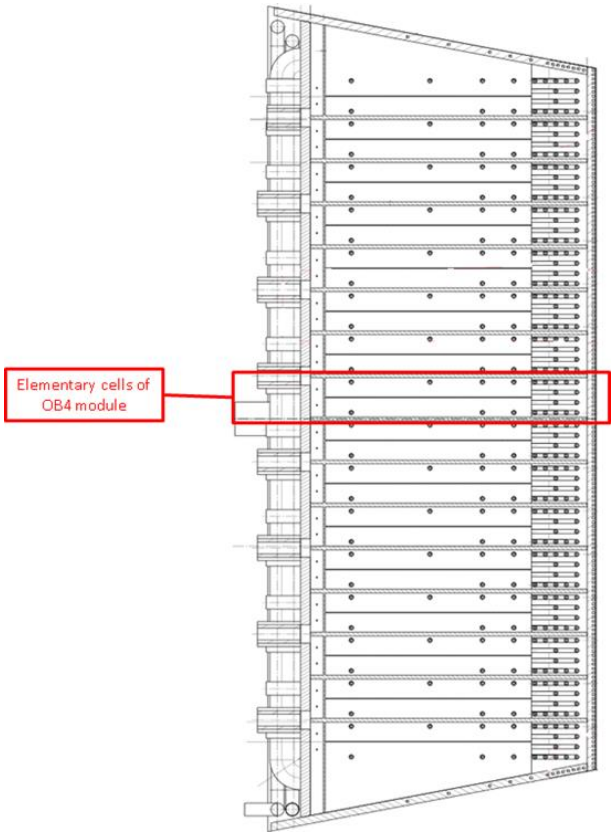

Figure 77: *Poloidal section of OB4 module for the 2015 concept but it is analogous to the 2016 concept* [163].

In summary, In order to guarantee the structural integrity of each segments against the over pressurization, the WCLL BB segments are equipped with internal stiffening plates, placed along poloidal-radial (PR) and toroidal-radial (TR) planes. In detail each modules has five PR stiffening plates 16 mm in thickness and about 100 TR ribs 12 mm thickness. In order to guarantee the Pb Li circulation, about 100 baffle plates for each module (inboard and outboard) with 2 mm thick have been placed along toroido-radial direction. The distance between TR stiffening plates and baffle plates is 135 mm and is calculated on a curvilinear coordinate. The TR ribs and baffle plates are planar and locally normal the face plasma BB curve. The overall segment is formed of about 100 breeding units distributed in poloidal direction. Each breeding unit is divided in 6 channels in toroidal direction. The breeding unit has a total height of 135 mm (including top and bottom radial-toroidal stiffening plates), a radial thickness of 450 mm in the inboard and 800 mm in the outboard segment [161][162].

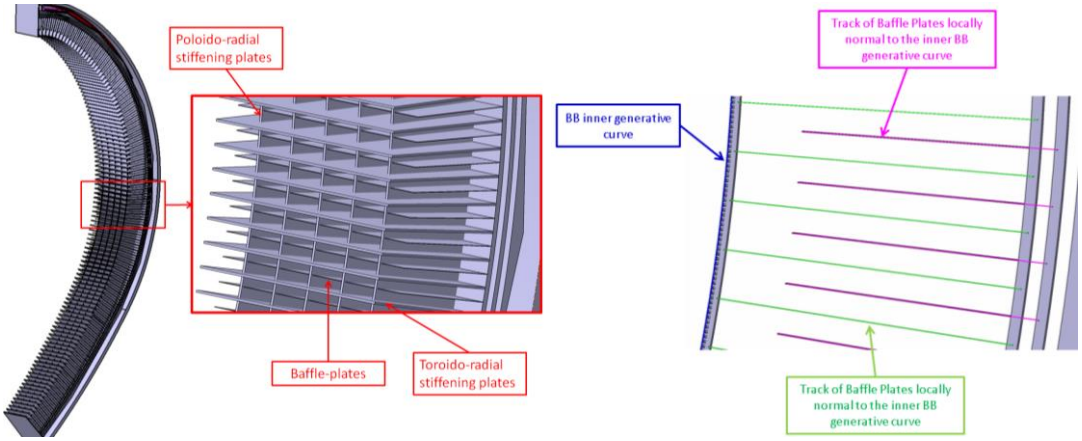

a) Stiffening and baffle plates

b) baffle plates and TR stiffening plates

Figure 78: *WCLL BB outboard segment internal structure* [161][162].

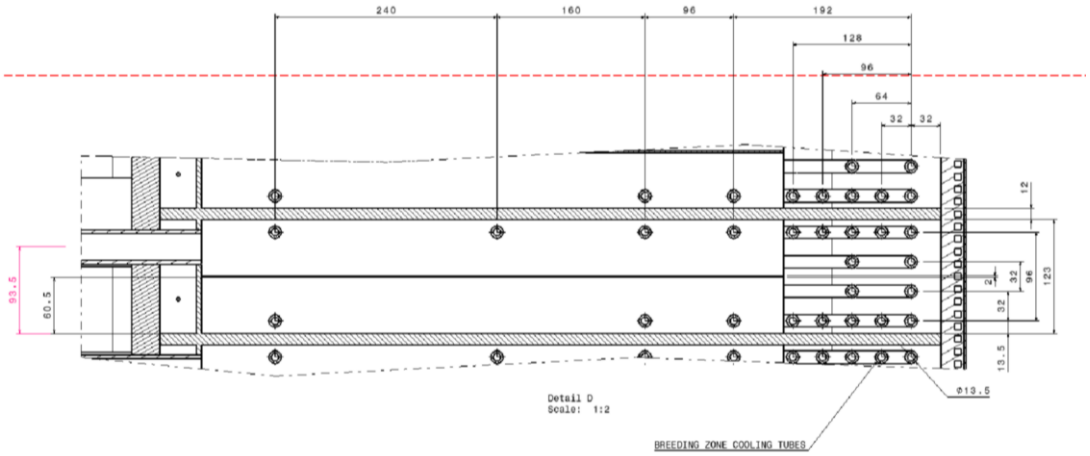

Figure 79: Radial-poloidal section of breeding unit [161][162].

4.6.3 First Wall

The front part of the WCLL BB segment is the First Wall (FW), which is an U-shape Plate bended in radial direction, cooled by an independent system. The plasma facing area is covered by a tungsten layer of 2 mm thickness and the total thickness is 25 mm. The FW is constituted by EUROFER, and it is cooled with

water flowing in square channels with a section of 7×7 mm and the pitch between two of them is 13.5 mm. In each breeding unit there are 10 coolant channels.

As it was mentioned previously, the water flows in the channels in counter with an inlet temperature of 295 °C and an outlet temperature of 325 °C, at 15.5 MPa.

Hence, owing to the FW water circuit configuration, the cooling modelization of the FW will be similar to that implemented for the rest of the BBs designs replacing Helium by water.

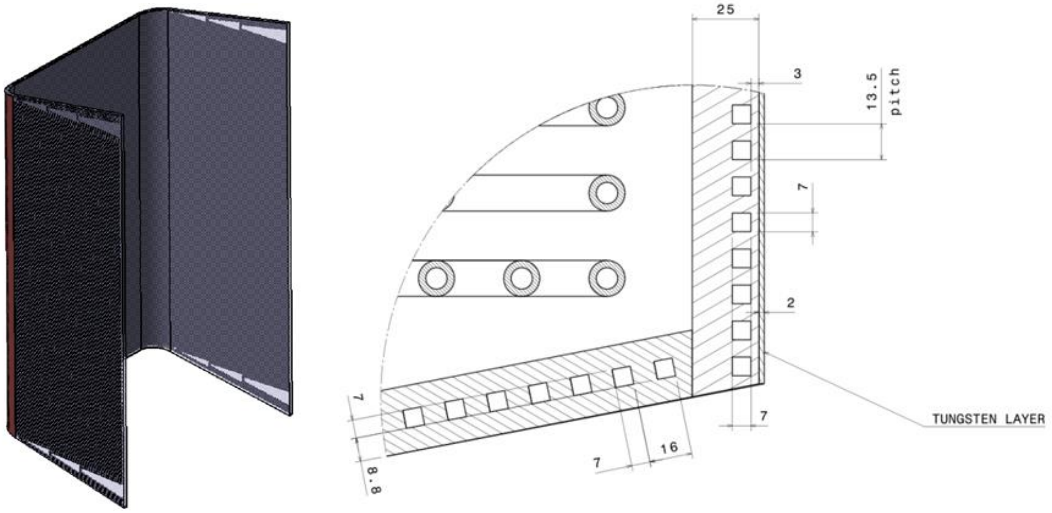

Figure 80: Cad model of OB4 First Wall and Layout of FW cooling channels [163].

4.6.4 BZ

The BZ is cooled with an independent system where also the water enters at 15.5 MPa and 295 °C, and exits at 328 °C. The tubes are radial-toroidal, displaced in a horizontal plane. The BZ tubes are double walled and have an external diameter of 13.5 mm, the internal one of 8 mm and the thickness is 1.25 mm [162]. The final configuration of these tubes is currently under investigation.

The Lead-Lithium (PbLi) enters in the breeding unit from the bottom of the elementary cell, flows in radial direction, from the back to the FW, goes up in poloidal direction and then flows from the FW to the back [162].

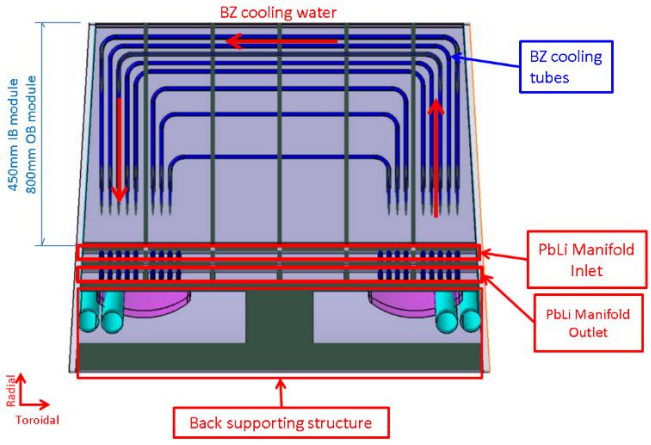

Figure 81: Section of the single module on toroidal-radial plane t [161].

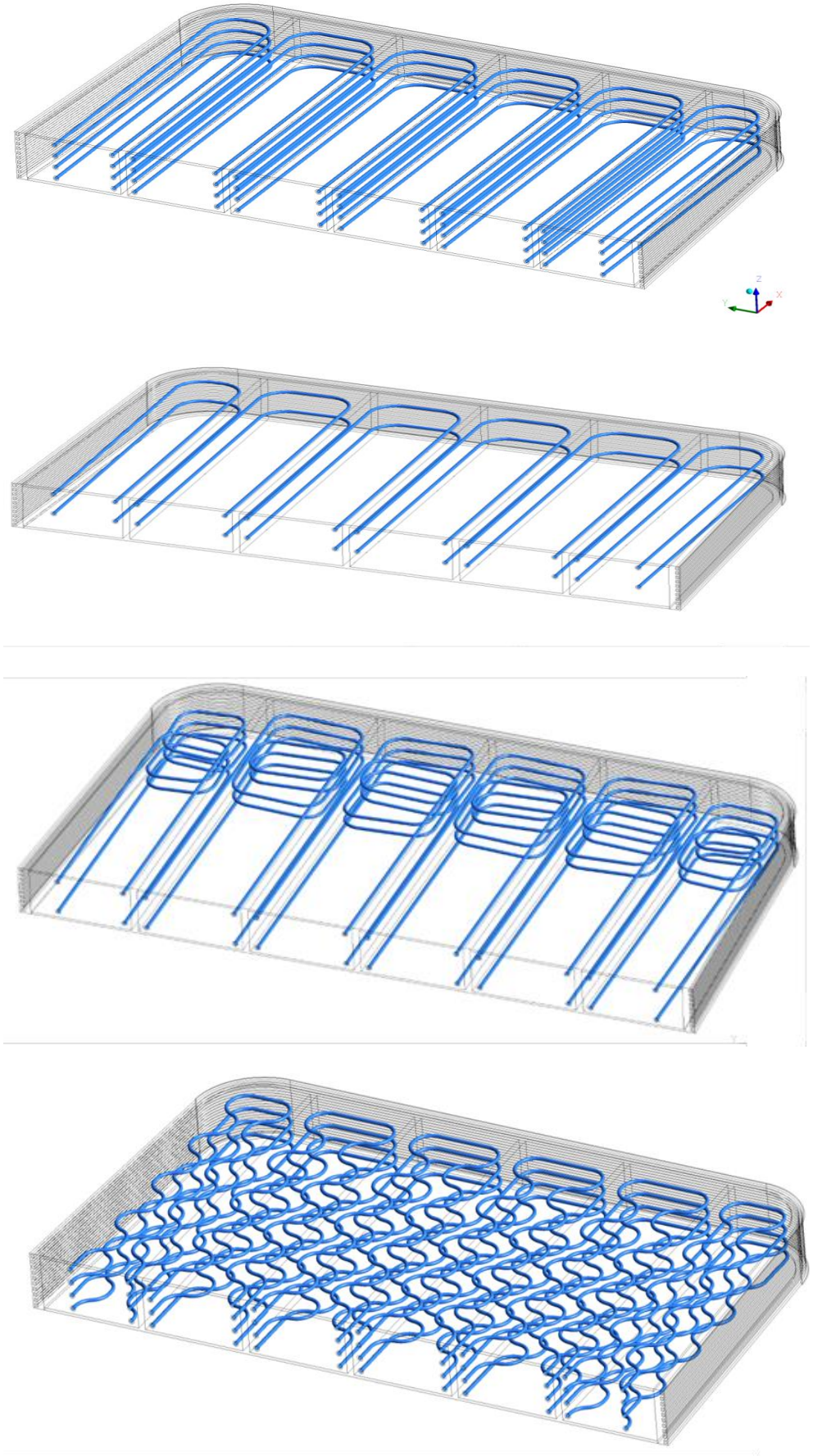

Figure 82: Cooling concepts 2016 for the Single breeding unit [160].

For AINA, the cooling effect caused by any of these configurations will be simulated as lateral cooling effect based on the Fabbri's methodology [2]. The PbLi along the BZ is not considered when the 1D segmentation is modeled and just two layers which represents the PbLi manifold tubes is implemented and is treated as a coolant layer. This criteria has been assumed since the most demanded area is the stiffening plates composed of EUROFER where a melting limit may be analyzed. It is even possible that the PbLi produces a soothing thermal effect due its flow but it has not been assumed either (conservative assumption).

4.6.5 Internal Stiffening and Baffle Plates

As stated on General Architecture section, Stiffening plates withstand an eventual over pressurization of the module due to a fault of the BZ water cooling tubes. The stiffening plates are placed on poloido-radial and toroido-radial planes. The internal structure is composed by 5 poloido-radial plates with 16 mm thickness [163].

In order to guarantee the Pb Li circulation, about 100 baffle plates for each module with 2 mm thick have been placed along toroido-radial direction. The distance between TR stiffening plates and baffle plates is 135 mm [161][162].

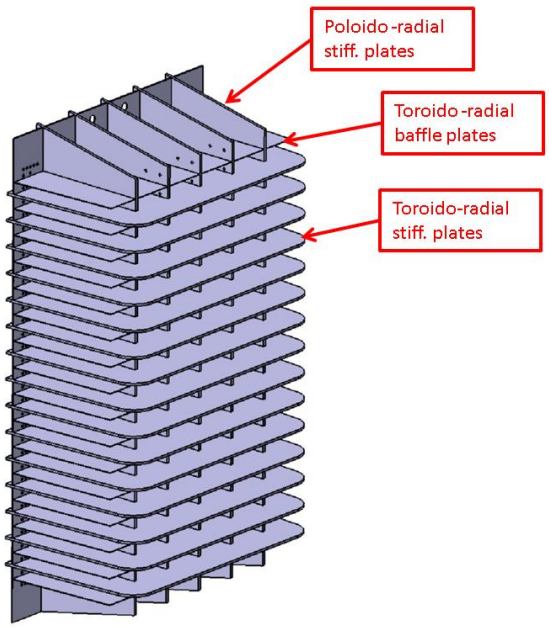

Figure 83: Plates of the OB4 module analogous to the 2016 concept [163].

4.6.6 Manifolds

The PbLi inlet and outlet manifolds are constituted by two gap of 40 mm. Three walls of 30 mm separate the inlet manifold from the breeding unit and the outlet manifold, and, vice versa, the outlet manifold from the inlet and the BSS. The PbLi is distributed (collected) in the six channels of the breeding unit through orifices [162].

The back walls of the modules are properly cut in the back area to save space for the BZ and FW cooling water manifolds [162].

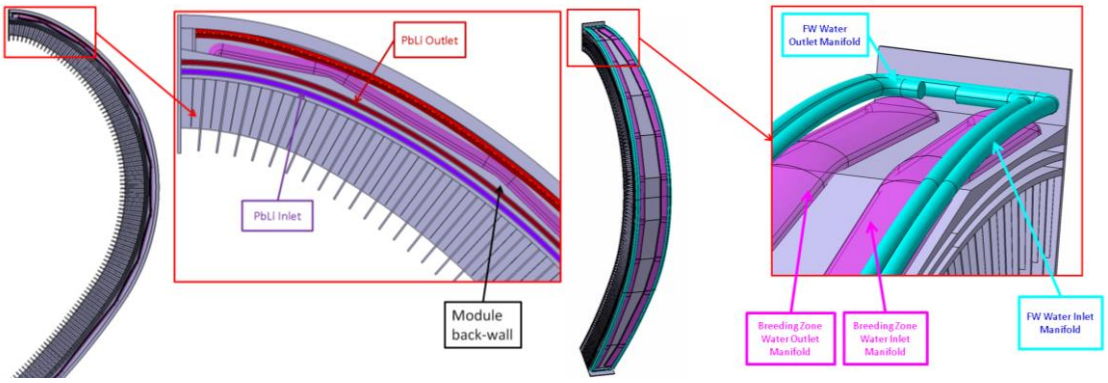

Figure 84: PbLi manifold region (left) and BZ and FW cooling water manifold [161].

4.6.7 Back Supporting Structure

The Back Supporting Structure (BSS) provides three distinct functions:

- Supporting the structural loads of the modules by mechanical attachment
- Holding feeding pipes
- Neutron shielding for the vacuum vessel

The BSS have T-shape and are joined to the sidewalls and the back walls of the modules. The BBS is connected to the back-wall of the modules through a proper rib 250 mm in thickness [161][162].

4.6.8 Material Properties

All materials properties employed in the AINA DEMO WCLL has already outlined throughout the analogous chapter for the AINA DEMO HCPB and DCLL, and the thermal model of the divertor.

4.6.9 Methodology to compute the lateral cooling

It should be recalled that the former AINA thermal wall model solver was not suitable to adapt to the most of DEMO designs because it was not able to take into consideration the influence of coolant channels not in line with the 1D segment. For this reason, a similar procedure to that used for the HCPB and HCLL model and based on the Fabbri's methodology [2] has been followed in order to implement the lateral cooling effect as a weighted convective negative flux as:

$$\dot{q} = h\,(T - T_{\infty}) \qquad (149)$$

where:

- $\dot{q}$ is the convective negative flux $[W/m^2]$
- h is the heat transfer coefficient $[W/m^2/K]$
- T is the material temperature $[K]$
- T_{∞} is the bulk coolant temperature $[K]$

Likewise, it is important to remember that $f_{WGT,R}$ and $f_{WGT,P}$ are the coolant factors for the no in lines tubes. They are discrete functions which take values only at the specified coolant positions and after a steady state crosscheck analysis. They have been outlined thorough Thermal Blanket Block Assembly section.

As already stated, owing to the water circuit configurations currently under investigation, the effect of water which flows through the BZ will be modeled as a single lateral cooling channel modeled by means of the Fabbri's methodology [2] and the specifications set out in Boundary Conditions section.

4.6.10 AINA WCLL Wall model

The 1D AINA WCLL thermal blanket model is based on the methodology used to develop the 1D AINA HCPB, DCLL and HCLL thermal model [2] doomed to represent the behavior of the more complex 3D CFD models. Therefore, a 1D simplified model has been built and consolidated using the results extracted from the thermal-hydraulic analysis performed by Martelli et al [160].

4.6.10.1 Model Description

The AINA WCLL thermal blanket model shall aim to represent the most conservative thermal behavior of the whole WCLL BB in the simplest possible way in order to check if EUROFER exceeds its melting limit (550 °C) in the worst case. Currently, a CFD model of the breeding units has been developed to obtain a complete and detailed temperature distribution in the solid structures [160]. The maximum EUROFER temperatures drawn from this study will be used to recreate a 1D segmentation along the blanket composed of the worst case for each layer depth.

In all previous blankets, the model has been based on the OBC equatorial module (OB4). However, as stated previously, a general breeding unit will be modeled for this blanket configuration. The 1D model dimensions have been taken from the following tables and the configuration described previously.

Component	Thickness (mm)	Tungsten	LiPb	H_20	Eurofer
Armour	2	100	-	-	-
First Wall	3	-	-	-	100
	7	-	-	50.74	49.26
	15	-	-	1.65	98.35
Breeding Zone	25	-	91.11	-	8.89
	14	-	61.91	10.26	27.83
	32	-	84.79	2.25	12.96
	32	-	78.98	4.26	16.76
	32	-	84.11	2.46	13.43
	32	-	83.67	2.5	13.83
	80	-	80.8	1.38	17.83
	80	-	80.56	1.41	18.03
	80	-	81.87	0.95	17.18
	80	-	81.34	1.19	17.47
	80	-	81.86	0.99	17.15
	80	-	81.93	0.98	17.1
	80	-	80.64	1.44	17.92
	73	-	81.71	1.07	17.22
LiPb manifolds	30	-	-	-	100
	40	-	38.23	-	61.77
	30	-	-	-	100
	40	-	38.18	-	61.82
Back Plate	30	-	-	-	100
H_20 manifolds	200	-	-	93.36	6.64
Back supporting structure	100	-	-	-	100

Table 59: Radial segmentation of the SMS WCLL BB model with materials volume percentage for each layer [160].

WCLL OB (DEMO 2016)							
Radial Subdivision (%)	0,15%	1,92%	61,44%		5,76%	30,72%	100,00%
Material	**Armour (2mm)**	**FW (t=25mm)**	**Breeding module**	**Caps**	**Backplates/ Internal Manifolds**	**BSS**	**Vol. (%)**
EUROFER [%]		86,090	16,130	95,098	97,200	44,900	30,957
Water [%]		13,914	1,460	4,902	0,910	54,100	17,837
PbLi (90% Li_6) [%]			82,410		1,890		50,745
Tungsten [%]	100,000						0,154
Void (Vacuum) [%]						1,000	0,307
Total	**100,0**	**100,0**	**100,0**	**100,0**	**100,0**	**100,0**	**100,0**

Table 60: Blanket material composition for the OBC [152].

Considering that the BZ back zone temperatures are mainly driven by the coolant outlet conditions and the BSS temperatures are very low the 1D AINA WCLL thermal blanket model domain ends at the backplate. The 1D segmentation selected passes through a stiffening plate along the BZ and assuming the lateral cooling of the water tubes. This choice causes conservative results. The resulting material layers, the thicknesses and the nodalization assumed are described in the next table and it is based on the truncation error and model discretization method exposed by Fabbri [2] in order to couch a realistic variation of the response functions as the temperature distributions and ensuring an acceptable computational time by means of the refinement of the model nodal mesh fixing time discretization (Δt=0.02 s). Contrary to HCPB blanket, in this case is not necessary scaling factors to compensate unrealistic results.

Layer No.	Material	Thickness [mm]	No. Nodes
1	Tungsten	2	102
2	EUROFER	3	500
3	Water Coolant	7	1
4	EUROFER	15	500
5	EUROFER	160	500
6	EUROFER	160	500
7	EUROFER	160	500
8	EUROFER	160	500
9	EUROFER	160	500
10	EUROFER	30	500
11	PbLi	40	1
12	EUROFER	30	500
13	PbLi	40	1
14	EUROFER	30	500

Table 61: Material Type, thickness and nodalization.

The water coolant layer for the FW assumes a f_{COOL} which is equal to the relative surface of the coolant tubes to the total surface of the module section, with an approximately value of 0.52 based on the dimensions FW model [163]; and 0.62 for the PbLi manifolds. Besides, the material emissivity used for irradiation during 100% LOCA is equal to 0.3 as in the HCPB, DCLL and HCLL models [2]. On the other hand, a huge EUROFER layer has been split out into five layers (from layer 5 to 9) with the aim of accomplishing realistic results keeping in mind the truncation error and model discretization method exposed by Fabbri [2].

4.6.10.2 Numerical Model

The numerical model is the same as used in the thermal HCPB, DCLL and HCLL blanket block and the thermal divertor blocks based on the research carried out by Marco Fabbri during his thesis development [2]. Likewise, the steady state and transient approaches follow the same structure; for this reason, the necessary boundary conditions and the nuclear heat deposition are presented in the following sections.

4.6.10.3 Boundary Conditions

- **FW Water Channel:** the water flows in the channels in counter with an inlet temperature of 295 °C and an outlet temperature of 325 °C, at 15.5 MPa [160][161][162][163][164][165]; thus, a temperature of 325 °C is assumed in conjunction with the thermal results of the Martelli's study [160]. Besides, the mass flow per cooling channel is set at 0.054 kg/s [162].
- **BZ Water Channels:** As stated above, the water coolant channels in the BZ has been modeled as lateral cooling. Based on Martelli's thermal hydraulic analysis [160], a conservative range from 359 °C to 343 °C has been set out. Besides, the mass flow per cooling channel is set at 0.0421 kg/s [160] and the water inlet pressure is equal to 155 bar [160][161][162][163][164][165].

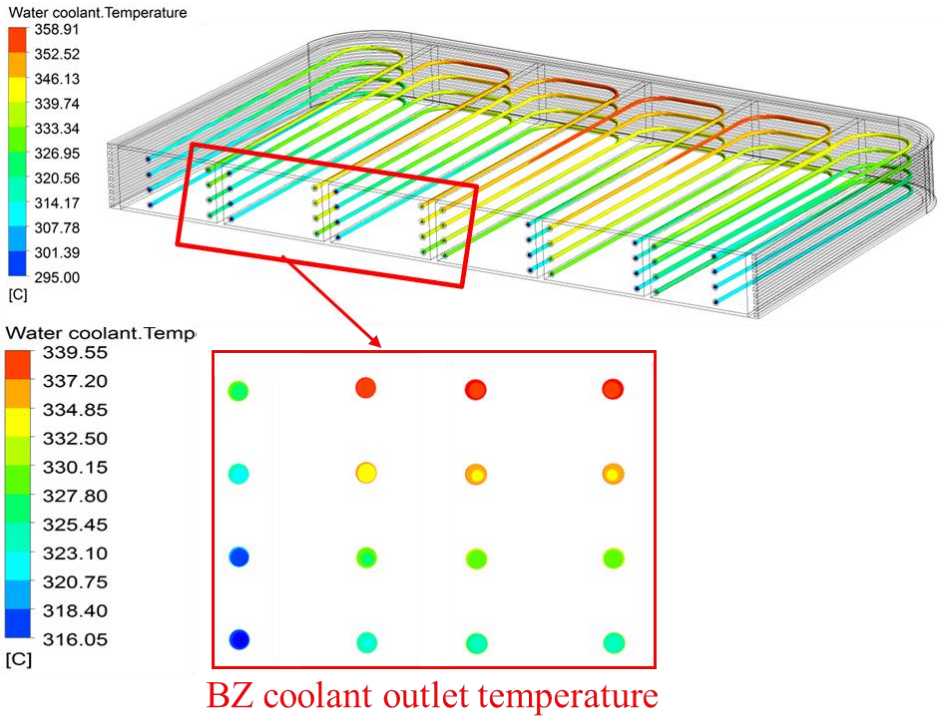

Figure 85: Water temperatures throughout the BZ [160].

- **PbLi Manifold**: The temperature is fixed at 325 °C [162][163][164][165] and the mass flow at 0.146 kg/s [161][163].
- **Last node:** For the last node, which represents the backplate, a temperature of 323.8 °C is assumed [160][161].
- **FW/first node**: in the first node a total load due to the radiation effect against the wall is applied. For the validation phase a heat flux on the FW of 0.5 MW/m^2 is assumed [160]. In addition, the power density for the first node (Tungsten) which is extrapolated for new NWL values when AINA runs is equal to 26.8 W/cm^3 [160].
- **Power deposition**: For the validation phase it is applied a mean neutron wall loading (NWL) of 1.05 MW/m^2 [160]. The corresponding power density profiles for a NWL of 0.97 MW/m^2 are also depicted in the following figure.

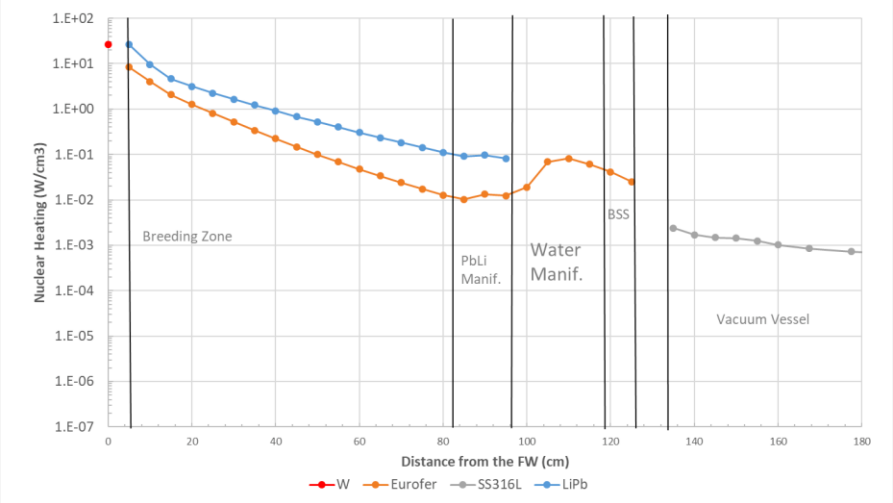

Figure 86: Radial distributions of the power density (W/cm3) along the outboard in W armour, Eurofer and LiPb [160].

Therefore, the nuclear distribution accepted for the EUROFER along the stiffening plate slice, manifold layers and backplate region and which is extrapolated for new NWL values when AINA runs is extracted from the previous graph.

It is important to remember that the power density for the first Tungsten nodes is equal to 26.8 W/cm^3 [160].

4.6.10.4 Model Validation

With the goal of validating the one-dimensional thermal-hydraulic behavior of the WCLL blanket AINA it would be desirable to cross-check its corresponding outcomes with results extracted from a more detailed (three-dimensional) thermal hydraulic analysis. A thermal-hydraulic model was performed by Martelli et al [160] with which to assess temperature distribution under steady state conditions and based on the geometry and the specifications exposed above.

From this analysis it was concluded that the maximum EUROFER temperature in the models is reached in the FW and is around 416.5 °C and it is always below 550 °C. The following table summarizes the highest temperatures obtained in different regions of the wall.

Component	Parameter	Value
Tungsten	Maximum W temperature	423.91 °C
FW	Maximum EUROFER temperature	416.5 °C
BS Stiffening plates	Maximum EUROFER temperature	402.9 °C

Table 62: HCLL hot spots [160].

In general, the EUROFER temperatures along the model is far below to the melting limit of 550 °C.

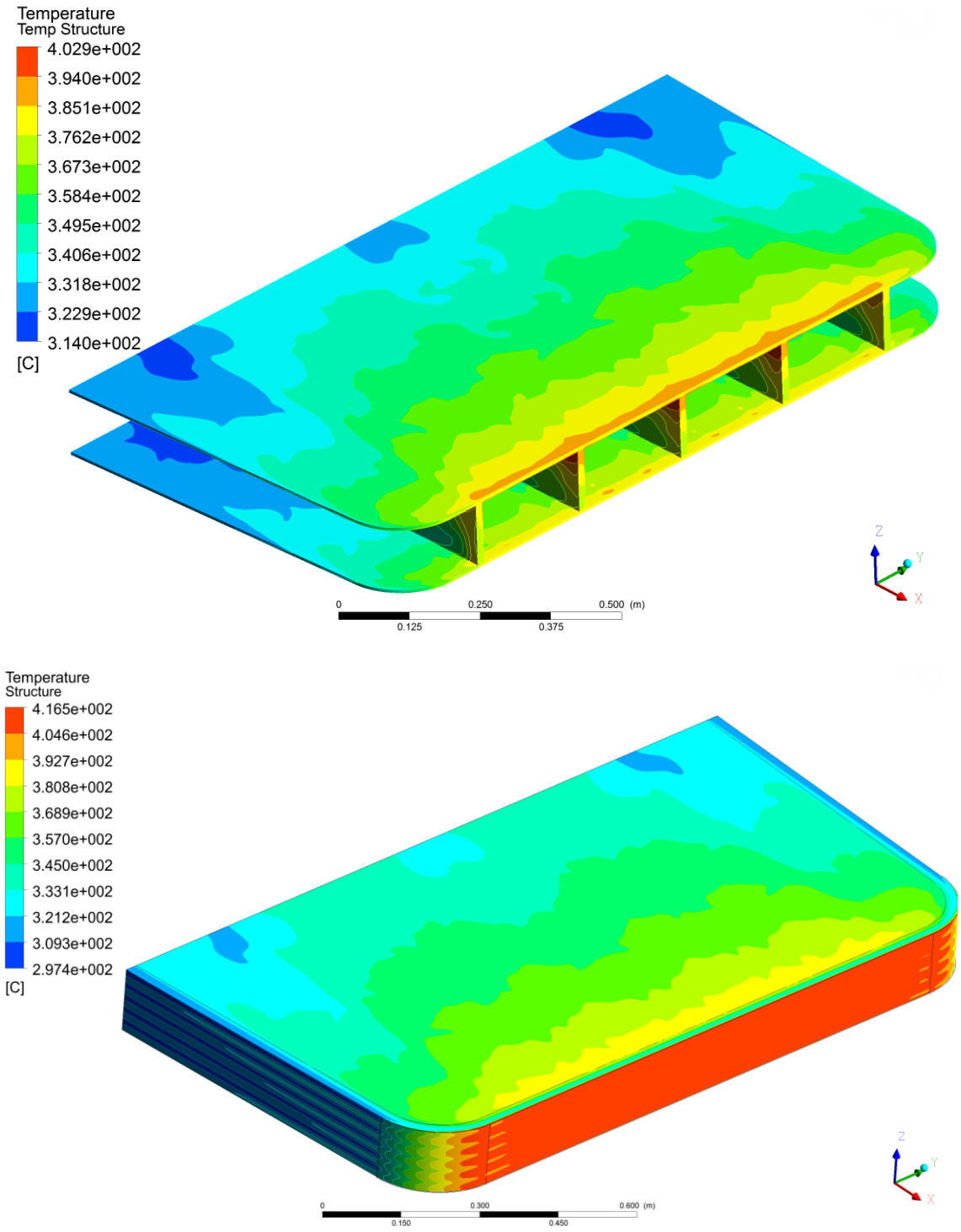

Figure 87: Thermal results for the stiffening (up) and the total structure (down) [160].

4.6.10.5 Cross-checks

The temperature WCLL 1D radial profile are computed by AINA and is reported in the following figure. These results refers to the thermal blanket block not coupled with the plasma model and, as already stated, forcing a mean neutron wall loading (NWL) of 1.05 MW/m^2 and a heat flux on the FW of 0.5 MW/m^2.

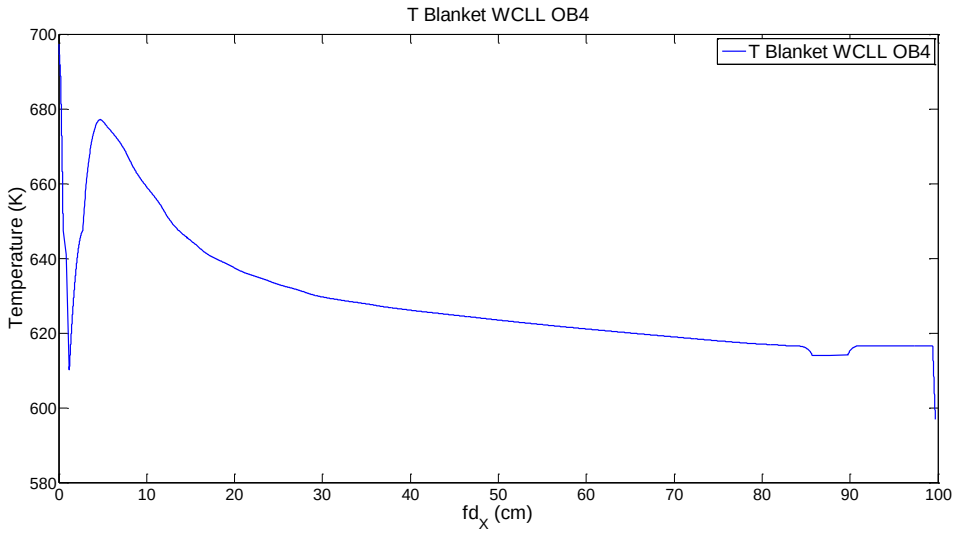

Figure 88: WCLL AINA 1D Temperature profile.

To validate the 1D WCLL AINA thermal-hydraulic behavior the following outcomes have been cross-checked with the 3D Finite Element (FE) detailed ones (referenced in the section above) and reported in the following table:

	3D WCLL FE	AINA WCLL	Relative difference (%)
Tungsten Temperature in the FW (°C)	423.91	424.1	+0.04
EUROFER Temperature in the FW (°C)	416.5	416.2	-0.07
Maximum EUROFER Temperature in the BZ (°C)	402.9	404	+0.27

Table 63: AINA 1D WCLL results cross-check.

4.6.11 Conclusions

The 1D WCLL AINA thermal behavior has resulted coherent and representative of the WCLL BB global behavior analyzed by means of 3D detailed FE. No meaningful discrepancies have been found. Indeed, the maximum temperature relative difference is less than 0.3% and is based on a conservative point of view.

On the other hand, the EUROFER limit of 550 °C is not exceeded both in 3D case and AINA simulation contrary to the rest of the blankets. Moreover, it is foreseeable that for the most demanding conditions estimated for DEMO1 by AINA this limit will not be surpassed. Thus, the design of the WCLL concept seems to be a proper and satisfactory solution.

Taking all these conclusions into account, all the simplifications done, the results and the development stage, the model fulfils the current work proposal. Unfortunately and as were the HCPB, DCLL and HCLL cases, the 1:1 temperature distribution along X-axis comparison has not been carried out because the data is not unavailable and so the verification has been only limited to specific hot spots. However and due to the model resulted coherent, conservative, representative and the run time is extremely short, a more complex model is not needed.

4.7 AINA Study as a Contribution to Safety Analyses of WCLL DEMO

As in the HCPB, DCLL and HCLL cases, AINA 4.0 has been the tool used to carry out the following safety study, DEMO1 is the reference scenario [11] and all the data and assumptions are based on DEMO BB Safety Data List document [120]. The difference to the previous cases is the design of the BB implemented in AINA, the modeled design is known as WCLL2016.v0.1 [160][161].

4.7.1 Types of Accidents

According to the criterion and the process of the previous safety analyses where the most representative 21 PIEs [129] for the deterministic assessments are kept in mind in order to check the compliance with safety limits and to give rationales for the selection of the reference DEMO reactor model, the following load or accident scenarios have been simulated by AINA for the WCLL case as well:

- Plasma disruption or structural material melting due to a LOPC. The perturbations that AINA may simulate and induce to this kind of scenario are: a failure in the external power supply system, a failure in the fuel source system, a variation in the confinement system and an entrance of an undesired quantity of impurities.
- In-vessel melt either of FW, blanket structure and/or divertor modules because of thermal stresses due to a LOCA. It is necessary to remember that AINA cannot simulate consequences of this kind of accident as a leakage, a release or a penetration of coolant or radioactive products into other structure regions.

4.7.2 Steady State Scenario DEMO1

The characteristics of the steady state scenario used to develop the safety study are the same as those used in the HCPB, DCLL and HCLL cases; the DEMO1 scenario ones [11][133]. Inputs and the relevant PROCESS crosschecking have been exposed in the HCPB case where no meaningful discrepancies have been found between AINA and PROCESS outputs.

Unlike for the HCPB and HCLL cases and in the same way as the DCLL case, there is no temperatures infringement for the WCLL steady state case as the following table summarizes. Specifically, EUROFER suffers this problem. For this reason, it would not be necessary to undertake a design review. It is important to note that this European DEMO blanket design has the biggest temperature safety margin according to AINA simulations.

Material	Temperature Limit $[^{o}C]$	T $[^{o}C]$
Tungsten	3422	365.5
EUROFER	550	422.8

Table 64: WCLL AINA DEMO1 SS maximum temperature.

All figures extracted from AINA and used in the following analysis are contained in Annex D.

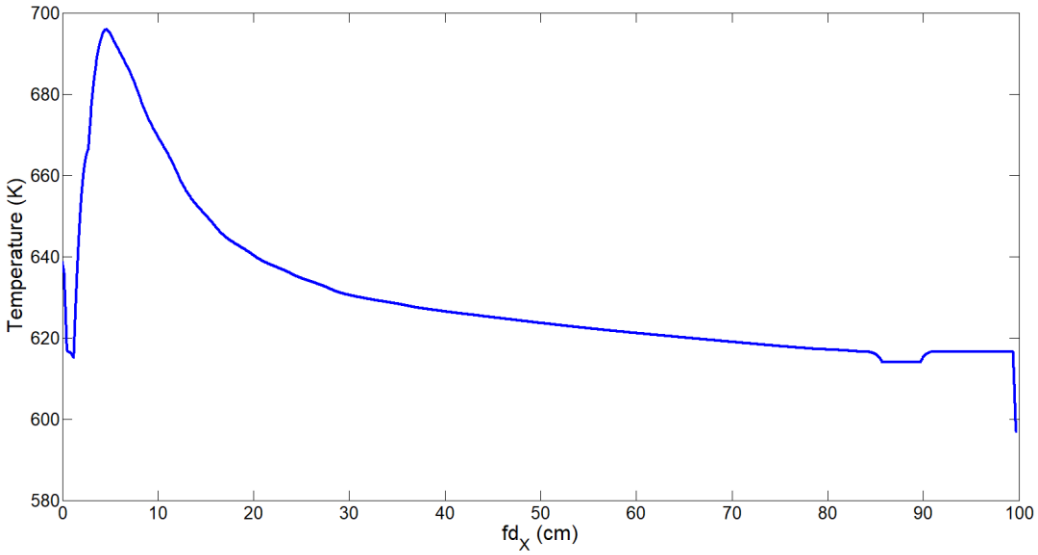

Figure 89: WCLL AINA 1D Temperature profile for DEMO1.

4.7.3 LOPC Accidents

The behavior of the plasma physics for this kind of anomalies is the same as the HCPB, DCLL and HCLL simulations. Therefore and once again only the temperatures reached by the BB materials require a particular attention since regarding the other conclusions are shared.

4.7.3.1 Failure in the External Power Supply System

As stated in the preceding safety analyses, the external power input is required for the fusion technologies not only to achieve an operational state but also to keep the plasma hot since most of the energy produced by fusion is carried away by the neutrons. In addition, currently, it is not clear yet whether ignition will be the optimum operating regime. For this reason the possible consequences of failures from the external power supply system should be studied. These failures are classified into three different scenarios which are outlined hereunder.

4.7.3.1.1 Auxiliary heating cut-off or decrease

Accident description: An unexpected and sudden auxiliary heating cut-off or decrease takes place at second t=0.1 s while the WCLL DEMO reactor is operating on DEMO1 steady state.

Event sequence: The reactor converges at a new steady state which produces a higher fusion power (2420 MW for the cut-off case and 2197 MW for a 50% external power decrease). So, the ignition point is achieved theoretically despite the increase of NWL through the blanket which induces a temperature increase for the BB materials but within the allowed range (Tungsten: 376.1 ºC and EUROFER: 433 ºC). In summary, the WCLL design, as in the DCLL case, would be capable of withstanding an ignition scenario with no risks apparently according to AINA results due to its cooling specifications.

4.7.3.1.2 Auxiliary heating increase up to a multiplication factor of 6.3

Accident description: An unexpected and sudden increase of auxiliary heating up to a multiplication factor of 6.3 takes place at second 0.1 while WCLL DEMO reactor is operating on DEMO1 steady state.

Event sequence: OB5 region becomes the worst (it receives the maximum load flux $NWL + P_{RAD}$) between the second 0.3-0.5 s depending on the multiplication factor which affect external power. An

initial and abrupt fusion power increment takes place although it finally decreases rapidly achieving a new steady state which produces less fusion power than DEMO1 and where the BB temperatures are lower except in the FW where the Tungsten temperature increases a bit. Ideally, these incidents should be detected for the purpose of foreseeing an important power fusion decrease since the new scenario does not represent any risk unless the external power keeps increasing and it reaches the following level of accident.

4.7.3.1.3 Auxiliary heating increase with a multiplication factor larger than 6.3

Accident description: An unexpected and sudden increase of auxiliary heating with a multiplication factor larger than 6.3 takes place at second 0.1 while WCLL DEMO reactor is operating on DEMO1 steady state.

Event sequence: This level of auxiliary heating perturbation causes a plasma disruption due to the beta limit infringement (the higher multiplication factor is, the faster plasma collapse is) and OB5 region becomes the worst (it receives the maximum load flux $NWL + P_{RAD}$) at second 0.3 s. Once again, fusion power and densities quickly diminish, except the impurity percentage of Tungsten which rises. The plasma thermal energy (U) reaches 1.5 GJ for a multiplication factor of 6.4; so, the overcoming of the EUROFER limit [135] takes place. Nevertheless and in spite of these severe consequences, it is important to stress that it is highly unlikely to achieve auxiliary heating as high as those due to the installed external power capacity would not exceed 150 MW.

4.7.3.1.4 Auxiliary heating perturbation summary

Mult. factor	Plasma termination	Plasma termination time $[s]$	Consequences	Mitigation	Observations
0 (cut-off)	Stabilized	-	Fusion power increase.	Not necessary.	Ignition scenario is achieved.
0.5	Stabilized	-	Fusion power increase.	Not necessary.	New SS more energetic.
2	Stabilized	-	Fusion power decrease. BB temperature decrease except in the FW.	Not necessary.	New SS less energetic.
3	Stabilized	-	Fusion power decrease. decrease except in the FW.	Not necessary.	New SS less energetic.
4	Stabilized	-	Fusion power decrease. decrease except in the FW.	Not necessary.	New SS less energetic.

5	Stabilized	-	Fusion power decrease. BB temperature decrease except in the FW.	Not necessary.	New SS less energetic.
6.4	Beta Limit	88.5	Excessive plasma thermal energy (1.5 GJ).	External power variation detection.	In principle, it is not possible to reach such high external power.
7	Beta Limit	12.8	Excessive plasma thermal energy (1.5 GJ).	External power variation detection.	In principle, it is not possible to reach such high external power.
8	Beta Limit	3.6	Excessive plasma thermal energy (1.5 GJ).	External power variation detection.	In principle, it is not possible to reach such high external power.
9	Beta Limit	2	Excessive plasma thermal energy (1.5 GJ).	External power variation detection.	In principle, it is not possible to reach such high external power.

Table 65: Auxiliary heating perturbation summary

4.7.3.2 Failure in the Fuel Source System

The fueling system provides the required D-T fuel mixture to maintain the equilibrium of the plasma as foreseen by the operating scenarios [136], therefore the consequences of its possible failures have to be analyzed. Four different scenarios analogous to the HCPB, DCLL and HCLL cases may take place.

4.7.3.2.1 Fueling rate cut-off

Accident description: An unexpected and instantaneous fueling rate cut-off takes place at second t=0.1 s while the WCLL DEMO reactor is operating on DEMO1 steady state.

Event sequence: A fueling source stop induces a fusion power and densities decrease, except the impurities percentages. With regard to structural conditions, all of this leads the reactor to a reduction in BB temperatures (Tungsten: 348 ºC and EUROFER: 389 ºC). Moreover OB5 becomes the worst region from the second 0.4 and a transition mode is detected after 22.9 seconds which leads to a plasma collapses at 25.5 s by an overshoot beta limit disruption. The plasma thermal energy (U) achieves values of up to 0.5 GJ; consequently this disruption could be mitigated by a disruption mitigation system [135] and, thereby, the BB material would be safeguarded from this energy release. Nevertheless and as concluded in the previous blanket cases it would be useful to detect a fueling cut off for the purpose of conducing the plasma to a better and controlled plasma shutdown if it is possible.

4.7.3.2.2 Fueling rate decrease

Accident description: An unexpected and sudden decrease of fueling rate takes place at second t=0.1 s while the WCLL DEMO reactor is operating on DEMO1 steady state.

Event sequence: As in the fueling cut-off case, OB5 becomes the worst region after 0.6 s. and the reactor is driven to a fusion power and temperatures decrease (Tungsten: 348 ºC and EUROFER: 394 ºC for a half of fueling). In conclusion, beyond this failure does not cause any risk but the generation of fusion power is much lower

4.7.3.2.3 Fueling rate increase up to 25%

Accident description: An unexpected and sudden increase of fueling rate up to 25% takes place at second t=0.1 s while the WCLL DEMO reactor is operating on DEMO1 steady state.

Event sequence: As in the previous case, a new steady state scenario is achieved, however in this conditions the fusion power expands greatly, the OB5 becomes the worst region after 5.5 s and the material temperatures rise, Tungsten reaches 416 ºC after 250 s and EUROFER 470 ºC. This means that the EUROFER functional temperature limit is not exceeded despite the failure. Even then, it is essential to be able to guarantee a quick detection and actuation of a fueling increase in order to prevent a new fueling rate increase which could induce the dangerous scenario analyzed in the following case.

4.7.3.2.4 Fueling rate increase above 25%

Accident description: An unexpected and sudden increase of fueling rate above 25% takes place at second t=0.1 s while the WCLL DEMO reactor is operating on DEMO1 steady state.

Event sequence: Fusion power, densities and confinement time are continuously growing until plasma collapses due to a Greenwald limit disruption. Logically, the higher fueling rate multiplication factor is, the earlier collapse takes place. Contrary to the previous blankets, for a fueling rate of 50% the EUROFER melting scenario is not exceeded (510 ºC) before the plasma collapse. The subsequent high energetic disruption causes structural damage, hence it is necessary to detect an increase of fueling rapidly and activate a FPSS. It is important to remember once again that in ITER, the fueling rate capacity can cover up to $7.8 \cdot 10^{19}$ $/_{m^3 s}$ (above a multiplication factor of 10 for DEMO1) [16] and hence this kind of dramatic scenarios might come about.

Multiplication factor	Plasma termination time $[s]$	Plasma Thermal energy U $[GJ]$	Max. Tungsten T $[ºC]$	Max. EUROFER T $[ºC]$
1.5	74.7	2.1	460.4	510
6	1.7	1.3	370.1	424.2

Table 66: Disruption time and plasma thermal energy for an excessive fueling rate increase.

4.7.3.2.5 Fueling rate perturbation summary

Mult. factor	Plasma termination	Plasma termination time $[s]$	Consequences	Mitigation	Observations
0 (cut-off)	Beta Limit	25.5	A plasma thermal energy with a rate of 0.5 GJ.	Disruption mitigation system.	-
0.5	Stabilized	-	Fusion power decrease.	Not necessary.	New steady state with lower material temperatures.
1.25	Stabilized	-	Fusion power increase. EUROFER limit exceeded at 50.6 s.	Fueling rate variation detection.	No risks but if the fueling still growing it is possible the skip to the next case.
1.5	Greenwald Limit	74.7	Fusion power increase.	Fueling rate variation	This is the worst scenario due to the

			Excessive plasma thermal energy (2.1 GJ).	detection and a FPSS activation.	high temperatures and the high plasma thermal energy.
6	Greenwald Limit	1.7	Fusion power increase. Excessive plasma thermal energy (1.3 GJ).	Fueling rate variation detection and a FPSS activation.	Structural damage due to the plasma thermal energy.

Table 67: Fueling rate perturbation summary.

4.7.3.3 Improvement in the Confinement System

It is important to remember that, historically, AINA has been used in safety analyses to scan the influence of an increase in confinement time [16][19][37] due to, among other reasons, the H mode discovery.

Accident description: An unexpected and sudden permanent increase of confinement time takes place at second t=0.1 s while the WCLL DEMO reactor is operating on DEMO1 steady state.

Event sequence: This kind of perturbation produces fast ion and electron temperatures increase as well as densities and an overall raise of fusion power until plasma terminates disruptively on account of the beta limit infringement. The region OB5 becomes the most demanded region promptly (~ 0.3 s) and PFCs temperatures quickly grow due to the load flux $NWL + P_{RAD}$ rise although melting limits are not surpassed before the collapse. The plasma thermal energy release during the beta disruption causes structural damage and melting in any case. Consequently, it is necessary, once again, to detect instantaneously an unexpected variation in confinement time with the aim of conducing the reactor to a controlled plasma shutdown.

Multiplication factor	Plasma termination time $[s]$	Plasma Thermal energy U $[GJ]$	Max. EUROFER T $[^{o}C]$	Max. P_{fus} $[MW]$
1.5	31.7	2.4	478	4708
5	3	2.4	430	5565

Table 68: Disruption time and plasma thermal energy for a confinement time improvement.

Moving on to other issues, it is important to remember, once again, that it is foreseeable that any confinement time reduction induces a loss of plasma confinement during the first seconds after the perturbation (< 5 s) with a fusion power drop; however, it is not possible to extract the precise consequences of these events from AINA owing to the numerical restrictions derived from the confinement law expressions implemented in the code. Therefore, it might be advisable to detect rapidly a failure in the confinement system which could lead to this kind of no discussed situation.

4.7.3.4 Occasional Variation of Confinement Time

A punctual confinement time variation may or may not take place due to an unexpected behavior during the operation time, hence the evolution of this kind of phenomena may be necessary.

As it was outlined in the HCPB, DCLL and HCLL safety analyses, the impact of these events is highly dependent on the duration of the confinement time variation and, in contrast, it does not depend so much on the variation factor suffered. Therefore, when the confinement time rises abruptly but decreases after 0.1 s, the effects are not severe and the steady state is recovered in less than 20 s not only for a low multiplication factor of 3 but also a high multiplication factor of 10. During this transition,

an instantaneous fusion power peak is reached due to a fast and short increase of plasma temperatures. Consequently, the BB temperatures remain practically unchanged. In case the duration of the confinement time variation is longer, the operations steady state is supposedly recovered as long as the perturbation disappears before the corresponding termination time tracked down in the previous section. For instance, an increase of the confinement time due to a multiplication factor with a value of 3 leads the plasma to a transitional state which can be intrinsically recovered as long as the perturbation lasts less than 3.7 s. However, it has been detected an unpredictable episode where the plasma collapses due to the Greenwald limit violation in less than 22 s and where the FW and internal BB temperatures rise sharply. This transient takes place when the occasional variation of confinement time lasts equal to or more than 3 s. In view of these circumstances, it is necessary to detect instantaneously an unexpected variation in confinement time with the aim of conducing the reactor to a controlled plasma shutdown if this variation is long enough to be critical.

Multiplication factor	Perturbation duration $[s]$	Max. EUROFER T $[^{o}C]$	Max. Tungsten T $[^{o}C]$	Max. P_{fus} $[MW]$
3	0.1	423.7	365.3	2096
3	0.5	425	367.6	2423
3	1	425.8	372	2803
3	3	459	463	4790
10	0.1	423.8	365.4	2117

Table 69: Maximum temperature increase and fusion power peak for an occasional confinement time improvement.

4.7.3.5 Entrance of an Undesired Quantity of Impurities

A flux of particles enter the plasma may induce several undesirable effects as a PFC damage or beneficial effects as shutting down the fusion due to an increase of Bremsstrahlung and line radiation. For this reason, this kind of perturbations must be studied.

4.7.3.5.1 Punctual impurity increase up to 300%

Accident description: A punctual increase of the impurities presence (Xe and W) up to 300% takes place at second t=0.1 s while the WCLL DEMO reactor is operating on DEMO1 steady state. This kind of perturbation can recreate the consequences of a leakage.

Event sequence: In this case it is noteworthy that the reactor suffers a sudden rise fusion power and an increase of the BB temperatures without exceeding the respective limits. Nevertheless, a recovery of the initial steady state takes place at last. Accordingly, the steady state temperatures are also recovered after 60 s for the 1.5 multiplication factor case and 140 s for the 2.9 multiplication factor case, the worst one. In conclusion, this case has no associated risks.

Multiplication factor	Max. Tungsten T $[^{o}C]$	Max. EUROFER T $[^{o}C]$	Max. P_{fus} $[MW]$
1.5	377.2	428	2299
2.9	434.1	462	4196

Table 70: Maximum temperature increase and fusion power peak for a punctual impurity increase.

4.7.3.5.2 Punctual impurity increase equal or above 300%

Accident description: A punctual increase of the impurities presence (Xe and W) equal to 300% takes place at second t=0.1 s while the WCLL DEMO reactor is operating on DEMO1 steady state. This kind of perturbation can recreate the consequences of a leakage.

Event sequence: The plasma skips instantaneous (at 0.1 s) to the L mode; hence, the steady state is not recovered after the perturbation. The fusion power grows (until a peak of 4365 MW) and, consequently, the temperature in the BB rises rapidly without exceeding limits. The EUROFER reaches 443.2 ºC and the Tungsten reaches 450.4 ºC for an impurity increase equal to 300%. Finally, the Greenwald limit is infringed due to densities are continuously growing. The disruption takes place at 12 s and it releases 1.8 GJ of thermal energy which would damage the reactor structure. For this reason, it is necessary to detect this kind of perturbation instantly and leading the reactor to a controlled plasma shutdown.

4.7.3.5.3 Tungsten permanent entrance increase

Accident description: An increase of the Tungsten impurity production takes place from second t=0.1 s while the WCLL DEMO reactor is operating on DEMO1 steady state. The previous cases could recreate the consequences of a leakage, however, in this case the simulation recreates a variation of the production rate and, consequently, the number of impurities which arrive to the plasma core permanently. These phenomena might occur due to the deterioration of the PFCs.

Event sequence: Fusion power, densities and confinement time grows slowly but continuously. Depending on the level of the new impurity production rate the plasma may reach a new steady state or it might collapse by mean of the Greenwald limit infringement. It should be noted that a huge Tungsten source is necessary in order to the second case takes place. A fourfold of tungsten entrance does not cause a plasma collapse and the EUROFER temperature reaches 444 ºC and Tungsten reaches 400.8 ºC that are lower than their limits due to this particular blanket design. Moreover, any alternative is not instantaneous; consequently the detection system which does not seem to be very complex has enough time to act before a collapse.

4.7.4 LOCA Accidents

Firstly, it should be underlined once again that, as in the HCPB, DCLL and HCLL cases, LOCA perturbations only affect the temperature profile along the BB and the divertor; however, the production rate of Tungsten by sublimation process (depending on surface material temperature) is greatly lower than physical sputtering process (independent of surface material temperature). Therefore, conditions inside the plasma remain practically unchanged. On the other hand, it is important to remember once again that the divertor modeling used in AINA is a preliminary configuration which would be advisable to improve and update when a more detailed thermo-hydraulic assessment for the final design of the divertor carries out; for this reason, the conclusions drawn from the LOCA simulations where the divertor is affected must be taken with a grain of salt. Moreover, LOCAs where just the divertor is affected have already been studied throughout the HCPB safety analysis.

4.7.4.1 BB LOCA 30%

Accident description: an small LOCA simulation where the water FW channel and the water and PbLi coolant loops of the BB architecture loses 30% of the mass flow rate at second t=0.1 s while the WCLL DEMO reactor is operating on DEMO1 steady state. The perturbation is applied using a step function and hence the progressive decrease of the mass flow rate has not been taken into account.

Event sequence: As it is well known, only the material temperatures of the BB structure changes; the plasma parameters remain virtually unchanged. This temperature distribution is affected in magnitude due to the modification of the cooling features and, as logic, enhanced variations are placed in most loaded areas where the coolant effect is lower. In this case, a new steady state for the thermal system is

found at 50 s. The Tungsten temperatures of the FW have increased to 372.4 ºC and the maximum EUROFER temperatures reaches 436 ºC which, in contrast with the previous blanket, is not higher than the design limit. Hence, this incident does not induce a dramatic scenario; however, it is advisable to be able to guarantee a quick detection if a LOCA takes place in any coolant channel in order to proceed to a proper mitigation action since, as will be pointed in the following cases, if the LOCA is greater, the structural damage would be possible.

4.7.4.2 BB LOCA 60%

Accident description: a medium LOCA simulation the water FW channel and the water and PbLi coolant loops of the BB architecture loses 60% of the mass flow rate at second t=0.1 s while the WCLL DEMO reactor is operating on DEMO1 steady state. The perturbation is applied using a step function and hence the progressive decrease of the mass flow rate has not been taken into account.

Event sequence: Obviously and following the trend of the previous case, the EUROFER temperature is greater and closer to the design limit but is not surpassed. The new steady state is found at 80 s. The Tungsten temperature reaches 386 ºC and EUROFER temperature rises to 458 ºC. As previously, it is recommended to be able to guarantee a very quick detection if a LOCA takes place with the objective of proceeding to a proper mitigation action although there is not a dangerous event due to the particular and proper coolant system configuration of the WCLL blanket.

4.7.4.3 BB LOCA 90%

Accident description: a big LOCA simulation where the water FW channel and the water and PbLi coolant loops of the BB architecture loses 90% of the mass flow rate at second t=0.1 s while the WCLL DEMO reactor is operating on DEMO1 steady state. The perturbation is applied using a step function and hence the progressive decrease of the mass flow rate has not been taken into account.

Event sequence: The overall behavior of the reactor is analogous to the previous cases although the current one causes a greater and faster temperature impact closer to the melting damage. The new thermal equilibrium is achieved after 150 s and the Tungsten temperature reaches 432.2 ºC and the EUROFER rises to 522 ºC. Thus, a very quick detection is necessary as well as a proper and fast mitigation action such as a fast plasma shutdown (FPSS) due to the possibility of structural damage taking place. It is important to remember that the thermal results obtained by AINA are approximations; for this reason, despite the fact that the AINA simulations do not foresee design limit infringements it will necessary to perform a more detailed thermal analysis to draw firm conclusions.

4.7.4.4 Divertor and BB LOCA 30% or 60% or 90%

Accident description: a LOCA simulation where the CB and the PFC cooling loops of the divertor architecture and the water FW channel and the water and PbLi coolant loops of the BB architecture loses 30% or 60% or 90% of the mass flow rate at second t=0.1 s while the WCLL DEMO reactor is operating on DEMO1 steady state. The perturbation is applied using a step function and hence the progressive decrease of the mass flow rate has not been taken into account. This kind of accident may be due to a loss of the cooling mass flow in the Primary Heat Transfer System (PHTS) which might affect the overall cooling system.

Event sequence: In summary, the consequences of this kind of accident are the sum of both phenomena discussed previously separately throughout the BB WCLL LOCA study and throughout the divertor HCPB

LOCA study. As has been pointed previously, the most relevant effect is a possible structural damage scenario due to the EUROFER temperatures reached. Thus, it would be necessary to assure a proper detection system in order to identify rapidly a loss of the cooling mass flow and to lead the reactor to a safe shutdown.

4.7.5 Conclusions

First of all, it is important to highlight the fact that, unlike for the HCPB and HCLL cases where certain functional temperature limits are slightly exceeded in the worst poloidal region (OB4) at the DEMO1 scenario, there is no temperatures infringement for the WCLL steady state case, in a similar way to the DCLL blanket. For this reason, it would not be necessary to undertake a DCLL design review.

With regard to LOCAs, it is necessary to remember, once again, that this kind of failure does not affect the internal plasma conditions from AINA outcomes. These perturbations lead the reactor to a more demanding scenario from a thermal point of view but the design limits are not exceeded in contrast with the rest of the blanket designs. Logically, the greater mass flow loss is, the higher structural temperatures are. Despite this positive evolution due to the particular and proper coolant system configuration of the WCLL blanket, it is recommended to be able to guarantee a very quick detection if a LOCA takes place with the objective of proceeding to a proper structural damage mitigation action.

On the other hand and concerning LOPC cases, broadly speaking, there are three possible scenarios when a LOPC takes place. At best, a new steady state with a fusion power decrease and less structural stress due to lower wall loads and, consequently, temperatures decrease. This case would be safe and a mitigation system or action would not be necessary. Those perturbations which induce to this option are: an increase of the external power injection between 200% and 630% and a decrease of the fueling injection rate (not fueling cut-off). In contrast, another potential consequence would involve a risk of structural damage due to a very energetic plasma termination which may discharge a great amount of thermal energy against the internal reactor walls. From AINA outcomes, an increase of the external power injection above 630% would disrupt within a short period of time (89 s at best) and transferring 1.5 GJ of thermal energy against the walls that damages and melts the structure. Notwithstanding, this situation would be highly unlikely since, in principle, it would not be possible to reach such high external power. Likewise, a cut-off of the fueling injection may induce to a plasma collapse in 25 s; however the thermal power released and around 0.5 GJ could be mitigated by a proper disruption mitigation system and, thereby, safeguarding the BB material. Finally, the third potential consequence arisen from a LOPC is the same as the impacts emerged when a LOCA takes place, a more demanding scenario from a thermal point of view but where the design limits are not exceeded. This situation might occur due to a decrease or a cut-off of the external power injection, a fueling rate injection increase up to 25%, an occasional variation of confinement time beneath the corresponding termination time and a punctual impurity increase up to 300%. All these situations seem to no have associated risk; however, for some of them it would be recommended to guarantee a quick detection and actuation by means of a proper system depending on the affected equipment since a new failure level increase could induce to a dangerous event. The mitigation action would be the activation of a fast plasma shutdown (FPSS) for all the cases. Last but not least, there are certain incidents which may drive the reactor to suffer both a structural temperatures increase scenario and a very energetic plasma disruption at the same time. These triggers are an increase of fueling injection above 50%, a permanent improvement in the confinement time and a punctual impurity increase above 300%. Therefore and owing to the double effect, these are the most critical failures and a special attention in order to avoid them will be necessary.

The measures to be taken are the mitigation systems and actions for the particular cases explained previously.

5 AINA Study as a Contribution to Safety Analyses of DEMO2

Firstly, it is important to highlight that the tool used to carry out this safety study has been AINA 4.0, the reference scenario is DEMO2 [12] , all the data and assumptions are based on DEMO BB Safety Data List document [120] and the design of the modeled Blanket is the HCLL Advanced-plus option [153]. Thanks to the previous safety analyses for the DEMO1 scenario where internal plasma parameters evolve in the same way without depending on the blanket simulated; the HCLL design can be used as reference. Likewise, the wall material response which varies depending on the blanket modeled shall be extrapolated from this singular case based on the previous experience as well.

It should be remembered that the safety and environmental goals of a fusion power plant design are to protect workers from radiation, electromagnetic fields, chemical and other hazards; the public from radioactive and toxic materials and the environment from pollutants and waste [121]. The general safety principals document for DEMO [122], the four DEMO Fundamental Safety Functions [122][123], the Propose Safety Importance Classification Scheme for DEMO Systems, Structures and Components [124] have already been set out in DEMO1 chapter. In such a case, as well as in previous DEMO1 case, this safety study is faced to figure out, on one hand, if the in vessel components fulfill the following safety functions in support of confinement and, on the other hand, the possible consequences if these functions are not satisfied:

- Control of plasma energy
- Control of thermal energy
- Control of coolant energy

5.1 Types of Accidents

As it has noted throughout this report, common objective of the FFMEAs done for the various DEMO systems [126][127][125][128] was, at first, to provide a complete list of potential accident initiating events (IEs). Among those, the Selection of reference accident scenarios for the DEMO plant document [129] has identified 21 PIEs (Postulated Initiating Events) as the most representative for the deterministic assessments to be performed in the first phase of the DEMO design activities both to check the compliance with safety limits and to give rationales for the selection of the reference DEMO reactor model. The vast majority of these 21 PIEs could induce the following load or accident scenarios which AINA is able to simulate:

- Plasma disruption or structural material melting due to a LOPC: disruptions represent the highest risk for DEMO integrity and it is assumed that they are only caused by instabilities induced by failures in the systems operating to confine, diagnose and feed the plasma or by accidental events leading to the entrance of undesired elements [130]. By means of AINA, it is possible to identify those failures which can lead to the maximum wall damage due to the electromagnetic and thermal load [131]. Likewise, some failures can not lead the plasma to a disruption event, however this perturbation can affect the plasma physics and damage the materials which make up the in vessel structure and containment. The perturbations that AINA can simulate are:
    - a failure in the external power supply system.
    - a failure in the fuel source system.
    - a variation in the confinement system.

- an entrance of an undesired quantity of impurities.

- In-vessel melt either of FW, blanket structure and/or divertor modules because of thermal stresses due to a LOCA: the Blanket is designed with sufficient cooling ability under normal operational conditions, however, it is necessary to study the temperature evolution in the Blanket structure when a LOCA takes place [132]. AINA is able to replicate this phenomena by means of the variation of the coolant mass flow rate through the cooling sections. They can affect the cooling loops in the BB, the cooling channel of the FW, the cooling regions in the CB of the divertor and the cooling channel of the PFCs of the divertor. It is necessary to remember that AINA cannot simulate consequences of this kind of accident as a leakage, a release or a penetration of coolant or radioactive products into other structure regions.

5.2 Steady State Scenario DEMO2

First of all, it is important to remember the characteristics of the steady state scenario used to develop the safety study. Thus, AINA 4.0 steady state simulation of DEMO2 scenario is presented in this section. The basic tokamak reactor parameters used both as inputs and to compare the AINA values have been based on the output data from the DEMO2 reference reactor configuration released on November 2014 by PROCESS (or document: DEMO2_Reference_Design_-_2015_May_(_EU_D_2MD7E6_v1_1.dat) [12].

INPUTS	**DEMO1**	
Major Radius (m)	7.5	
Minor Radius (m)	2.885	
Toroidal Field (T)	5	
q95	3	
Vp (m^3)	2217	
Sp (m^2)	1253	
P_{fus} (MW)	3255	
T_i (keV)	18.067	
OUTPUTS	**AINA 4.0**	**PROCESS**
T_e (keV)	16.70	18.7
S_H ($m^{-3}s^{-1}$)	1.1e19	4.7e18
n_e (m^{-3})	9.74e19	9.93e19
n_e (m^{-3})	8.53e19	8.25e19
n_H (m^{-3})	7.54e19	7.38e19
n_α (m^{-3})	9.74e18	8.75e18
n_{Ztotal} (m^{-3})	1.10e17	9.94e16
n_{ZXe} (m^{-3})	1.01e17	-
n_{ZW} (m^{-3})	1.01e16	-
f_{Xe} (%)	0.1	0.1
f_W (%)	0.01	0.01
P_{ext} (MW)	183	133
Q	17.74	24.46
P_α (MW)	636	650
P_{ie} (MW)	101	-
P_{Ohm} (MW)	1.78	2.21e-10*
P_{Br} (MW)	217	210
P_{syn} (MW)	40.1	57.7
P_{li} (MW)	105 (f_{core} fraction) / 420	368
P_{edge} (MW)	332	318

P_{core_rad} (MW)	362	318
P_{rad_total} (MW)	698	636
P_{SOL} (MW)	458	-
β_{total} (%)	3.9	5.1
β_t (%)	3.6	5.2
β_p (%)	0.58	1.71
$\tau_{E,e}$ (s)	3.74	4.027
Plasma Current (MA)	28.1	21.6
$f_{bootstrap}$	0.14	0.48
NWL (MW/m^2)	1.71	1.911
P_{rad_FW} (MW/m^2)	0.4	0.5

Table 71: Main global parameters of the DEMO2 computed by means of AINA 4.0 and compared with PROCESS results.

These values obtained from the AINA 4.0 simulation are similar to those achieved from the PROCESS simulation and no meaningful discrepancies have been found. However due to the P_{core_rad} and P_{edge} values, AINA estimates a conservative scenario, not only on plasma model but on thermal blanket model as well. Therefore, it can be concluded that AINA 4.0 is a suitable and fast tool to analyze the time evolution behavior of theses parameters assuming this starting point. Nevertheless, it is important to note that AINA estimated that an external power of 183 MW will be required to maintain the DEMO2 operational state even though the installed external power capacity is expected to not exceed 150 MW.

*The Ohmic Power value outlined from PROCESS may be assumed as 0 by comparison with the rest of powers.

Notwithstanding, it is necessary to highlight that for the DEMO2 scenario certain functional temperature limits may be slightly exceeded in the worst poloidal region (OB4) for the HCLL and the HCPB blanket designs; on the contrary, the DCLL and the WCLL models this phenomena does not take place:

Material	**Temperature Limit** $[^{o}C]$	**T** $[^{o}C]$
Tungsten	3422	481
EUROFER	550	610

Table 72: HCLL AINA DEMO2 SS maximum temperature.

Accordingly, it would be advisable to undertake a design review focused on ensuring a suitable operating temperature range for all the materials which make up the HCPB and the HCLL BB.

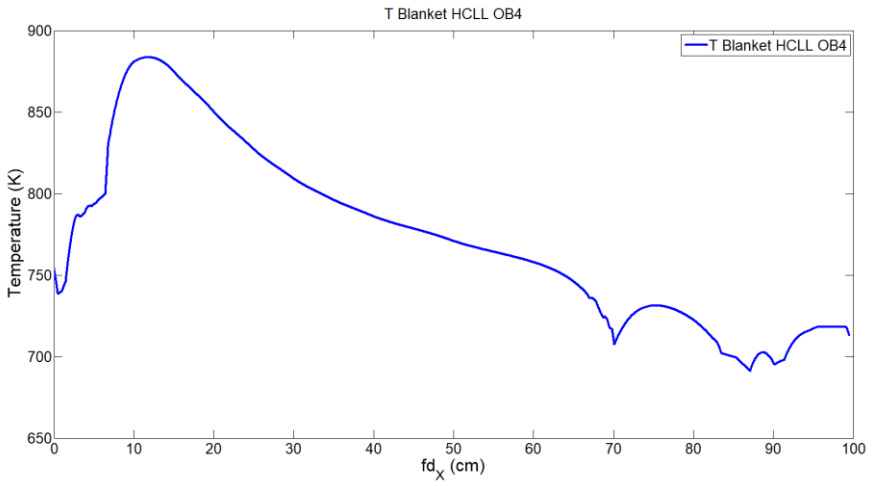

Figure 90: HCLL AINA 1D Temperature profile for DEMO2.

All figures extracted from AINA and used in the following analysis are contained in Annex E.

5.3 LOPC Accidents

5.3.1 Failure in the External Power Supply System

External power input is required for the fusion technologies not only to achieve an operational state but also to keep the plasma hot since most of the energy produced by fusion is carried away by the neutrons and, nowadays, it is not clear yet whether ignition will be the optimum operating regime, at which the production of hot helium is enough to sustain the plasma and the external energy sources can be turned off. Tokamaks use as this external heating supply a neutral beam injection and sources of high-frequency electromagnetic waves which are sensible technologies, for this reason the consequences of their possible failures must be studied.

5.3.1.1 Auxiliary heating cut-off

Accident description: An unexpected and instantaneous auxiliary heating cut-off takes place at second t=0.1 s while the HCLL DEMO reactor is operating on DEMO2 steady state.

Event sequence: This failure produces a fast decrease of ion and electron temperatures, an important densities increase and confinement time rises leading to fusion power increase which leads plasma to terminate due to the Greenwald limit infringement after 88.7 s. The maximum fusion power reached is 7936 MW; thus, neutronic heat flux (NWL) through the blanket vastly increases and induces the overtaking of the functional temperature limits wider than in the DEMO2 state for any BB design. For this reason it is necessary to conclude that it is really important to detect rapidly an external power cut-off in order to proceed with a fast plasma shutdown (FPSS) [132] (by means of the control of the confinement system) during the first seconds for the purpose of preventing blanket melting on account of thermal energy release by the plasma collapse or NWL rising.

5.3.1.2 Auxiliary heating decrease

Accident description: An unexpected and sudden decrease of auxiliary heating takes place at second t=0.1 s while the HCLL DEMO reactor is operating on DEMO2 steady state.

Event sequence: An analogous and scaled sequence to the previous one takes place when this accident occurs with the fundamental difference that the disruption takes longer to occur and the material temperature increase is less marked. In short, any auxiliary heating reduction must be detected instantly in order to proceed with a fast plasma shutdown (FPSS) and thereby avoiding the BB material collapse.

5.3.1.3 Auxiliary heating increase

Accident description: An unexpected and sudden increase of auxiliary heating takes place at second 0.1 while HCLL DEMO reactor is operating on DEMO2 steady state.

Event sequence: As soon as the incident takes place ion and electron temperatures increase and all the species densities fall; except the impurity percentage of Tungsten which rise due to the sputtering processes. All of this leads to a rapidly decrease of the fusion power achieving a new steady state which produces less fusion power than DEMO2 depending on the multiplication factor applied to the external power, the higher multiplication factor is, the lower fusion power is. Thus, the wall loads are lower with the exception of the P_{RAD} against the divertor which produces a slight increase of the Tungsten FW

temperature although it may be different when the divertor models will be updated. For this reason this kind of scenarios could be interesting since the functional temperature limits of the BB materials are not widely exceeded or they are not exceeded. In summary, this kind of perturbation does not represent a risk scenario. Moreover, it is important to remember that it the installed external power capacity probably will not exceed 150 MW.

Multiplication factor	New SS Fusion Power $[MW]$	Max. SS EUROFER T $[K]$
2	2362	594
7	724	577

Table 73: Fusion power and maximum EUROFER temperature when a new SS is reached for an excessive auxiliary heating increase

5.3.1.4 Auxiliary heating perturbation summary

Mult. factor	Plasma termination	Plasma termination time $[s]$	Consequences	Mitigation	Observations
0 (cut-off)	Greenwald limit	88.7	Fusion power increase and excessive plasma thermal energy.	External power variation detection.	-
			Temperature limits exceeded.	A controlled fast plasma shutdown.	
0.5	Greenwald limit	< 200	Fusion power increase and excessive plasma thermal energy.	External power variation detection.	-
			Temperature limits exceeded.	A controlled fast plasma shutdown.	
2	Stabilized	-	Fusion power decrease.	Not necessary.	Increasing the external power leads to closer to the BB operating temperatures.
			BB temperature decrease.		
7	Stabilized	-	Fusion power decrease.	Not necessary.	Increasing the external power leads to closer to the BB operating temperatures.
			BB temperature decrease.		

Table 74: Auxiliary heating perturbation summary

5.3.2 Failure in the Fuel Source System

The fueling system must provide the required D-T fuel mixture to maintain the plasma as foreseen by the plasma scenarios [136]. This system in DEMO is composed of two types of equipment, the pellet injection system which will deposit material in the plasma core and the gas injection which will supply the material needed for pre-fill, ramp up and plasma enhancement gases [136]. For AINA simulations,

only the pellet injection system is considered since DEMO1 is a steady state scenario, and, moreover, almost 100 % of particles injected arrive into the plasma core and the fueling of DEMO can be only ensured by pellets injected from the HFS (High Field Side) [137][138][139]. This complex system is necessary in order to maintain the equilibrium of the plasma, for this reason the consequences of its possible failures must be studied.

5.3.2.1 Fueling rate cut-off and decrease

Accident description: An unexpected and instantaneous fueling rate cut-off or an unexpected and sudden decrease of fueling rate takes place at second t=0.1 s while the HCLL DEMO reactor is operating on DEMO2 steady state.

Event sequence: In case fueling is stopped or reduced, it is possible to observe how fusion power quickly diminish as well as densities, except the impurities percentages due to physical sputtering driven by the increase in ion and electron temperatures. This growth takes place basically as a result of auxiliary heating injection, reaching more than 30 keV for the cut-off case. Moreover, the lower the impurities percentages, the lesser the power losses; for this reason the confinement time increases to 17 s for the fuel stopping scenario. All of this leads to a reduction in BB temperatures, including the surface temperature of the Tungsten. Finally, plasma collapses at 15.6 s for the cut off case by an overshoot beta limit disruption. Despite this, at the time of the collapse, the plasma thermal energy (U) achieve values of up to 0.5 GJ, and this disruption extend could be mitigated by a disruption mitigation system [135] and, thereby, the BB material would be safeguarded. Nevertheless, it would be useful to detect a fueling cut off or reduction instantaneously for the purpose of conducing the plasma to a better and controlled plasma shutdown if it is possible.

5.3.2.2 Fueling rate increase

Accident description: An unexpected and sudden increase of fueling rate takes place at second t=0.1 s while the HCLL DEMO reactor is operating on DEMO2 steady state.

Event sequence: In this case; fusion power, densities and confinement time are continuously growing until a Greenwald limit disruption takes place. The higher fueling rate multiplication factor is, the earlier collapse happens. Therefore, for a fueling rate of 50% the crucial risk involves an initial melting scenario and a subsequent high energetic disruption whilst for a higher fueling rate the crucial risk involves an instantaneous and very energetic plasma termination. In short, it is necessary to detect a increase of fueling rapidly and activate a fast plasma shutdown (FPSS) since all these perturbations cause structural damage. It is important to note that, for example, for ITER the fueling rate capacity can cover up to $7.8 \cdot 10^{19}$ $/_{m^3 s}$ (above a multiplication factor of 10 for DEMO1) [9] and hence the dealt scenarios may occur.

Multiplication factor	Plasma termination time $[s]$	Plasma Thermal energy U $[GJ]$	Max. EUROFER T $[^{o}C]$
1.5	173.6	3.1	724
2	47.8	2.9	687

Table 75: Disruption time and plasma thermal energy for an excessive fueling rate increase.

5.3.2.3 Fueling rate perturbation summary

Mult. factor	Plasma termination	Plasma termination time $[s]$	Consequences	Mitigation	Observations
0 (cut-off)	Beta Limit	15.6	A plasma thermal energy with a rate of 0.5 GJ.	Disruption mitigation system.	-
1.5	Greenwald Limit	173.6	All temperature limits widely exceeded. Excessive plasma thermal energy Fusion power increase.	Fueling rate variation detection and a FPSS activation.	This is the worst scenario due to the high temperatures and the high plasma thermal energy
6	Greenwald Limit	47.8	All temperature limits widely exceeded. Excessive plasma thermal energy Fusion power increase.	Fueling rate variation detection and a FPSS activation.	-

Table 76: Fueling rate perturbation summary.

5.3.3 Improvement in the Confinement System

Historically, AINA has been used in safety analyses to scan the influence of an increase in confinement time [16][19][37] owing, among other reasons, to the H mode discovery occurred on 4 February 1982. Following this path, at first, the behavior of plasma parameters in case of a permanent increase of confinement time will be simulated and discussed.

Accident description: An unexpected and sudden permanent increase of confinement time takes place at second t=0.1 s while the HCLL DEMO reactor is operating on DEMO2 steady state.

Event sequence: Confinement time improvement produces a fast increase of ion and electron temperatures as well as densities, which drive to an overall raise of fusion power until plasma terminates disruptively due to the beta or the Greenwald limit infringement depending on the scale of the perturbation. For example, if the confinement time improvement is less than twice, the collapse is due to the Greenwald limit infringement. In contrast, if the improvement is higher, the disruption takes place by the Beta limit overcoming. In general, the region OB5 becomes the worst in the first few seconds (< 3 s) and the BB material temperatures reach very high values which lead the reactor to a global melting scenario. The lower the multiplication factor is the grater maximum temperatures are achieved due to the plasma collapse takes place later. Nevertheless, the plasma thermal energy discharged during the disruption cause structural damage and melting in any case, hence, it is necessary to detect instantaneously an unexpected variation in confinement time with the aim of conducing the reactor to a controlled plasma shutdown.

Multiplication factor	Plasma termination time $[s]$	Plasma Thermal energy U $[GJ]$	Max. EUROFER T $[^{o}C]$	Max. P_{fus} $[MW]$
1.5	94.9	3.6	708	1016
5	3.9	3.8	614	7323

Table 77: Disruption time and plasma thermal energy for a confinement time improvement.

It is important to note that any confinement time reduction induces a loss of plasma confinement during the first seconds after the perturbation (< 5 s) with a fusion power drop; however, it is not possible to extract the precise consequences of these events from AINA owing to the numerical restrictions derived from the confinement law expressions implemented in the code. Therefore, it must be necessary to detect rapidly a failure in the confinement system which could lead to this kind of situation.

5.3.4 Occasional Variation of Confinement Time

In line with the previous cases, a punctual confinement time variation may happen due to an unexpected behavior during the operation time. Despite the fact these events might not take place, it was concluded, after an experts' discussion, that analyzing the evolution of this kind of phenomena may be useful.

The impact of these events is highly dependent on the duration of the confinement time variation and it does not depend so much on the variation factor suffered. Therefore, when the confinement time rises abruptly but decreases after 0.1 s, the effects are not severe since both a multiplication factor of 3 and 10 excites the plasma but the steady state is recovered in less than 20 s. During this transition an instantaneous fusion power peak is reached due to a fast increase of ion and electron temperatures, as well as the BB materials temperatures rise slightly but they are stabilized rapidly. On the other hand, in case the duration of the confinement time variation is longer, the operations steady state is recovered whilst the perturbation disappears before the corresponding termination time tracked down in the previous section. For instance, an increase of the confinement time due to a multiplication factor with a value of 3 leads the plasma to a transitional state which can be intrinsically recovered as long as the perturbation lasts less than 10 seconds. Nevertheless and in spite of the recovery, the longer the duration of the perturbation is the greater maximum temperatures are achieved. In view of these circumstances, as in the previous case, it is necessary to detect an unexpected variation in confinement time which extends in time with the aim of conducing the reactor to a controlled plasma shutdown.

Multiplication factor	Perturbation duration $[s]$	Max. EUROFER ΔT $[^{o}C]$	Max. P_{fus} $[MW]$
3	0.1	0.15	3348
3	0.5	0.8	3751
3	1	2	4307
3	3	20	6773
10	0.1	0.2	3381

Table 78: Maximum temperature increase and fusion power peak for an occasional confinement time improvement.

Moreover, in all the cases the region OB5 becomes the most demanded after 0.3 s.

5.3.5 Entrance of an Undesired Quantity of Impurities

As already stated, when the reactor is operating, a flux of particles enter the plasma as impurities due to the erosion phenomena which is inherent to the nature of plasma wall interaction. It can be cause of several undesirable effects as a PFC damage or beneficial effects as shutting down the fusion due to an increase of Bremsstrahlung and line radiation, becoming a passive safety mechanism, for instance, if a

LOCA takes place. For these reasons the consequences of an undesired quantity of impurities must be studied.

5.3.5.1 Punctual impurity increase up to 150%

Accident description: A punctual increase of the impurities presence (Xe and W) up to 250% takes place at second t=0.1 s while the HCLL DEMO reactor is operating on DEMO2 steady state. This kind of perturbation can recreate the consequences of a leakage.

Event sequence: This event produces a sudden rise of confinement time, densities, fusion power, power losses (Bremsstrahlung and line radiation); a decrease of the ions and electrons temperatures and, after a few seconds, the recovery of the initial steady state; however, the detection of this kind of perturbation and a controlled plasma shutdown must be fast since the material temperatures rise rapidly.

5.3.5.2 Punctual impurity increase among 150% and 200%

Accident description: A punctual increase of the impurities presence (Xe and W) among 150% and 250% takes place at second t=0.1 s while the HCLL DEMO reactor is operating on DEMO2 steady state. This kind of perturbation can recreate the consequences of a leakage.

Event sequence: This event produces the same initial effects as in the previous case but after a few seconds the fusion power picks rapidly. Therefore, the detection of this kind of perturbation and a controlled plasma shutdown must be fast since the material temperatures rise rapidly.

Multiplication factor	Max. EUROFER ΔT [ºC]	Max. P_{fus} [MW]
1.5	19.5	4180
2	70	7395

Table 79: Maximum temperature increase and fusion power peak for a punctual impurity increase.

5.3.5.3 Punctual impurity increase equal or above 250%

Accident description: A punctual increase of the impurities presence (Xe and W) equal to 250% takes place at second t=0.1 s while the HCLL DEMO reactor is operating on DEMO2 steady state. This kind of perturbation can recreate the consequences of a leakage.

Event sequence: Differing from the previous case, the plasma equilibrium is not recovered after a perturbation of this magnitude. As soon as the perturbation takes places, the plasma skips instantaneous to the L mode and a disruption occurs due to the P_{SOL} limit infringement releasing a thermal energy of 1.82 GJ which can damage the reactor structure. Therefore, it is necessary to detect an important important leakage instantly (in less than 0.1 s) and leading the reactor to a controlled plasma shutdown in order to mitigate or prevent these possible an undesirable consequences.

5.3.5.4 Tungsten permanent entrance increase

Accident description: An increase of the Tungsten impurity production takes place from second t=0.1 s while the HCLL DEMO reactor is operating on DEMO2 steady state. The previous cases could recreate the consequences of a leakage, however, in this case the simulation recreates a variation of the production rate and, consequently, the number of impurities which arrive to the plasma core permanently. These phenomena might occur due to the deterioration of the PFCs.

Event sequence: In this case; fusion power, densities and confinement time are continuously and slowly growing. Depending on the new impurity production rate the plasma may reach a new steady state or it might collapse by mean of the infringement of the Greenwald limit. Nevertheless, any alternative is not instantaneous, so the incident detection must be previous to the endpoint in order to prevent a melting scenario which could take place for any case.

5.4 LOCA Accidents

LOCA perturbations only affect the temperature profile along the BB and the divertor materials; however, the production rate of Tungsten by sublimation (depending on material temperature) process is greatly lower than physical sputtering process (virtually independent of temperature). Consequently since the entrance of impurity is not affected by this kind of perturbations, conditions inside the plasma remain practically unchanged.

5.4.1 BB LOCA 30%

Accident description: an small LOCA simulation where the PbLi coolant loops of the BB architecture loses 30% of the mass flow rate at second t=0.1 s while the HCLL DEMO reactor is operating on DEMO2 steady state. The perturbation is applied using a step function and hence the progressive decrease of the mass ow rate has not been taken into account.

Event sequence: As indicated above, only the internal material temperatures of the BB structure changes; the plasma parameters remain virtually unchanged. This temperature distribution is affected in magnitude, the most relevant variations are placed in most loaded areas. At 40 s a new steady state is found even though EUROFER temperature reached is even greater than design limit (EUROFER: 624 ºC). The spatial position of this temperature peak is unchanged and around 11.5 cm. The FW is not affected during this transition. In summary, it is essential to be able to guarantee a very quick detection if the LOCA takes place in the internal loops in order to proceed to a proper mitigation action such as a fast plasma shutdown (FPSS) injecting impurity gases (e.g. Ne, Ar, etc.) as in ITER. Thus, it would be possible to prevent a melting damage inside the internal structure of the BB. In spite of this, it is important to note that these conclusions can be extrapolated to the HCPB design; however, the DCLL and WCLL maintain the structural temperature peak close to the limit. Therefore, this incident does not induce a critical scenario for the DCLL and WCLL designs; however, it is advisable to be able to guarantee a quick detection if the LOCA takes place in order to proceed to a proper mitigation action since, as will be pointed in the following cases, if the LOCA is worse, the melting scenario occurs.

5.4.2 BB LOCA 60%

Accident description: a medium LOCA simulation where the Helium and PbLi coolant loops of the BB architecture loses 30% of the mass flow rate at second t=0.1 s while the HCLL DEMO reactor is operating on DEMO2 steady state. The perturbation is applied using a step function and hence the progressive decrease of the mass ow rate has not been taken into account.

Event sequence: Once again, only the internal material temperatures of the BB structure changes; the plasma parameters remain virtually unchanged. A new steady state is found at 70 s even though, as in the previous case, EUROFER reaches a temperature peak that are far greater than design limits (EUROFER: 642 ºC). The spatial position of this material temperature peak remains unchanged (11.5 cm) and the FW remains unaltered. As previously, with the objective of proceeding to a proper mitigation

action it is essential to be able to guarantee a very quick detection if the LOCA takes place in the internal loops. Thus, it would be possible to prevent a melting damage inside the internal structure of the BB. In addition, at this level of cooling loss, the four European DEMO designs suffer analogous consequences and require similar responses.

5.4.3 BB LOCA 90%

Accident description: a big LOCA simulation where the Helium and PbLi coolant loops of the BB architecture loses 30% of the mass flow rate at second t=0.1 s while the HCLL DEMO reactor is operating on DEMO2 steady state. The perturbation is applied using a step function and hence the progressive decrease of the mass ow rate has not been taken into account.

Event sequence: The overall behavior of the reactor is analogous to the previous cases although it causes a greater and faster temperature impact. The new steady state is found at 160 s. In this simulation and getting worse the previous cases, the EUROFER design limit is excessively surpassed and thus a global melting would be nearly instantaneous (EUROFER: 680 ºC). In addition, the temperature distribution shape is slightly affected although the FW remains practically unchanged. In summary, a very quick detection, if the LOCA takes place in the internal loops, is extremely necessary as well as a proper and fast mitigation action such as a fast plasma shutdown (FPSS) injecting impurity gases (e.g. Ne, Ar, etc.) as in ITER which may stop the reactor in less than 3 s [132]. As in the medium LOCA case, these findings are valid for the four European DEMO designs.

5.4.4 Internal and FW BB LOCA 30%

Accident description: an small LOCA simulation where the Helium FW channel and the Helium and PbLi coolant loops of the BB architecture loses 30% of the mass flow rate at second t=0.1 s while the HCLL DEMO reactor is operating on DEMO2 steady state. The perturbation is applied using a step function and hence the progressive decrease of the mass ow rate has not been taken into account.

Event sequence: As in the internal BB LOCA cases, the plasma parameters remain virtually unchanged and just the temperature distribution is affected in magnitude and shape. As in the previous 30% LOCA case, at 40 s a new steady state is found even though EUROFER temperature reached is even greater than design limit (EUROFER: 624 ºC; the same value than in the internal BB LOCA 30% case). The spatial position of this temperature peak is unchanged and around 11.5 cm. Unlike the previous case, the FW is affected during this transition due to the minor mass flow through the Helium FW channel; the maximum Tungsten temperature reached is 496.5 ºC. In summary, it is essential to be able to guarantee a very quick detection if a LOCA takes place in order to proceed to a proper mitigation action such as a fast plasma shutdown (FPSS) injecting impurity gases (e.g. Ne, Ar, etc.) as in ITER. Thus, it would be possible to prevent a melting damage inside the internal structure of the BB. In spite of this, it is important to note that these conclusions can be extrapolated to the HCPB design; however, the DCLL and WCLL maintain the structural temperature peak close to the limit. Therefore, this incident does not induce a critical scenario for the DCLL and WCLL designs; however, it is advisable to be able to guarantee a quick detection if the LOCA takes place in order to proceed to a proper mitigation action since, as will be pointed in the following cases, if the LOCA is worse, the melting scenario occurs.

5.4.5 Internal and FW BB LOCA 60%

Accident description: a medium LOCA simulation where the Helium FW channel and the Helium and PbLi coolant loops of the BB architecture loses 30% of the mass flow rate at second t=0.1 s while the HCLL

DEMO reactor is operating on DEMO2 steady state. The perturbation is applied using a step function and hence the progressive decrease of the mass ow rate has not been taken into account.

Event sequence: When a medium LOCA takes place the Tungsten temperature of the FW increases 49 ºC (from 480.9 ºC to 529.3 ºC) and the internal EUROFER until to 645 ºC in less than 80 s. Logically, the temperature increase is higher than in the previous case; hence with the objective of proceeding to a proper mitigation action it is essential to be able to guarantee a very quick detection if the LOCA occurs. In this way it would be possible to prevent a melting damage inside the internal structure of the BB. In addition, at this level of cooling loss, the four European DEMO designs suffer analogous consequences and require similar responses.

5.4.6 Internal and FW BB LOCA 90%

Accident description: a big LOCA simulation where the Helium FW channel and the Helium and PbLi coolant loops of the BB architecture loses 30% of the mass flow rate at second t=0.1 s while the HCLL DEMO reactor is operating on DEMO2 steady state. The perturbation is applied using a step function and hence the progressive decrease of the mass ow rate has not been taken into account.

Event sequence: in line with the previous cases, when a big LOCA takes place the temperature stabilization occurs after 100 s suffering a Tungsten temperature increase of 185 ºC (from 480.9 ºC to 666ºC) and a EUROFER temperature increase until to 695 ºC. As earlier cases, with the objective of preventing the structural damage a fast detection of the accident and a fast appropriate response would be necessary.

5.5 Conclusions

First and foremost, it is necessary to recall the fact that, on the basis of the information drawn from AINA simulations, EUROFER temperature reached during an operational scenario according to the steady state DEMO2 permanently exceed the design melting limit for the HCLL and the HCPB cases. Specifically, this transgression affects the internal BB architecture. For this reason, all the outcomes and all the conclusions which may be derived from the HCPB and HCLL AINA safety analysis must be judged according to this tenet and keeping in mind a possible design review focused on ensuring a suitable operating temperature range for the EUROFER.

With regard to LOCAs, from AINA outcomes, it concludes that this kind of failure inside the cooling system does not affect the internal plasma conditions but, undoubtedly, even a slight loss of the mass flow (about 30%), leads the reactor to an overall melting scenario for the HCLL and HCPB cases rapidly since EUROFER temperature increases drastically during the first seconds after the cooling channel rupture. In DCLL and WCLL cases, from a medium LOCA (about 60% of the mass flow loss) the structural damage due to an EUROFER temperature increase is analogous. For this reason, it is indispensable the installation of a quick response system capable of detecting a cooling anomaly rapidly and activating a proper mitigation action such as a fast plasma shutdown FPSS injecting impurity gases (e.g. Ne, Ar, etc.) as in ITER.

On the other hand and broadly speaking, there are four possible scenarios when a LOPC takes place. At best, the same DEMO2 steady state or a new steady state with a fusion power decrease and lower temperatures along the BB and divertor structure may be achieve. These cases would be safe and a mitigation system or action would not be necessary. Further, it could be considered that a new steady

states achieved, for the HCLL and HCPB cases, could be better candidates for DEMO operation from the point of view of temperature limits no exceedance and despite the generation of lower fusion power and, consequently, less gain. An increase of the external power injection rate leads the reactor to this new non-dangerous steady state situation and a punctual impurity increase up to 150% drive the reactor to DEMO2 again after a slightly transition. Another potential consequence would involve a risk of structural damage due to a plasma termination wich may discharge an acceptable amount of thermal energy (< 0.5 GJ) when an unexpected and instantaneous fueling rate cut-off or an unexpected and sudden decrease of fueling rate takes place. This disruption extend could be mitigated by a disruption mitigation system. The third potential consequence arisen from a LOPC is the same as the impacts emerged when a LOCA takes place, a melting process due to a rapidly temperature increase. From the analysis of the AINA simulations, this situation might occur due to an occasional variation of confinement time beneath the corresponding termination time and a punctual impurity increase betweem 150% - 250%. In contrast to LOCA detection system which must identify a failure in the cooling system, in this case it is essential to be able to guarantee a quick detection and actuation by means of a proper system depending on the affected equipment because just an increase temperature detection system must not be fast enough. Last but not least, there are certain incidents which may drive the reactor to suffer not only a melting scenario and a very energetic plasma disruption at the same time. These triggers are a decrease or a cut-off of the external power injection, a fueling rate increase, a permanent improvement in the confinement time and a punctual impurity increase over 250%. Therefore and owing to the double effect, there are the most critical failures and a special attention in order to avoid them will be necessary. The measures to be taken are the mitigation systems and actions for the particular cases explained previously.

6 Conclusion

First of all, it is important to note that tasks and challenges which make up the collaborative project between EUROfusion and Polytechnic University of Catalonia-BarcelonaTech, in cooperation with CIEMAT, (where this thesis is framed) have been successfully completed with a good acceptance by all involved agents.

The first milestone achieved was the recognition that AINA 3.0 was not a universal software to be used for a wide range of designs and scenarios. Moreover, its low level of flexibility, friendliness and reliability led to the development of a totally new AINA version for the four European designs of DEMO.

Currently, AINA 4.0 is a reliable and flexible tool able to estimate some steady state scenarios for DEMO similar than generated ones by PROCESS and show its evolution when some perturbation are inserted. Moreover, AINA 4.0 ensures the use of the most recognized numerical models, the most recent design versions and the creation of a more friendliness tool due to its modular/branching structure to be modified and updated.

Therefore, AINA 4.0 can be used to contribute to the safety analyses for DEMO designs. Specifically, contributions and recommendations to future safety operators and designers have been outlined from several safety analyses carried out using AINA 4.0 during the years when this thesis has been elaborated.

One of the most important findings of this study is that for the DEMO 1 and DEMO2 scenarios certain functional temperature limits may be slightly exceeded in the worst poloidal region (OB4) for the HCLL and the HCPB blanket designs; on the contrary, for the DCLL and the WCLL models this phenomena does not take place due to the particular architecture and cooling scheme of each design.

With regard to LOCAs perturbations, from AINA outcomes, it concludes that this kind of failure inside the cooling system does not affect the internal plasma conditions but, undoubtedly, even a slight loss of the mass flow (about 30%), leads the reactor to an overall temperature increase for all the designs and levels. For this reason, it is indispensable the installation of a quick response system capable of detecting a cooling anomaly rapidly and activating a proper mitigation action such as a fast plasma shutdown FPSS injecting impurity gases (e.g. Ne, Ar, etc.) as in ITER.

Concerning LOPC cases there is a wide variability of situations depending on the perturbation simulated. Broadly speaking, there are three possible scenarios as when a LOPC takes place and one more critical for all the designs. At best, a new steady state with a fusion power decrease and lower blanket temperatures may be achieved. This case would be safe and a mitigation system or action would not be necessary. An increase of the external power injection between 200% and 630% and a decrease of the fueling injection rate are those anomalies may lead the reactor to this kind of non-dangerous situation. In contrast, another potential consequence would involve a risk of structural damage due to a very energetic plasma termination which may discharge a great amount of thermal energy against the internal reactor walls. An increase of the external power injection above 630% and a fueling rate cut-off would be the possible initiators. The third potential consequence arisen from a LOPC is the same as the impacts emerged when a LOCA takes place, a more critical melting scenario than the DEMO1 steady state. This situation might occur due to a decrease or a cut-off of the external power injection, a fueling rate injection increase up to 25%, an occasional variation of confinement time beneath the corresponding termination time and a punctual impurity increase up to 300%. Last but not least, there

are certain incidents which may drive the reactor to suffer both a melting scenario and a very energetic plasma disruption at the same time. Owing to the double effect, these are the most critical failures and a special attention in order to avoid them will be necessary. These triggers are an increase of fueling injection above 50%, a permanent improvement in the confinement time and a punctual impurity increase above 300%.

Finally, it is necessary to point out that AINA 4.0 shall be easily updated and improved in the future when the final DEMO design are dealt and more accurate models are assumed.

7 Scientific Production

7.1 Papers and Publications

“Contribution to safety analyses of DEMO HCPB using AINA code”

E. Baeza, A. de Blas, A. Riego and M. Fabbri

Fusion Engineering and Design. (2018). doi:10.1016/J.FUSENGDES.2018.11.030.

“**Development of the safety code AINA for the European DEMO designs**”

E. Baeza, A. de Blas, A. Riego and M. Fabbri

Fusion Engineering and Design. (2018). doi:10.1016/J.FUSENGDES.2018.04.074.

“**Desarrollo del código de seguridad para reactores de fusión AINA 4 para los análisis de seguridad de los diseños europeos de DEMO”**

E. Baeza, A. De Blas, A. Riego and M. Fabbri

Reunión Anual SNE, Ponencias. (2017). http://hdl.handle.net/2117/112696.

“Metodologia per incorporar la fusió nuclear dins d'una programació educativa de tecnologia”

E. Baeza

TFM, Màster de Formació del Professorat d’Educació Secundària Obligatòria i Batxillerat, Formació Professional i Ensenyament d’Idiomes. (2017). http://hdl.handle.net/2117/111212.

“**Methodology for the improvement of the AINA Code wall-model applied to DEMO WCPB blanket”**

M. Fabbri, A. de Blas, A. Riego, I. Zamora and E. Baeza

Fusion Engineering and Design. 124 (2017) 1195–1198. doi:http://dx.doi.org/10.1016/j.fusengdes.2017.05.027.

7.2 Congresses/workshops

"Contribution to safety analyses of DEMO HCPB using AINA code"

E. Baeza, A. de Blas , A. Riego, J. Dies and M. Fabbri

30th Symposium on Fusion Technology (SOFT)

Sicily (Italy), September 2018.

"Desarrollo del código de seguridad para reactores de fusión AINA 4 para DEMO"

E. Baeza, A. de Blas , A. Riego, J. Dies and M. Fabbri

Sociedad Nuclear Española (SNE)

Málaga (Spain), October 2017.

"Development of the safety code AINA for the European DEMO designs"

E. Baeza, A. de Blas , A. Riego, J. Dies and M. Fabbri

13th International Symposium on Fusion Nuclear Technology (ISFNT)

Kyoto (Japan), September 2017.

"Methodology for the improvement of the AINA Code wall-model applied to DEMO WCPB blanket"

M. Fabbri, A. de Blas , A. Riego, J. Dies, I. Zamora and E. Baeza

29th Symposium on Fusion Technology (SOFT)

Prague (Czech Republic), September 2016.

7.3 Posters

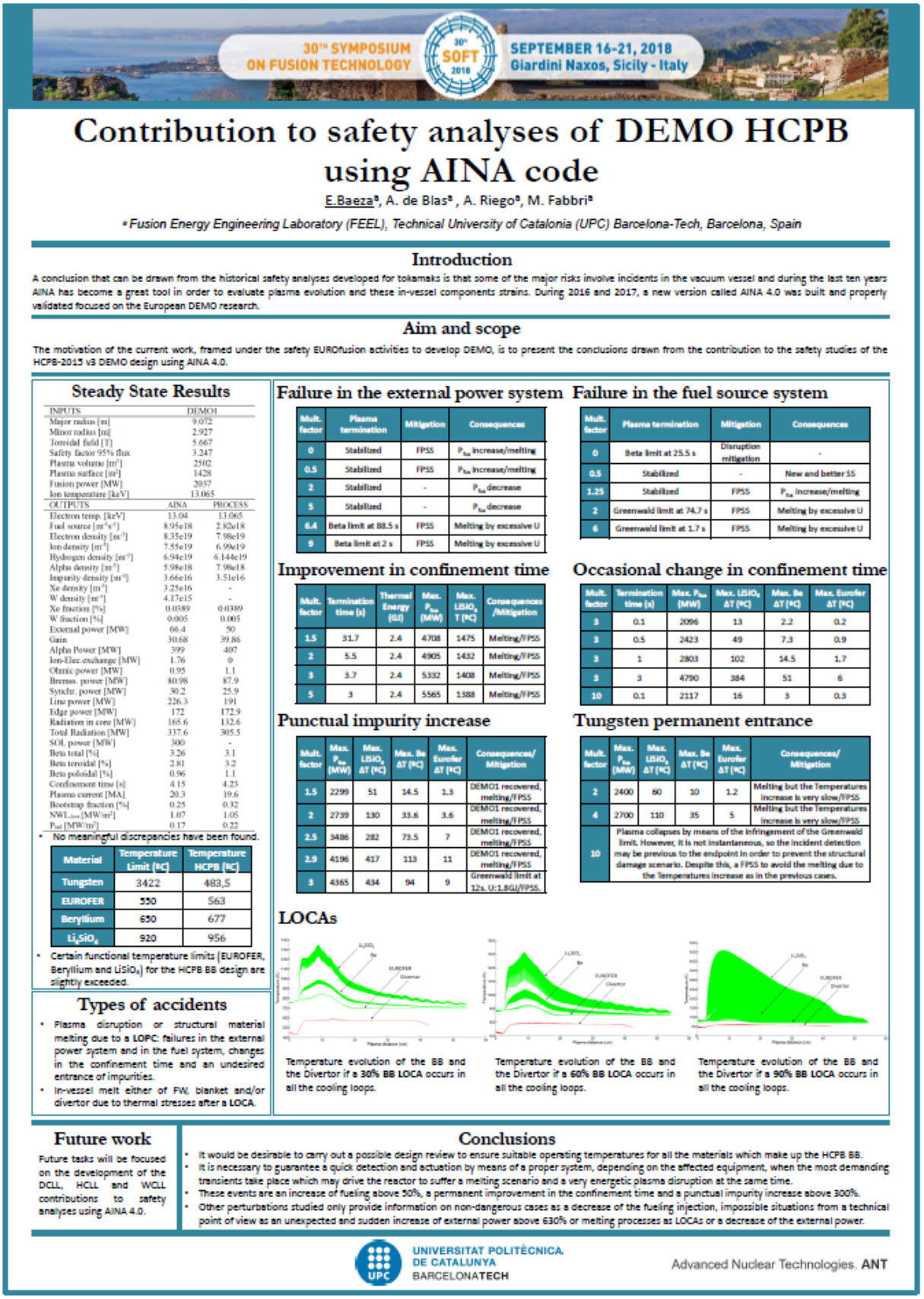

30TH SYMPOSIUM ON FUSION TECHNOLOGY — 30th SOFT 2018 — SEPTEMBER 16-21, 2018 Giardini Naxos, Sicily - Italy

Contribution to safety analyses of DEMO HCPB using AINA code

E.Baeza[a], A. de Blas[a] , A. Riego[a], M. Fabbri[a]

[a] Fusion Energy Engineering Laboratory (FEEL), Technical University of Catalonia (UPC) Barcelona-Tech, Barcelona, Spain

Introduction

A conclusion that can be drawn from the historical safety analyses developed for tokamaks is that some of the major risks involve incidents in the vacuum vessel and during the last ten years AINA has become a great tool in order to evaluate plasma evolution and these in-vessel components strains. During 2016 and 2017, a new version called AINA 4.0 was built and properly validated focused on the European DEMO research.

Aim and scope

The motivation of the current work, framed under the safety EUROfusion activities to develop DEMO, is to present the conclusions drawn from the contribution to the safety studies of the HCPB-2015 v3 DEMO design using AINA 4.0.

Steady State Results

INPUTS	DEMO1	
Major radius [m]	9.072	
Minor radius [m]	2.927	
Toroidal field [T]	5.667	
Safety factor 95% flux	3.247	
Plasma volume [m³]	2502	
Plasma surface [m²]	1428	
Fusion power [MW]	2037	
Ion temperature [keV]	13.065	
OUTPUTS	AINA	PROCESS
Electron temp. [keV]	13.04	13.065
Fuel source [m⁻³s⁻¹]	8.95e18	2.82e18
Electron density [m⁻³]	8.35e19	7.98e19
Ion density [m⁻³]	7.55e19	6.99e19
Hydrogen density [m⁻³]	6.94e19	6.144e19
Alpha density [m⁻³]	5.98e18	7.98e18
Impurity density [m⁻³]	3.66e16	3.51e16
Xe density [m⁻³]	3.25e16	-
W density [m⁻³]	4.17e15	-
Xe fraction [%]	0.0389	0.0389
W fraction [%]	0.005	0.005
External power [MW]	66.4	50
Gain	30.68	39.86
Alpha Power [MW]	399	407
Ion-Elec.exchange [MW]	1.76	0
Ohmic power [MW]	0.95	1.1
Brems. power [MW]	80.98	87.9
Synchr. power [MW]	30.2	25.9
Line power [MW]	226.3	191
Edge power [MW]	172	172.9
Radiation in core [MW]	165.6	132.6
Total Radiation [MW]	337.6	305.5
SOL power [MW]	300	-
Beta total [%]	3.26	3.1
Beta toroidal [%]	2.81	3.2
Beta poloidal [%]	0.96	1.1
Confinement time [s]	4.15	4.23
Plasma current [MA]	20.3	19.6
Bootstrap fraction [%]	0.25	0.32
NWL_{Ave} [MW/m²]	1.07	1.05
P_{wall} [MW/m²]	0.17	0.22

- No meaningful discrepancies have been found.

Material	Temperature Limit (ºC)	Temperature HCPB (ºC)
Tungsten	3422	483,5
EUROFER	550	563
Beryllium	650	677
Li_4SiO_4	920	956

- Certain functional temperature limits (EUROFER, Beryllium and Li_4SiO_4) for the HCPB BB design are slightly exceeded.

Types of accidents

- Plasma disruption or structural material melting due to a LOPC: failures in the external power system and in the fuel system, changes in the confinement time and an undesired entrance of impurities.
- In-vessel melt either of FW, blanket and/or divertor due to thermal stresses after a LOCA.

Failure in the external power system

Mult. factor	Plasma termination	Mitigation	Consequences
0	Stabilized	FPSS	P_{fus} increase/melting
0.5	Stabilized	FPSS	P_{fus} increase/melting
2	Stabilized	-	P_{fus} decrease
5	Stabilized	-	P_{fus} decrease
6.4	Beta limit at 88.5 s	FPSS	Melting by excessive U
9	Beta limit at 2 s	FPSS	Melting by excessive U

Failure in the fuel source system

Mult. factor	Plasma termination	Mitigation	Consequences
0	Beta limit at 25.5 s	Disruption mitigation	-
0.5	Stabilized	-	New and better SS
1.25	Stabilized	FPSS	P_{fus} increase/melting
2	Greenwald limit at 74.7 s	FPSS	Melting by excessive U
6	Greenwald limit at 1.7 s	FPSS	Melting by excessive U

Improvement in confinement time

Mult. factor	Termination time (s)	Thermal Energy (GJ)	Max. P_{fus} (MW)	Max. $LiSiO_4$ T (ºC)	Consequences /Mitigation
1.5	31.7	2.4	4708	1475	Melting/FPSS
2	5.5	2.4	4905	1432	Melting/FPSS
3	3.7	2.4	5332	1408	Melting/FPSS
5	3	2.4	5565	1388	Melting/FPSS

Occasional change in confinement time

Mult. factor	Termination time (s)	Max. P_{fus} (MW)	Max. $LiSiO_4$ ΔT (ºC)	Max. Be ΔT (ºC)	Max. Eurofer ΔT (ºC)
3	0.1	2096	13	2.2	0.2
3	0.5	2423	49	7.3	0.9
3	1	2803	102	14.5	1.7
3	3	4790	384	51	6
10	0.1	2117	16	3	0.3

Punctual impurity increase

Mult. factor	Max. P_{fus} (MW)	Max. $LiSiO_4$ ΔT (ºC)	Max. Be ΔT (ºC)	Max. Eurofer ΔT (ºC)	Consequences/ Mitigation
1.5	2299	51	14.5	1.3	DEMO1 recovered, melting/FPSS
2	2739	130	33.6	3.6	DEMO1 recovered, melting/FPSS
2.5	3486	282	73.5	7	DEMO1 recovered, melting/FPSS
2.9	4196	417	113	11	DEMO1 recovered, melting/FPSS
3	4365	434	94	9	Greenwald limit at 12s. U:1.8GJ/FPSS.

Tungsten permanent entrance

Mult. factor	Max. P_{fus} (MW)	Max. $LiSiO_4$ ΔT (ºC)	Max. Be ΔT (ºC)	Max. Eurofer ΔT (ºC)	Consequences/ Mitigation
2	2400	60	10	1.2	Melting but the Temperatures increase is very slow/FPSS
4	2700	110	35	5	Melting but the Temperatures increase is very slow/FPSS
10	Plasma collapses by means of the infringement of the Greenwald limit. However, it is not instantaneous, so the incident detection may be previous to the endpoint in order to prevent the structural damage scenario. Despite this, a FPSS to avoid the melting due to the Temperatures increase as in the previous cases.				

LOCAs

Temperature evolution of the BB and the Divertor if a 30% BB LOCA occurs in all the cooling loops.

Temperature evolution of the BB and the Divertor if a 60% BB LOCA occurs in all the cooling loops.

Temperature evolution of the BB and the Divertor if a 90% BB LOCA occurs in all the cooling loops.

Future work

Future tasks will be focused on the development of the DCLL, HCLL and WCLL contributions to safety analyses using AINA 4.0.

Conclusions

- It would be desirable to carry out a possible design review to ensure suitable operating temperatures for all the materials which make up the HCPB BB.
- It is necessary to guarantee a quick detection and actuation by means of a proper system, depending on the affected equipment, when the most demanding transients take place which may drive the reactor to suffer a melting scenario and a very energetic plasma disruption at the same time.
- These events are an increase of fueling above 50%, a permanent improvement in the confinement time and a punctual impurity increase above 300%.
- Other perturbations studied only provide information on non-dangerous cases as a decrease of the fueling injection, impossible situations from a technical point of view as an unexpected and sudden increase of external power above 630% or melting processes as LOCAs or a decrease of the external power.

UNIVERSITAT POLITÈCNICA DE CATALUNYA BARCELONATECH

Advanced Nuclear Technologies. ANT

"Contribution to safety analyses of DEMO HCPB using AINA code" E. Baeza, A. de Blas , A. Riego, J. Dies and M. Fabbri. 30th Symposium on Fusion Technology (SOFT)**.** Sicily (Italy), September 2018.

ISFNT-13 2017 KYOTO 13th International Symposium on Fusion Nuclear Technology

September 25-29, 2017 – Kyoto, Japan

Development of the safety code AINA for the European DEMO designs

E.Baeza[a], A. de Blas[a] , A. Riego[a], M. Fabbri[a]

[a] Fusion Energy Engineering Laboratory (FEEL), Technical University of Catalonia (UPC) Barcelona-Tech, Barcelona, Spain

Introduction

A conclusion that can be drawn from the historical safety analyses developed for tokamaks fusion reactors is that some of the major risks involve incidents in the vacuum vessel. In order to evaluate plasma evolution and in-vessel components strains, a safety code called AINA has been developing during the last ten years for different fusion reactors designs as ITER and the Japanese DEMO design WCPB. This work describes the new AINA code which is being adapted for the four European DEMO designs (HCPB, DCLL, HCLL and WCLL).

Aim and scope

The main goal of this project is developing a new AINA that becomes a proper, reliable, versatile and flexible tool in order to preform future safety studies of the European DEMO designs. The basic structure of the code and the most relevant models and numerical methods exposed in this poster have been implemented from scratch after an in-depth critical analysis of the former AINA versions and an intensive checking process carried out during the last year.

AINA Scheme

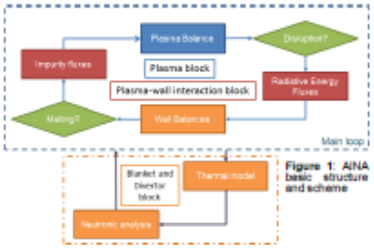

Figure 1: AINA basic structure and scheme

- AINA is a code comprised of a 0D plasma dynamics approach and a 1D thermal model for the blanket and the divertor.
- These two blocks feed-back constantly each other by means of the plasma-wall interaction block.

Plasma Block

- It is a mass and energy balance.
- All the terms are calculated through volume and radial profiles of plasma density and temperature.
- AINA determines a SS scenario of the plasma using an average ion temperature and a specified power fusion as inputs and solving the system by the Newton method.
- The time evolution is estimated by the Euler method.

$$\frac{dn_{He}}{dt} = S_{He} - 2S_{\alpha} - \frac{n_{He}}{\tau_{p,He}}$$

$$\frac{dn_{\alpha}}{dt} = S_{\alpha} - \frac{n_{\alpha}}{\tau_{p,\alpha}}$$

$$\frac{dn_{Imp}}{dt} = S_{Imp} - \frac{n_{Imp}}{\tau_{p,I}}$$

$$\frac{dn_{DT}}{dt} = S_{DT} - \frac{n_{DT}}{\tau_{p,I}}$$

Figure 2: Numerical model

$$\frac{3}{2}\frac{d(n_e T_i)}{dt} = f_{\alpha e} P_{\alpha} + f_e P_{\alpha} - P_{ie} - \frac{3 n_e T_e}{2 \tau_{E,I}}$$

$$\frac{3}{2}\frac{d(n_e T_e)}{dt} = (1 - f_{\alpha e}) P_{\alpha} + (1 - f_e) P_{\alpha} + P_{ie} + P_{Brem} - P_{Br} - P_{Sy} - P_{\Omega} - \frac{3 n_e T_e}{2 \tau_{E,e}}$$

$$n_e = n_i + 2n_{\alpha} + \sum_{j=1}^{n} \langle Z_j \rangle n_{Zj}$$

Thermal Divertor Block

- Both the numerical model and the solver and all the requirements are the same as used in the thermal blanket block although they are adapted to the divertor configuration.

Layer No.	Material	Thickness [mm]	No. Nodes
1	Tungsten	2	10
2	Copper	1	500
3	CuCrZr	1.6	500
4	Tungsten Contact	12	1
5	CuCrZr	1.5	500
6	Copper	1	500
7	Tungsten	1	500
8	EUROFER	10	500
9	Tungsten Contact	70	1
10	EUROFER	10	500
11	Tungsten Contact	70	1
12	EUROFER	10	500
13	Tungsten Contact	70	1
14	EUROFER	10	500
15	Tungsten Contact	70	1
16	EUROFER	10	500

Figure 4: Specifications of the 1D Divertor model

Steady State Results

INPUTS	DEMO1
Major radius [m]	9.072
Minor radius [m]	2.927
Toroidal field [T]	5.667
Safety factor 95% flux	3.247
Plasma volume [m³]	2502
Plasma surface [m²]	1428
Fusion power [MW]	2037
Ion temperature [keV]	13.065

OUTPUTS	AINA	PROCESS
Electron temp. [keV]	13.04	13.065
Fuel source [m⁻³s⁻¹]	8.95e18	2.82e18
Electron density [m⁻³]	8.35e19	7.98e19
Ion density [m⁻³]	7.55e19	6.99e19
Hydrogen density [m⁻³]	6.94e19	6.144e19
Alpha density [m⁻³]	5.98e18	7.98e18
Impurity density [m⁻³]	3.66e16	3.51e16
Xe density [m⁻³]	3.25e16	-
W density [m⁻³]	4.17e15	-
Xe fraction [%]	0.0389	0.0389
W fraction [%]	0.005	0.005
External power [MW]	66.4	50
Gain	30.68	39.86
Alpha Power [MW]	399	407
Ion-Elec.exchange [MW]	1.76	0
Ohmic power [MW]	0.95	1.1
Bremss. power [MW]	80.98	87.9
Syncht. power [MW]	30.2	25.9
Line power [MW]	226.3	191
Edge power [MW]	172	172.9
Radiation in core [MW]	165.6	132.6
Total Radiation [MW]	337.6	305.5
SOL power [MW]	300	-
Beta total [%]	3.26	3.1
Beta toroidal [%]	2.81	3.2
Beta poloidal [%]	0.96	1.1
Confinement time [s]	4.15	4.23
Plasma current [MA]	20.3	19.6
Bootstrap fraction [%]	0.25	0.32
NWL$_{ave}$ [MW/m²]	1.07	1.05
P$_{wall}$ [MW/m²]	0.17	0.22

Region	Material	T limit [°C]	T max [°C]
BB/Div	Tungsten	3422	505 / 182
BB/Div	EUROFER	550	578 / 317
BB	Be	650	816
BB	Li_4SiO_4	920	1360
Div	Cu	980	158
Div	CuCrZr	1050	156

- No meaningful discrepancies have been found.
- Certain functional temperature limits (EUROFER, Beryllium and Li_4SiO_4) for the HCPB BB design are slightly exceeded.

Thermal Blanket Block

Figure 3: Transient solver approach and numerical model

$$\rho(T,x)c(T,x)\frac{\partial T}{\partial t} = \frac{\partial}{\partial x}\left(\left(1 - f_{Conv_{ij}}\right)k_i(T,x)\frac{\partial T(x,t)}{\partial x}\right) + f_{Conv_{ij}} f_{Geo_{ij}} h_{ij}\left(T(x,t) - T_{j,n}(x,t)\right) + \dot{q}(x,t)$$

- Thermal-hydraulics routines based on the finite differences.
- Coolant channels not in line with the 1D segment are considered using a weighted convective negative flux effect.

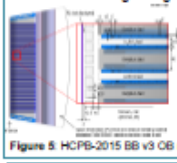

Layer No.	Material	Thickness [mm]	No. Nodes
1	Tungsten	2	10
2	EUROFER	3	500
3	15Mass Coolant	13.5	1
4	EUROFER	8.5	500
5	Be/Li_4SiO_4/EUR	516	500

Figure 5: HCPB-2015 BB v3 OB region concept and its specifications for AINA

Plasma-Wall Interaction Block

- Estimation of the loads (P_{wall} and NWL) for the thermal equilibrium calculation.
- Estimation of the impurity fluxes to the plasma core.

Wall Loads

$$NWL_{ave} = \frac{S_p \cdot (m)_{eff} \cdot E_i}{S_{wall}} \cdot \Gamma_{wall}$$

$$P_{wall} = RWL + RDL - \dot{q}_{RadVol,P} - \dot{q}_{Conv}$$

$$RWL_{ave} = \frac{P_{He} + P_{\alpha} + P_i + P_{Imp}}{S_{wall}} + \frac{P_n \cdot 2 \cdot f_{Refl}}{S_{wall}}$$

$$RDL = \frac{P_{Brd} - P_{Brd,refl}}{S_{wall}}$$

Figure 6: Numerical models

$$P_{DIV} = P_{ion} + P_n - P_{Br} - P_{Sy} - P_{\Omega}$$

Impurities

- A constant fraction of Xe.
- W produced by two main sources:

$$\Gamma_{Plasma}(R_i) = Q \cdot S_i(a)\left(1 - \left(\frac{R_{in}}{R_i}\right)^{\alpha}\right)\left(1 - \frac{R_{in}}{R_0}\right)^{\beta}$$

$$\Gamma_{Self} = \frac{2.6 \cdot 10^{14}}{\sqrt{M_i \cdot T}} \cdot 10^{\frac{E_{th}}{T}}$$

$$S_i(t) = C_{Armor_i} \cdot (t - \tau_{Ex})$$

Figure 7: Physical sputtering, thermal sublimation and transport

Transients Results

AINA is able to simulate:

- Plasma disruption or structural material melting due to a LOPC.
- In-vessel melt either of FW, blanket structure and/or divertor regions due to thermal stresses after a LOCA.

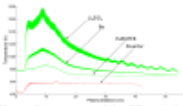

Figure 8: Increase of the BB and divertor temperatures after an external power cut-off

Figure 9: Surface divertor temperature after a loss of 90% of the mass flow rate in the PFC loop

Future work

- Development of the HCPB safety analysis by means of the new AINA.
- Thermal blanket block adaptation for the rest of the European blanket designs (DCLL, HCLL and WCLL) and development of the their pertinent safety analyses.
- Implementation of models which estimate the radiation reflected for every module of the blanket and the energy flux emitted due to impurity flux leaving the wall.

Conclusions

- The new AINA has become a proper, reliable, versatile and flexible tool in order to preform future safety studies for the European DEMO designs.
- Several potential risk scenarios as LOPCs and LOCAs can be simulated consequently the most critical ones will be identified.
- It would be advisable to undertake a design review focused on ensuring a suitable operating temperature range for all the materials which make up the HCPB blanket.

UNIVERSITAT POLITÈCNICA DE CATALUNYA BARCELONATECH

Advanced Nuclear Technologies. ANT

"Development of the safety code AINA for the European DEMO designs" E. Baeza, A. de Blas , A. Riego, J. Dies and M. Fabbri. 13th International Symposium on Fusion Nuclear Technology**.** Kyoto (Japan), September 2017.

8 Agraïments

Cada un dels esforços que he hagut de dur a terme per realitzar aquesta tesis els i vull dedicar, molt especialment, al meu pare, en Pedro Baeza Giménez. Et faré present a cada passa de per vida.

Tanmateix agraeixo a ma mare, la Viky Pérez Andreu, haver apuntalat sempre els meus dies i no deixar-me defallir mai. Ets l'exemple etern.

Tots dos éreu, sou i sereu bondat.

També a la meva companya de viatge, la Laura Fros Gaetan, qui il·lumina els instants foscos i li dóna sentit a tot amb un somriure. Aquesta tesis també és teva, té moltíssim de tu. Gràcies per ensenyar-me tant.

La resta de la família directa, el Pedro Baeza Pérez, el Juan Manuel Baeza Pérez, la Mònica, la Txell, la Coral, l'Alicia i el Carlos; entre totes heu aconseguit molt sovint fer-me oblidar els maldecaps de tot aquest procés i altres dissorts dibuixant-me un somriure a la cara.

Agraeixo també la feina dels meus dos tutors, l'Alfredo de Blas del Hoyo i l'Albert Riego Pérez, i a les companyes de la secció: el Pedro, el Roger, en Marco, la Maria, la Idoia, la Mercè, la Luisa, l'Agustí, la Maria Amor per haver-me fet riure tant. I a les amigues que m'he anat trobant pel camí: Ger, Gina, Dani, Andrea, Marc, Toni, Tomàs, Adri, Sandy, Carlos, Txela, Juan, Artur, Fàbrega, Martin, Laura, Torra, Ruben, Andrea, Guille, Jasmina, Carlos, Isra, Paco... un gràcies per compartir via.

I, finalment, un gràcies enorme a totes les companyes de lluites.

Per cert, també toca donar la benviguda a l'Aina Fàbrega Herrera; que tinguis sort i que tinguis joia.

Salut!

9 References

[1] EUROfusion, EUROfusion Web page, (2018). https://www.euro-fusion.org/.

[2] M. Fabbri, Neutronics analysis and thermodynamics studies of several DEMO breeding blankets for the development of the AINA safety code, Universitat Politècnica de Catalunya, 2017.

[3] E. Baeza, Human reliability assessment in remote handling tasks as a contribution to RAMI reviews of IFMIF, (2013).

[4] ITER-Organization, ITER web page, (2018). https://www.iter.org/.

[5] J.D. Lawson, Some Criteria for a Power Producing Thermonuclear Reactor, Proceedings of the Physical Society. Section B. 70 (1957) 6–10. doi:10.1088/0370-1301/70/1/303.

[6] Woodbank Communications Ltd, Electropaedia, (2018). http://www.mpoweruk.com/nuclear_practice.htm.

[7] D. Clery, The bizarre reactor that might save nuclear fusion, Science. (2015). doi:10.1126/science.aad4746.

[8] ITER, 60 YEARS OF PROGRESS, (n.d.). https://www.iter.org/sci/BeyondITER.

[9] J. Izquierdo, Iter Safety Assessment: In-vessel simulation of tokamak events and component reliability approach, 2008.

[10] C.L. Smith, S. Cowley, The path to fusion power, Philosophical Transactions of the Royal Society A: Mathematical, Physical and Engineering Sciences. 368 (2010) 1091–1108. doi:10.1098/rsta.2009.0216.

[11] R. Wenninger, DEMO1 Reference Design - 2015 April ("EU DEMO1 2015"), 2MDKFH. (2015).

[12] R. Wenninger, DEMO2 Reference Design - 2015 May ("EU DEMO2 2015"), 2MBDKZ. (2015).

[13] R. Wenninger, Scenario Modelling, 2LMSDR. (2014).

[14] J. Dies, M. Dapena, M. Ramon, J. Garcia, J.C. Rivas, A. Calvo, S. Reyes, AINA safety code, a review of loss of plasma control transients in ITER: sudden increase in fuelling rate, sudden increase of auxiliary heating, Fusion Science and Technology. 56 (2009) 31–37.

[15] J.C. Rivas, J. Dies, Upgrading of plasma wall interaction model for tokamak transient modeling code aina 2.0, used in safety studies of iter plasma instability events, Fusion Science and Technology. 60 (2011) 825–829.

[16] J.C. Rivas, J. Dies, Safety studies: Review of loss of plasma control transients in ITER with AINA 3.0 code, Fusion Engineering and Design. 88 (2013) 2709–2713. doi:10.1016/j.fusengdes.2013.02.134.

[17] J.C. Rivas, J. Dies, ITER safety studies: The effect of two simultaneous perturbations during a loss of plasma control transient, Fusion Engineering and Design. 89 (2014) 2043–2047. doi:10.1016/j.fusengdes.2014.04.010.

[18] J.C. Rivas, J. Dies, X. Fajarnés, Revisiting the analysis of passive plasma shutdown during an ex-vessel loss of coolant accident in ITER blanket, Fusion Engineering and Design. 98-99 (2015) 2206–2209. doi:10.1016/j.fusengdes.2015.06.143.

[19] J.C. Rivas, M. Nakamura, Y. Someya, K. Hoshino, N. Asakura, H. Takase, Y. Miyoshi, H. Utoh, K. Tobita, J. Dies, A. de Blas, A. Riego, M. Fabbri, Safety studies of plasma-wall events with AINA code for Japanese DEMO, Fusion Engineering and Design. (2015). doi:10.1016/j.fusengdes.2015.10.037.

[20] Sandia National Laboratories, MELCOR, (2017). http://energy.sandia.gov/energy/nuclear-energy/nuclear-energy-safety-technologies/melcor/.

[21] B.J. Merrill, Recent Updates to the MELCOR 1 . 8 . 2 Code for ITER Applications Applications, (2007).

[22] B.J. Merrill, New version of MELCOR-Fusion Now Available, (n.d.).

[23] B. Chuilon, Analysis_of_the_impacts_of_LOCA_events_-_2M7SWU_v1_2, (2016).

[24] G. Caruso, M. Nobili, F. Giannetti, A. Naviglio, M. Frullini, Interim_report_on_accident_analyses__WCL_2MLL8T_v1_1, (2016).

[25] D. Carloni, B. Gonfiotti, S. Paci, L.V. Boccaccini, LOCA accident for the DEMO helium cooled blanket, Fusion Science and Technology. 68 (2015) 353–357. doi:dx.doi.org/10.13182/FST14-924.

[26] E. Urbonavičius, Identify_required_safety_analysis_code_d_2MH2PZ_v1_1, (2015).

[27] P. Norajitra, M. Oron-Carl, Project_Deliverable_D1A02_(112-01-A)__DD_2MCQCX_v1_2, (2015).

[28] M. Ebolia, N. Forgionea, A. Del Nevo, Implementation of the Chemical PbLi / Water Reaction in the SIMMER Code, (2015).

[29] M. Ebolia, N. Forgionea, A. Del Nevo, M.T. Porfiri, Set_up_safety_analysis_code_SIMMER_III_f_2MCTPT_v1_0, (2014).

[30] M. Kovari, R. Kemp, H. Lux, P. Knight, J. Morris, D.J. Ward, " PROCESS " : A systems code for fusion power plants Part 1: Physics, Fusion Engineering and Design. 89 (2014) 3054–3069. doi:10.1016/j.fusengdes.2014.09.018.

[31] M. Kovari, F. Fox, C. Harrington, R. Kemp, P. Knight, H. Lux, J. Morris, "PROCESS": a systems code for fusion power plants - Part 2: Engineering (submitted to Fusion Engineering and design), (2015).

[32] ANSYS Team, ANSYS, (n.d.). http://www.ansys.com/products/multiphysics.

[33] F. Hernandez, Q. Kang, P. Pereslavtsev, CAD, Thermo-hydr./-mechanical analyses 2014, EFDA_D_2MEVJZ. (2014).

[34] L. V Boccaccini, G. Zhou, F. Hern, H. Chen, M. Ye, Preliminary structural analysis of the new HCPB blanket for EU DEMO reactor, 1 (2016) 7–9.

[35] I. Balboa, M. Clever, R. Dejarnac, I. Coffey, Y. Corre, S. Devaux, L. Frassinetti, E. Gauthier, J. Horacek, M. Knaup, K. Krieger, S. Marsen, A. Meigs, P. Mertens, R.A. Pitts, T. Puetterich, MEMOS Code Validation on JET Transient Tungsten Melting Experiments, (2014).

[36] S. Pestchanyi, A. Boboc, B. Bazylev, I. Landman, Optimization of MGI in JET using TOKES Code, (2014).

[37] J.C. Rivas, Development of AINA code for the study of loss of plasma control events in ITER and DEMO, and contribution to the systems study of DEMO, Universitat Politècnica de Catalunya,

2016.

[38] H.-S. Bosch, G.. Hale, Improved formulas for fusion cross-sections and thermal reactivities, Nuclear Fusion. 33 (2002) 1919–1919. doi:10.1088/0029-5515/33/12/513.

[39] T. HONDA, H.-W. BARTELS, N.A. UCKAN, Y. SEKI, T. OKAZAKI, Development of Time Dependent Safety Analysis Code for Plasma Anomaly Events in Fusion Reactors, Journal of Nuclear Science and Technology. 34 (1997) 229–239. doi:10.1080/18811248.1997.9733655.

[40] R.J. Goldston, P.H. Rutherford, Introduction to Plasma Physics, Bristol, UK, 1995.

[41] F. Albajar, Radiation Transport Modelling in a Tokamak Plasma : Application to Performance Prediction and Design of Future Machines, (2001).

[42] F. Albajar, M. Bornatici, F. Engelmann, RAYTEC: a new code for electron cyclotron radiative transport modelling of fusion plasmas, Nuclear Fusion. 49 (2009) 115017. doi:10.1088/0029-5515/49/11/115017.

[43] D.E. Post, R. V. Jensen, C.B. Tarter, W.H. Grasberger, W.A. Lokke, Steady-state radiative cooling rates for low-density, high-temperature plasmas, Atomic Data and Nuclear Data Tables. 20 (1977) 397–439. doi:10.1016/0092-640X(77)90026-2.

[44] J. Sheffield, The physics of magnetic fusion reactors, Reviews of Modern Physics. 66 (1994) 1015–1103.

[45] Y. Ding, Modelling of the radiative power loss from the plasma of the Tore Supra tokamak, (2008).

[46] R. Neu, Tungsten as a plasma facing material in Fusion Devices, (2003). doi:10.1016/B978-0-08-056033-5.00118-X.

[47] J. Wesson, Tokamaks, Third edit, 2004.

[48] G. Giruzzi, J.F. Artaud, M. Baruzzo, T. Bolzonella, E. Fable, L. Garzotti, I. Ivanova-Stanik, R. Kemp, D.B. King, M. Schneider, R. Stankiewicz, W. Stepniewski, P. Vincenzi, D. Ward, R. Zagórski, Modelling of pulsed and steady-state DEMO scenarios, Nuclear Fusion. 55 (2015) 073002. doi:10.1088/0029-5515/55/7/073002.

[49] P.C. Stangeby, The Plasma Boundary of Magnetic Fusion Devices, (2000). doi:10.1088/0741-3335/43/2/702.

[50] C. Reux, L. Di Gallo, F. Imbeaux, J.-F. Artaud, P. Bernardi, J. Bucalossi, G. Ciraolo, J.-L. Duchateau, C. Fausser, D. Galassi, P. Hertout, J.-C. Jaboulay, A. Li-Puma, B. Saoutic, L. Zani, DEMO reactor design using the new modular system code SYCOMORE, (2014). doi:10.1088/0029-5515/55/7/073011.

[51] ITER TEAM and others, ITER physics basis, Nucl Fusion. 39 (1999).

[52] N.A. Uckan, S. Putvinski, J. Wesley, H.-W. Bartels, T. Honda, T. Amano, D. Boucher, N. Fujisawa, D. Post, M. Rosenbluth, Iter physics-safety interface: models and assessments, 1 (1996).

[53] A.R. Polevoi, M. Shimada, V.S. Mukhovatov, ITER plasma performance assessment on the basis of newly-proposed scalings, Plasma Phys. Control. Fusion. 48 (2006).

[54] H.. Wilson, Bootstrap current scaling in tokamaks, Nuclear Fusion. 32 (1992) 257–263. doi:10.1088/0029-5515/32/2/I05.

[55] F. Troyon, R. Gruber, H. Saurenmann, S. Semenzato, S. Succi, MHD-Limits to Plasma Confinement, Plasma Physics and Controlled Fusion. 26 (2002) 209–215. doi:10.1088/0741-3335/26/1A/319.

[56] M. Greenwald, Density limits in toroidal plasmas, Plasma Physics and Controlled Fusion. 44 (2002) R27–R53. doi:10.1088/0741-3335/44/8/201.

[57] ANSYS Team, ANSYS Fluent (C) User Manual, 2015.

[58] M. Fabbri, A. de Blas, A. Riego, I. Zamora, E. Baeza, Methodology for the improvement of the AINA Code wall-model applied to DEMO WCPB blanket., Fusion Engineering and Design. 124 (2017) 1195–1198. doi:http://dx.doi.org/10.1016/j.fusengdes.2017.05.027.

[59] F.A. Hernández, Q. Kang, B. Kiss, P. Norajitra, G. Nádasi, P. Pereslavtsev, C. Zeile, HCPB Design Report 2015. Internal_Deliverable_BB-1.2.1-T002-D001__2MNBH9_v1_0, D_2LGL9U (2016).

[60] H. Petersen, The properties of helium: density, specific heats, viscosity, and thermal conducdivity at pressures from 1 to 100 bar and from room temperature to about 1800 K, Danish Atomic Energy Comission, Research Establishment Risö, Risö. 224 (1970) 1–42.

[61] F.A. Hernández, Thermo-hydraulic analyses of HCPB BB segment, EFDA_D_ 2HF7KU_v1.1. (2016).

[62] F. Incropera, D. DeWitt, Fundamentos de transferencia de calor, 1999.

[63] V. Gnielinski, New equations for heat and mass transfer in the turbulent flow in pipes and channels, Jahrestreffen Der Verfahrensingenieure. 41 (1975) 8–16.

[64] B.S. Petukhov, Heat Transfer and Friction in Turbulent Pipe Flow with Variable Physical Properties, Advances in Heat Transfer. 6 (1970) 503–564. doi:10.1016/S0065-2717(08)70153-9.

[65] F. Gillemot, E. Gaganidze, S. Ildikó, Material property handbook on EUROFER97 (2015-MTA, MAT-1.2.1.02, D-2MRP77,. (2016).

[66] J.W. Davis, P.D. Smith, ITER material properties handbook, Journal of Nuclear Materials. 233 (1996) 1593–1596. doi:10.1016/S0022-3115(96)00202-4.

[67] A. Abou-Sena, F. Arbeiter, L. V. Boccaccini, G. Schlindwein, Measurements of the purge helium pressure drop across pebble beds packed with lithium orthosilicate and glass pebbles, Fusion Engineering and Design. 89 (2014) 1459–1463. doi:10.1016/j.fusengdes.2013.12.009.

[68] A. De Blas, A. Riego, E. Baeza, M. Fabbri, Á. Cubí, Report on development of new AINA code for DEMO HCPB (models and numerical methods), (2016).

[69] J.J. Zielinski, H.J. Van Der Meiden, T.W. Morgan, M.H.J. 'T Hoen, D.C. Schram, G. De Temmerman, Self-shielding of a plasma-exposed surface during extreme transient heat loads, Applied Physics Letters. 104 (2014) 5–8. doi:10.1063/1.4869486.

[70] P. Frosi, S. Villari, G. Ramogida, V. Cocilovo, Load Specification for Divertor Cassette and steel supporting structure for Vertical Target and Dome. DIV-1-T001-D006_Load_Specification_for_D_2LLS49_v1_0, (2015).

[71] G. Mazzone, P. Frosi, D. Coccorese, R. Villari, D. Marzullo, P.A. Di Maio, V. Cocilovo, D. De Meis, D. Dongiovanni, Divertor cassette Design Description Document. DIV-1-T001-D001_-_Divertor_cassette_Desi_2MW2KD_v1_0, (2015).

[72] D.N. Dongiovanni, G. Ramogida, Functional Requirements Verification Report. FR_-_AWP15_-_DIV-1-T001-D011__Verificati_2MC88V_v1_0, (2015).

[73] P.A. Di Maio, G. Mazzone, S. Garitta, E. Vallone, DEMO Divertor - Thermo-hydraulic assessment report. FR_-_AWP15_-_DIV-1-T001-D010_Thermo-hydr_2MY45W_v1_0, (2015).

[74] G. Mazzone, WP-DIV - DEMO Divertor design status Nov. 2016, (2016).

[75] G. Di Gironimo, D. Marzullo, D. Coccorese, CAD Model of the Divertor CB system. FR_-_AWP15_-_DIV-1-T001-D005-CAD_Model_o_2M5EEF_v1_0 (1), (2015).

[76] F. Domptail, T. Barrett, M. Fursdon, Divertor Target Technology: Thermal break concept 1st phase design assessment. FR_-_AWP15_-_DIV-2.2.2-T001-D001___DEMO__2MPLQF_v1_1, (2015).

[77] I. Smid, J. Schlosser, J. Boscary, F. Escourbiac, G. Vieider, Comparison between various thermal hydraulic tube concepts for the ITER divertor, in: Fusion Technology 1996, 1997: pp. 263–266. doi:10.1016/B978-0-444-82762-3.50036-7.

[78] S. Dudarev, J.-L. Boutard, Advances in modelling the performance of fusion steels, (2009). https://www.euro-fusion.org/newsletter/advances-in-modelling-the-performance-of-fusion-steels/.

[79] M.T. Porfiri, G. Mazzini, DEMO Accident Selection and Description. 2MEWTE_v1_0, (2015).

[80] M. Fursdon, T. Barret, F. Domptail, S. McIntosh, Updated Monoblock Elastic Analysis Procedure (MEAP) guidelines. FR_-_AWP15_-_DIV-2.9.3-T001-D001__Elasti_2CYH6Q_v1_2, (2015) 18–24.

[81] Adene, Revised Release on the IAPWS Industrial Formulation 1997 for the Thermodynamic Properties of Water and Steam, Energy and Buildings. 31 (2013). doi:10.1177/0037549714528744.

[82] C.F. Beaton, Heat Exchanger Design Handbook, (1986). doi:10.1615/AtoZ.s.steam_tables.

[83] B. Wischnewski, Calculation of thermodynamic properties of water, (n.d.). http://www.peacesoftware.de/einigewerte/wasser_dampf_e.html.

[84] F.P. Incropera, D.P. DeWitt, T.L. Bergman, A.S. Lavine, Fundamentals of Heat and Mass Transfer, 2007. doi:10.1073/pnas.0703993104.

[85] V. Barabash, ITER Materials Property Handbook (baseline). ITER_D_29DDBF, 2009.

[86] T. Barrett, D. Hancock, M. Kalsey, W. Timmis, M.P. Ccfe, Water-Cooled Divertor Target Design Study – Alternative CuCrZr Concepts. Water-Cooled_Divertor_Target_Design_Stud_2AQ5UZ_v1_0, (2012) 1–44.

[87] R. Villari, G. Mariano, Neutronic Analysis Report for Divertor Cassette and PFC 2015. FR_-_AWP15_-_DIV-1-T001-D008_-_Neutronic_2MN2H3_v1_0, (2016).

[88] R. Villari, D. Flammini, Neutron transport analysis through openings in in-vessel components. PMI.3.3-008_Neutron_transport_analysis_t_2MEP2U_v1_0, (2016).

[89] M. Li, J.-H. You, Modelling of failure features for thermal break concept. FR_-_AWP15_-_DIV-2.2.2-T002-D002-Modelli_2M4YKZ_v1_0, (2015).

[90] ITER-Organization, GSSR Volume 11 - Models and Codes, XI (2001).

[91] A. Loarte, Introducción a la física de la interacción Plasma-Pared en dispositivos de fusión nuclear, (2005).

[92] R.J. Walker, M.R. Gilbert, Neutron activation of impurity seeding gases within a DEMO environment, Fusion Engineering and Design. (2016) 1–4. doi:10.1016/j.fusengdes.2017.01.057.

[93] G. Federici, C.. Skinner, J.. Brooks, J.. Coad, C. Grisolia, A.. Haasz, A. Hassanein, V. Phillips, C.. Pitcher, J. Roth, W.. Wampler, D.. Whyte, Plasma material interactions in current tokamaks and their implications for next step fusion reactors, Nuclear Fusion. 41 (2001) 1967–2137. doi:10.1088/0029-5515/41/12/218.

[94] W. Eckstein, J.. Stephens, R.E.. Clark, J.. Davisc, A.. Haasz, E. Vietzked, Y. Hirooka, Atomic and Plasma-Material Interaction Data for Fusion, 7 (2001) Part B.

[95] IAEA, Iter physics, (1991).

[96] A. Hassanein, A. Konkashbaev, I. Konkashbaev, Erosion of melt layers developed during a plasma disruption, (1994).

[97] C. Linsmeier, Plasma-Wall Interactions, (2014).

[98] P. Sigmund, Theory of sputtering. I. Sputtering yield of amorphous and polycrystalline targets, Physical Review. 184 (1969) 383–416.

[99] Y. Yamamura, J. Bohdansky, Few collisions approach for threshold sputtering, Vacuum. 35 (1985) 561–571. doi:10.1016/0042-207X(85)90316-1.

[100] W.D. Wilson, L.G. Haggmark, J.P. Biersack, Calculations of nuclear stopping, ranges, and straggling in the low-energy region, Physical Review B. 15 (1977) 2458–2468. doi:10.1103/PhysRevB.15.2458.

[101] C. García-Rosales, W. Eckstein, J. Roth, Revised formulae for sputtering data, Journal of Nuclear Materials. 218 (1995) 8–17. doi:10.1016/0022-3115(94)00376-9.

[102] K. Krieger, A. Geier, X. Gong, H. Maier, R. Neu, V. Rohde, Erosion and migration of tungsten employed at the main chamber first wall of ASDEX Upgrade, Journal of Nuclear Materials. 313-316 (2003) 327–332. doi:10.1016/S0022-3115(02)01351-X.

[103] A. Geier, K. Krieger, J.D. Elder, R. Pugno, V. Rohde, Modeling of tungsten transport in the SOL for sources at the central column of ASDEX Upgrade using DIVIMP, Journal of Nuclear Materials. 313-316 (2003) 1216–1220. doi:10.1016/S0022-3115(02)01519-2.

[104] G. Janeschitz, R. König, L. Lauro-Taroni, J. Lingertat, G. Matthews, M. Stamp, G. Vlases, D. Campbell, S. Clement, L. De Kock, W. Eckstein, J. Ehrenberg, N. Gottardi, P. Harbour, L. Horton, H. Jäckel, M. Lesourd, A. Loarte, C. Lowry, J. Roth, G. Saibene, D. Summers, J.A. Tagle, P.R. Thomas, M. von Hellermann, Divertor performance on carbon and beryllium targets in JET, Journal of Nuclear Materials. 196-198 (1992) 380–385. doi:10.1016/S0022-3115(06)80064-4.

[105] S. Putvinski, N. Fujisawa, D. Post, N. Putvinskaya, M.. Rosenbluth, J. Wesley, Impurity fueling to terminate Tokamak discharges, Journal of Nuclear Materials. 241-243 (1997) 316–321.

[106] K. Mccarthy, D. Petti, B. Kolbasov, V.P. Shestakov, Beryllium interaction with steam or air in ITER under accident conditions, (2014).

[107] P. Galli, A. Cherubini, R. De Angelis, F. De Luca, M. Erba, R. Giannella, G. Gorini, A. Jacchia, H. Jäckel, P. Mnatica, V.. Parail, L. Porte, A. Taroni, Transient heat transport studies using laser

ablated impurity injection in JET, Nuclear Fusion. 38 (1998).

[108] W. Horton, W. Rowan, Impurity transport studies in the Texas Experimental Tokamak (TEXT), Physics of Plasmas. 1 (1994) 901–908. doi:10.1063/1.870749.

[109] K.W. Gentle, W.L. Rowan, R. V. Bravenec, G. Cima, T.P. Crowley, H. Gasquet, G.A. Hallock, J. Heard, A. Ouroua, P.E. Phillips, D.W. Ross, P.M. Schoch, C. Watts, Strong nonlocal effects in a Tokamak perturbative transport experiment, Physical Review Letters. 74 (1995) 3620–3623. doi:10.1103/PhysRevLett.74.3620.

[110] R. Behrisch, G. Federici, A. Kukushkin, D. Reiter, Material erosion at the vessel walls of future fusion devices, Journal of Nuclear Materials. 313-316 (2003) 388–392. doi:10.1016/S0022-3115(02)01580-5.

[111] F. Militello, W. Fundamenski, Multi-machine comparison of drift fluid dimensionless parameters, Plasma Physics and Controlled Fusion. 53 (2011). doi:10.1088/0741-3335/53/9/095002.

[112] N. Asakura, K. Shimizu, K. Tobita, Simulation of Power Exhaust in Edge and Divertor of the SlimCS Tokamak Demo Reactor, (2010).

[113] M. Beckers, W. Biel, M. Tokar, U. Samm, Investigations of the First-Wall Erosion of DEMO with the CELLSOR Code, 22nd PSI. (2016).

[114] M. Wischmeier, Modelling power exhaust, (2014).

[115] K. Hoshino, N. Asakura, K. Shimizu, S. Tokunaga, T. Takizuka, Y. Someya, M. Nakamura, H. Utoh, Y. Sakamoto, K. Tobita, Divertor study on DEMO reactor, Plasma and Fusion Research. 9 (2014) 1–8. doi:10.1585/pfr.9.3403070.

[116] F. Subba, L. Aho-Mantila, R. Ambrosino, D.. Coster, V. Pericoli-Ridolfini, A. Uccello, R. Zanino, Efficiency of non-standard divertor configurations in DEMO, 22nd PSI. (2016).

[117] G.Y. Zheng, Y.D. Pan, K.M. Feng, H. Da He, X.W. Cui, Super-X Divertor Simulation for HCSB-DEMO Conception Design, Chinese Physics Letters. 29 (2012) 105202. doi:10.1088/0256-307X/29/10/105202.

[118] M. Wischmeier, M. Groth, A. Kallenbach, A. V. Chankin, D.P. Coster, R. Dux, A. Herrmann, H.W. Müller, R. Pugno, D. Reiter, A. Scarabosio, J.G. Watkins, Current understanding of divertor detachment: Experiments and modelling, Journal of Nuclear Materials. 390-391 (2009) 250–254. doi:10.1016/j.jnucmat.2009.01.081.

[119] A. Loarte, Física de plasmas en contacto con materiales: El sheath, (2005).

[120] M.T. Porfiri, G. Mazzini, DEMO BB Safety Data List (SDL)_2MF8KU_v2_0, (2016).

[121] P. Norajitra, D. Carloni, Safety relevant aspects identified for the HCPB BB_Internal Deliverable _D-111-02__Safety_re_2JQ2P3_v1_0, (2014).

[122] N. Taylor, General_Safety_Principles_2LJVZ7_v1_0, (2014).

[123] J. Johnston, Plant Safety Requirements Document_2MKFDY_v3_1, (2016).

[124] D. Carloni, S. Ciattaglia, Propose Safety Importance Classification Scheme for DEMO Systems, Structures and Components_2MAZHF_v1_0, (2015).

[125] D. Carloni, T. Pinna, Functional Failure Mode and Effect Analysis (FFMEA) for the DEMO water

cooling systems of the Divertor. D-WBS-2.16_2M4REM, (2014).

[126] D. Carloni, T. Pinna, Report on FBS and PBS to analyse with the FFMEA of the HCPB Breeding system, Magnet and Vacuum Vessel systems. Report on FFMEA of the HCPB Breeding system, Magnet and Vacuum Vessel systems with indications for the selection of reference accident scenarios, (2015).

[127] T. Pinna, Failure Mode and Effect Analysis for the European Helium Cooled Pebble Bed (HCPB), (2006).

[128] D.N. Dongiovanni, T. Pinna, D. Carloni, RAMI analysis for DEMO: Helium Cooled Pebble Bed cooling system. EFDA_D_2KZVUG v1.0, (2013).

[129] T. Pinna, Selection of reference accident scenarios for the DEMO plant. 2MA6TU_v1_0, (2016).

[130] F. Maviglia, Disruptions physics Analysis. PMI-5.3.2-T006_EFDA_D_2MTZ9D, (2016).

[131] C. Bachmann, DEMO Plant Load Specification. 2MY7H3_v1_2, (2017).

[132] X.Z. Jin, Interim report on selected accident analyses: BB LOCA for the HCPB concept. 2M7KNN_v1_0, (2017).

[133] UKAEA Fusion, Plasma and Equilibrium description. 2LJFN7_v1_1, (2015).

[134] A. Paknezhad, A.S. Elahi, M. Ghoranneviss, Plasma Thermal Energy Measurement based on the Plasma Diamagnetic Effect in the IR-T1 Tokamak, 3 (2013) 145–148. doi:10.5923/j.jnpp.20130305.04.

[135] R. Wenninger, The DEMO Wall Load Challenge, (2016).

[136] B. Ploeckl, Fuelling technology for DEMO , state of the art, (2016).

[137] A. Frattolillo, F. Bombarda, C. Day, P.T. Lang, S. Migliori, B. Pégourié, An innovative approach for DEMO core fuelling by inboard injection of high-speed pellets, Fusion Engineering and Design. (2016). doi:10.1016/j.fusengdes.2017.03.067.

[138] B. Pégourié, C. Day, A. Frattolillo, F. Koechl, P.T. Lang, Physical constraints on the design of the DEMO pellet fueling system, (2016) 3–6.

[139] P.T. Lang, C. Day, E. Fable, Y. Igitkhanov, F. Köchl, R. Mooney, B. Pegourie, B. Ploeckl, R. Wenninger, H. Zohm, Considerations on the DEMO pellet fuelling system, Fusion Engineering and Design. 96-97 (2015) 123–128. doi:10.1016/j.fusengdes.2015.04.014.

[140] D. Rapisarda, I. Fernández, I. Palermo, F. Roca, M. Gonzalez, T. Melichar, O. Frybort, L. Vala, L. Maqueda, D. Alonso, H. Neuberger, P. Norajitra, M. Reungoat, M. Utili, Design Description Document 2015 for DCLL (update of DDD 2014) BB-4.1.2-T004-D001_EFDA_D_2MT44J, (2016).

[141] I. Fernández, I. Palermo, F.R. Urgorri, L. Maqueda, D. Alonso, J. Olalde, DCLL Design Report 2016 BB-4.2.1-T003-D001_EFDA_D_2MMM6Q, (2017).

[142] I. Fernández, DCLL Design Report 2015 BB-4.2.1-T002-D001_EFDA_D_2MYHGZ, (2016).

[143] I. Fernández, F.R. Urgorri, Updated design of the DCLL BB CIEMAT_2N787X_v1, (2016).

[144] D. Rapisarda, The DCLL Blanket Concept NBI integration meeting 2MQDDK_v1_0, (2016).

[145] I. Fernández, CAD Model Outboard Equatorial Modul for DCLL (part of Internal Deliverable BB-

4.2.1-T003-D001), (2017). https://idm.euro-fusion.org/?uid=2N7PNT.

[146] I. Fernández, CAD Model Inboard Equatorial Modul for DCLL (part of Internal Deliverable BB-4.2.1-T003-D001), (2017). https://idm.euro-fusion.org/?uid=2NFRL9.

[147] E. Mas de les Valls, L.A. Sedano, L. Batet, I. Ricapito, A. Aiello, O. Gastaldi, F. Gabriel, Lead-lithium eutectic material database for nuclear fusion technology, Journal of Nuclear Materials. 376 (2008) 353–357. doi:10.1016/j.jnucmat.2008.02.016.

[148] J. Rao, H. Sankar, Magneto Hydro-Dynamics and Heat Transfer in Liquid Metal Flows, edited by M.A. Dos Santos, (2011). http://cdn.intechopen.com/pdfs/19884/InTech-Magneto_hydro_dynamics_and_heat_transfer_in_liquid_metal_flows.pdf.

[149] M. Abdou, N.B. Morley, S. Smolentsev, A. Ying, S. Malang, A. Rowcliffe, M. Ulrickson, Blanket/first wall challenges and required R&D on the pathway to DEMO, Fusion Engineering and Design. 100 (2015) 2–43. doi:10.1016/j.fusengdes.2015.07.021.

[150] I. Fernández-Berceruelo, D. Rapisarda, I. Palermo, L. Maqueda, D. Alonso, T. Melichar, O. Frýbort, L. Vála, Á. Ibarra, Thermal-hydraulic design of a DCLL breeding blanket for the EU DEMO, Fusion Engineering and Design. (2016). doi:10.1016/j.fusengdes.2017.03.108.

[151] J. Sanz, Interim report on activation analyses and related studies on DCLL DEMO SAE-2.17.1-T01-D08, (2017).

[152] Blanket Material Composition For Neutron 2N5LUV_v1_0_2017, (2017).

[153] J. Aubert, G. Bongiovi, R. Boullon, J.-C. Jaboulay, A. Morin, J. Peyraud, B. Kiss, G. Porempovics, P.K. Domalapally, Final Report DDD 2016 for HCLL Internal_Deliverable_BB-2.1.2-T005-D001__2MYUAF_v1_0, (2017).

[154] J. Aubert, G. Bongiovi, R. Boullon, J.-C. Jaboulay, A. Morin, J. Peyraud, Final Report HCLL Design Report 2016 Internal_Deliverable_BB-2.2.1-T003-D001__2N8YZS_v1_0, (2017).

[155] U. Fischer, Final Report “Review of the specific DEMO Models (HCPB, HCLL, DCLL, WCLL) and associated nuclear analyses” Internal_Deliverable_BB-9.2.3-T003-D001__2MVP68_v1_0, (2017).

[156] L. V Boccaccini, EU blanket design and R & D for DEMO Outline, (2014) 1–26.

[157] P.K. Domalapally, Final Report CAD, Therm-hydr & Therm-mech analysis (activities in 2016) Internal_Deliverable_BB-2.2.3-T002-D001__2MMB8Z_v1_0, (2017).

[158] Technical Meeting on Failure Analysis/Proposed (draft version) manufacturing scenario (HCLL) V3-_BB-_FR_-_HCLL_2N7PB5_v1_0, (2017).

[159] CAST3M, HTTP://WWW-CAST3M.CEA.FR. (2016).

[160] E. Martelli, A. Del Nevo, P. Arena, G. Caruso, G. Di Gironimo, P.A. Di Maio, M. Eboli, N. Forgionea, WCLL Design Report 2017_BB-3.2.1-T004-D001__2MYHNE_v1_0, (2018).

[161] E. Martelli, A. Del Nevo, P. Arena, G. Caruso, G. Di Gironimo, P.A. Di Maio, M. Eboli, N. Forgionea, WCLL Design Report 2016_BB-3.2.1-T003-D001__2MTZP6_v1_1, (2017).

[162] E. Martelli, A. Del Nevo, P. Arena, G. Bongiovi, Integration for WCLL – DDD 2016 for WCLL (update of DDD 2015)_BB-3.1.2-T005-D001__2N4XN5_v1_1, (2017).

[163] E. Martelli, A. Del Nevo, P. Arena, G. Bongiovi, WCLL DESIGN REPORT 2015_Internal_Deliverable_BB-3.2.1-T002-D001__2N6WLQ_v1_0, (2016).

[164] M. Nobili, G. Caruso, F. Giannetti, M. D'Onorio, Interim report on parametric accident analyses: LOFA in WCLL blanket_2MNV3U_v2_1, (2017).

[165] G. Caruso, F. Giannetti, M. D'Onorio, M. Frullini, Interim report on accident analyses: WCLL blanket in-box LOCAs__WCLL_2MND5X_v1_2, (2018).